INVESTIGATING ANCIENT BISON MIGRATION IN ALASKA: A BOTTOM UP APPROACH USING ISOTOPES.

By

Juliette Marie Funck, MSc

A Dissertation Submitted in Partial Fulfillment of the Requirements

for the Degree of

Doctorate of Philosophy

in

Biogeochemistry and Paleoecology:

Interdisciplinary Program

University of Alaska Fairbanks

May 2020

APPROVED:
Dr. Matthew Wooller, Committee Chair
Dr. Patrick Druckenmiller, Committee Member
Dr. Kris Hundertmark, Committee Member
Dr. Joshua Ruether, Committee Member
Dr. Paul McCarthy, Department Chair
Department of Geoscience
Dr. Kinchel C. Doerner, Dean
College of Natural Science and Mathematics
Dr. Michael Castellini
Dean of the Graduate School

Abstract

Once abundant in the Arctic, bison (*Bison bison)* declined almost to extinction in the North but have subsequently been reintroduced into Alaska. The predecessors of these modern bison were the ancient steppe bison (*Bison priscus*), which were abundant throughout the Northern Hemisphere before their extinction during the Holocene. This thesis investigates the ecology and landscape-use of both the present-day wood bison (*Bison bison athabascae*) and the ancient steppe bison in Alaska using stable isotopes, among other methods. The stable carbon and nitrogen isotope compositions of animal tissues are traditionally used to investigate diet. However, this thesis uses the isotope composition of tail hairs from present day wood bison as a proxy for their nutritional stress. Nutritional stress of some wood bison appears to be influenced not only by food shortage during hard seasons, but also due to long-distance mobility. This insight provides a key to understanding the challenges of reintroduction of the species into Alaska today, and can also be applied to understand the nutritional stress and cost of dispersal by ancient animals. Whereas the mobility of present-day bison can be tracked using sophisticated satellite tracking technologies, studies of the paleo-mobility of ancient bison rely on isotopic markers such as strontium and oxygen isotope ratios preserved in their teeth. To aid this approach using isotopic geolocation, this thesis creates a map of bioavailable strontium modeled and based on strontium isotope composition of present-day rodent teeth from across Alaska. It then compares this map, together with an existing oxygen isotope map of precipitation in Alaska, with the strontium and oxygen isotopes preserved in a suite of ancient bison from Northern Alaska. This comparison brings to light some of the major habitation regions used by *Bison* on the North Slope of Alaska over the last ~50,000 years. Finally, these findings subsequently contribute to a detailed paleoecological investigation of a mostly articulated and complete ancient steppe bison found on the North Slope of Alaska. This final study reveals the life-history of an individual bison that dispersed from the coastal plain to the foothills of the Brooks Range early in his life, and shows that the trip was nutritionally costly. This information is combined with a suite of other paleoecological methods to provide a vivid life history of this ancient bison. We introduce new

methodologies for studying these ancient animals that seek to bridge the gap between how we study present-day and the past.

Table of Contents

List of Figures

Page

List of Tables

Page

Acknowledgments

This thesis was funded and supported by a number of organizations. The Alaska Stable Isotope Facility (ASIF) provided technical support and analyzed many of the samples used here within. Tim Howe, Norma Haubenstock, Karen Spaleta, Dr. Ben Barst and Stormy Fields in particular contributed their expertise, advice and support. Strontium analysis were conducted by Dr. Diego Fernandez at the University of UTAH and his team. The University of Alaska Museum of the North Earth Science and Mammalogy collections provided many samples and the curators, Dr. Katherine Anderson and Aren Gunderson, worked with me extensively.

Chapter 1, Tom Seaton from the Department of Fish and Game, was a key co-author for the 1st data chapter, providing not only samples of plant materials and bison but also a wealth of background knowledge about wood bison. Cade Kellam helped extensively with sampling the bison tail hairs and plants for this chapter and helped write the early stages of the manuscript.

The assistance with the analysis for data chapter 2 was contributed by Dr. Clement Bataille. He also helped with editing and writing the final manuscript for this paper. The Geist Fund Award of 2016 and 2017 supported the radiocarbon analysis and strontium analysis of the steppe bison for this chapter. The National Park Service through Dr. Jeff Rassic provided funding for strontium analysis of the rodents in this study.

Data chapter 3 was supported by experts from a wide range of disciplines utilized in the production of this chapter. Dr. Nancy Bigelow supervised the plant macrofossil analysis and identification and provided support in writing this section. Dr. Jean-Bernard Hauchet analyzed the insect fossils and wrote the sections pertaining to this analysis, which I then revised and integrated into the paper. Dr. Holly McKiney wrote a report of her taphonomic assessment of the specimen from, which I wrote the sections on this topic. Dr. Pat Druckenmiller provided his expert insight and helped to develop the manuscript particularly, integrating the various taphonomic elements. Ancient DNA analysis was conducted by Dr. Beth Shaprio's laboratory, with the support of Dr. Peter Heintzman and Dr. Gemma Murrat all of whom were co-authors. They provided analysis and wrote the methodologies for the ancient DNA in this

section. The Quaternary Center through the David and Rachel Hopkins Fellowship of 2016 and 2017 funded analysis of the strontium of UAMES 29458 ('Bison Bob') in this chapter and a pilot study of rodent's strontium isotopes used in both data chapters 2 and 3.

My committee members, Dr. Josh Ruether, Dr. Kris Hundertmark and Dr. Pat Druckenmiller, provided input into the planning of these projects, and pushed me to go further when necessary. They have all provided extensive notes and edits on these chapters. Finally, I want to acknowledge the work and patience of my supervisor, Dr. Matthew Wooller who over saw all the steps of this work, including planning, data analysis, interpretation, writing and editing. Without his ongoing support this thesis would not have been possible.

General Introduction

The ecology of the Arctic is changing rapidly (Shepherd, 2016), and we may be approaching what some believe to be the next great extinction (Ceballos et al., 2017). The challenges we currently face in the Anthropocene are different from those of the Pleistocene: the temperatures are rising at a faster rate; wilderness is shrinking; and humans take an ever-greater toll on the ecosystem services. Unfortunately, we understand only imperfectly the dynamics at play, as the instrumental record in the Arctic and the temporal extent of ecological and environmental monitoring efforts are relatively short. To supplement these efforts, we can however look at the long trends of paleoecological history. If we can decipher the clues from the past, then we can tap into a record of how ecosystems have adapted to previous cycles of rapid environmental change. Megafauna are particularly at risk, they are less suitable for rapid adaptation, because their long lifespans and specialized diets. They also often function as "ecosystem engineers" (de Silva and Leimgruber, 2019; Fritz, 2017); their disappearance from an ecosystem can thus have significant consequences to it. Fortunately for paleoecologists seeking to understand past successes and failures of adaptation, the remains of ancient megafauna can preserve into the present. This information can help to better calibrate our responses to current adaptation challenges.

The bison is emblematic of the American frontier and wilderness, but for much of human prehistory, they spread across the entire Northern Hemisphere. These animals were a key component of many northern ecosystems (Geremia et al., 2019), and some even believe that their return could help stop the feedback cycle of a thawing Arctic (Zimov et al., 2011). Bison are intrinsically as worthy of study as any other megafauna, but their abundance in the paleontological record (Mann et al., 2013) and continued presence on the landscape makes them easier to study, hence more useful for developing analytical methods.

Stable isotope techniques are the primary methodologies of investigation within the three chapters that follow because they can be measured on both living and long-dead individuals and can provide valuable perspectives on animal ecology (Clementz, 2012) and mobility (Glassburn et al., 2018; Widga et al., 2010). The stable isotope composition (the ratio of heavy to light isotopes sometimes expressed

relative to the isotope ratio of a standard) of animal tissues can be used to infer diet (O'Brien, 2015), nutritional stress (Lee et al., 2012), geolocation (Juarez, 2008), and even past climates and environments (Balasse, 2002). To better understand the effects of the ecosystem and of mobility on the stable isotopes of bison, it is beneficial to broaden the investigation to modern bison living under controlled conditions or whose life history is relatively well known and recorded. Equipped with this understanding, it is then feasible to employ some of these same tools, as well as additional paleoecological techniques to better understand the lives of ancient bison.

In Chapter 1, we follow a herd of wood bison through their reintroduction into the wilds of the Innoko Flats in Alaska, and the first hurdles these animals face. To address the question of: What can the stable carbon and nitrogen isotope tissues of present-day bison can tell us about their ecological physiology? The tail hairs of these animal were sampled before release, during exams of wild individuals and in cases of mortality after death. This provided a compelling natural experiment to study differences in the stable isotopes in the hairs of these wood bison during these periods in order to gain better understanding of the mobility and landscape use of ancient animals.

In Chapter 2, we use strontium paired with oxygen data to determine the provenance of bison tissues to look at how can we track larger scale and long-term landscape use by animals. To determine provenance, we first build a map the strontium bio-availability of Alaska, using present-day georeferenced small mammal specimens and Global Information System (GIS)-based rasters. We then use this map to track the potential landscape use of ancient steppe bison from the teeth of their maxillae and mandibles (dentaries) found in the banks of the Ikpikpuk River on the North Slope of Alaska. The findings update previous models of strontium isoscape of Alaska (Bataille et al., 2014) allowing for stronger inferences about the provenance and movement of ancient megafauna.

Finally, Chapter 3 explores the life history of a charismatic megafauna specimen, affectionately known as "Bison Bob," a steppe bison whose skeleton was discovered, unusually well-preserved, on the banks of the Ikpikpuk River. A detailed, interdisciplinary analysis of all the tissues and materials associated with this specimen, allows us to reconstruct the different parts of its life. Our approach us

combines isotope analysis ($^{87}Sr/^{86}Sr$, $\delta^{18}O$, $\delta^{13}C$, $\delta^{15}N$), ancient DNA, radiocarbon dating, taphonomic analysis, plant macrofossil analysis, and forensic entomology. By "fleshing out" the skeleton of this bison, we are able to carry out an ecological reconstruction of its development, life, and death. This level of analytical depth allows us to place an ancient specimen in its ecological context and provides a review of the analytical methods available.

In the approach presented here, research findings go both ways. What we learn about the reintroduced wood bison of the Innoko Flats regions helps us understand the fate of ancient steppe bison from the Ikpikpuk river region. Conversely, a better understanding of landscape use by ancient megafauna can in the future help better manage reintroduction and re-adaptation programs, such as in the case the modern herds of the Innoko Flats region. More generally, the methods introduced in this thesis can be used to examine adaptation challenges over large landscapes and timespans.

Chapter 1: Stable isotopic signatures in modern wood bison (Bison bison athabascae) hairs as telltale biomarkers of nutritional stress

Juliette Funck[1, 3*], Cade Kellam[2], Thomas C. Seaton[4], Matthew J. Wooller[3, 5*]

1. Department of Geology and Geoscience, University of Alaska Fairbanks, Fairbanks, AK 99775, USA.
2. Department of Biology and Wildlife, University of Alaska Fairbanks, Fairbanks, AK 99775, USA.
3. Alaska Stable Isotope Facility, Water and Environmental Research Center, Institute of Northern Engineering, University of Alaska Fairbanks, Fairbanks, AK 99775, USA.
4. Wood Bison Restoration Project, Alaska Department of Fish and Game, Fairbanks, AK 99701, USA.
5. College of Fisheries and Ocean Sciences, University of Alaska Fairbanks, Fairbanks, AK 99775, USA.

*Corresponding author contact e-mails: jmfunck@alaska.edu, mjwooller@alaska.edu

1.1 Abstract

Assessing the challenges faced by wildlife populations is key to providing effective management but is problematic when dealing with populations in remote locations. Analyses of the stable carbon and nitrogen isotope composition (expressed as $\delta^{13}C$ and $\delta^{15}N$ values) of sequentially grown tissues, such as hairs, can be used to track changes in the eco-physiology of organisms. We generated $\delta^{13}C$ and $\delta^{15}N$ values from sequentially sampled (n = 465) hairs taken from wood bison (n = 27, *Bison bison athabascae* (Rhoads, 1897)). Samples were taken from individuals prior to and after their release from captivity as part of a larger herd (n = 130) into the lower Innoko-Yukon river area of Alaska in 2015. Twenty months after release individuals had a distinct seasonal pattern in $\delta^{13}C$ values. Hairs from individuals that experienced food scarcity or long-distance movement were sampled as case studies. Nutritional stress in these cases lead to a rise in $\delta^{15}N$ values and a decrease in $\delta^{13}C$ values. Applications of $\delta^{13}C$ and $\delta^{15}N$ analyses of bison tail hairs could provide wildlife managers a valuable and minimally invasive tool to better understand bison seasonal metabolic status and determine the historical health and behaviour of living and dead individuals.

Key words: Nutritional stress, wood bison (*Bison bison athabascae* (Rhoads, 1897)), carbon, nitrogen, stable isotopes, hair-growth

1.2 Introductions

In areas where bison (*Bison* sp. (Hamilton Smith, 1827)) had been a dominant species for millennia, they have become rare or extinct in the last few hundred years, but through reintroduction programs bison are returning to the wild (Larter *et al.*, 2000; Olech and Perzanowski, 2002; Freese *et al.*, 2007). Reintroduction of captive animals poses many diverse challenges including: their ability to forage, adaptation to local predators, disease, and hardiness in a challenging environment (Kleiman, 1989; Viggers, Lindenmayer and Spratt, 1993). All of these issues can be compounded if the population size is relatively small. Understanding the causes of death in unsuccessful individuals and correctly assessing challenges faced by populations are key to providing proper management of herds (Armstrong and Seddon, 2008). Stable isotope analysis of hairs could provide key insights into the behavior of bison.

Wood bison (*Bison bison athabascae* (Rhoads, 1897)) are a sub-species of bison adapted to the boreal forest (Stephenson *et al.*, 2001; Gardner and DeGange, 2003; Seaton, 2016). They were thought to have gone extinct until a herd was located in 1957 in remote reaches of Canada (Banfield and Novakowski, 1960; Gates and Larter, 1990). Due to breeding and release programs in Canada (Mitchell and Gates, 2002) and subsequently in Alaska (Seaton 2016), their numbers have increased (Alberta Environment and Parks and Alberta Conservation Association, 2017). Wildlife managers need information to track the health status of individual bison over time, but this can be both a challenging and expensive process, especially in remote and inaccessible regions, such as Alaska. We investigated the application of stable carbon and nitrogen isotope analyses (expressed as $\delta^{13}C$ and $\delta^{15}N$ values, respectively) in segments taken from along the length of tail and forelock hairs of individual wood bison released as part of a herd (n = 130) into the lower Innoko-Yukon river area, Alaska (Figure 1), in the spring of 2015 (Seaton 2016).

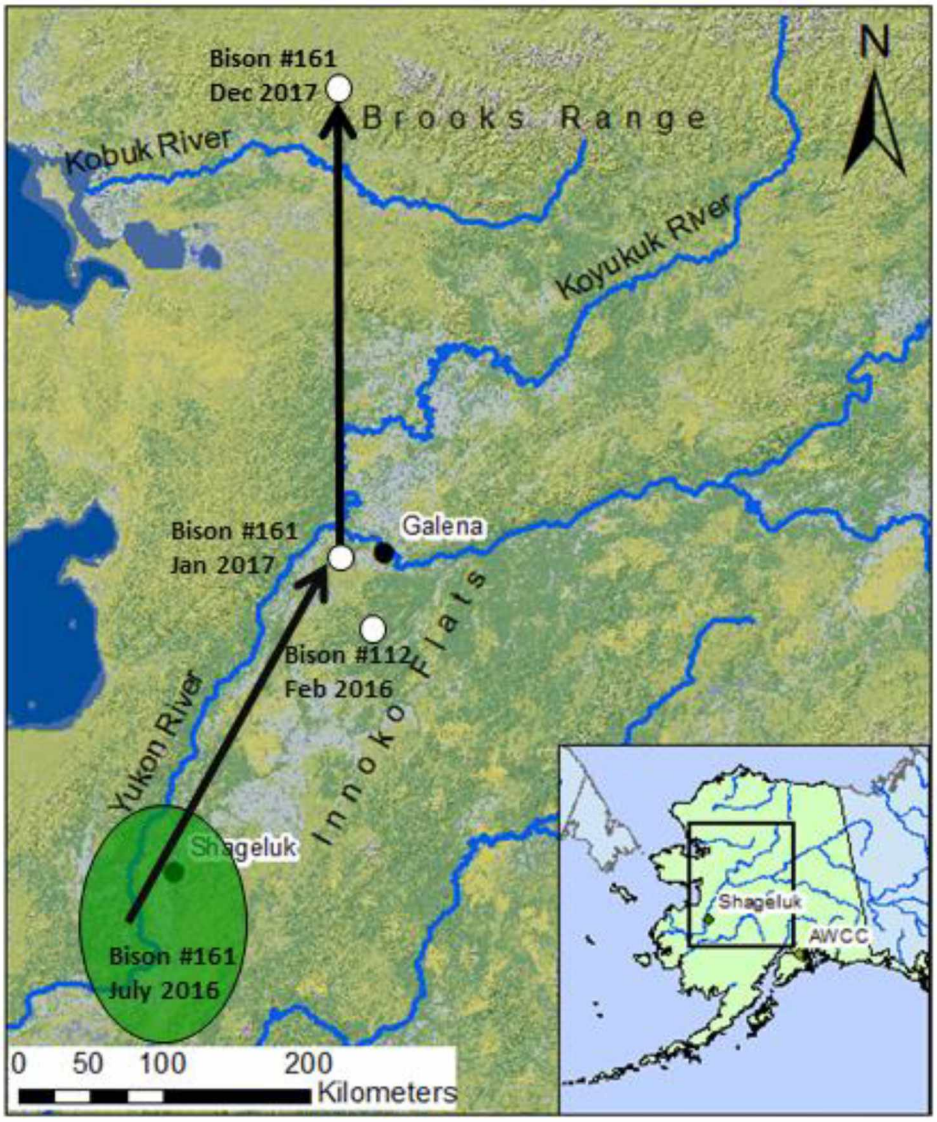

Figure 1.1 A map showing the home range of wood bison (Bison athabascae) (green circle), bison hair sampling, and track directions for bison 161 (solid black line) and location of bison 112

Analyzing the $\delta^{13}C$ and $\delta^{15}N$ values along tissues that grow sequentially, such as hairs, can provide a temporal record of an animal's past feeding ecology and physiology (Darimont and Reimchen, 2002; Cerling and Viehl, 2004; Iacumin, Davanzo and Nikolaev, 2005; Cerling *et al.*, 2006). For example, analyses of $\delta^{15}N$ values from tissues of organisms can be used to determine the trophic level of an organism and/or consumption of marine resources (Minagawa and Wada, 1984). However, fluctuations in $\delta^{15}N$ values in tissues of large terrestrial herbivores, such as bison on a boreal landscape,

would most likely be related to body condition, nutrition and physiology because marine resources are unlikely to enter the food web of an inland bison. When nutritional input does not meet the nutritional need the body will begin depleting fat reserves, leading to the breakdown of lean muscle by an organism, as a result of an individual 'recycling' its own muscle tissues (Waterlow, 1986; Habran *et al.*, 2010). This can, in turn, cause an increase in $\delta^{15}N$ values as if an animal were shifting to a higher trophic level (Minagawa and Wada, 1984; Kelly, 2000; Fuller *et al.*, 2005; Habran *et al.*, 2010). For example, ground squirrels fasting through winter hibernation break down their fat and muscle reserves in order to construct new molecules resulting in significant fractionation of nitrogen isotopes and higher $\delta^{15}N$ values (Lee *et al.*, 2012). This type of isotopic response can stem from a lack of food and fasting (Hobson and Clark, 1992; Hobson, Alisauskas and Clark, 1993; Voigt and Matt, 2004; Mekota *et al.*, 2006). For example, Mekota (et al. 2006) studied human patients recovering from anorexia nervosa and showed a decrease in $\delta^{15}N$ values as their body conditions improved. The physical toll of morning sickness, gestation, and lactation in humans can also cause increases in $\delta^{15}N$ values (Fuller et al. 2005). In addition, sustained physical exertion, disease, injury, or hibernation can result in increased $\delta^{15}N$ values (Delgiudice *et al.*, 2000; Habran *et al.*, 2010; Lee *et al.*, 2012; Rode *et al.*, 2016). We use the term nutritional stress here to include events such as fasting as well as physical exertion which surpasses replacement of calories and results in catabolism of tissues producing a shift to higher $\delta^{15}N$ values. The isotopic data generated from sequentially grown tissues, such as hairs, can thus be used upon necropsy to understand if and when individuals experienced past nutritional stress.

Cortisol is another noninvasive chemical indicator of stress in wildlife and is believed to hormonally mediate catabolism during nutritional stress (Saltz and White, 1991). Blood cortisol can be used to determine acute nutritional stress (Saltz and White, 1991), but in remote populations such as the reintroduced wood bison, blood samples are impractical to obtain. Alternatively, cortisol from hair tends to be homogenous and indicative of long-term stress (Macbeth *et al.*, 2010). The resolution of cortisol from hair is further reduced because it requires an order of magnitude more mass than $\delta^{15}N$ analysis

(Macbeth *et al.*, 2010; Schillaci *et al.*, 2019). As such $\delta^{15}N$ of hair seems a more relevant tool for investigating acute stress, in serial hair samples from bison in a remote, wilderness location.

The $\delta^{13}C$ values of organisms can also be used to identify changes in an organism's diet and health status. The $\delta^{13}C$ values of organisms are often used to track dietary carbon sources, most often for distinguishing consumption of differing proportions of plants using either the C3 or C4 photosynthetic pathways (Connin, Betancourt and Quade, 1998; Feranec, Hadly and Paytan, 2009). However, C4 plants are exceedingly rare at high latitudes and in Alaska (Wooller *et al.*, 2007; Zazula and Wooller, 2008). Instead, $\delta^{13}C$ values of plants at high latitudes can be related to different environmental conditions, including plant water-use efficiency (Wooller *et al.*, 2007) and vegetation coverage (Drucker *et al.*, 2008). The $\delta^{13}C$ values of a consumer can also decrease as a result of using fat reserves, which have relatively low $\delta^{13}C$ values compared with other tissues (Graves *et al.*, 2012; Wolf *et al.*, 2015; Rode *et al.*, 2016, 2018).

Bison can, to some degree, buffer nutritional stresses, such as those associated with supporting long-distance travel and enduring harsh conditions, partially due to their large muscle and fat reserves (Stuth, 1992). Wood bison have been referred to as grazers (Mitchell and Gates, 2002), living on fluctuating/perennial wetlands, and grass meadows (Larter and Gates 1991, Waggoner and Hinkes 1986). However, browse can also be included in the diet of wood bison (Larter and Gates 1991, Waggoner and Hinkes 1986). Wood bison tend to get most of their annual metabolic gain from young sedges (e.g. *Carex* spp.) and grasses (e.g. *Calamagrostis* spp.) throughout the early summer months, before these plants mature and become more fibrous and less nutritious in the mid to late summer (Larter and Gates, 1991). Sedges can also comprise most of the diet of wood bison throughout the winter months and into the spring (Reynolds, Hansen and Peden, 1978; Larter and Gates, 1991). Some sedge stems freeze in a green state in winter, which is presumed to be more palatable and nutritious than other brown, senescent graminoids available in the winter. Frozen ground can also give bison the opportunity to access grazing areas that are often too cumbersome to move through during summer months, because of high water. These swampy areas, which are sometimes dominated by aquatic sedges and horsetails, follow the rise

and fall of water levels, changing access to forage and providing a diversity of forage ages, including highly palatable young plants, when they are not normally available in late summer (Seaton personal observation). Some northern bison also consume significant amounts of willow (Waggoner and Hinkes, 1986), which could also be utilized by wood bison.

We investigated the $\delta^{13}C$ and $\delta^{15}N$ values of sequentially sampled wood bison hairs, with an overarching goal to better understand the seasonal feeding ecology and stress physiology of a herd of wood bison (*Bison bison athabascae)* recently released into the lower Innoko-Yukon river area, Alaska. Our study aimed to determine if we could detect isotopic signatures of nutritional stress and to characterize the typical pattern of isotopic variation in hairs from individuals in the herd before, during and after release. Our analysis includes hairs from a series of individuals with documented behaviours including long-distance movement, nutritional stress, wolf predation, and a winter mortality event. We used these as case studies to examine if they had adopted isotopic signatures that marked nutritional stress in their hairs and distinguished them from the rest of the herd.

1.3 Methods

1.3.1 Sample acquisition

Plant samples

In August of 2015, 53 plant samples were collected at 21 sites where bison had been grazing in the previous two months. Evidence of grazing was sought out, and then whole, un-grazed plants of the same type were sampled near the grazed plants. Plants were classified into four broad groups (grass, sedge, equisetum and herb), then ground and homogenized before being analyzed for their stable isotopic composition (described below).

Baseline bison herd

Guard hairs were routinely pulled from wood bison during handling events, and when dead bison were inspected in the field. Hairs were pulled with the follicle using nitrile-gloved fingers and then stored in a dry paper envelope. An attempt was made to remove the full length of the hair including the follicle, with a sample size of around 20 hairs per individual. Handling procedures included squeeze chutes and chemical immobilizations. The animal care and use committee of the Alaska Department of Fish and Game approved all of the handling and sampling methods. Guard hairs were most often pulled from the end of the tail, but sometimes pulled from the forelock (top of the head, between the horns) when the tail was missing from dead bison due to predation, scavenging, or rotting.

In 2008, a herd of 53 wood bison (*Bison bison athabascae*) was transported to the Alaska Wildlife Conservation Center (AWCC), Alaska, USA, from Elk Island, Canada. The bison were kept in pastures totalling 65 acres, and were fed a diet of live grasses in summer and hay during winter. After a breeding program at the facility, the herd was large enough to be released. Bison underwent medical evaluations in a squeeze shoot and tail hairs were collected prior to their release. Every individual was given an individual identification number (PID). Eight individuals were selected for this study to generate baseline isotope values from captivity (PIDs 102, 116, 112, 124, 138, 142, 149, and 202). A herd of 130 individuals (male 30 / female 100) were transported from the AWCC in 2015 and released to the lower Innoko-Yukon river area (Seaton 2016) near Shageluk, Alaska (Figure 1). In a continued effort to monitor and manage the wellbeing of the herd, a subset of 9 individuals were chemically immobilized 20 months after release in December 2016 to evaluate their health and attach new radio-collars (PIDs 091, 106, 137, 028, 093, 048, 105, 092, 183). All individuals were determined to be in very good body condition during their evaluations and tail hairs were collected. This sampling served as the baseline of wild individuals in good condition.

Case Study 1: North dispersing cow 112

After release in April 2015, a two-year-old female wood bison (112) from the lower Innoko-Yukon river herd dispersed ~260 km north from the herd and settled in a new habitat by September 2015 (Figure 1). This individual was chemically immobilized in February of 2016 (10 months after release), fitted with a radio-collar, and tail hairs were sampled and analyzed for their stable isotope composition (described below). Wood bison 112 was deemed healthy and had no detectable abnormalities at the time of capture. Wood bison 112 was previously sampled before release.

Case Study 2: North dispersing bull 161

One year after the 2015 release, in July of 2016, a five-year-old male wood bison (161) from the lower Innoko-Yukon river herd shed his radio-collar in the southern extent of the wood bison range and dispersed north (Figure 1). He was located by biologists in January 2017, and chemically immobilized in March 2017, 22 months after release (Figure 1). He was fitted with a new radio-collar, and tail hairs were sampled. Wood bison 161 was deemed healthy with no detectable abnormalities. This individual had only localized movements from January 2017 to May 2017, when he then continued on dispersal north. Wood bison 161 was viewed alive in poor body condition in October of 2017, high in the Brooks Range mountains. He died there of unknown causes in December 2017 (Figure 1). Hairs from the bull's forelock were collected and analyzed for their stable isotope composition (described below). The radio collar was collected from the carcass upon death. The movement data was compared to stable isotope values of hair using hair growth estimates discussed below.

Case Study 3: Wolf-killed yearling PID 224

The remains of a wild-born, female wood bison (224) estimated to be 22 months old at the time of death were located and necropsied. Significant injuries to the throat and nose occurred while the bison was alive, and dimensions of canine holes in the bones and soft tissues of the skull indicated wolf predation as

the cause of the bison's death. Hairs were sampled from the forelock and analyzed for their stable isotope composition (described below).

Case Study 4: Winter mortality event

The late winter of 2018 produced an exceptional late-season snow load in Alaska. The snow was also deep and firm, significantly reducing the bison's access to forage. The difficult and extended late winter conditions pushed many bison beyond the extent of their body reserves and approximately 35% of the population died that season. The high death rate was also recorded in a sympatric moose population in Alaska (ADF&G records). Harassment and predation from wolves, breakdown of the bison social hierarchy, the overlap of the metabolic demands of calving season and the lack of access to forage all seemed to have played a role in the late winter mortality event (Seaton personal observation). The tail or forelock hairs of 9 individuals (051, 052, 054, 091, 138, 141, 168, 174, 226) were collected and analyzed for their stable isotope composition (described below). Individual 138 was previously sampled before release.

1.3.2 Sample preparation and stable isotope analyses of samples

Hairs sampled from bison were wiped with a methanol soaked Kimwipe® to remove any non-keratinous substances from their surfaces. The waxy cuticle was also removed from each hair by scraping the base of the hair with a razor blade on all sides. Tail hairs were sectioned into 1-3 cm length subsamples for isotope analysis to reach target weights of between 0.3 and 0.6 mg. These samples were placed into 7 mm tin cups. Hairs collected from dead individuals were sub-sampled more intensively near the root in order to have a higher temporal resolution for the period leading up to their death. Two hairs were sampled in 0.5 cm sections and combined for the first 3 cm of the hair to obtain a large enough mass for analysis over a smaller hair length. Subsequent samples were collected from a single hair. Samples were analyzed to produce $\delta^{15}N$ and $\delta^{13}C$ values using an elemental analyzer (EA) Flash 2000 Organic Elemental Analyzer connected via a Conflo IV to an isotope ratio mass spectrometer (IRMS - Delta V Plus) at the Alaska

Stable Isotope Facility, University of Alaska Fairbanks. Stable isotope ratios are expressed in δ notation as parts per thousand (‰) relative to international standards (Vienna Pee Dee Belemnite – VPDB for carbon and AIR for nitrogen):

$$\delta X‰ = \left[\left(\frac{R_{Sample}}{R_{Standard}}\right) - 1\right] * 1000$$

Where *X* is the element of interest, *R* is the ratio of the heavy to light isotope measured for that element, *Sample* is the sample of interest, and *Standard* is the standard used, VPDB for carbon or AIR for nitrogen. Reference checks using peptone (No. P-7750 meat-based protein. Sigma Chemical Company, Lot #76f-0300) were run every 10th sample, and blanks every 20th sample. Repeated measurements of standards provided the run instrument errors (expressed as 1 standard deviation), which were ±0.2‰ and ±0.1‰ for $\delta^{15}N$ and $\delta^{13}C$ values respectively.

Estimation of tail hair growth-rate

Several studies have previously estimated the growth rates of tail hairs for domestic cattle (Bos Taurus (Linnaeus, 1758)) and horses (*Equus ferus callabus* (Linnaeus, 1758) (Schwertl, Auerswald and Schnyder, 2003; Ayliffe *et al.*, 2004; West *et al.*, 2004; Zazzo *et al.*, 2007; Auerswald *et al.*, 2011). Lacking the resources and ability to replicate their efforts and considering the consistency of approximate growth-rates across species, the growth-rate of bison hairs was estimated as an average of 0.76 ±0.03 mm/day from the previously published studies (Table 1). This was then extrapolated to days and months from death to determine the approximate timing of events in the isotope records from the bison hairs.

Table 1.1 Hair growth rates for a selection of mammals.

Taxon	*Number of samples*	*Hair Growth-rate mm/day*	*1 SD*	*Citation*
Cow (*Bos taurus*)	9	0.76	0.06	Zazzo et al. 2007
Cow (*Bos taurus*)	1	0.76	n.d.	Auerswald et al. 2011
Cow (*Bos taurus*)	5	0.69-1.06	n.d.	Schwertl et al. 2003
Horses (*Equus ferus caballus)*	18	0.72	0.03	West et al. 2004
Horses (*Equus ferus caballus)*	2	0.73	n.d.	Ayliffe et al. 2004
Mean		**0.74**	**0.03**	

1.3.3 Statistics

In order to compare $\delta^{13}C$ and $\delta^{15}N$ differences between wood bison and plant groups a Mann-Whitney *U*-test was used. Distribution of data was evaluated using a Shapiro-Wilks Test of Normality. The mean of all values measured for an individual bison was used as the primary unit of analysis because measurements were not independent. To evaluate differences along the length of the hair, data was binned in equal units of distance from the cuticle, where the width of bins depended on the time scale of interest (3 cm length for multi-season trends, and 1.5 cm length for short scale events). Bins were limited to four due to the small sample number. All measurements in a bin for an individual were averaged. One-way repeated-measures ANOVA was then used to evaluate change between bins along the length of hair. The data were evaluated for this analysis using a Shapiro-Wilks Test of Normality and Mauchly's Test of Sphericity. Differences between the bins were established using a pairwise *t*-test.

Data interpretation

To account for trophic discrimination between plants and consumer's tissue we used a fractionation factor of $\Delta 3.4 \pm 1‰$ (Post, 2002). In addition, a correction of $\Delta+3.1‰$ for bison $\delta^{13}C$ values was used to account for fractionation from diet to hair (Sponheimer *et al.*, 2003; Ayliffe *et al.*, 2004; Drucker *et al.*, 2008).

1.4 Results

The mean $\delta^{15}N$ value for the 36 plants measured was $2.3 \pm 2.1‰$ (All results reported to ± 1 standard deviation). Plants were split into groups by taxa, herbs, equisetum, grasses, and sedges (Figure S1 supplementary documents). Herbs showed the greatest variability in $\delta^{15}N$ values, ranging between -1.7‰ and 6.7‰. All plant groups had no significant difference in their mean $\delta^{15}N$ values ($p = 0.20$). The mean $\delta^{13}C$ value of the herbs was significantly different from the grasses and sedges (graminoids) ($p = 0.002$) with a lower (2.5‰). The mean $\delta^{13}C$ values from analyses of grasses, sedges and equisetum were not distinguishable from each other ($-27.9 \pm 1.5‰$, $-27.4 \pm 1.8‰$, $-28.2 \pm 0.8‰$ respectively ($p = 0.52$). The $\delta^{13}C$ mean value of $-25.3 \pm 2.1‰$ for the plants adjusted by $\Delta+3.1‰$ to account for fractionation in

digestion (Drucker *et al.*, 2008) was only slightly different to the yearly mean of the overall baseline $\delta^{13}C$ value of the bison from this study (overall mean bison $\delta^{13}C$ value in -24.5 ±0.6‰) (described in more details below).

Wood bison in captivity had no obvious synchronous patterns in $\delta^{13}C$ values and showed little variation in $\delta^{15}N$ values (Figure 2*a* and *c*). The $\delta^{13}C$ values ranged from -24.4 to -26.7 ±0.1‰. The tail hairs collected from wood bison 20 months after release into the wild had nearly identical ranges in $\delta^{13}C$ values (-23.3‰ to -26.6‰) compared to the values from captive individuals, though means for individuals were statistically different ($p < 0.000$, Effect Size= 0.64). The bison in captivity had no apparent synchronous temporal pattern of $\delta^{13}C$ values and statistically hair length bins could not be distinguished from one another (one-way repeated measures ANOVA $p = 0.22$) (Figure 2*a*). In contrast, the $\delta^{13}C$ values from the 20-month released individuals showed an apparent synchronous temporal pattern (Figure 2*b*). The values are closely grouped by length and distinctly different to other lengths of hair (one-way repeated measures ANOVA $p > 0.000$). Based on estimates of hair growth-rate (Table 1) it appears that the hairs reached their lowest $\delta^{13}C$ values during the fall and highest values during the mid-summer.

The range of $\delta^{15}N$ values from the 20-month wild individuals was 4.0‰ to 6.5‰, which is slightly smaller than that of those from captivity (4.4‰ to 8.7‰) and neither group showed any apparent seasonal pattern (Figure 2*c* and *d*) (one-way repeated measures ANOVA: wild, $p = 0.60$ and captive, $p = 0.59$). The means from the two groups were not significantly different ($p = 0.074$ Effect Size = 0.5).

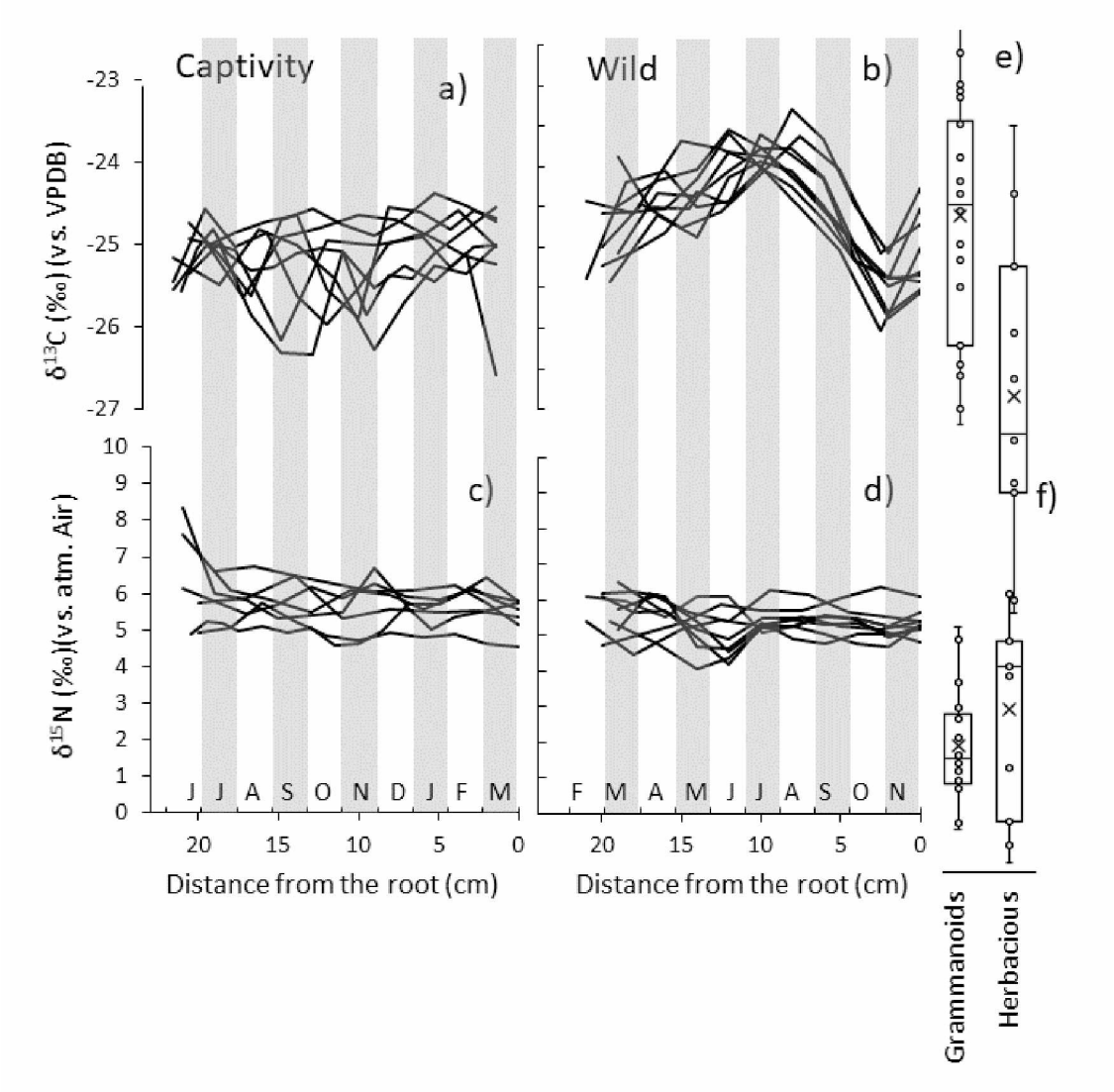

Figure 1.2 The δ13C and δ15N values from wood bison (Bison athabascae) in captivity (a and c) and in the wild (b and d). The δ13C and δ15N values of the forage plants (e and f respectively) are shown as adjusted by +3.1‰ to reflect trophic fractionation (Drucker et al 2008)

Wood bison 112 (Case Study 1) had a punctuated departure from her baseline isotopic values beginning ~8 cm from the base of the cuticle. The $\delta^{13}C$ values decreased by -2.0‰, and the $\delta^{15}N$ values increased to 9.4‰, which was >3‰ higher than her baseline isotopic values earlier on in the hair and relative to the baseline isotopic values for the rest of the herd (Figure 3*a*). At 5 cm $\delta^{15}N$ values began to shift back to her baseline.

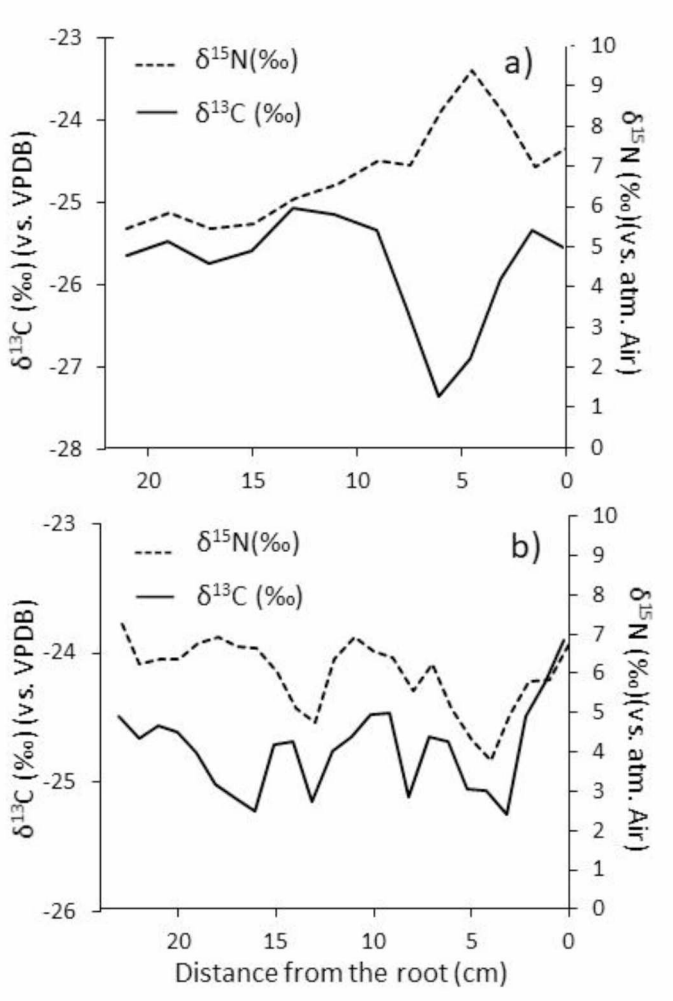

Figure 1.3 The δ13C and δ15N values of tail hair segments from: a) Case Study 1 - Galena cow (112) and b) Case Study 2 - Brooks Range bull (161)

Over the length of the hair from wood bison 161 (Case Study 2) the $\delta^{15}N$ values varied from 3.8‰ to 7.4‰ (Figure 3*b*) and the mean $\delta^{15}N$ value was 6.0 ±0.9‰. The record from this individual also showed two large decreases in $\delta^{15}N$ values, down to 3‰ and 4‰. The $\delta^{13}C$ values for this male showed very little fluctuation (no more than a ~1‰ change) around a mean of -24.7 ±0.3‰ (Figure 3*b*), until approximately the last month of hair growth where both $\delta^{13}C$ and $\delta^{15}N$ values increased rapidly. The supporting radio-collar information from this male showed that this individual had periods of mobility interspersed between periods of rest. The periods of rest coincided with decreases in $\delta^{15}N$ values based on estimates of hair growth (Figure 4).

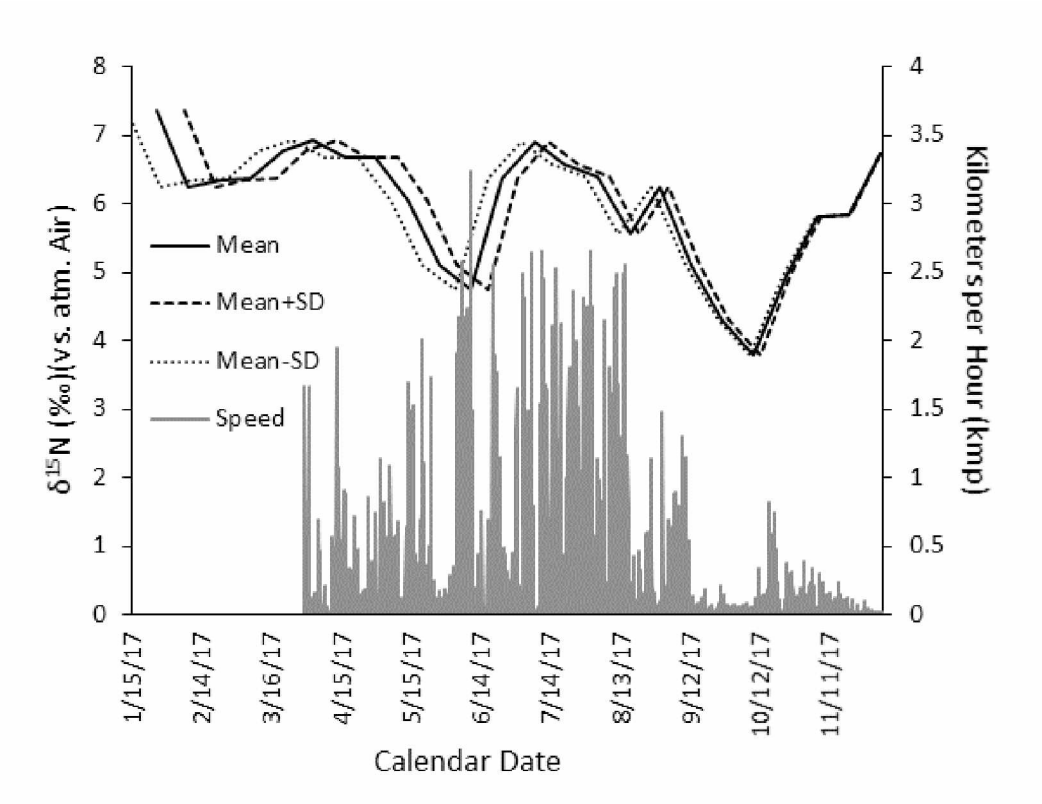

Figure 1.4 The δ15N values of Case Study 2 - Brooks Range bull (161) plotted according to estimates of dates, based on hair growth rates (see text) and relative to radio-collar km/hr.

The wolf killed yearling, wood bison 224 (Case Study 3) (Figure 5), had fluctuating $\delta^{13}C$ values that were initially consistent with the baseline of other wild individuals, with a decrease in the fall followed by a rise mid-winter. However, at the end of this individual's life the values levelled off. Shortly before death, the $\delta^{15}N$ values of this individual increased by ~1.5‰.

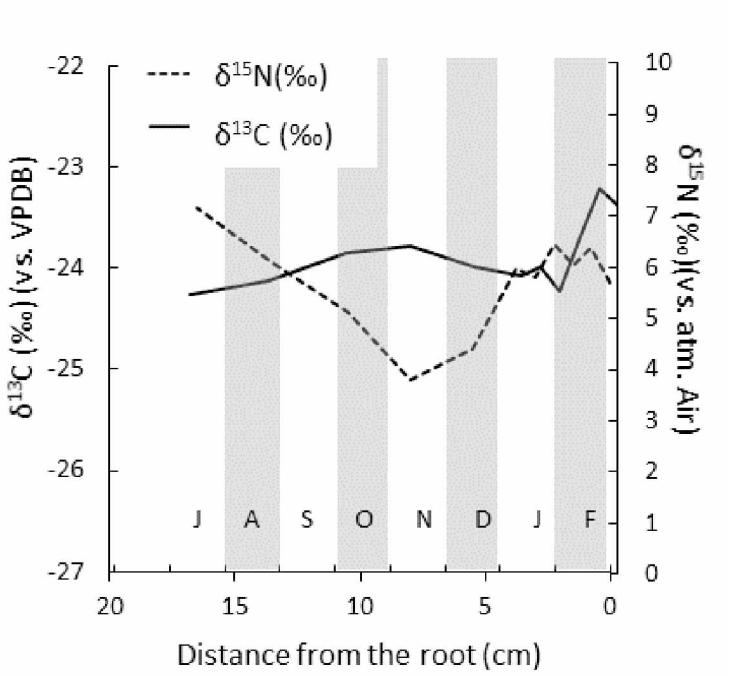

Figure 1.5 The δ13C and δ15N values of tail hair segments from Case Study 3 - Wolf kill calf (224)

All but one (052) of the individuals that died during a winter high mortality event (Case study 4) showed an increase (between 0.6‰ to 1.5‰) in $\delta^{15}N$ values in the last 0.5-1 cm of their tail hairs before death (Figure 6*b*). The difference between their base $\delta^{15}N$ values and the values shortly before death are further accentuated when normalized to individuals' mean $\delta^{15}N$ value (Figure 6*c*). When $\delta^{15}N$ values from the hairs were binned in four groups of 1.5 cm in length, the $\delta^{15}N$ values showed a significant difference in one-way repeated measures ANOVA ($p = 0.002$), but the $\delta^{13}C$ values did not. Post hoc pairwise *t*-test showed that the $\delta^{15}N$ values of the bin closest to the cuticle was significantly different from the others, while the other bins were not. The $\delta^{13}C$ values showed some of the lowest values at ~2 cm, which increased between 5 and 10 cm from the follicle (Figure 6*a*).

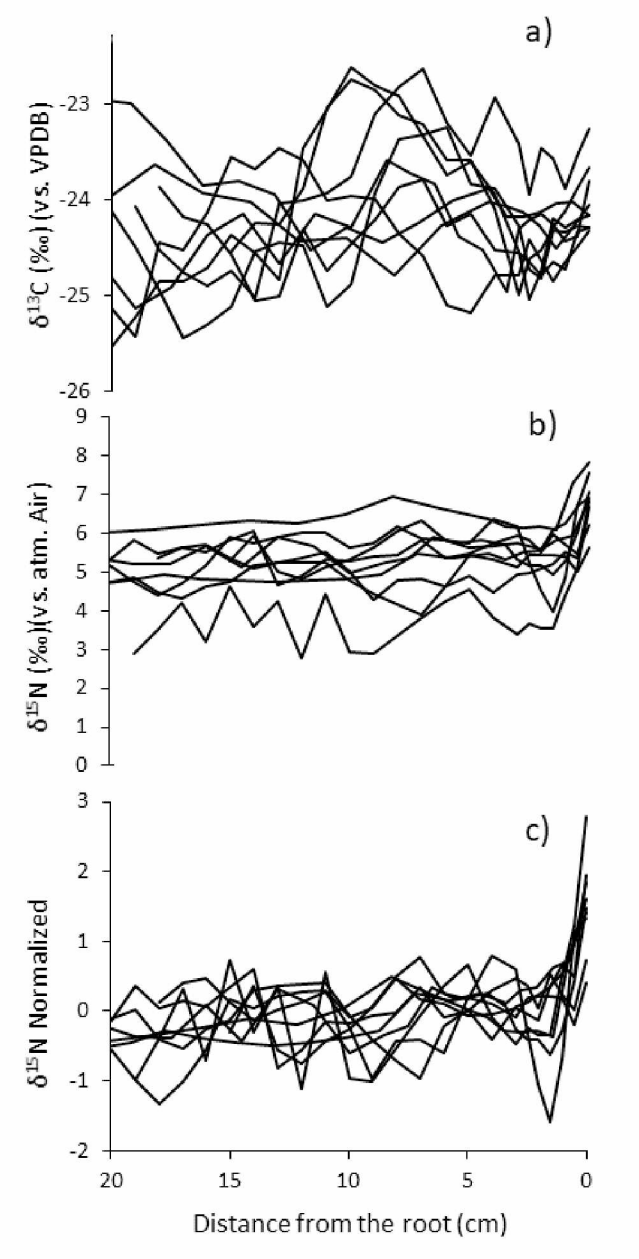

Figure 1.6 The δ13C and δ15N values (a and b respectively) of Case Study 4 - Winter mortality event and c) δ15N values normalized to the mean δ15N value of each individual.

1.5 Discussion

The release of the lower Innoko-Yukon river wood bison herd into the wilds of Alaska provided us with a natural experiment to examine how the stable isotope composition of individuals were influenced by life

in the wild. This release also provided an opportunity to characterize the stable isotopic composition of captive and wild individuals, along with individuals that had adopted behaviours outside the norm for the herd (i.e., our individual case studies). Overall, nearly all of the bison that encountered some form of nutritional stress showed a distinct increase in $\delta^{15}N$ values during the period of stress (e.g. harsh winter conditions or significant movement across the landscape), which in most of the case studies lead to their death. This isotopic pattern contrasted markedly with the pattern from the wild population during a time of minimal nutritional stress, where the $\delta^{15}N$ was relatively stable over time.

The $\delta^{13}C$ values from analyses of captive bison showed very little coherent synchronous seasonal patterns (Figure 2*b*) most likely because steady forage resources were provided year-round, including summer cut grass hay ad libitum throughout the winter. This contrasted with the more synchronous shifts in $\delta^{13}C$ values for the wild bison (Figure 2*b*). All of the wild individuals showed an increase in $\delta^{13}C$ values followed by a decrease in the spring before rising into the summer, but this second event is less synchronous potentially because of variability in hair growth-rate or differences in feeding behaviour. The pattern is consistent with a greater reliance on herbaceous plants in the fall, and graminoids in the summer based on a comparison to the $\delta^{13}C$ values of plants from the region (Figure 2*e* and *f*). This most likely reflected the seasonality of available forage in the wild system and the development of the bison's seasonal foraging strategy obligating the herd to synchronize. There was a consistent decrease in $\delta^{13}C$ values near the follicles from the wild bison (Figure 2*b*), with the lowest values approximately 2 to 3 cm from the base of the hair (estimated to ~October) and highest 8 to 12 cm from the base (estimated to ~June-August). This shift could represent a switch to herbaceous food sources in the fall.

The $\delta^{15}N$ values from both the baseline (captive) and wild bison showed very little variation, which might be expected as the $\delta^{15}N$ values of the plants had only a small range. Based on a trophic level increase in $\delta^{15}N$ values of 3.4 ±1‰ between a herbivore and its diet (Post, 2002) the wild individuals are consistent with being approximately one trophic level above the mean value of the plants measured (2.3 ±2.1‰). In addition, the captive wood bison did not experience stressors like dispersal or starvation. Similarly, a visual assessment of the body condition of the wild herd confirmed that the animals were

uniformly healthy and well-fed during all times except the late winter mortality event of 2018. The relatively flat $\delta^{15}N$ values in the 20-month wild bison and the captive herd are indicative of stable overall health, which allowed us to compare them with the values from the case studies.

The north-dispersing cow (112, Case Study 1) showed an increase in $\delta^{15}N$ values (+3‰) and a decrease in $\delta^{13}C$ values (-2‰) (Figure 3*a*), suggesting major nutritional stress in her most recent past. Her hair was collected in February, ~5 months after she was first spotted in Galena, 260 km (September 10th) to the north of the rest of the herd (Figure 1). During the late summer, when the rest of the herd were focused on grazing and creating body reserves for the oncoming winter, wood bison 112 was engaged in long-distance movement, which may have necessitated the use of her body reserves. Based on hair growth estimates the $\delta^{15}N$ was gradually rising, and the $\delta^{13}C$ values were slowly declining before her arrival in Galena in September, and during the onset of winter both values changed drastically. The decrease in $\delta^{13}C$ values likely represents a draw on her lipid stores (Rode *et al.*, 2018), which typically have lower $\delta^{13}C$ values compared to other body tissues (DeNiro and Epstein, 1977). The increase in $\delta^{15}N$ values in this individual is also consistent with increased use of endogenous nitrogen (Lee *et al.*, 2012). Based on current knowledge of hair growth in domestic cattle, it seems likely that hair could reduce in growth rate during times of extreme nutritional stress (West *et al.*, 2004; Auerswald *et al.*, 2011; Burnik Šturm *et al.*, 2015). It is difficult to interpret the exact timing of the greatest changes in $\delta^{13}C$ and $\delta^{15}N$ values and whether they occurred during her period of rapid mobility or during the portion of winter that followed. However, individual 112 underwent nutritional stress during the time before the hair was collected, where her protein and fat expenditure was greater than her intake. Upon arriving at a new home range, she may have used more body reserves in early winter, but eventually returned to normal baseline values exhibited by the rest of the herd (Figure 3*a*).

The north dispersing bull (161, Case Study 2) had more variable stable isotope values than expected. However, when connected to the radio-collar mobility data from this individual, the oscillation in the $\delta^{15}N$ values seemed to be at least partly associated with periods of extensive mobility interspersed with periods of rest (Figure 4). The $\delta^{15}N$ values appeared to increase sharply during periods of mobility

and decrease when this individual decreased its mobility (Figure 4). The $\delta^{15}N$ values of this individual never increased higher than the Galena cow (112) who survived her journey (Figure 3). However, based on his poor body condition at the last observation, two months prior to his death, wood bison 112 had a diminished pool of tissue available for catabolism. Thus, the change of $\delta^{15}N$ values ($\Delta\delta^{15}N$) is not so much a quantitative indication of the nutritional state as more likely a qualitative signature relative to an individual's overall body condition. At the end of life for wood bison 161, his speed of travel decreased as the $\delta^{15}N$ values increased in this individual. This could have been caused by an injury, illness, or lack of access to forage in the weeks before death. His dispersal event ended high in the Brooks Range of mountains, far above the Arctic Circle (Figure 1).

The wolf killed yearling (224, Case Study 3) showed $\delta^{15}N$ values that increased by 1.5‰ (Figure 5) in the last 2 cm of its hairs, suggesting an acute change in nutrition. Perhaps an illness or injury leads to a lack of forage intake while its herd maintained stable conditions. There was some evidence of recent bone injury of wood bison 224 along the incisor tooth row, which had partially healed on the mandible. The increased $\delta^{15}N$ values from wood bison 224 may provide evidence that it was predisposed to predation, with predation being the proximal but not ultimate cause of death.

The harsh winter conditions of 2018 tested the limits of the lower Innoko-Yukon river wood bison herd and led to a winter mortality event, the physiological cost of which was recorded in their hairs (Case Study 4) (Figure 6*b*-*c*). This case study indicated that eight of the nine individuals analyzed had $\delta^{15}N$ increases from analyses of their tail hairs that were consistent with the individuals having suffered nutritional stress in the weeks leading to their death. Wood bison 052 was the only individual without this distinct pattern; one explanation may be that wood bison 052 died before a significant change in the body chemistry was deposited in the hair or from a different cause (i.e. illness). As part of future research, it will be interesting to examine if residual isotopic evidence of the winter mortality event remains in hairs from individuals that survived. Other tissues may also record these stress events. For example, horn sheaths that grow incrementally over the lifetime of an individual are, like hair, composed of keratin. Since hairs must be analyzed in segments, the data for any single segment is an average of the time it took

to grow that segment of hair. Because of this, acute changes in the deposition of carbon and nitrogen along the hair stem may be somewhat dampened by our sampling methods. Further research into the use of cortisol alongside $\delta^{15}N$ values as markers of nutritional stress would be a beneficial tool for understanding acute and long-term nutritional stress in animals.

A future study documenting hair growth rate in wood bison could aid estimates of the timing of isotopic events preserved in the tail hairs, which could improve this tool as a predictor of historic events in the lives of wood bison. The similarity between the timing of movement in wood bison 161 and fluctuations in isotopic variation dated with estimates of growth rate lend support to the growth rates found in other studies. However, factors such as seasonal differences, domestication, and nutritional stress itself can all play a role in mediating hair growth-rates (West *et al.*, 2004; Auerswald *et al.*, 2011; Burnik Šturm *et al.*, 2015). Auerswald et al. (2011) found seasonal differences in the growth-rate of tail hairs from domestic cows was +0.09 mm/day during the summer. Given the extreme seasonality of forage availability and quality in Alaska, there could be differences in seasonal hair growth-rates. Furthermore, nearly all studies used to estimate tail-hair growth have been conducted on domestic species in captive conditions (Ayliffe *et al.*, 2004; West *et al.*, 2004; Schwertl *et al.*, 2005; Behkami *et al.*, 2017). One study of domestic and wild horses (*Equus ferus przewalskii* (L.S. Poliakov, 1881)) and ass (*Equus hemionus* (Pallas, 1775)) in captive conditions found that wild species had slower growth-rates (Przewalski's horse = 0.57 $\pm$0.06 mm/day and Asiatic wild ass = 0.52 $\pm$0.06 mm/day) than the rate found for domestic horses from the same area (0.79 $\pm$0.11 mm/day) (Burnik Šturm *et al.*, 2015). Although domestic cattle have many physiological similarities to bison, and there is strong consistency between more distantly related species of domestic cattle and horse, we cannot account for the potential effects of colder northern winter and periods of nutritional stress that a wild existence could have had on the growth-rate in wood bison tail hairs.

1.6 Conclusion

The $\delta^{15}N$ and $\delta^{13}C$ values along the timeline associated with hairs in wild wood bison are a valuable tool to document changes that were important in the life history of individual animals. Stable isotope values were shown to detect periods of change that were mainly associated with nutritional stress. These changes were associated with long-distance dispersal, winter stress events, and the weakening of an animal that may have predisposed it to predation death. Wood bison that have reduced access to forage or dispersed a long distance had increased $\delta^{15}N$ values around the time of the nutritionally stressful experience. This contrasted with baseline isotopic values from individuals in the wild and captive herds. Data from a series of case studies demonstrated the utility of $\delta^{15}N$ values for monitoring wood bison health, investigating potential causes of death, and have implications for interpreting paleontological specimens. In addition, $\delta^{13}C$ values appeared to highlight features of the herd's seasonal foraging cycle. Intra-hair analysis can be used to monitor the way that large mammals use the landscapes, food resources and potentially across climatic periods. With an increased understanding of tail-hair growth-rates in wood bison and other species, the timing of nutritional stress and dietary shifts can be more precisely understood. In particular, $\delta^{15}N$ values from hair may be an important tool for wildlife managers as a marker for monitoring physiological status.

1.7 Acknowledgments

We would like to recognize the efforts of the many interest groups involved in the wood bison release and restoration program without which this research would not have been possible. In particular, the ongoing support of the Alaska Wildlife Conservation Center and the communities of the lower Innoko-Yukon river area have been instrumental in accessing the necessary materials. The wider community has also played a hand in monitoring the bison's movement and reporting sightings. Tim Howe and Norma Haubenstock at the Alaska Stable Isotope Facility provided guidance and advice from their wealth of

experience facilitating isotopic data collection. Jen Roach from Alaska Department of fish and game helped us with the radiolocation information. Thomas Funck and Ben Barst discussed and aided with statistics for this work. In addition we appreciate the efforts of the reviewers for improving our manuscript. The animal care and use committee of the Alaska Department of Fish and Game approved all of the handling and sampling methods

1.8 References

Alberta Environment and Parks and Alberta Conservation Association. 2017. Status of the American Bison (Bison bison) in Alberta : Update 2017. *In* Alberta Wi. Alberta Environment and Parks, Edmonton, AB.

Armstrong, D.P., and Seddon, P.J. 2008. Directions in reintroduction biology. Trends Ecol. Evol. **23**(1): 20–25. doi:10.1016/j.tree.2007.10.003.

Auerswald, K., Rossmann, A., Schäufele, R., Schwertl, M., Monahan, F.J., Schnyder, H., Grünlandlehre, L., München, T.U., and Akademie, A. 2011. Does natural weathering change the stable isotope composition (2H , 13C , 15N , 18O and 34S) of cattle hair? Rapid Commun. Mass Spectrom. **25**(August): 3741–3748. doi:10.1002/rcm.5284.

Ayliffe, L.K., Cerling, T.E., Robinson, T., West, A.G., Sponheimer, M., Passey, B.H., Hammer, J., Roeder, B., Dearing, M.D., and Ehleringer, J.R. 2004. Turnover of carbon isotopes in tail hair and breath CO2 of horses fed an isotopically varied diet. Oecologia **139**(1): 11–22. doi:10.1007/s00442-003-1479-x.

Banfield, A.W.., and Novakowski, N.S. 1960. The survival of the wood bison (Bison bison athabascae Rhoads) in the Northwest Territories. Queen's Printer.

Behkami, S., Zain, S., Gholami, M., and Bakirdere, S. 2017. Isotopic ratio analysis of cattle tail hair : A potential tool in building the database for cow milk geographical traceability. Food Chem. **217**: 438–444. Elsevier Ltd. doi:10.1016/j.foodchem.2016.08.130.

Burnik Šturm, M., Pukazhenthi, B., Reed, D., Ganbaatar, O., Sušnik, S., Haymerle, A., Voigt, C.C., and Kaczensky, P. 2015. A protocol to correct for intra- and interspecific variation in tail hair growth to align isotope signatures of segmentally cut tail hair to a common time line. Rapid Commun. Mass Spectrom. **29**(11): 1047–1054. doi:10.1002/rcm.7196.

Cerling, T.E., and Viehl, K. 2004. Seasonal diet changes of the forest hog (Hylochoerus meinertzhageni Thomas) based on the carbon isotopic composition of hair. Afr. J. Ecol. **42**(2): 88–92. doi:10.1111/j.1365-2028.2004.00500.x.

Cerling, T.E., Wittemyer, G., Rasmussen, H.B., Vollrath, F., Cerling, C.E., Robinson, T.J., and Douglas-Hamilton, I. 2006. Stable isotopes in elephant hair document migration patterns and diet changes. Proc. Natl. Acad. Sci. U. S. A. **103**(2): 371–373. doi:10.1073/pnas.0509606102.

Connin, S.L., Betancourt, J., and Quade, J. 1998. Late Pleistocene C 4 Plant Dominance and Summer Rainfall in the Southwestern United States from Isotopic Study of Herbivore Teeth. Quat. Res. **193**: 179–193. Available from doi:10.1006/qres.1998.1986.

Darimont, C.T., and Reimchen, T.E. 2002. Intra-hair stable isotope analysis implies seasonal shift to salmon in gray wolf diet. Can. J. Zool. **80**(9): 1638–1642. doi:10.1139/z02-149.

Delgiudice, G.D., Kerr, K.D., Mech, L.D., and Seal, U.S. 2000. Prolonged winter undernutrition and the interpretation of urinary allantoin : creatinine ratios in white-tailed deer. Can. J. Zool. **78**: 2147–2155. Available from https://doi.org/10.1139/z00-151.

DeNiro, M.J., and Epstein, S. 1977. Mechanism of Carbon Isotope Fractionation Associated with Lipid Synthesis. Am. Assoc. Adv. Sci. **197**(4300): 261–263. Available from https://www.jstor.org/stable/1744515.

Drucker, D.G., Bridault, A., Hobson, K. a., Szuma, E., and Bocherens, H. 2008. Can carbon-13 in large herbivores reflect the canopy effect in temperate and boreal ecosystems? Evidence from modern and ancient ungulates. Palaeogeogr. Palaeoclimatol. Palaeoecol. **266**: 69–82. doi:10.1016/j.palaeo.2008.03.020.

Feranec, R.S., Hadly, E. a., and Paytan, A. 2009. Stable isotopes reveal seasonal competition for resources between late Pleistocene bison (Bison) and horse (Equus) from Rancho La Brea, southern California. Palaeogeogr. Palaeoclimatol. Palaeoecol. **271**(1–2): 153–160. Elsevier B.V. doi:10.1016/j.palaeo.2008.10.005.

Freese, C.H., Aune, K.E., Boyd, D.P., Derr, J.N., Forrest, S.C., Cormack Gates, C., Gogan, P.J.P., Grassel, S.M., Halbert, N.D., Kunkel, K., and Redford, K.H. 2007. Second chance for the plains bison. Biol. Conserv. **136**(2): 175–184. doi:10.1016/j.biocon.2006.11.019.

Fuller, B.T., Fuller, J.L., Sage, N.E., Harris, D.A., O'Connell, T.C., and Hedges, R.E.M. 2005. Nitrogen balance and δ15N: why you're not what you eat during nutritional stress. Rapid Commun. Mass Spectrom. **19**(18): 2497–2506. doi:10.1002/rcm.2090.

Gardner, C., and DeGange, A. 2003. A review of information on wood bison in Alaska and adjacent Canada, with particular reference to the Yukon Flats. *In* Alaska Department of Fish and Game. Available from https://www.wc.adfg.state.ak.us/static/species/speciesinfo/woodbison/pdfs/appendix_a.pdf.

Gates, C.C., and Larter, N.C. 1990. Growth and dispersal of an erupting large herbivore population in northern Canada: the Mackenzie wood bison (Bison bison athabascae). Arctic **43**(3): 231–238. Available from http://www.jstor.org/stable/40511262.

Graves, G.R., Newsome, S.D., Willard, D.E., Grosshuesch, D.A., Wurzel, W.W., and Fogel, M.L. 2012. Nutritional stress and body condition in the Great Gray Owl (Strix nebulosa) during winter irruptive migrations. Can. J. Zool. **90**: 787–797. doi:10.1139/Z2012-047.

Habran, S., Debier, C., Crocker, D.E., Houser, D.S., Lepoint, G., Bouquegneau, J.M., and Das, K. 2010. Assessment of gestation, lactation and fasting on stable isotope ratios in northern elephant seals (Mirounga angustirostris). Mar. Mammal Sci. **26**(4): 880–895. doi:10.1111/j.1748-7692.2010.00372.x.

Hobson, K.A., Alisauskas, R.A.Y.T., and Clark, R.G. 1993. Stable-Nitrogen Isotope Enrichment in Avian Tissues Due to Fasting and Nutritional Stress : Implications for Isotopic Analyses of Diet. Condor **95**(2): 388–394. Available from https://www.jstor.org/stable/1369361.

Hobson, K.A., and Clark, R.G. 1992. Assessing Avian Diets Using Stable Isotopes II : Factors Influencing Diet-Tissue Fractionation. Condor **94**(1): 189–197. Available from https://www.jstor.org/stable/1368808.

Iacumin, P., Davanzo, S., and Nikolaev, V. 2005. Short-term climatic changes recorded by mammoth hair in the Arctic environment. Palaeogeogr. Palaeoclimatol. Palaeoecol. **218**(3): 317–324. doi:10.1016/j.palaeo.2004.12.021.

Kelly, J.F. 2000. Stable isotopes of carbon and nitrogen in the study of avian and mammalian trophic ecology. Can. J. Zool. **78**(1): 1–27. doi:10.1139/z99-165.

Kleiman, D.G. 1989. Reintroduction of Captive Mammals for Conservation. Bioscience **39**(3): 152–161. doi:10.2307/1311025.

Larter, N.C., and Gates, C.C. 1991. Diet and habitat selection of wood bison in relation to seasonal-changes in forage quantity and quality. Can. J. Zool. **69**(10): 2677–2685. doi:10.1139/z91-376.

Larter, N.C., Sinclair, A.R.E., Ellsworth, T., Nishi, J., and Gates, C.C. 2000. Dynamics of reintroduction in an indigenous large ungulate: the wood bison of northern Canada. Anim. Conserv. **3**(4): 299–309. doi:10.1111/j.1469-1795.2000.tb00115.x.

Lee, T.N., Buck, C.L., Barnes, B.M., and O'Brien, D.M. 2012. A test of alternative models for increased tissue nitrogen isotope ratios during fasting in hibernating arctic ground squirrels. J. Exp. Biol. **215**: 3354–61. doi:10.1242/jeb.068528.

Macbeth, B.J., Cattet, M.R.L., Stenhouse, G.B., Gibeau, M.L., and Janz, D.M. 2010. Hair cortisol concentration as a noninvasive measure of long-term stress in free-ranging grizzly bears (Ursus arctos): considerations with implications for other wildlife. Can. J. Zool. **88**(10): 935–949. doi:10.1139/Z10-057.

Mekota, A.-M., Grupe, G., Ufer, S., and Cuntz, U. 2006. Serial analysis of stable nitrogen and carbon isotopes in hair: monitoring starvation and recovery phase of patients suffering from anorexia nervosa. Rapid Commun. Mass Spectrom. **20**: 1604–1610. doi:10.1002/rcm.

Minagawa, M., and Wada, E. 1984. Stepwise enrichment of 15N along food chains : Further evidence and the relation between d15N and animal age. Geoch **48**: 1135–1140. Available from doi.org/10.1016/0016-7037(84)90204-7.

Mitchell, J.A., and Gates, C.C. 2002. Status of the Wood Bison (Bison bison athabascae) in Alberta. . Alberta Sustainable Resource Development, Fish and Wildlife Division, and Alberta Conservation Association, Edmonton, AB.

Olech, W., and Perzanowski, K. 2002. A genetic background for reintroduction program of the European bison (Bison bonasus) in the Carpathians. Biol. Conserv. **108**(2): 221–228. doi:10.1016/S0006-3207(02)00108-8.

Post, D.M. 2002. Using Stable Isotopes to Estimate Trophic Position: Models, Methods and Assumptions. Ecology **83**(3): 703–718.

Reynolds, H.W., Hansen, R.M., and Peden, D.G. 1978. Diets of the Slave River Lowland Bison Herd, Northwest Territories, Canada. J. Wildl. Manage. **42**(3): 581–590. Available from https://www.jstor.org/stable/3800821 DIETS O.

Rode, K.D., Stricker, C.A., Erlenbach, J., Robbins, C.T., Cherry, S.G., Newsome, S.D., Cutting, A., Jensen, S., Stenhouse, G., Brooks, M., Hash, A., and Nicassio, N. 2016. Isotopic Incorporation and the Effects of Fasting and Dietary Lipid Content on Isotopic Discrimination in Large Carnivorous Mammals. Physiol. Biochem. Zool. **89**(3): 182–197. doi:10.1086/686490.

Rode, K.D., Wilson, R.R., Douglas, D.C., Muhlenbruch, V., Atwood, T.C., Regehr, E. V., Richardson, E.S., Pilfold, N.W., Derocher, A.E., Durner, G.M., Stirling, I., Amstrup, S.C., St. Martin, M., Pagano, A.M., and Simac, K. 2018. Spring fasting behavior in a marine apex predator provides an index of ecosystem productivity. Glob. Chang. Biol. **24**(1): 410–423. doi:10.1111/gcb.13933.

Saltz, D., and White, G.C. 1991. Urinary cortisol and urea nitrogen responses in irreversibly undernourished mule deer fawns. J. Wildl. Dis. **27**(1): 41–46. doi:10.7589/0090-3558-27.1.41.

Schillaci, M.A., Lintlop, J., Sumra, M., Pizarro, M., and Jones-Engel, L. 2019. Hair cortisol and stable carbon and nitrogen isotope ratios in barbary macaques (Macaca sylvanus) from Gibraltar. Rapid Commun. Mass Spectrom. **33**(9): 831–838. doi:10.1002/rcm.8413.

Schwertl, M., Auerswald, K., Schäufele, R., and Schnyder, H. 2005. Carbon and nitrogen stable isotope composition of cattle hair: Ecological fingerprints of production systems? Agric. Ecosyst. Environ. **109**(1–2): 153–165. doi:10.1016/j.agee.2005.01.015.

Schwertl, M., Auerswald, K., and Schnyder, H. 2003. Reconstruction of the isotopic history of animal diets by hair segmental analysis. Rapid Commun. Mass Spectrom. **17**(12): 1312–1318. doi:10.1002/rcm.1042.

Seaton, C.T. 2016. Bringing Alaska's wood bison back: The American conservation story that almost wasn't. Wildl. Prof. **10**(3): 20–24.

Sponheimer, M., Robinson, T., Ayliffe, L., Passey, B., Roeder, B., Shipley, L., Lopez, E., Cerling, T., Dearing, D., and Ehleringer, J. 2003. An experimental study of carbon-isotope fractionation between diet , hair , and feces of mammalian herbivores. **876**: 871–876. doi:10.1139/Z03-066.

Stephenson, R.O., Gerlach, S.C., Guthrie, R.D., Harington, C.R., Mills, R.O., and Hare, G. 2001. Wood Bison in Late Holocene Alaska and Adjacent Canada: Paleontological, Archaeological and Historical Records. *In* People and Wildlife in Northern North America. BAR International Series. pp. 125–148.

Stuth, J. 1992. Comparative Nutrition of Bison and Cattle For Parameterizing the Nutbal DSS. Department of Rangeland Ecology and Management, College Station.

Viggers, K.L., Lindenmayer, D.B., and Spratt, D.M. 1993. The importance of disease in Reintroduction programmes. Wildl. Res. **20**(5): 687–698. doi:10.1071/WR9930687.

Voigt, C.C., and Matt, F. 2004. Nitrogen stress causes unpredictable enrichments of 15N in two nectar-feeding bat species. J. Exp. Biol. **207**(10): 1741–1748. doi:10.1242/jeb.00929.

Waggoner, V., and Hinkes, M. 1986. Summer and Fall Browse Utilization by an Alaskan Bison Herd. J. Wildl. Manag. **50**(2): 322–324.

Waterlow, J.C. 1986. Metabolic Adaptation to Low Intakes of Energy and Protein. Annu. Rev. Nutr. **6**(1): 495–526. doi:10.1146/annurev.nu.06.070186.002431.

West, A.G., Ayliffe, L.K., Cerling, T.E., Robinson, T.F., Karren, B., Dearing, M.D., and Ehleringer, J.R. 2004. Short-term diet changes revealed using stable carbon isotopes in horse tail-hair. Funct. Ecol. **28**: 616–624. Available from doi.org/10.1111/j.0269-8463.2004.00862.x.

Wolf, N., Newsome, S.D., Peters, J., and Fogel, M.L. 2015. Variability in the routing of dietary proteins and lipids to consumer tissues influences tissue-specific isotopic discrimination. Rapid Commun. Mass Spectrom. **29**: 1448–1456. doi:10.1002/rcm.7239.

Wooller, M.J., Zazula, G.D., Edwards, M., Froese, D.G., Boone, R.D., Parker, C., and Bennett, B. 2007. Stable carbon isotope compositions of Eastern Beringian grasses and sedges: Investigating their potential as paleoenvironmental indicators. Arct. Antarct. Alp. Res. **39**(2): 318–331. doi:10.1657/1523-0430(2007)39[318:SCICOE]2.0.CO;2.

Zazula, G.D., and Wooller, M.J. 2008. Comment on "Environmental setting (micro) morphologies and stable C-O isotope composition of cold climate carbonate - a review and evaluation of their potential as paleoclimatic proxies" by Denis Lacelle. Quat. Sci. Rev. **26**: 1670–1689. Available from doi:10.1016/j.quascirev.2008.05.001.

Zazzo, A., Harrison, S.M., Bahar, B., Moloney, A.P., Monahan, F.J., Scrimgeour, C.M., and Schmidt, O. 2007. Experimental determination of dietary carbon turnover in bovine hair and hoof. Can. J. Zool. **85**(12): 1239–1248. doi:10.1139/Z07-110.

1.9 Supplementary figures

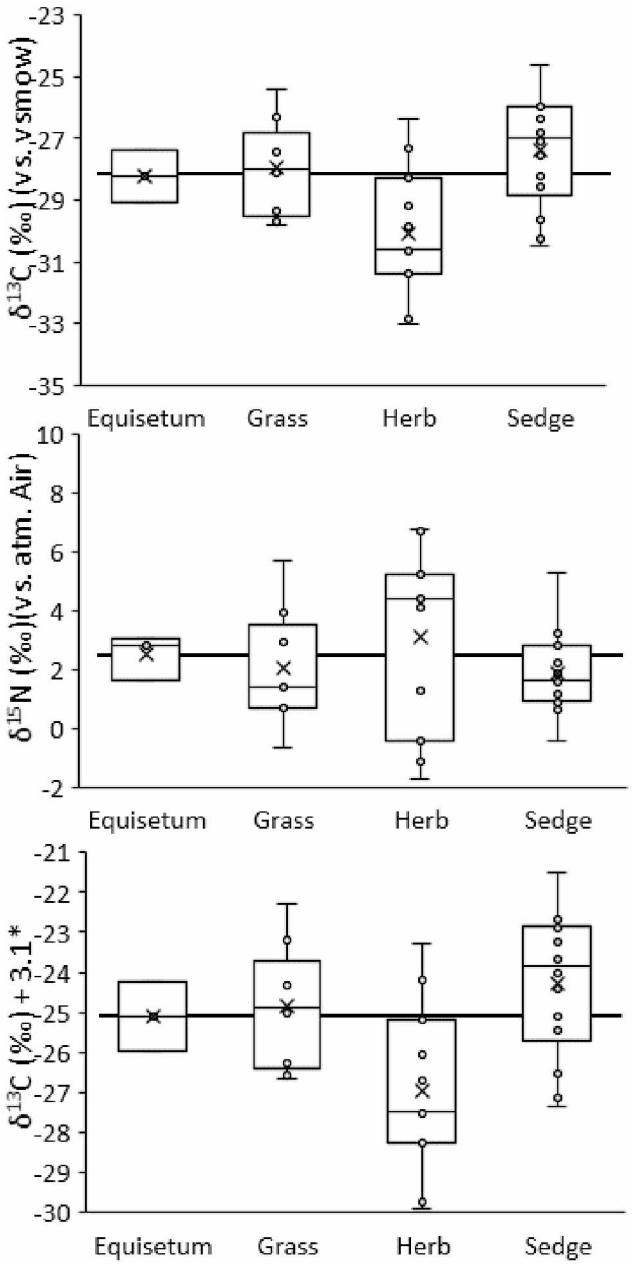

Figure 1.7S1 The δ13C and δ15N values of forage plants (a and b respectively) and the δ13C values of plants corrected for Δδ13C (‰) Diet-Hair +3.1‰ conversion (Drucker et al. 2003)

Chapter 2: Rode(ent)-map of bio-available strontium for Beringia: A tool for tracking landscape-use of Pleistocene megafauna in Eastern Beringia.

Juliette Funck[1,2*], Clement Bataille[3], Jeffrey Rasic[4], Matthew J. Wooller[1, 5]

1. Alaska Stable Isotope Facility, Water and Environmental Research Center, Institute of Northern Engineering, University of Alaska Fairbanks, Fairbanks, AK 99775, USA.

2. Department of Geosciences, University of Alaska Fairbanks, Fairbanks, AK 99775, USA.

3. Department of Earth and Environmental Sciences, University of Ottawa, Ottawa, Ontario K1N 6N5, Canada.

4. National Park Service, Fairbanks, AK 99709, USA.

5. College of Fisheries and Ocean Sciences, University of Alaska Fairbanks, Fairbanks, AK 99775, USA.

* Contact e-mail : jmfunck@alaska.edu

Keywords: Bio-available Strontium, Rodents, Migration, Random-Forest, Isoscape, Steppe B

2.1 Abstract:

Numerous paleoecological questions concern the paleomobility of the rich paleofauna of Eastern Beringia, not least because the region was an entry point for ancient people into North America. Mobility in ancient animals and humans can be difficult to ascertain from physical evidence in the fossil and archaeological records. Strontium (Sr) isotope ratio ($^{87}Sr/^{86}Sr$) analysis has emerged recently as a powerful tool for detecting mobility and determining provenance of ancient biological materials, because it can be used as a geological tracer. To utilize this tool, it is important to characterize $^{87}Sr/^{86}Sr$ variation across a landscape. We measured the $^{87}Sr/^{86}Sr$ composition of teeth from n = 162 present-day herbivorous rodents sampled from across Eastern Beringia to estimate the local bioavailable $^{87}Sr/^{86}Sr$ values. We added the very limited number of published strontium isotope data from water, soil and plant values from the region. We then used this bioavailable dataset and a machine learning, random-forest regression to predict bioavailable $^{87}Sr/^{86}Sr$ variations across Eastern Beringia from geoenvironmental covariates. The model used climate and geological variables as the main predictors. Lastly, we measured the strontium isotope values ($^{87}Sr/^{86}Sr$) and oxygen stable isotope values ($\delta^{18}O‰$) of five ancient (14,215, 34,880, 42,210, 42,440, 44,930 to 45,000 calibrated years Before Present) steppe bison (*Bison priscus*) molars from Arctic Alaska as a case study utilizing our new$^{87}Sr/^{86}Sr$ isoscape. We then compared these values to our bioavailable $^{87}Sr/^{86}Sr$ 'isoscape' and an adjusted $\delta^{18}O‰$ isoscape to estimate the probable landscape-use of these ancient steppe bison. Our model provides an important foundation for a wide range of additional applications, including studies of the paleo-mobility of ancient people and their material trade, other megafaunal taxa, and present-day fauna across Eastern Beringia.

2.2 Introduction

2.2.1 Beringia and bison:

Beringia is the massive landmass that once extended from the Lena River, Russia, in the west and the Mackenzie River, Canada, in the east (Elias and Crocker, 2008; Lloyd et al., 2013) (Figure 1). The region has experienced changes in the extent of glacial barriers and temporary continental connections between Eastern and Western Beringia via the Bering Land Bridge (BLB) (Burns, 2010; Elias and Crocker, 2008; Kaufman and Manley, 2004). This dynamic physiographic backdrop has prompted questions about ecological processes that include spatial interconnectivity, biogeography and discontinuity in the landscape (Elias et al., 2000; Elias and Crocker, 2008; Froese et al., 2017; Goebel et al., 2008; Heintzman et al., 2016; Mann et al., 2013; Potter et al., 2017; Zazula et al., 2017). Spatial and biogeographic questions also surround many aspects of Beringian paleoecology, including the paleo-mobility of animals (Froese et al., 2017; Heintzman et al., 2016; Mann et al., 2013) and people in Beringia (Goebel et al., 2008; Potter et al., 2017). Moreover, there are many questions

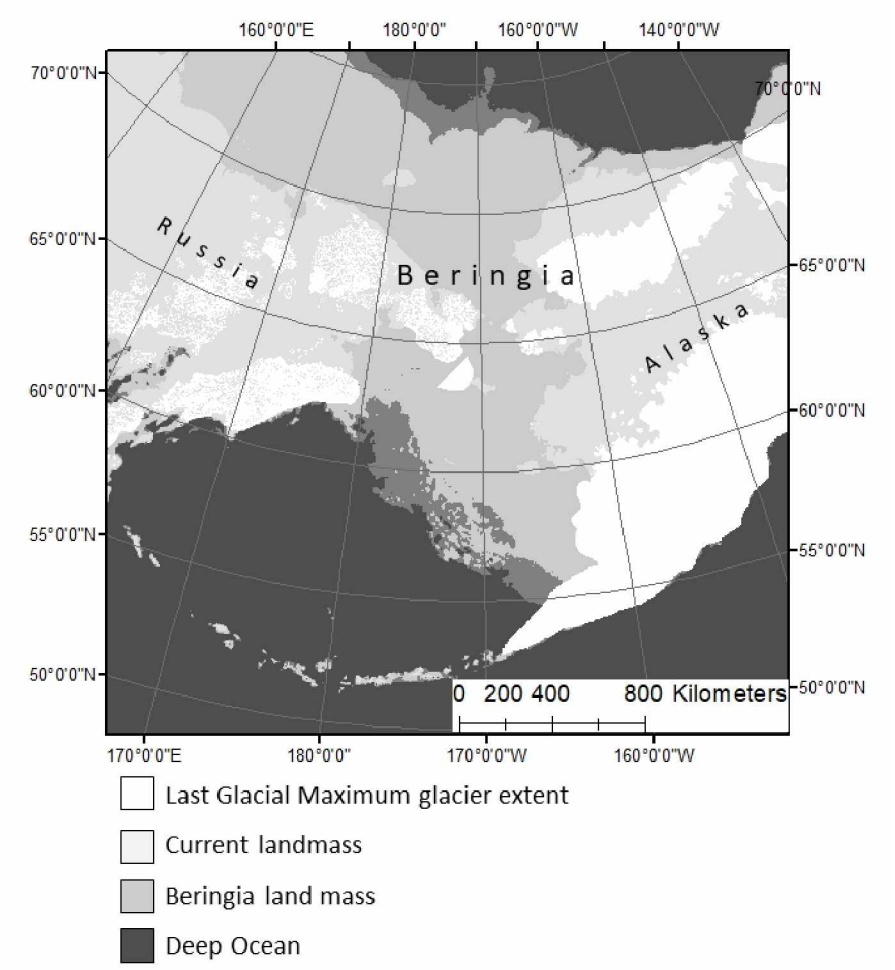

Figure 2.1 The Beringian landmass and glacier coverage modelled for Last Glacial Maximum.

surrounding the mobility of present-day megafauna, including caribou and moose (Cameron et al., 2018; Dussault et al., 2005; Joly et al. 2019).

The paleo-mobility of steppe bison is a particular quandary because these large mobile ungulates were once spread throughout the northern hemisphere (Mann et al., 2013; Shapiro et al., 2004) but became extinct at some point during the Holocene (Rasic and Matheus, 2007; Stephenson et al., 2001; Zazula et al., 2017). The wood bison, Plains bison and European wisent that replaced them are known to have varying degrees of mobility in their modern habitat, but much of their true ecological niche and life history is not well known because they were forced to near extinction in the 19th and 20th centuries due to overhunting and habitat degradation (Banfield and Novakowski, 1960; Freese et al., 2007; Larter and Gates, 2017; Massilani et al., 2016; Stephenson et al. 2001). To better understand the *Bison genus*, we can reconstruct prehistoric behavior, for example how they responded to and persisted through climate change. That knowledge can also help inform current reintroduction and management programs (Cannon, 2001). To help examine the paleo-mobility of steppe bison in the north there are a large number of ancient steppe bison fossils to draw from due to regional permafrost, dry conditions and high sedimentation rates (Shapiro and Cooper, 2003). The primary aim of our study is to improve and increase the resources to conduct research into megafaunal paleo-mobility in Eastern Beringia by creating a baseline of $^{87}Sr/^{86}Sr$ variation (isoscape) across Eastern Beringia This $^{87}Sr/^{86}Sr$ isoscape will be used to reconstruct the paleomobility of a series of steppe-bison individuals to showcase its applicability in paleoecology studies.

2.2.2 Isoscapes and paleomobility:

Isotope ratios of several elements are especially valuable tools for reconstructing the paleomobility of organisms. For example, oxygen isotope composition ($\delta^{18}O$ values) have been used for decades to reconstruct movements because variation in $\delta^{18}O$ values preserved in tissues usually reflect that of the water ingested (e.g., O'Brien and Wooller, 2007). As meteoric water has predictable spatial patterns of $\delta^{18}O$ values following climate regimes (Bowen et al., 2005), changes in $\delta^{18}O$ signatures in tissues can help reconstruct the paleo-mobility of ancient animals and populations (Widga et al., 2010). However, $\delta^{18}O$ values alone are limited in their ability to precisely and confidently determine an organism's provenance,

particularly when considering paleo-landscapes where climate regimes can differ significantly from the present-day (Gaglioti et al., 2017; Rasmussen et al., 2014). By contrast, strontium (Sr) isotope ratios ($^{87}Sr/^{86}Sr$) in inorganic tissues derive from an essentially static geological substrate underlying the habitat of a given individual (Britton, 2009; Julien et al., 2012; Widga et al., 2010). As bedrock geology alters very little over millenial timescales, present-day geology closely informs past $^{87}Sr/^{86}Sr$ variations in Late-Quaternary landscapes.

As an individual animal develops, different tissues of its body incorporate the $^{87}Sr/^{86}Sr$ value of local food sources. In the case of tooth enamel, which grows in discrete, incremental daily layers (Risnes, 1998), each growth layer incorporates the local bioavailable $^{87}Sr/^{86}Sr$ value at the time of development. By taking serial, intra-tooth samples it is possible to track the degree of movement of an organism during tooth development based on the most probable geological origin of the specific $^{87}Sr/^{86}Sr$ value in the tissue (Balasse et al., 2002; Hoppe et al., 1999; Hoppe, 2004; Koch et al., 1995). In animals that cannot be directly observed, such as archeological (Viner et al., 2010), paleontological (Hoppe et al., 1999), or forensic specimens (Juarez, 2008), $^{87}Sr/^{86}Sr$ values can be used to determine provenance and movement that would otherwise be unknown. Reliable isoscapes, of $^{87}Sr/^{86}Sr$ and $\delta^{18}O$ values are needed to predict the variation that exists across landscapes (West et al., 2009). Several products from previous research have generated $\delta^{18}O$ isoscapes covering Eastern Beringia (Bowen et al., 2005; Lachniet et al., 2016). Currently there is no terrestrial bioavailable $^{87}Sr/^{86}Sr$ isoscape for Eastern Beringia. Alaska has a complex geology that leads to high variation in $^{87}Sr/^{86}Sr$ values (Bataille et al., 2014) which makes it an ideal place for $^{87}Sr/^{86}Sr$ geolocation applications.

2.2.3 Limitations of existing $^{87}Sr/^{86}Sr$ isoscape across Beringia:

Bataille et al. (2014) predicted $^{87}Sr/^{86}Sr$ values in rocks across Alaska based on the age and lithology of rock units by leveraging data from rock geochemical databases. While geological regimes dominate $^{87}Sr/^{86}Sr$ variations in terrestrial ecosystems (Bataille and Bowen, 2012), other factors can contribute to this $^{87}Sr/^{86}Sr$ variation before it enters biological systems(Capo et al., 1998). The mixing of strontium

from the geosphere to the biosphere is primarily driven by hydrological processes (Capo et al., 1998). For example, differential weathering of minerals with isotopically distinct signatures, can lead to different isotopic values between soil water and rocks (Bataille et al., 2014; Shand et al., 2009). Strontium from external sources can also be added to soils by deposition from aerosols, sea spray and airborne sediments (Bataille et al., 2012; Chadwick et al., 2009; Graustein and Armstrong, 2009; Hartman and Richards, 2014). Soil processes and plant physiology can further modulate the mixing of isotopically-distinct Sr sources in soil water and their uptake by ecosystems (Graustein and Armstrong, 2009); Podzwa et al., 2004; Hartmann and Richards, 2014). Consequently, a simple geological model, such as that used by Bataille et al. (2014) to create an $^{87}Sr/^{86}Sr$ isoscape primarily serving the freshwater realm is not sufficient to explain the distribution of $^{87}Sr/^{86}Sr$ values across terrestrial ecosystems and cannot be used for more precise terrestrial paleo-mobility research.

2.2.4 Bioavailable $^{87}Sr/^{86}Sr$:

Previous archeological and paleoecological research has defined the concept of 'bioavailable Sr' (Price et al., 2002), to describe the $^{87}Sr/^{86}Sr$ entering the biological system, which can differ from the local geology, as mentioned above. It is possible to define the local $^{87}Sr/^{86}Sr$ signature available to organisms in an area by sampling organisms with a local and limited home range. Rodents have proven to be useful indicators of local bioavailable $^{87}Sr/^{86}Sr$ values in terrestrial systems because they have low mobility, are herbivorous and common in most ecosystems (Barberena et al., 2019; Hoppe et al., 1999; Kootker et al., 2016; Price et al., 2002). A problem with this empirical approach, however, is that when the spatial scale increases, large dataset of $^{87}Sr/^{86}Sr$ values are required to characterize the baseline at sufficiently high spatial resolution for paleo-mobility studies. In our case, Eastern Beringia covers a massive area and high-resolution sampling and analysis of $^{87}Sr/^{86}Sr$ values in local organisms is not logistically or financially feasible. To solve this issue, we used a hybrid empirical and predictive approach. First, we produced a relatively large dataset of $^{87}Sr/^{86}Sr$ values from analyses of archived, extant rodents across Eastern Beringia. Second, we extracted the geological, climatological and environmental conditions for the

documented geolocations of these rodents using open-access environmental and geological maps. Lastly, we applied a random forest regression approach, developed by Bataille et al. (2018), to predict bioavailable $^{87}Sr/^{86}Sr$ dataset across Eastern Beringia. As a case study, to demonstrate the applicability of our new bioavailable $^{87}Sr/^{86}Sr$ isoscape, we combined our $^{87}Sr/^{86}Sr$ isoscape with an existing $\delta^{18}O$ isoscape (Lachniet et al., 2016) and evaluated the probable landscape use of a suite of radiocarbon dated steppe bison (*Bison priscus*) from Eastern Beringia.

2.3 Materials and Methods:

2.3.1 Rodent sampling:

We sampled rodent specimens from the University of Alaska Museum Mammal Collection (UAM:Mamm) for this study and selected them based on a series of criteria, including coverage of unique locations (Figure 2), the accuracy of the georeference related to each specific specimen, and the species of interest. Damaged and redundant specimens were favored in order to minimize impacts from destructive sampling on museum specimens. Coverage of locations was determined by mapping the coordinates of all (n= >36,000) rodent specimens in the UAM:Mamm collection database (arctosdb.org) for visual inspection. Additional sites were included from areas with variable geology, such as the Seward Peninsula and Brooks Range Mountains. For five sites from across the geological spectrum a subset of 4 to 5 individuals was sampled in order to determine the site-specific population variance. The accuracy of the georeference information for the analyzed specimens are reported in the UAM database and range from 6 to 3615 m. Specimens collected more recently have higher accuracy due to improvement in Global Positioning System (GPS) and were favored during our sampling whenever possible. In a few cases specimens with less precise geographic coordinates were used for some unique locations where only a few specimens were available. Museum curators assigned georeferences to specimens without GPS coordinates using protocols described in VertNet (2016). We selected species of *Microtus* (voles),

Myodes (red-backed voles), *Lemmus* (lemming) and *Dicrostonyx* (collard lemming). These species are all herbivorous and unlikely to have large dispersal distances or to have consumed non-local plants. Beavers and muskrats, which are primarily aquatic, were excluded because they are more likely to be infused by alluvial rather than local terrestrial material. We removed molars or incisors from n = 162 selected rodent specimens and placed them in a sterile sample tube ready for $^{87}Sr/^{86}Sr$ analyses (described below). A full list of specimens and museum accession numbers is included in the supplementary information (Table S1).

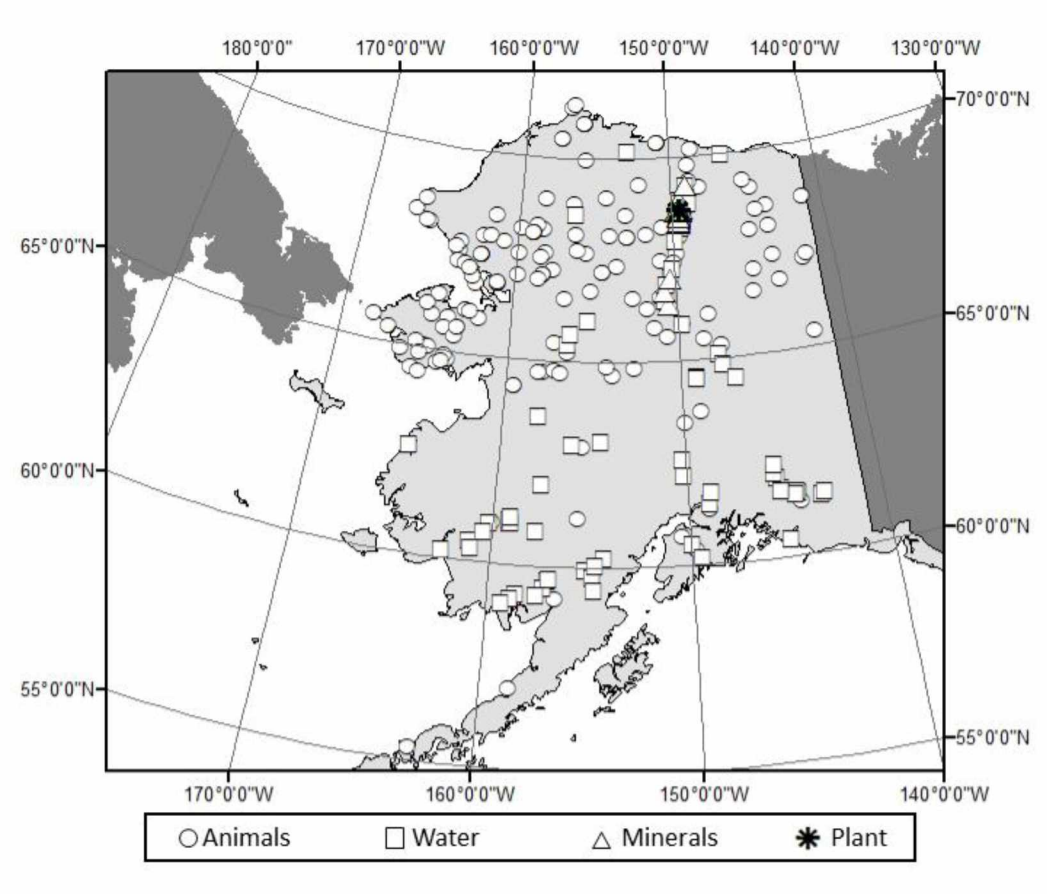

Figure 2.2 Sampling scheme for georeferenced rodents, and samples from previous studies (Bataille et al., 2014; Brennan et al., 2015; Keller et al., 2007).

2.3.2 Pleistocene steppe bison:

Steppe bison mandibles and maxillae from the Ikpikpuk River of the North Slope of Alaska (Figure 3) were recovered where the river cuts through the fossil-rich deposits of the "Pleistocene Sand Sea" (Carter,

1981). They are curated in the University of Alaska Museum Earth Science (UAMES) collection. We prepared collagen from samples of nine mandibles and maxillae at the Alaska Stable Isotope Facility (ASIF) using a previously published protocol (Misarti et al., 2009). We subsequently sent the collagen for radiocarbon analysis at the University of Georgia's Center for Applied Isotope Studies. Finite ^{14}C ages within the range of calibration were calibrated using Calib 7.1 Radiocarbon Calibration (Stuiver et al., 2019). We then used the teeth of the finite specimens to serially sample the enamel for $^{87}Sr/^{86}Sr$ and $\delta^{18}O$ analyses.

Samples were collected in a laminar flow hood in the ASIF. We targeted the tallest section of each tooth and cleaned the external surface by abrading the exterior enamel surface using a Dremel buffing bit. Subsequently, we used a Dremel diamond-coated circular saw bit to divide samples along each tooth parallel to the growth plane. We then used a dental pick to break off chips from the enamel surface, which were then subdivided and placed into labeled, sealable vials. This method has been found to introduce fewer potential contaminates than removing enamel as a ground powder (Fernandez personal communication, ICP-MS Metals Lab, 2016). Half of each sample was analyzed for $^{87}Sr/^{86}Sr$ isotope ratios and the other half for $\delta^{18}O$ values (described below). Previously published isotope values from water, plant, and soil samples were also included in our model (Bataille et al., 2014; Brennan et al., 2015; Keller et al., 2007) (Table S2).

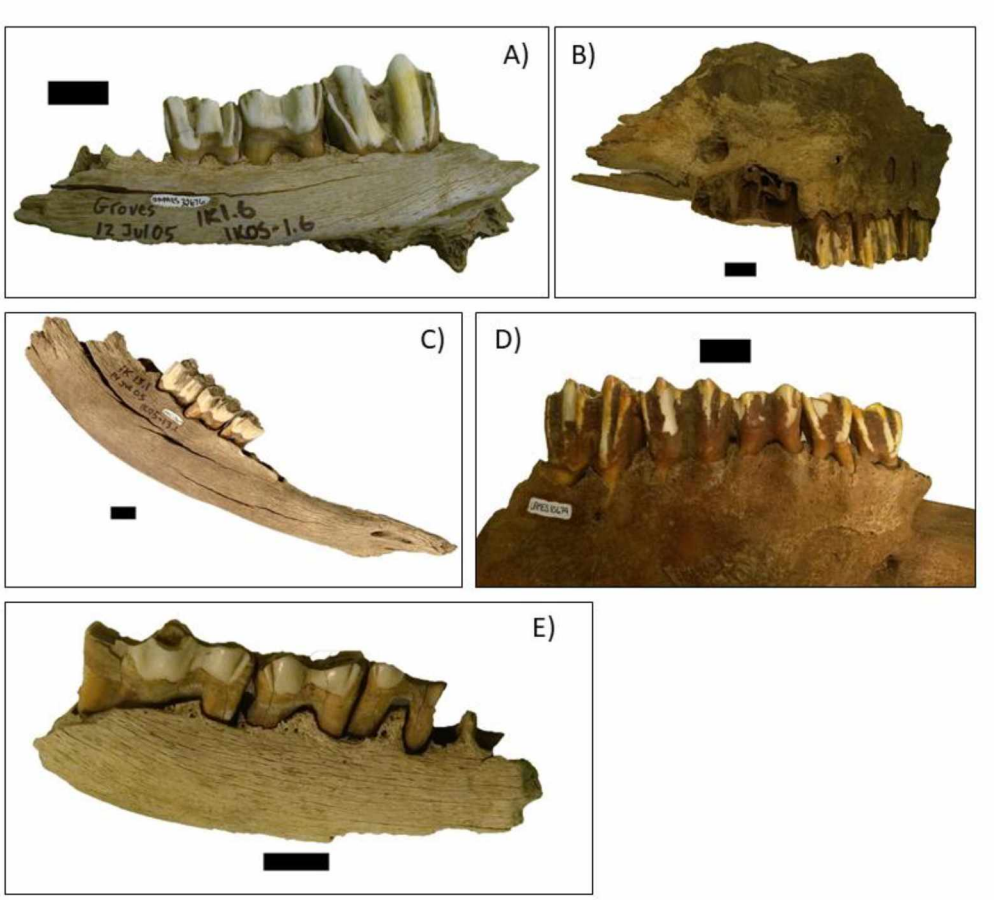

Figure 2.3 Steppe bison dentaries sampled for enamel A) UAMES 32676, B) UAMES 10679, C) UAMES 32669, D) UAMES 10679, and E) UAMES 11332

2.3.3 $^{87}Sr/^{86}Sr$ isotope ratio analysis:

The University of Utah, Department of Geology and Geophysics, ICPMS facility prepared samples and conducted $^{87}Sr/^{86}Sr$ analysis on the rodent specimens. Any dentine was removed and physically cleaned from each sample. Samples were analyzed for their $^{87}Sr/^{86}Sr$ composition using a previously published solution method (Mackey and Fernandez, 2011). Analysis was conducted using a multi-collector inductively coupled plasma mass spectrometer (MC-ICPMS - ThermoFisher Scientific, High Resolution NEPTUNE, Bremen, Germany). Samples were purified for the analyses using an introduction system of aqueous solution using an inline chromatographic column (Mackey and Fernandez, 2011). An analytical mean error for this methodology of 0.00001 was calculated by comparing sample results with measures of

NIST standard reference sample SRM 987 and a lab-specific reference blank. Individual sample errors are reported in Table S1.

2.3.4. $\delta^{18}O$ analysis:

The remaining half of each bison enamel sample was analyzed to produce $\delta^{18}O$ (and $\delta^{13}C$) values from carbonate using a Thermo Scientific GasBench II carbonate analyzer attached to a Thermo Scientific DeltaV^{Plus} Isotope Ratio Mass Spectrometer (IRMS) at ASIF, following previously published protocols (Glassburn et al., 2018). Stable carbon and $\delta^{18}O$ values are reported in δ notation as parts per thousand (‰) relative to the international standard Vienna Pee Dee Belemnite (VPDB). We ran samples with laboratory standards of calcium carbonate (Merck, Suprapur 99.95% Lot # B510959 313) every 10 samples to determine analytical precision for $\delta^{13}C$ and $\delta^{18}O$ values, which were 0.3‰ and 0.2‰ respectively (all errors are expressed to one standard deviations unit). We analyzed a blank every 20 samples.

2.3.5 Isoscapes:

A prerequisite before geographic assignment is to have an isoscape calibrated to the tissue of interest. In this study, we applied isotope provenance using teeth to assess the paleomobility of steppe bison using $\delta^{18}O$, $^{87}Sr/^{86}Sr$ and combined $\delta^{18}O$ - $^{87}Sr/^{86}Sr$. The data analysis of stable isotope values to assignment of provenance probability is outlined in Figure 4 and is detailed below.

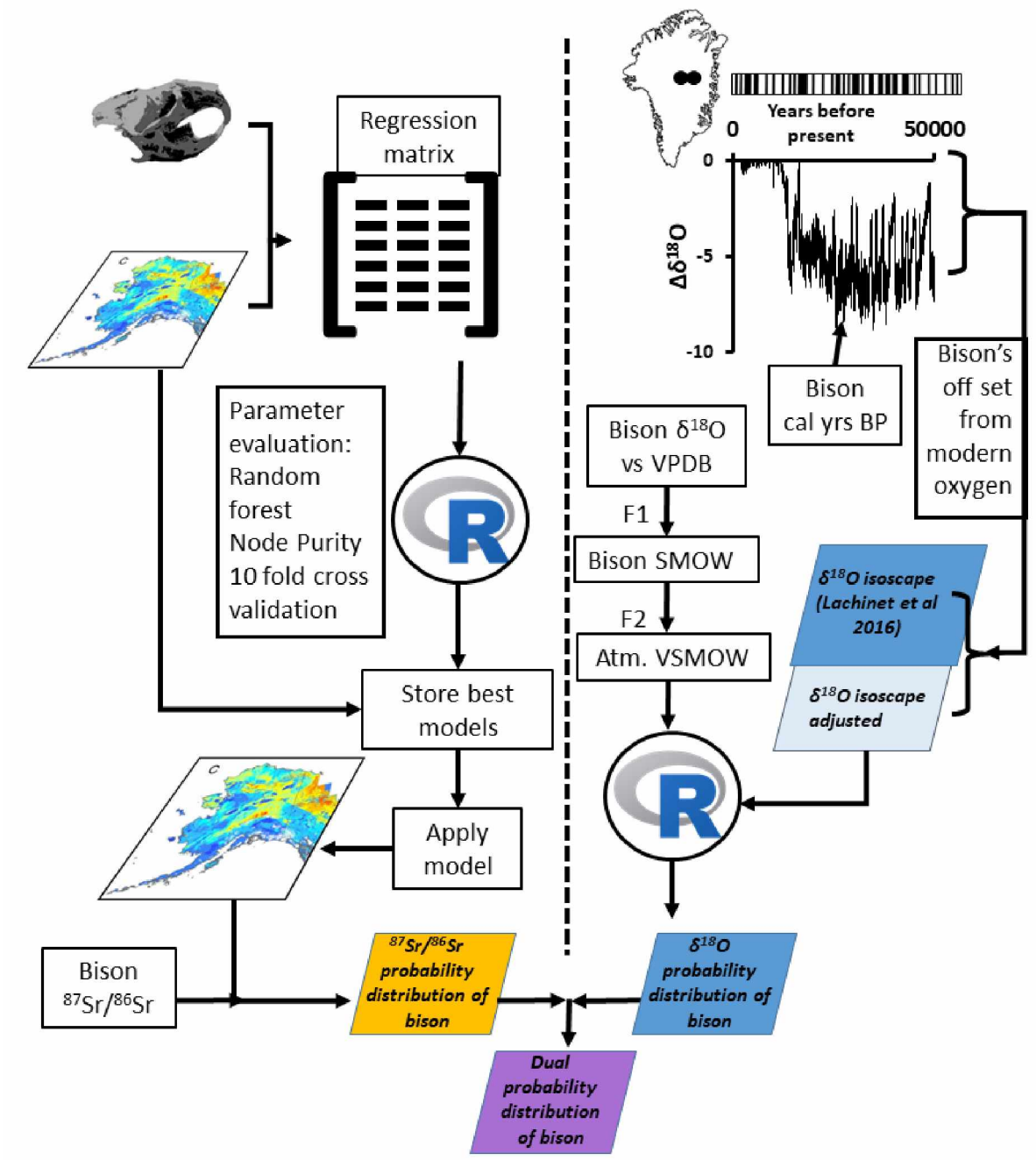

Figure 2.4 Work flow of analysis for generating a bioavailable strontium isotope model and adjusted stable oxygen isotope model for strontium and oxygen isotope probability distribution of provenance.

2.3.5.1 Modeling bioavailable $\delta^{18}O$ values for steppe bison:

The $\delta^{18}O$ and $\delta^{13}C$ values of steppe bison were initially determined relative to VPDB, but the $\delta^{18}O$ values were subsequently converted to the Vienna Standard Mean Ocean Water (VSMOW) scale to allow the

comparison with water $\delta^{18}O$ isoscape. We converted the $\delta^{18}O$ values to VSMOW using equation 1 (Verkouteren and Klinedinst, 2004) and then equation 2, which is a conversion developed by Hoppe et al (2006) and Velivetskaya et al (2016) to compare bison enamel to meteoric water $\delta^{18}O$ values:

$$\delta^{18}O\ VSMOW_{carb} = 30.92+1.03092^{*}\ \delta^{18}O\ VPDB_{carb} \qquad (Eq.1)$$

$$\delta^{18}O\ VSMOW_{water} = 0.7(\pm0.12)^{*}\ \delta^{18}O\ VSMOW_{carb} - 30.06(\pm1.40) \qquad (Eq.2)$$

The present-day $\delta^{18}O$ isoscape for surface water (Lachniet et al., 2016) cannot be directly used for provenance applications of steppe bisons because of the different climate and ice volume during the Late Pleistocene when steppe bison were in existence (129,000 to 11,700 cal yrs Before Present). In order to estimate the difference in the isoscape at the time when our steppe bison samples lived we used the long climatic $\delta^{18}O$ record contained in the Greenland ice-cores, as an indicator of global $\delta^{18}O$ value at the time when each steppe bison sample was alive. However; we first had to determine if the $\delta^{18}O$ values from the Greenland ice-cores (Rasmussen et al., 2014) are appropriate for adjusting eastern Beringian $\delta^{18}O$ isoscape models. To do this we used local (Alaska) records that cover the Younger Dryas (YD; 12,800 to 11,500 cal yrs Before Present) as a fixed point of comparison to the Greenland ice core record. The two local records based on analyses of ice wedges and willows (Gaglioti et al., 2017; Meyer et al., 2010) from the North Slope had similar $\Delta\ \delta^{18}O$ offsets of -6‰ between present and the peak of the YD, which was equivalent to the $\Delta\ \delta^{18}O$ offsets in the Greenland ice-cores record. Because the offset for the YD in these records are the same, we proceeded to use the Greenland ice-core record to extend back past the range of the local records to estimate the contemporaneous $\delta^{18}O$ values for each of our steppe bison samples.

The mean annual meteoric $\delta^{18}O$ value from the most recent (modern) layers of the Greenland ice-cores ($\delta^{18}O$ = -35‰) was subtracted from the annual $\delta^{18}O$ value from the whole record to calculate the global atmospheric offset of $\delta^{18}O$ ($\Delta\ \delta^{18}O$). We then identified the offset value ($\Delta\ \delta^{18}O$) at the date of each bison specimen, we averaged the $\Delta\ \delta^{18}O$ range of values represented within the 2 standard deviation

associated with the calibration range for the radiocarbon dates associated with each bison specimen (Figure 5, Table 1). We also conducted a series of sensitivity analysis tests using no adjustment and adjustment $\delta^{18}O$ values at the temporally closest maximum peak in $\delta^{18}O$ values as recorded in the Greenland ice-core record (Figure 5), to determine the strength of effects associated with modified $\delta^{18}O$ isoscapes. Sensitivity tests are essential in this step because of the uncertainties involved in the assumptions made using past $\delta^{18}O$ isoscapes. The distribution of $\delta^{18}O$ values is determined by atmospheric circulation and distance from shorelines (Gat and Gonfiantini, 1981). Lower sea levels, and ice sheets would naturally alter these factors in the past.

Table 2.1 Summary isotope results from five steppe bison from the North Slope of Alaska.

UAMES	cal yr BP	Tooth	$^{87}Sr/^{86}Sr$ Average	$^{87}Sr/^{86}Sr$ SD	$\delta^{18}O$ VPDB Mean	$\delta^{18}O$ SD of tooth	$\delta^{18}O$ SMOW	$\delta^{18}O$ SMOW atm.	$\delta^{18}O$ adj. factor
9885	14,215	M1	0.71106		-15.3	0.2	15.2	-19.4	
		M2	0.71107		-14.4	0.2	16.1	-18.8	
		M3	0.710897	0.00041	-16.1	0.1	14.3	-20.1	-1.6
11332	34,880	M1	0.71086		-19.0	0.1	11.3	-22.1	
		M2	0.71105	0.00033	-17.6	0.1	12.7	-21.1	-4.7
32676	42,215	M1	0.71168		-18.4	0.1	12.0	-21.7	
		M2	0.71093	0.00092	-16.9	0.1	13.5	-20.6	-5.3
32669	42,440	M1	0.71027		-17.0	0.1	13.4	-20.7	
		M2	0.71037	0.00028	-16.8	0.2	13.6	-20.5	-4.6
10679	44,930	M1	0.71197		-18.1	0.1	12.2	-21.5	
		M2	0.71128		-17.3	0.2	13.1	-20.9	
		M3	0.71111	0.00112	-18.1	0.02	12.2	-21.5	-4.5
Mean			0.71105	0.00061	-17.1	0.1	13.3	-20.7	-4.2

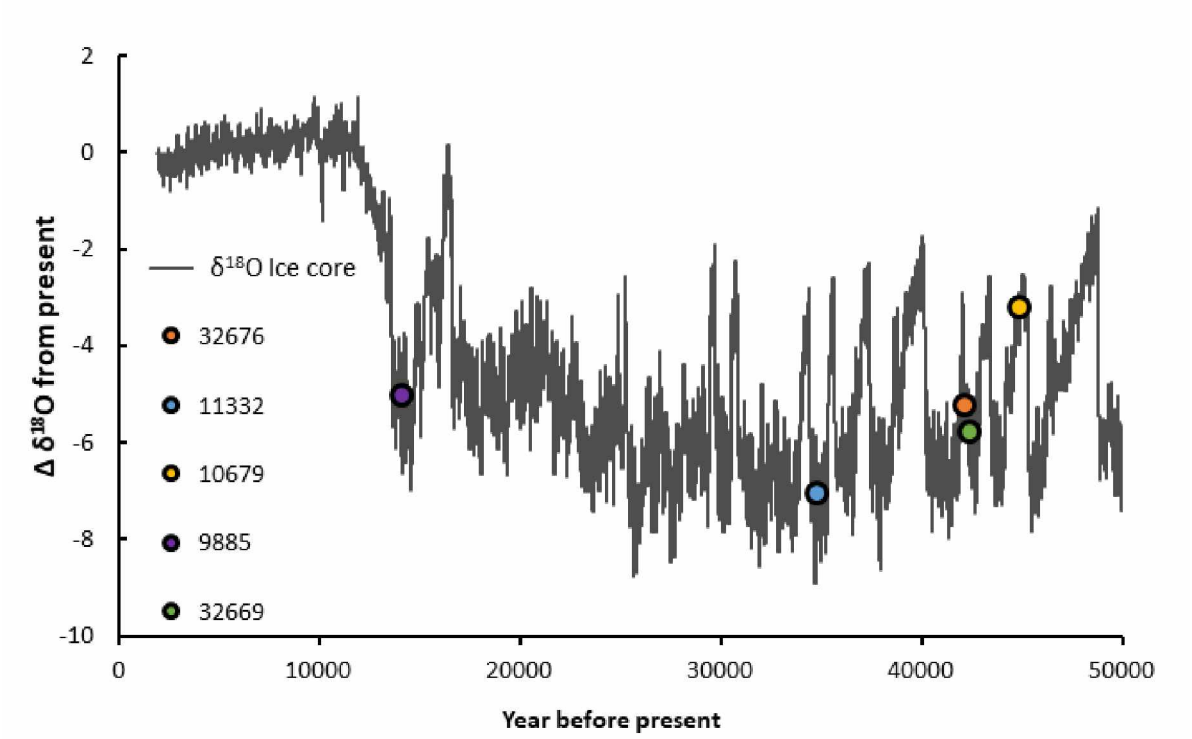

Figure 2.5 Steppe bison 14C dates plotted on the δ18O values recorded in the Greenland Ice cores (Rasmussen et al., 2014) adjusted by -35‰ to represent the difference between present values and ancient values (Δ from present).

2.3.5.4 Modeling bioavailable $^{87}Sr/^{86}Sr$ values:

Our modeling approach was previously described in details by Bataille et al. (2018). Briefly, we used the $^{87}Sr/^{86}Sr$ values of rodent teeth as a response variable to calibrate a multivariate regression model (Figure 4). Using the location of the collection site for each rodent tooth, we extracted the environmental, climatological and geological conditions from open-access auxiliary rasters (Table 2). We selected auxiliary variables that were likely to influence the bioavailable $^{87}Sr/^{86}Sr$ distribution as in Bataille et al. (2018). The only major difference of our approach compared with that employed by Bataille et al. (2018) is that we used as covariate the previously constructed $^{87}Sr/^{86}Sr$ isoscape for bedrock geology across Alaska (Bataille et al., 2014). Once the regression matrix was compiled, we used the VSURF algorithm to select the most appropriate predictors of $^{87}Sr/^{86}Sr$ variations and avoid redundancy between covariates. Once predictors were selected, a multivariate random forest regression was applied and validated using a n-fold cross-validation. The resulting model was used in combination with selected predictors to predict

the mean and interquartile range of $^{87}Sr/^{86}Sr$ variations across Eastern Beringia. We have assumed a large degree of geological and hyrdrological stability in the bioavalible $^{87}Sr/^{86}Sr$ over time.

Table 2.2 All rasters included in the strontium isoscape model.

Variables	Description	Transf.	Res.	Type	Source
r.xx	GLiM 1st lithological class attribute		1km	D	(Hartmann and Moosdorf, 2012)
r.litho	GLiM 2nd lithological class attribute		1km	D	(Hartmann and Moosdorf, 2012)
r.maxage_geol.t	GLiM age attribute	Log	1km	D	(Hartmann and Moosdorf, 2012)
r.minage_geol.t	GLiM age attribute	Log	1km	D	(Hartmann and Moosdorf, 2012)
r.meanage_geol.t	GLiM age attribute	Log	1km	D	(Hartmann and Moosdorf, 2012)
r.age	Terrane age attribute		1km	D	(Mooney et al., 1998)
r.salt.t	CCSM.3 simulation	Log	1.4°	C	(Mahowald et al., 2006)
r.dust.t	Multi-models average	Log	1°	C	(Mahowald et al., 2006)
r.elevation	SRTM		90m	C	(Jarvis et al., 2008)
r.cec	Cation Exchange Capacity		250m	C	(Hengl et al., 2017)
r.ph	Soil pH in H2O solution		250m	C	(Hengl et al., 2017)
r.phkcl	Soil pH in KCl solution		250m	C	(Hengl et al., 2017)
r.clay	Clay (weight %)		250m	C	(Hengl et al., 2017)
r.silt	Silt (weight %)		250m	C	(Hengl et al., 2017)
r.sand	Sand (weight %)		250m	C	(Hengl et al., 2017)
r.orc	Soil organic carbon (weight %)		250m	C	(Hengl et al., 2017)
r.bulk	Bulk density (kg m−3)		250m	C	(Hengl et al., 2017)
r.bouguer	WGM2012_Bouguer		2min	C	(Balmino et al., 2012)
r.soilthickness	Global soil thickness		1km	C	(Pelletier et al., 2015)
r.map.t	Mean annual precipitation (mm.yr-1)	Log	30-arc sec	C	(Hijmans et al., 2005)
r.pet	Global Potential Evapo-Transpiration		30-arc sec	C	(Zomer et al., 2008)
r.ai	Global Aridity Index		30-arc sec	C	(Zomer et al., 2008)
r.lc	Global Land Cover 2009		300m	D	(Arino et al., 2012)

2.5.4. Probability geographic assignments for steppe bison:

We compared the observed isotopic values in step bison tooth with that of the constructed isoscapes for Alaska. Assignment was based on the average of each tooth's $^{87}Sr/^{86}Sr$ and bulk $\delta^{18}O$ values for the tooth. We used a continuous-surface assignment framework to estimate the most likely developmental origins of each tooth (z^*). This required comparing observed $\delta^{18}O$ or $^{87}Sr/^{86}Sr$ values (x^*) with those predicted by spatially-explicit models. z^* was determined by evaluating the likelihood at each cell (c) of the isoscape knowing the mean over the entire study area (μ_c) and the standard deviation (σ) of values from the same locality:

$$z^* = \frac{x^* - \mu_C}{\sigma} \qquad \text{(Eq. 3)}$$

The probability that any given cell represents a potential origin for a feather [$f(z^*|c)$] was then evaluated using a normal probability density function:

$$f(z^* \mid c) = \left(\frac{1}{\sqrt{2\pi}}\right) \exp\left[-\frac{z^{*2}}{2}\right] \qquad \text{(Eq. 4)}$$

This equation is valid when using a single isotope system for assignment. Under the assumption of independence between the two variables, the combined probability density for both $\delta^{18}O$ and $^{87}Sr/^{86}Sr$ isotopes is:

$$f(z_O^*, z_{Sr}^* | c) = \left(\frac{1}{\sqrt{2\pi}}\right) exp\left[-\frac{z_O^{*2} + z_{Sr}^{*2}}{2}\right] \qquad \text{(Eq. 5)}$$

Where z^*_O and z^*_{Sr} are the observed values for each tooth. This joint function is the product of the marginal functions of each isotope system, and yields high likelihood estimates when both marginal probability densities are also high.

2.4 Results:

2.4.1 Descriptive statistics of rodents:

The mean $^{87}Sr/^{86}Sr$ values among the n =162 rodents were 0.71172 ± 1SD = 0.0043 with a range of 0.70492 to 0.73519. $^{87}Sr/^{86}Sr$ values of the rodents have a positively skewed distribution.

At the five localities where multiple rodent samples were taken (n = 4 or n = 5) the population range varied depending on location. The lowest $^{87}Sr/^{86}Sr$ range was at the Colville River (range = 0.000873), and at the highest range was the Toolik Lake Research Station (range = 0.00825), which was much higher than the other sites measured (Figure 6).

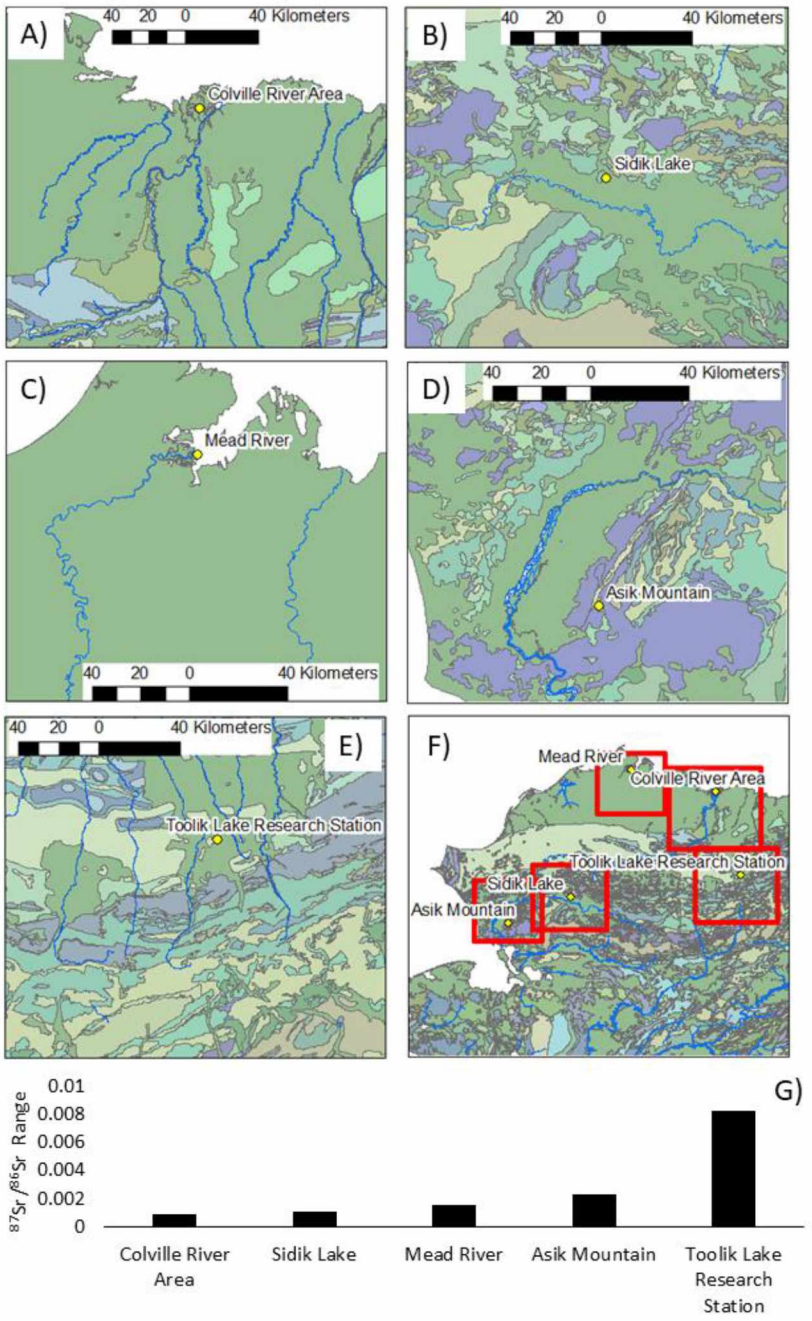

Figure 2.6 Geological map of rodent population samples at A) Colville River Area, B) Sidik Lake, C) Mead River, D)Asik Mountain and E) Toolik Lake Research Station. F) Location of regional maps A-E in Alaska G) Depicts the range of 87Sr/86Sr values found within ea

2.4.2. Steppe bison:

All collagen samples of the bison passed a quality control evaluation of their composition (%C, %N, and C:N; (Van Klinken, 1999). Five out of the nine dated fossils produced finite radiocarbon dates ranging from 14,200 ± 30 to 44,930 ±210 cal yr BP that were included in this study (Table 3).

*Table 2.3 Radiocarbon dates for five steppe bison from the North Slope of Alaska. *calibrated using Calib (Stuiver et al., 2019)*

UAMES	*Latitude*	*Longitude*	*^{14}C age, years BP*	±	*Median Age cal**	*Conc N(%)*	*Conc C(%)*	*C/N*	*$\delta^{15}N$ At-air (‰)*	*$\delta^{13}C$ VPDB (‰)*
9885	69.46667	-154.917	12,300	30	14,215	17.9	47.9	3.1	3.3	-20.1
11332	69.35215	-154.668	31,000	100	34,880	8.4	22.1	3.1	6.2	-20.3
32676	69.6725	-154.834	37,970	160	42,220	16.4	44.4	3.2	4.3	-20.3
32669	69.71355	-154.878	38,340	160	42,440	15.5	42.5	3.2	3.7	-20.1
10679	69.34347	-154.643	41,480	210	44,930	15.5	42.0	3.2	4.0	-20.3
10909	69.71355	-154.878	46,820	350	>50,000	15.8	42.4	3.1	4.9	-20.8
26400	69.5833	-154.95	50,260	490	>50,000	11.4	32.0	3.3	5.3	-19.9
23488	69.58864	-154.96	52,570	650	>50,000	17.0	45.8	3.1	4.0	-20.2
								error	0.11	0.08

The $^{87}Sr/^{86}Sr$ of the steppe bison were relatively stable within each individual's molars. However, two individuals, UAMES 32676 and 10679 (42,214 ±160 cal yrs BP and 44,927 ±210 cal yrs BP respectively), showed characteristics consistent with long-distance movement and possibly migration. These two individuals had an overall range of $^{87}Sr/^{86}Sr$ values of 0.00092 and 0.00112 respectively, while the other specimens (UAMES 9885 (14,215 ±30 cal yrs BP), UAMES 11332 (34,879 ±100 cal yrs BP), and UAMES 32669 (42,440 ±160 cal yrs BP)) had less than half the range of $^{87}Sr/^{86}Sr$ values (0.00028, 0.00041, and 0.00033). However, sample UAMES 10679 (44,930 ±210 cal yrs BP) may be somewhat biased because it appears to have died at a younger age as evidenced by retention of high teeth ridges that are typically worn and diminished in older individuals (Fuller, 1959) (Figure 3B). Thus, younger adult specimens with fully developed teeth have a more complete recorded period of its life, because the enamel was not worn away. In contrast, bison UAMES 11332 had less data because it likely died as an older individual with more worn-down teeth ridges that represented a smaller period of its life. The bison

grouped into two distinct geological areas based on the $^{87}Sr/^{86}Sr$ values. One group had $^{87}Sr/^{86}Sr$ values closer to 0.7105-0.711 and the other closer to 0.7116-0.712 (Table 3).

The average $\delta^{18}O$ value among the steppe bison teeth was -17.1‰ vs. VPDB (Table 1). After conversion from bison tooth bioapatite to meteoric $\delta^{18}O$ values (as described above) the mean among all of the bison was -20.7‰, about ~1‰ less than annual precipitation $\delta^{18}O$ value for the area (Bowen, 2018).

2.4.3. Model selection and performance:

Variable importance in the bioavailable $^{87}Sr/^{86}Sr$ isoscape model was determined through the VSURF algorithm as described in Bataille et al. (2018) (Figure 7). The raster selected as predictors of bioavailable $^{87}Sr/^{86}Sr$ variations include: maximum geological age (r.max), bedrock model (Bataille et al., 2014) (r.m1), the aridity index (r.ai), soil pH (r.ph), magnetic anomaly (r.ma), and potential evapotranspiration (r.pet) (Figure 7).

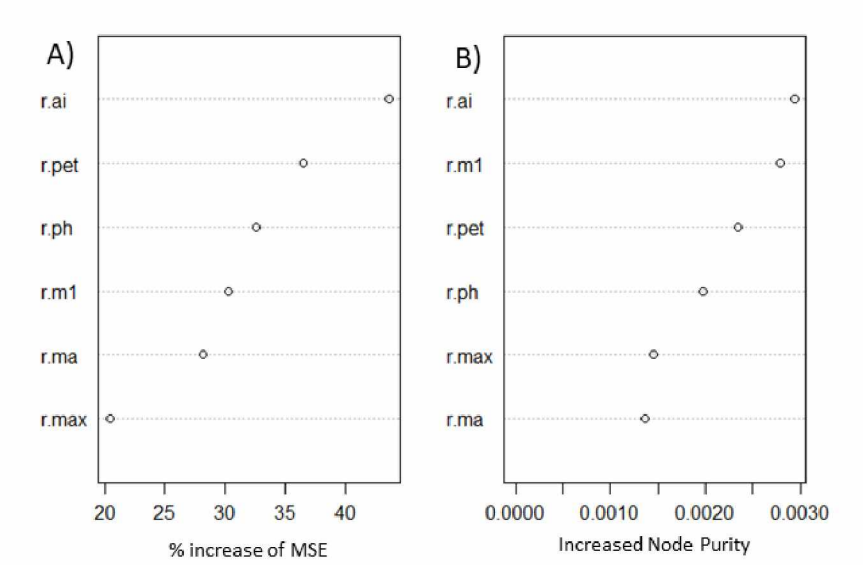

Figure 2.7 Variable importance for the best random forest model using 6 variables. r.max is maximum geological age, rm1 is the bedrock model from Bataille et al., (2014), r.ai is the aridity index (increasing as aridity decrease), r.ph (soil pH), r.ma (magnetic anomaly), r.pet (potential evapotranspiration).

The n-fold cross-validated R^2 and RMSE values were 0.62 and 0.0026, respectively (Figure 8). Residuals show an increasing trend with increasing $^{87}Sr/^{86}Sr$ values. We calculated that below 0.720 the RMSE of the model is at 0.0018 but when including higher $^{87}Sr/^{86}Sr$ values the RMSE increases largely. This trend in our residuals is logical, $^{87}Sr/^{86}Sr$ values in rocks are log-normally distributed with strong positive skewing. Consequently, $^{87}Sr/^{86}Sr$ values of older rocks to be much more variable and harder to predict (Figure 9).

The rodents $^{87}Sr/^{86}Sr$ values were also compared to those of the previous published $^{87}Sr/^{86}Sr$ isoscape (Bataille et al., 2014). We extracted the models predicted $^{87}Sr/^{86}Sr$ value for the location of each rodents to $^{87}Sr/^{86}Sr$ values measured for that rodent. The regression for the values from the older model were $R^2 = 0.21$.

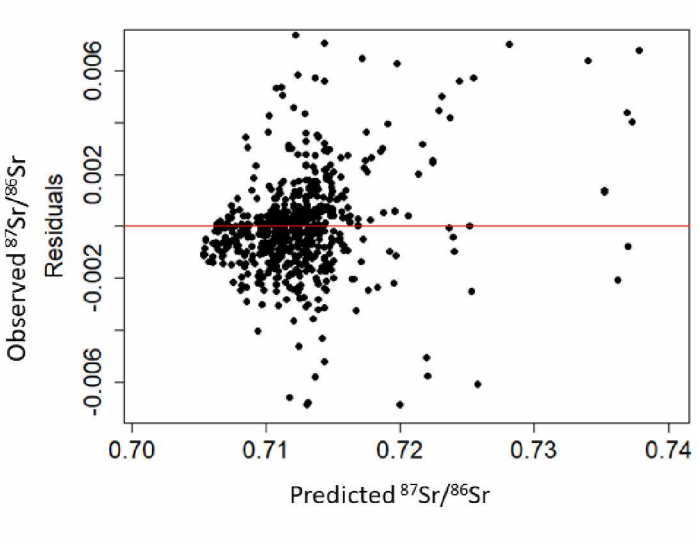

Figure 2.8 Scatterplot of observation vs. 10-fold cross-validation testing data.

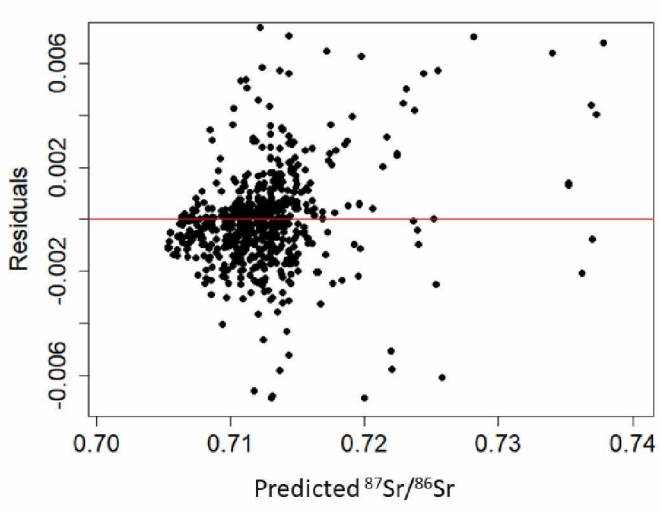

Figure 2.9 Residuals vs. predicted 87Sr/86Sr values for geolocations.

2.5 Discussion:

2.5.1 The bioavailable dataset:

Our sampling scheme helped mitigate the biggest challenge of research in Eastern Beringia, which is access. By utilizing rodents collected by other researchers over the last 65 years across a wide expanse of

Alaska we were able to thoroughly sample much of this large, remote and difficult to access region, whereas prior studies had largely been restricted to areas adjacent the limited road system, which touches on just of few of Alaska's several ecoregions in central Alaska (Brennan et al., 2014; Lachniet et al., 2016). This study substantially expanded the area and density of coverage in northern, western, and southwestern. Some geographic areas would still benefit from yet greater coverage, particularly isolated places with high heterogeneity, such as the region north of Bethel, Alaska, and the western North Slope (Figure 2). Furthermore, archeological and paleontological rodent samples could be included in future research to test the supposition that landscape $^{87}Sr/^{86}Sr$ values remain stable over time (Kootker et al., 2016). In areas with high loess deposition, for example, the primary source of bioavailable Sr could derive from non-local origins during high depositional periods (Kootker et al., 2016). While geological maps do document Quaternary surficial deposits, it is not clear if this uncertainty is adequately addressed in the current model and these variable merits more investigation.

Within-site population variance also seems to be the most potentially confounding factor for modeling the $^{87}Sr/^{86}Sr$ isoscape. Most of the populations from which multiple rodent samples were collected have acceptable levels of variation associated with them. However, Toolik Lake Research Station had relatively high levels of site specific $^{87}Sr/^{86}Sr$ variability (Figure 6G). Variability in the five site-specific sample populations (Figure 6F) seems to be driven by landscape heterogeneity and erosional forces. The Asik Mountain population had the second-highest range of variability and is in a heterogeneous geological environment with high energy erosion due to elevation and grade (Figure 6D). As a result, patches of the geologically unique substrate are likely available in close proximity to one another. The Toolik Lake Research Station location had similar properties with highly diverse geology particularly upstream from the site in the Brooks Range and high energy erosional process from the fast-moving streams in the area traveling short distances (Figure 6E). This may be compounded by the fact that research at Toolik extends over a broad area and may for convenience have reported all the rodent specimens to have come from that specific research station, while in fact they may have been from a broader area and had simply been assigned to the Toolik research station coordinates. In contrast, the

Colville River Delta (Figure 6A), the Meade River (Figure 6C), and Sidik Lake (Figure 6B) had the smallest ranges of variability, likely because they have a homogenized source mineral over the course of their drainages on relatively uniform geology (Figure 6A). The error associated with these five populations ranged can be attributed to the issues surrounding the modeling of bioavailable $^{87}Sr/^{86}Sr$ discussed earlier, including slope (Bataille et al., 2014), hydrology (Brennan et al., 2014), and sea spray (Rich et al., 2012). The small sample size of a population also makes it difficult to rule out some element of sampling bias.

As larger animals, such as caribou and bison, travel through these more heterogenous areas they will tend to average out the variability, so an estimated average should be compatible with modeling techniques. However, in the future, it would be useful to include animals that have a larger local range that should be considered for bio-available $^{87}Sr/^{86}Sr$ analyses. It has also been suggested that selecting local carnivores that collect an average of the local bioavailable $^{87}Sr/^{86}Sr$ might be a more effective comparison to migratory animals (Crowley et al., 2015).

2.5.2 A bioavailable $^{87}Sr/^{86}Sr$ isoscape for Eastern Beringia:

Our bioavailable $^{87}Sr/^{86}Sr$ isoscape across Eastern Beringia (Figure 10) performs well for our test data sets, explaining $R^2 = 0.62$ of the data. While still imperfect, it is an improvement from previous models that did not include biological samples and were geared towards aquatic systems (Bataille et al., 2014). Previous studies of variability in $^{87}Sr/^{86}Sr$ values across Alaska focused primarily on water samples, our focus on the terrestrial realm here improves estimates from $R^2 = 0.21$ for terrestrial bioavailable $^{87}Sr/^{86}Sr$ values making it more applicable for archeological, paleoecological, and wildlife studies. The diversity of geology in Eastern Beringia, and thus the documented total range of 0.04 $^{87}Sr/^{86}Sr$ values is large enough to tolerate moderate to high error associated with $^{87}Sr/^{86}Sr$ values and still be an effective tool of predicting probable provenance. We found that most residuals were below 0.0026, (Figure 9), which is less than 10% of the total range of $^{87}Sr/^{86}Sr$ values for the region. Not only does the region have a high degree of variability, they distinguish biologically and archeological meaningful units. For example The

Western Arctic Caribou Herd, which undergo a migration from the Seward Peninsula over the Brooks Range Mountains onto the North Slope of Alaska (Joly et al., 2019), travel through distinct $^{87}Sr/^{86}Sr$ ranges in each of those areas. These types of movements can now be examined with more accuracy in paleoecological specimens and used to augment biological models such as (Baltensperger and Joly, 2019). Furthermore, major cultural zones of the Yukon-Kuskokwim Delta, the Interior and Arctic Alaska have very distinct signals $^{87}Sr/^{86}Sr$ that could be meaningful for understanding trade connection in cultural and archeological materials (Potter et al., 2017, 2013).

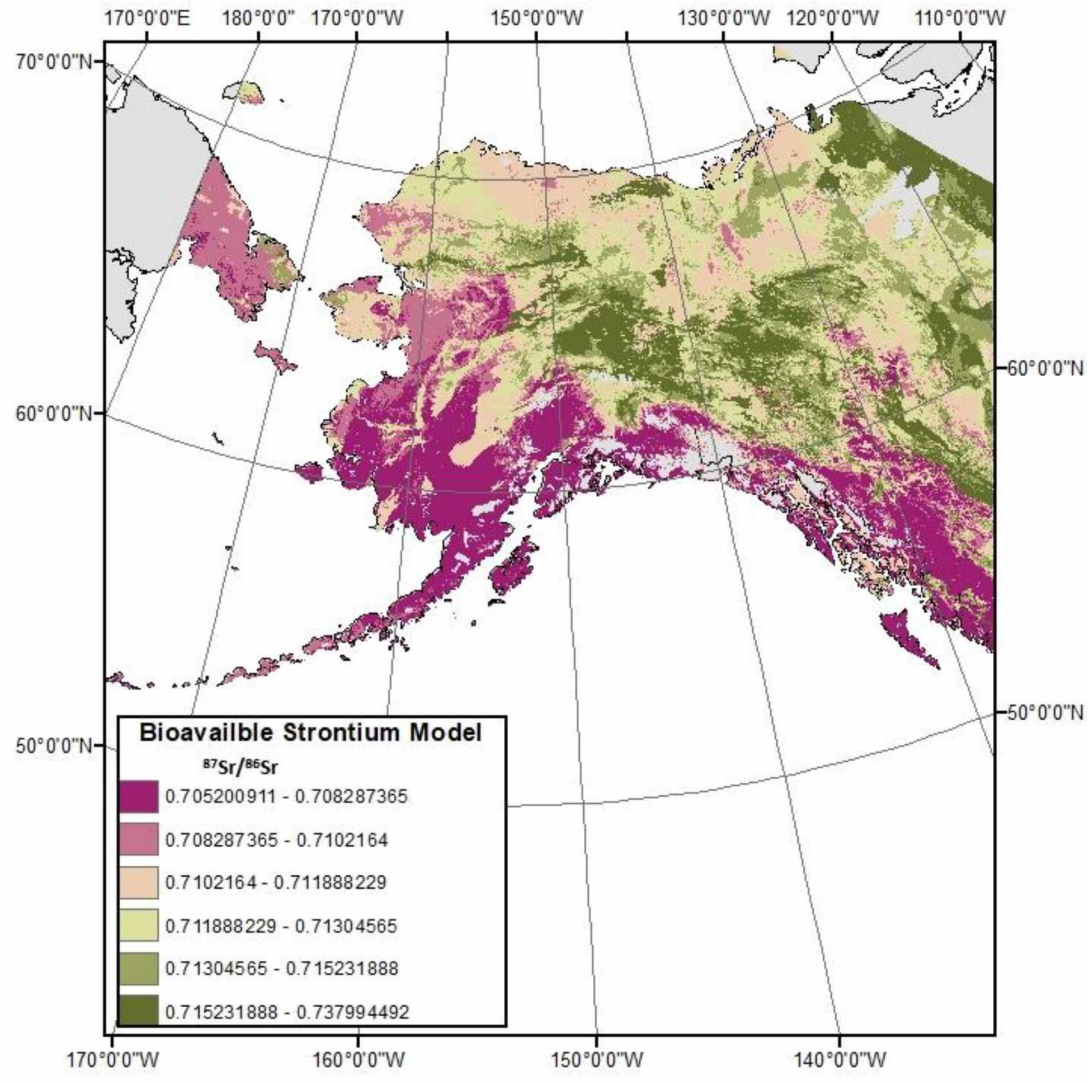

Figure 2.10 Model of bioavailable 87Sr/86Sr variation in Alaska.

The non-linear relationships between the target and predictor variables highlight the importance of machine learning over linear equations. Linear equations cannot capture the complexity of these systems (Figure 11). The bedrock model published Bataille et al. (2014) has a strong predictive capability, which demonstrates the strong link between bedrock and bioavailable $^{87}Sr/^{86}Sr$ (Figure 11C). However, for $^{87}Sr/^{86}Sr$ superior to ~0.74 (Figure 11C), the bedrock model is not able to predict bioavailable $^{87}Sr/^{86}Sr$. As expected, the maximum rock unit age (Figure 11A) has an exponential relationship with bioavailable $^{87}Sr/^{86}Sr$ before 1000 million years ago (mya). However, for every old rock units, age is not a strong predictor of $^{87}Sr/^{86}Sr$. This is probably due to the lack of accuracy of geological map where ages of older rock units are generally broadly classified as Precambrian. The magnetic anomalies can indicate differences in the underlying geology that are often mafic intrusions and volcanic fields in Alaska, which explains why these younger rocks would have lower $^{87}Sr/^{86}Sr$ values and a strong inverse linear relationship (Figure 11F; (Drake et al., 1963; Himmelberg and Loney, 1995). The aridity index and potential evapotranspiration (PET) (Figure 10B and 10E) have similar relationships with $^{87}Sr/^{86}Sr$ values with opposite patterns, areas that are more arid and areas that had more evaporation were strong predictors of $^{87}Sr/^{86}Sr$. In drier environments, there are likely to be more radiogenic aerosol dust in the regions that could influence the bioavailable $^{87}Sr/^{86}Sr$ values (Reynolds et al., 2012). Bioavailable $^{87}Sr/^{86}Sr$ also appear to increase with increasing pH. The main reason for this trend is that highly acidic soils correspond to areas with more volcanic ash, which as mentioned above have lower $^{87}Sr/^{86}Sr$ values.

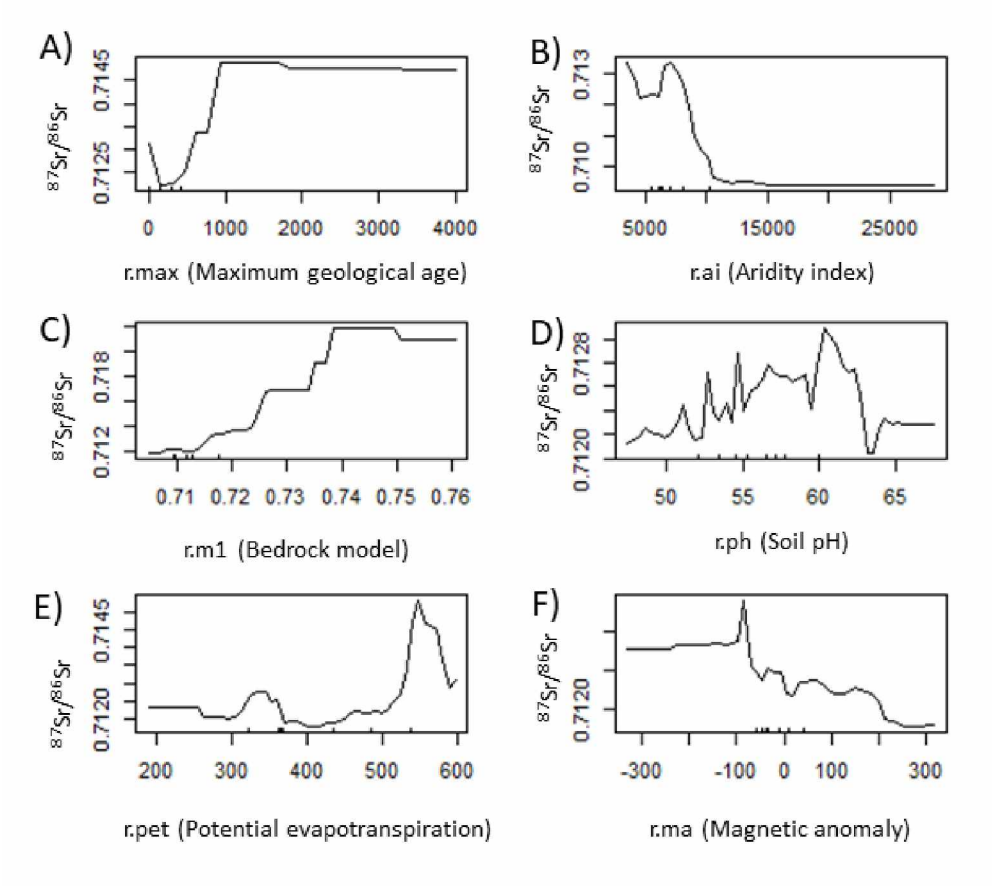

Figure 2.11 Partial plots for each predictor showing the relation between target variables and predictors.

2.5.3 Pleistocene steppe bison:

Our bioavailable $^{87}Sr/^{86}Sr$ isoscape can be used for a wide variety of applications. Here, we used serial sampling of Pleistocene steppe bison teeth as a case study to illustrate how landscape use and geolocation of paleo-fauna can be modelled by employing our $^{87}Sr/^{86}Sr$ isoscape coupled to an adjusted $\delta^{18}O$ isoscape. The steppe bison with finite radiocarbon dates for this case study were from before and after the Last Glacial Maximum (LGM) 28-19,000 yrs BP (Clark et al., 2009) (Table 1 and Figure 5). The assignment of bison tissues based on the bioavailable $^{87}Sr/^{86}Sr$ isoscape (Figure 10) without the $\delta^{18}O$ isoscape demonstrates two consistent patterns of landscape use (Figure 12). Two of the three oldest specimens, UAMES 32676 and UAMES 10679 (44,930 ±160 cal yrs BP and 42,210 ±210 cal yrs BP), showed

relatively high degrees of variability in their $^{87}Sr/^{86}Sr$ values over the serial sets of samples analyzed from their teeth (Supplemental Figure S1 and Table 1). This indicates they moved across a landscape with relatively diverse $^{87}Sr/^{86}Sr$ values (and geology) during the early period (~2.5 years) of their lives as represented by the specimens' molars. For these two individuals, the first molar (M1) were both assigned to the western end of the North Slope based on their $^{87}Sr/^{86}Sr$ values (Figure 12). The M1 tooth develops over approximately the first 3 months of life (Gadbury et al., 2000), and thus represents the calving grounds and summer range. In both individuals, the M2 $^{87}Sr/^{86}Sr$ values assigned them to the eastern end of the North Slope. The M2 develops over 2-14 months (Gadbury et al., 2000) and would represent mostly a winter season of habitation. The M3, which develops from 10-24 months, of specimen UAMES 32676 (44,930 ±160 cal yrs BP) showed a potential return to the same area of the M1 marking a potential full migratory cycle. The other three individuals who had a smaller range of $^{87}Sr/^{86}Sr$ values, UAMES 11332, UAMES 9885 and UAMES 32669 (34,890 ±100 cal yrs BP, 14,215 ±30 cal yrs BP, and 42,440 ±160 cal yrs BP) (Table 1 and Supplementary Figures S1), appeared, based on their $^{87}Sr/^{86}Sr$ values, to be consistently assigned to the eastern end of the North Slope area through the ~2 years represented by their period of tooth development. These bison showed a stability in their provenance from an area of the eastern end of the North Slope (Figure 12), similar to the current extent of the contemporary Central Arctic Herd of caribou (Nicholson et al., 2016). The fossil bison specimens were all found within an area of high probability of assignment based on their tooth $^{87}Sr/^{86}Sr$ values. This may indicate that they had a consistent home range and possibly an enduring pattern of habitat use.

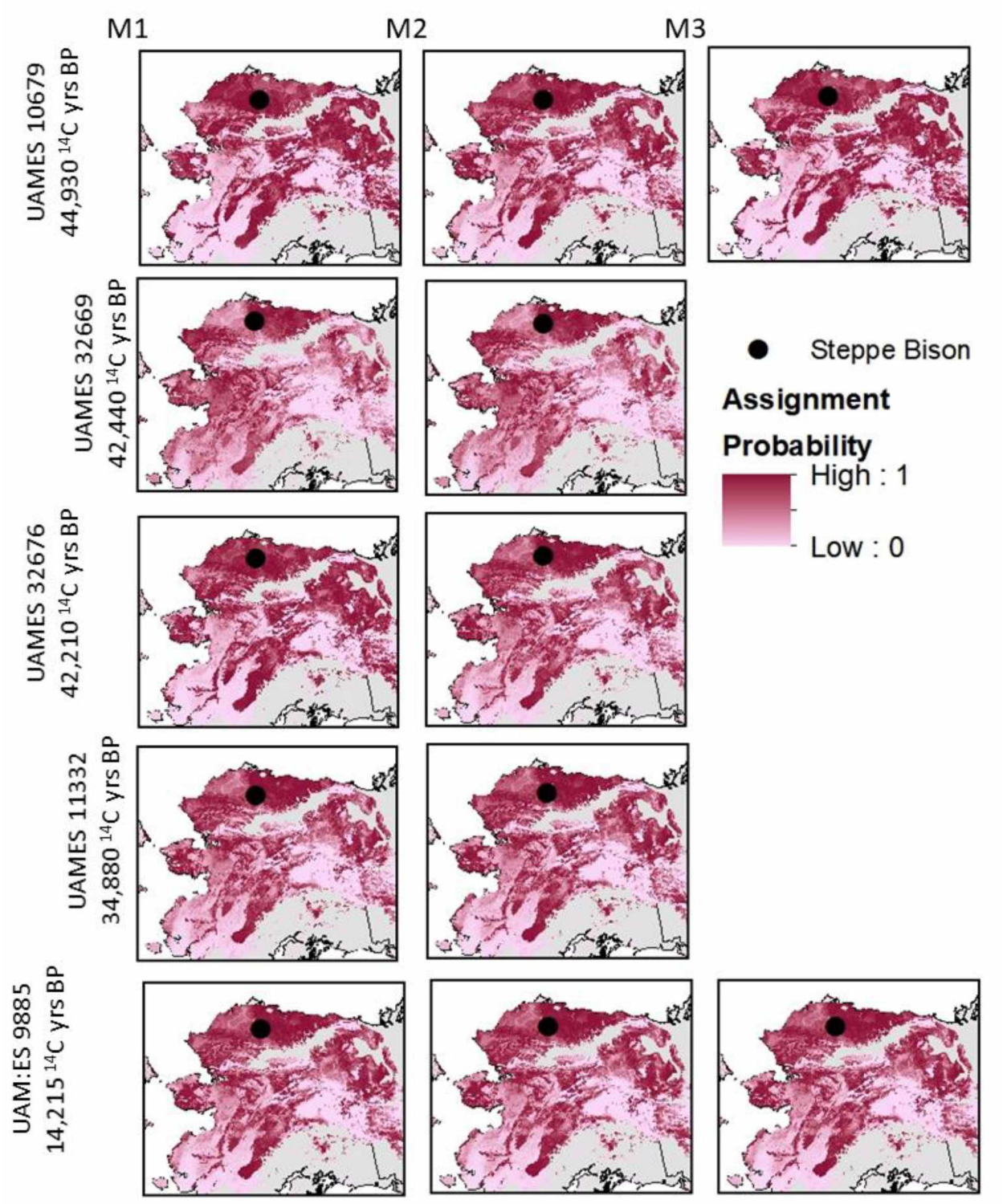

Figure 2.12 Assignment of bison molar 1 (M1), molar 2 (M2) and molar 3 (M3), with probability assignment based on model of bioavailable strontium isotope.

When a dual probability assignment using both the bioavailable $^{87}Sr/^{86}Sr$ isoscape and the $\delta^{18}O$ isoscape was added to the geolocation approach, a number of alternative inferences can be made about the paleomobility of the five steppe bison specimens with finite radiocarbon ages. For all the specimens the highest probabilities for a geolocation based on a dual $^{87}Sr/^{86}Sr$ and $\delta^{18}O$ isotope model is the Yukon-Kuskokwim region (Figure 13) and this is consistent with time spent in interior Alaska. Although the model is not able to rule out areas currently below sea level on the continental shelf of Beringia it does appear from the $\delta^{18}O$ isotope assignment that early in their lives the bison inhabited a different region than the one they would later die within north of the Brooks Range (Figure 13). In all of these cases, regardless of the magnitude of the $^{87}Sr/^{86}Sr$ variability displayed within their teeth, the distance between the bison's' modeled time spent in interior Alaska during their early life history and their death location on the North Slope of Alaska indicates a significant degree of dispersal during their later life. It is impossible to say whether this reflects development of a seasonal migratory pattern later life or a single episode of dispersal. As a whole these data imply that steppe bison may have employed varying degrees of paleomobility in Eastern Beringia over thousands of years, which is consistent with previous findings from ancient steppe bison (*Bison priscus*) and modern bison (*Bison bison*) previously analyzed from interior Alaska (Glassburn et al., 2015).

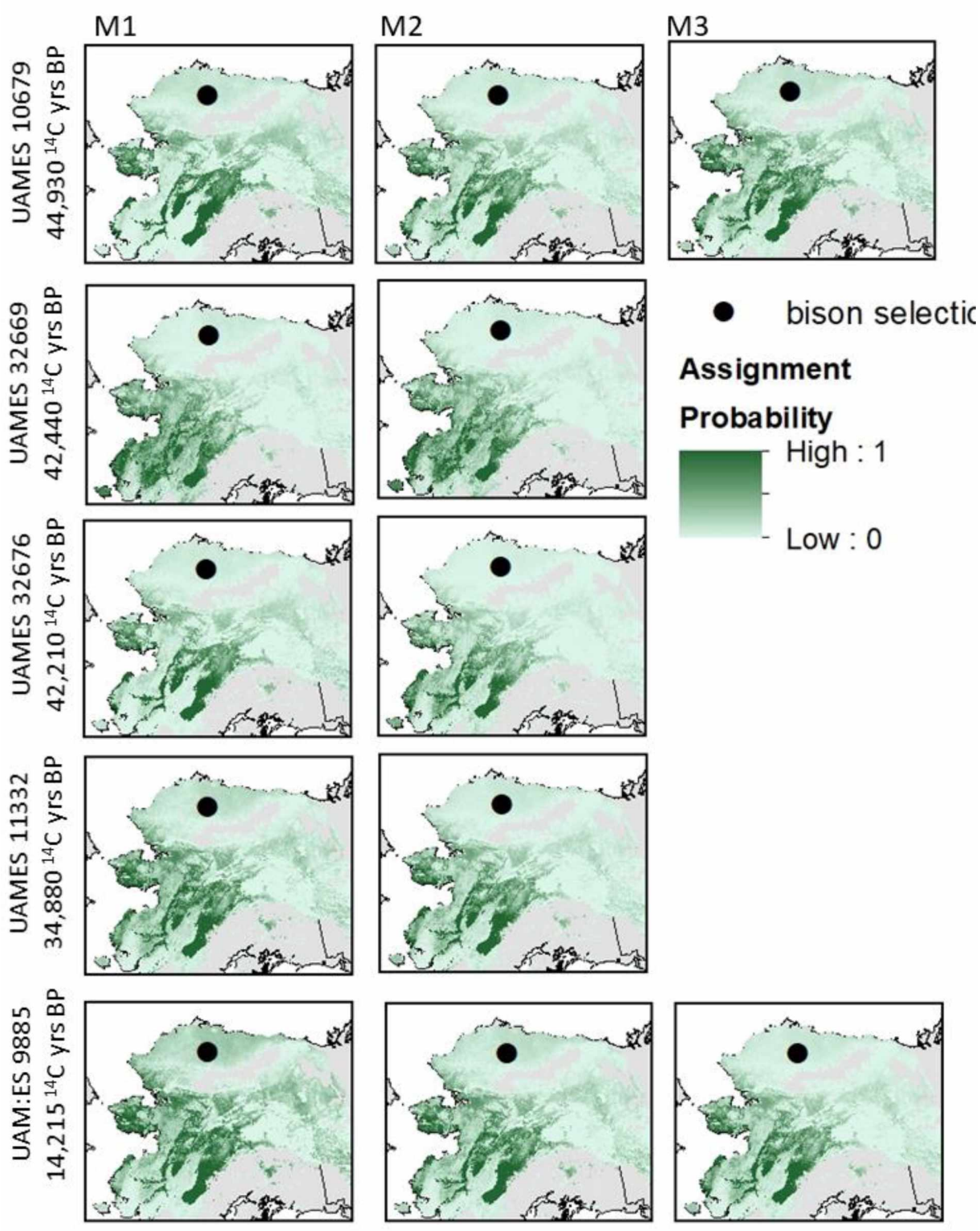

Figure 2.13 Assignment of bison molar 1 (M1), molar 2 (M2) and molar 3 (M3), with probability assignment based on dual models of bioavailable strontium isoscape and oxygen isoscape (Lachniet et al., 2016) adjusted by Δ δ18O offset of date range (Figure 11, Table 2)

Although little is known about the migration patterns of steppe bison in Alaska, we can compare the total ranges of $^{87}Sr/^{86}Sr$ values found to those found in other studies (Glassburn et al., 2018; Julien et al., 2012). The $^{87}Sr/^{86}Sr$ ranges of the two most mobile individuals—UAMES 32676 (0.00092, 44,930 ±210 cal yrs BP) and UAMES 10679 (0.00112, 42,210 ±160 cal yrs BP) (Table 1)—are similar to that of plains bison (*Bison bison bison*) in present day interior Alaska (Glassburn et al., 2018). These contemporary bison are known to conduct an annual migration of ~250 km from the highlands south of Delta, Alaska in the summer to river bottom settings along the Tanana and Delta Rivers in the winter (Glassburn et al., 2018). This migration pattern is typical of recorded yearly movement patterns of bison in other regions (Plumb et al., 2009). The three seemingly less mobile steppe bison individuals with lower $^{87}Sr/^{86}Sr$ ranges: UAMES 9885 = 0.00041, UAMES 11332 = 0.00033, and UAMES 32669 = 0.0028 (14,215 ±30 cal yrs BP, 34,890 ±100 cal yrs BP, 42,440 ±160 cal yrs BP respectively) are more similar to the low ranges of $^{87}Sr/^{86}Sr$ values from LGM steppe bison (*Bison priscus*) found near the Black Sea (Julien et al., 2012). These ancient Black Sea bison had $^{87}Sr/^{86}Sr$ values that matched the local geology and were believed to be non-migratory. It seems from our analysis that these five steppe bison that eventually died on the North Slope of Alaska utilized both migratory and non-migratory behaviors based on their total range of $^{87}Sr/^{86}Sr$ values.

The steppe bison we examined from the North Slope of Alaska have been assigned with high probability to interior Alaska using a dual isoscape analysis and they would have dispersed either around or over the Brooks Range to their place of death. Dispersal, described as movement without return (Stenseth et al., 1992), is a strategy that some present-day bison utilize (Gates and Larter, 1990; Larter et al., 2000; Plumb et al., 2009; Funck et al., accepted 2020). For example wood bison (*Bison bison athabascae*) recently released in Alaska in 2015 have dispersed 100s of km into their new domain (McFarland and Seaton, 2018; Funck et al., in review). One female wood bison was observed to travel ~160 km south, while a young bull was observed to travel ~300 km north and reached the Brooks Range before it died (McFarland and Seaton, 2018). Remains of a plains bison (*Bison bison*) discovered in the highlands of Northern Utah at 3840 m above sea level also illustrates that bison can travel to high altitudes (Cannon,

2007). A future, larger sample size of steppe bison from Alaska would allow us to determine if a dispersal or long-distance migration strategy was connecting interior and Arctic Alaska. Furthermore, a larger sample size would allow us to determine if paleo-mobility strategies changed over time in response to environmental change periods and sex.

The adjustment we used to adapt the $\delta^{18}O$ isoscape to the specific radiocarbon age for each steppe bison specimen was a somewhat rudimentary but reasonable approach to a complex question of how best to reconstruct a paleo $\delta^{18}O$ isoscape. However, modelling $\delta^{18}O$ values in an ancient system should ideally account for changes in sea level, glaciers and weather systems. We reported that the offset in $\delta^{18}O$ values of precipitation between present-day and those associated with YD found in the Greenland ice cores match local offsets for the YD (Gaglioti et al., 2017; Meyer et al., 2010). However, other factors may confound the $\delta^{18}O$ values of ancient bison specimens as a proxy for past precipitation. For example, lower sea levels during the Pleistocene mean the area where the bison were found would actually have been further inland, which can influence $\delta^{18}O$ values of precipitation via an increased degree of continentality (Bowen et al., 2005). Weather patterns are also likely to have been different during the Pleistocene further influencing paleo- $\delta^{18}O$ models (Gaglioti et al., 2017). $\delta^{18}O$ values are a key component of many provenance studies (Wunder, 2012), but currently are typically based on a contemporary $\delta^{18}O$ isoscape. To test the sensitivity of the $\delta^{18}O$ offset we applied, we had also conducted sensitivity tests using the present-day $\delta^{18}O$ isoscape as published by Lachniet et al., (2016). We had offset the present-day $\delta^{18}O$ isoscape using the average $\delta^{18}O$ offset for the median time period represented by the age range of each ancient steppe bison (Figure 13). We also used the offset values associated with the nearest maximum peak in $\delta^{18}O$ isotopes associated with the median age of each bison, which were Δ 0‰ for the youngest individual (UAMES 9885) and Δ -2.3‰ to -2.7‰ for the other four bison specimens (Supplementary Figure S2). The adjustment to the nearest peak (Figure 11) still indicates high probability geolocation assignment zones in interior Alaska (Figure S2). Assignments without adjusting the isoscape from modern values (Supplementary Figure S3) shifts the probabilities to include locations north of the Brooks Range. However, the present-day isoscape is a highly unlikely scenario for our ancient bison specimens

because records indicate that temperatures were colder during this period (Rasmussen et al., 2014) and would have shifted the $\delta^{18}O$ isoscape to lower $\delta^{18}O$ values (Porter et al., 2016). Some level of offset of the modern $\delta^{18}O$ isoscape seems appropriate to utilize in a dual isotope geolocation approach alongside our bioavailable $^{87}Sr/^{86}Sr$ isoscape.

2.6 Conclusions:

Our bioavailable $^{87}Sr/^{86}Sr$ isoscape performs well for most of the areas sampled. It is also an improvement over past models by providing a model more specifically for terrestrial geolocation studies and will allow for greater predictive power in terrestrial provenance studies. Our preliminary analyses from ancient bison demonstrated the model's applicability within a dual ($^{7}Sr/^{86}Sr$ and $\delta^{18}O$) isotope approach to geolocation. Our findings from these specimens, also revealed some interesting paleoecological and paleomobility inferences. The bioavailable $^{87}Sr/^{86}Sr$ model demonstrated a pattern of continued land use of the eastern end of the North Slope of Alaska, with some animals migrating to the western end of the North Slope during the summer season. The dual assignment indicated that bison may have dispersed from south of the Brooks Range to the North Slope where they died, or even migrated between the two regions. Our $^{87}Sr/^{86}Sr$ b nnnnisoscape based on bioavailable $^{87}Sr/^{86}Sr$ preserved in museum specimens of rodent across Eastern Beringia opens the potential for a wide range of future research of ancient and modern faunal and human mobility.

2.7 Acknowledgments:

The 2017 David and Rachel Hopkins Fellowship Application funded the initial pilot study of rodent $^{87}Sr/^{86}Sr$ analysis. The National Park Service (Gates of the Arctic National Park and Preserve) provided analytical funds for $^{87}Sr/^{86}Sr$ analysis of rodent samples. We thank the Alaska Stable Isotope Facility staff for their support of this study. Dr. Link Olson from the University of Alaska Museum of the North

Mammals Collection generously allowed us to sample UAMN rodent specimens. Aren Gunderson aided in the final selection of specimens and located all specimens in the University of Alaska Museum of the North Mammals Collection. University of Alaska Museum Earth Science helped selected and over saw sampling of the steppe bison specimens. Stormy Fields also aided in sampling specimens. Sample preparation and data analysis of the rodent teeth were diligently conducted by Dr. Diego Fernandez from the ICP MS Metals Laboratory at the University of Utah. Tim Howe at the Alaska Stable Isotope Facility ran conducted the $\delta^{18}O$ analysis.

2.8 References:

Arino, O., Ramos Perez, J.J., Kalogirou, V., Bontemps, S., Defourny, P., and Van Bogaert, E. 2012. Global Land Cover Map of 2009 (GlobCover 2009). Eur. Sp. Agency Univ. Cathol. Louvain. Available from https://doi.pangaea.de/10.1594/PANGAEA.787668.

Balasse, M., Ambrose, S.H., Smith, A.B., and Price, T.D. 2002. The seasonal mobility model for prehistoric herders in the south-western Cape of South Africa assessed by isotopic analysis of sheep tooth enamel. J. Archaeol. Sci. 29(9): 917–932. doi:10.1006/jasc.2001.0787.

Balmino, G., Vales, N., Bonvalot, S., and Briais, A. 2012. Spherical harmonic modelling to ultra-high degree of Bouguer and isostatic anomalies. J. Geod. 86(7): 499–520. doi:10.1007/s00190-011-0533-4.

Baltensperger, A.P., and Joly, K. 2019. Using seasonal landscape models to predict space use and migratory patterns of an arctic ungulate. Mov. Ecol. 7(1): 1–19. Movement Ecology. doi:10.1186/s40462-019-0162-8.

Banfield, A.W.., and Novakowski, N.S. 1960. The survival of the wood bison (Bison bison athabascae Rhoads) in the Northwest Territories. Queen's Printer.

Barberena, R., Tessone, A., Cagnoni, M., Gasco, A., Durán, V., Winocur, D., Benítez, A., Lucero, G., Trillas, D., Zonana, I., Novellino, P., Fernández, M., Bavio, M.A., Zubillaga, E., and Gautier, E.A. 2019. Bioavailable Strontium in the Southern Andes (Argentina and Chile): A Tool for Tracking Human and Animal Movement. Environ. Archaeol. 0(0): 1–13. Taylor & Francis. doi:10.1080/14614103.2019.1689894.

Bataille, C.P., and Bowen, G.J. 2012. Sr / 86 Sr variations in bedrock and water for large scale provenance studies. Chem. Geol. 304–305: 39–52. Elsevier B.V. doi:10.1016/j.chemgeo.2012.01.028.

Bataille, C.P., Brennan, S.R., Hartmann, J., Moosdorf, N., Wooller, M.J., and Bowen, G.J. 2014. A geostatistical framework for predicting variability in strontium concentrations and isotope ratios in Alaskan rivers. Chem. Geol. 389: 1–15. Elsevier B.V. doi:10.1016/j.chemgeo.2014.08.030.

Bataille, C.P., von Holstein, I.C.C., Laffoon, J.E., Willmes, M., Liu, X.M., and Davies, G.R. 2018. A bioavailable strontium isoscape for Western Europe: A machine learning approach. PLoS One 13(5): 1–27. doi:10.1371/journal.pone.0197386.

Bataille, C.P., Laffoon, J., and Bowen, G.J. 2012. Mapping multiple source effects on the strontium isotopic signatures of ecosystems from the circum-Caribbean region. Ecosphere 3(12): art118. doi:10.1890/es12-00155.1.

Bowen, G.J. 2018. WaterIsotopes.org.

Bowen, G.J., Wassenaar, L.I., and Hobson, K.A. 2005. Global application of stable hydrogen and oxygen isotopes to wildlife forensics. Oecologia 143(3): 337–348. doi:10.1007/s00442-004-1813-y.

Brennan, S.R., Fernandez, D.P., Mackey, G., Cerling, T.E., Bataille, C.P., Bowen, G.J., and Wooller, M.J. 2014. Strontium isotope variation and carbonate versus silicate weathering in rivers from across Alaska: Implications for provenance studies. Chem. Geol. 389: 167–181. Elsevier B.V. doi:10.1016/j.chemgeo.2014.08.018.

Brennan, S.R., Zimmerman, C.E., Fernandez, D.P., Cerling, T.E., Mcphee, M. V, and Wooller, M.J. 2015. Strontium isotopes delineate fine-scale natal origins and migration histories of Pacific salmon. (May): 1–6.

Britton, K. 2009. Reconstructing faunal migrations using intra- tooth sampling and strontium and oxygen isotope analyses : A case study of modern caribou (Rangifer tarandus granti). (August 2015). doi:10.1016/j.jas.2009.01.003.

Burns, J.A. 2010. Mammalian faunal dynamics in Late Pleistocene Alberta, Canada. Quat. Int. 217(1–2): 37–42. Elsevier Ltd and INQUA. doi:10.1016/j.quaint.2009.08.003.

Cameron, M.D., Joly, K., Breed, G.A., Parrett, L.S., and Kielland, K. 2018. Movement-based methods to infer parturition events in migratory ungulates. Can. J. Zool. 96(April): 1187–1195.

Cannon, K.P. 2001. What the past can provide: Contribution of prehistoric bison studies to modern bison management. Gt. Plains Res. 11(1): 145–174.

Cannon, K.P. 2007. "They Went as High as They Choose:" What an Isolated Skull Can Tell Us about the Biogeography of High-altitude Bison. Arctic, Antarct. Alp. Res. 39(1): 44–56. doi:10.1657/1523-0430(2007)39[44:TWAHAT]2.0.CO;2.

Capo, R.C., Stewart, B.W., and Chadwick, O.A. 1998. Strontium isotopes as tracers of ecosystem processes: theory and methods. Geoderma 82(1–3): 197-225 (pp.21). doi:10.1016/S0016-7061(97)00102-X.

Carter, L.D. 1981. A pleistocene sand sea on the alaskan arctic coastal plain. Science 211(4480): 381–3. doi:10.1126/science.211.4480.381.

Chadwick, O.A., Derry, L.A., Bern, C.R., and Vitousek, P.M. 2009. Changing sources of strontium to soils and ecosystems across the Hawaiian Islands. Chem. Geol. 267(1–2): 64–76. Elsevier B.V. doi:10.1016/j.chemgeo.2009.01.009.

Clark, P.U., Dyke, A.S., Shakun, J.D., Carlson, A.E., Clark, J., Wohlfarth, B., Mitrovica, J.X., Hostetler, S.W., and McCabe, A.M. 2009. The Last Glacial Maximum. Science (80-.). 325(5941): 710–714. doi:10.1126/science.1172873.

Crowley, B.E., Miller, J.H., and Bataille, C.P. 2015. Strontium isotopes (87 Sr/ 86 Sr) in terrestrial ecological and palaeoecological research: empirical efforts and recent advances in continental-scale models. Biol. Rev. 1: n/a-n/a. doi:10.1111/brv.12217.

Drake, C.L., Heirtzler, J., and Hirshman, J. 1963. Magnetic anomalies off eastern North America. J. Geophys. Res. 68(18): 5259. doi:10.1029/jz068i018p05259.

Dussault, C., Ouellet, J., Courtois, R., Huot, J., Jolicoeur, H., Kelt, D., and Breton, L. 2005. Linking moose habitat selection to limiting factors Linking. Ecography (Cop.). 28(5): 619–628.

Elias, S.A., Berman, D., and Alfimov, A. 2000. Late pleistocene beetle faunas of beringia: Where east met west. J. Biogeogr. 27: 1349–1363. doi:10.1046/j.1365-2699.2000.00503.x.

Elias, S.A., and Crocker, B. 2008. The Bering Land Bridge: a moisture barrier to the dispersal of steppe-tundra biota? Quat. Sci. Rev. 27: 2473–2483. Elsevier Ltd. doi:10.1016/j.quascirev.2008.09.011.

Freese, C.H., Aune, K.E., Boyd, D.P., Derr, J.N., Forrest, S.C., Cormack Gates, C., Gogan, P.J.P., Grassel, S.M., Halbert, N.D., Kunkel, K., and Redford, K.H. 2007. Second chance for the plains bison. Biol. Conserv. 136(2): 175–184. doi:10.1016/j.biocon.2006.11.019.

Froese, D., Stiller, M., Heintzman, P.D., Reyes, A. V., Zazula, G.D., Soares, A.E.R., Meyer, M., Hall, E., Jensen, B.J.L., Arnold, L.J., MacPhee, R.D.E., and Shapiro, B. 2017. Fossil and genomic evidence constrains the timing of bison arrival in North America. Proc. Natl. Acad. Sci. 114(13): 3457–3462. doi:10.1073/pnas.1620754114.

Fuller, W.A. 1959. The horns and teeth as indicators of age in bison. J. Wildl. Manage. 23(3): 342–344. doi:10.2307/3796894.

Gadbury, C., Todd, L., Jahren, A.H., and Amundson, R. 2000. Spatial and temporal variations in the isotopic composition of bison tooth enamel from the Early Holocene Hudson-Meng Bone Bed, Nebraska. Palaeogeogr. Palaeoclimatol. Palaeoecol. 157: 79–93. doi:10.1016/S0031-0182(99)00151-0.

Gaglioti, B. V., Mann, D.H., Wooller, M.J., Jones, B.M., Wiles, G.C., Groves, P., Kunz, M.L., Baughman, C.A., and Reanier, R.E. 2017. Younger-Dryas cooling and sea-ice feedbacks were prominent features of the Pleistocene-Holocene transition in Arctic Alaska. Quat. Sci. Rev. 169: 330–343. Elsevier Ltd. doi:10.1016/j.quascirev.2017.05.012.

Gat, J., and Gonfiantini, R. 1981. Stable isotope hydrology : deuterium and oxygen-18 in the water cycle. International Atomic Energy Agency (IAEA), Vienna Austria. Available from https://inis.iaea.org/search/search.aspx?orig_q=RN:13677657 [accessed 24 March 2020].

Gates, C.C., and Larter, N.C. 1990. Growth and dispersal of an erupting large herbivore population in northern Canada: the Mackenzie wood bison (Bison bison athabascae). Arctic 43(3): 231–238. Available from http://www.jstor.org/stable/40511262.

Glassburn, C.L., Potter, B.A., Clark, J.L., Reuther, J.D., Bruning, D.L., and Wooller, M.J. 2018. Strontium and Oxygen Isotope Profiles of Sequentially Sampled Modern Bison (Bison bison bison) Teeth from Interior Alaska as Proxies of Seasonal Mobility. Arctic 71(2): 185–202.

Glassburn, C.L., Potter, B.A., Clark, J.L., Reuther, J.D., Bruning, D.L., Wooller, M.J., Clark, J.L., Reuther, J.D., Bruning, D.L., and Wooller, M.J. 2015. Application of strontium and oxygen isotope analyses to sequentially-sampled modern bison (Bison bison bison) teeth from Interior Alaska as a proxy of seasonal mobility. (Masters Thesis).

Goebel, T., Waters, M.R., and Rourke, D.H.O. 2008. The Late Pleistocene Dispersal of Modern Humans in the Americas The Late Pleistocene Modern Humans Dispersal in the Americas of. Sci. New Ser. 319(5869): 1497–1502.

Graustein, W.C., and Armstrong, R.L. 2009. The Use of Strontium-87 / Strontium-86 Ratios to Measure Atmospheric Transport into Forested Watersheds. Science (80-.). 219(4582): 289–292.

Hartman, G., and Richards, M. 2014. Mapping and defining sources of variability in bioavailable strontium isotope ratios in the Eastern Mediterranean. Geochim. Cosmochim. Acta 126: 250–264. Elsevier Ltd. doi:10.1016/j.gca.2013.11.015.

Hartmann, J., and Moosdorf, N. 2012. The new global lithological map database GLiM: A representation of rock properties at the Earth surface. Geochemistry, Geophys. Geosystems 13(12): 1–37. doi:10.1029/2012GC004370.

Heintzman, P.D., Froese, D., Ives, J.W., Soares, A.E.R., Zazula, G.D., Letts, B., Andrews, T.D., Driver, J.C., Hall, E., Gregory Hare, P., Jass, C.N., Mackay, G., Southon, J.R., Stiller, M., Woywitka, R.,

Suchard, M.A., and Shapiro, B. 2016. Bison phylogeography constrains dispersal and viability of the Ice Free Corridor in western Canada. PNAS: 1–7. doi:10.1073/pnas.1601077113.

Hengl, T., De Jesus, J.M., Heuvelink, G.B.M., Gonzalez, M.R., Kilibarda, M., Blagotić, A., Shangguan, W., Wright, M.N., Geng, X., Bauer-Marschallinger, B., Guevara, M.A., Vargas, R., MacMillan, R.A., Batjes, N.H., Leenaars, J.G.B., Ribeiro, E., Wheeler, I., Mantel, S., and Kempen, B. 2017. SoilGrids250m: Global gridded soil information based on machine learning. In PLoS ONE. doi:10.1371/journal.pone.0169748.

Hijmans, R.J., Cameron, S.E., Parra, J.L., Jones, P.G., and Jarvis, A. 2005. Very high resolution interpolated climate surfaces for global land areas. Int. J. Climatol. 25(15): 1965–1978. doi:10.1002/joc.1276.

Himmelberg, G.R., and Loney, R.A. 1995. Characteristic and Petrogenesis of Alaskan-Type Ultramafic-Mafic Intrusions in Southeastern Alaska. Washington DC.

Hoppe, K. a, Koch, P.L., Carlson, R.W., and Webb, S.D. 1999. Tracking mammoths and mastodons : Reconstruction of migratory behavior using strontium isotope ratios. Geology 27(5): 439–442. doi:10.1130/0091-7613(1999)027<0439.

Hoppe, K.A. 2004. Late Pleistocene mammoth herd structure, migration patterns, and Clovis hunting strategies inferred from isotopic analyses of multiple death assemblages. Paleobiology 30(1): 129–145.

Jarvis, A.H.I., Reuter, A., Nelson, A., and Guevara, E. 2008. Hole-filled SRTM for globe Version 4, Available from the CGIAR-CSI SRTM 90m Database. CGIAT CSI Consort Spat. Inf.: 1–9. Available from http://srtm.csi.cgiar.org.

Joly, K., Gurarie, E., Sorum, M.S., Kaczensky, P., Cameron, M.D., Jakes, A.F., Borg, B.L., Nandintsetseg, D., Hopcraft, J.G.C., Buuveibaatar, B., Jones, P.F., Mueller, T., Walzer, C., Olson, K.A., Payne, J.C., Yadamsuren, A., and Hebblewhite, M. 2019. Longest terrestrial migrations and movements around the world. Sci. Rep. 9(1): 1–10. doi:10.1038/s41598-019-51884-5.

Juarez, C.A. 2008. Strontium and geolocation, the pathway to identification for deceased undocumented Mexican border-crossers: A preliminary report. J. Forensic Sci. 53(1): 46–49. doi:10.1111/j.1556-4029.2007.00610.x.

Julien, M., Bocherens, H., Burke, A., Drucker, D.G., Patou-mathis, M., Krotova, O., and Péan, S. 2012. Were European steppe bison migratory? d18O, d13C and Sr intra-tooth isotopic variations applied to a palaeoethological reconstruction. Quat. Int. 271: 106–119. Elsevier. doi:10.1016/j.quaint.2012.06.011.

Kaufman, D.S., and Manley, W.F. 2004. Pleistocene Maximum and Late Wisconsinan glacier extents across Alaska, U.S.A. Dev. Quat. Sci. 2(Part 2): 9–27. doi:10.1016/S1571-0866(04)80182-9.

Keller, K., Blum, J.D., and Kling, G.W. 2007. Geochemistry of soils and streams on surfaces of varying ages in arctic Alaska. Arctic, Antarct. Alp. Res. 39(1): 84–98. doi:10.1657/1523-0430(2007)39[84:GOSASO]2.0.CO;2.

Koch, P.L., Heisinger, J., Moss, C., Carlson, R.W., Fogel, M.L., and Behrensmeyer, A.K. 1995. Isotopic Tracking of Change in Diet and Habitat Use in African Elephants. doi:DOI 10.1126/science.267.5202.1340.

Kootker, L.M., van Lanen, R.J., Kars, H., and Davies, G.R. 2016. Strontium isoscapes in The Netherlands. Spatial variations in 87Sr/86Sr as a proxy for palaeomobility. J. Archaeol. Sci. Reports 6: 1–13. Elsevier Ltd. doi:10.1016/j.jasrep.2016.01.015.

Lachniet, M.S., Lawson, D.E., Stephen, H., Sloat, A.R., and Patterson, W.P. 2016. Isoscapes of d18O and d2H reveal climatic forcings on Alaska and Yukon precipitation. Water Resour. Res. 52(8): 6575–6586. doi:10.1002/2016WR019436.Received.

Larter, N.C., and Gates, C.C. 2017. American Society of Mammalogists Home-Range Size of Wood Bison : Effects of Age , Sex , and Forage. Am. Soc. Mammal. 75(1): 142–149.

Larter, N.C., Sinclair, A.R.E., Ellsworth, T., Nishi, J., and Gates, C.C. 2000. Dynamics of reintroduction in an indigenous large ungulate: the wood bison of northern Canada. Anim. Conserv. 3(4): 299–309. doi:10.1111/j.1469-1795.2000.tb00115.x.

Lloyd, A.H., Duffy, P. a., and Mann, D.H. 2013. Nonlinear responses of white spruce growth to climate variability in interior Alaska. Can. J. For. Res. 43: 331–343. doi:10.1139/cjfr-2012-0372.

Mackey, G.N., and Fernandez, D.P. 2011. High throughput Sr isotope analysis using an automated column chemistry system. In American Geophysical Union, San Francisco, California. AGU Fall. p. Meeting Abstracts 1:2525.

Mahowald, N.M., Muhs, D.R., Levis, S., Rasch, P.J., Yoshioka, M., Zender, C.S., and Luo, C. 2006. Change in atmospheric mineral aerosols in response to climate: Last glacial period, preindustrial, modern, and doubled carbon dioxide climates. J. Geophys. Res. Atmos. 111(10). doi:10.1029/2005JD006653.

Mann, D.H., Groves, P., Kunz, M.L., Reanier, R.E., and Gaglioti, B. V. 2013. Ice-age megafauna in Arctic Alaska: Extinction, invasion, survival. Quat. Sci. Rev. 70: 91–108. Elsevier Ltd. doi:10.1016/j.quascirev.2013.03.015.

Massilani, D., Guimaraes, S., Brugal, J.-P., Bennett, E.A., Tokarska, M., Arbogast, R.-M., Baryshnikov, G., Boeskorov, G., Castel, J.-C., Davydov, S., Madelaine, S., Putelat, O., Spasskaya, N.N., Uerpmann, H.-P., Grange, T., and Geigl, E.-M. 2016. Past climate changes, population dynamics and the origin of Bison in Europe. BMC Biol. 14(1): 93. BMC Biology. doi:10.1186/s12915-016-0317-7.

McFarland, H., and Seaton, T. 2018. Wood Bison News. In Department of Fish and Game, Division of Wildlife Conservation. Available from http://www.adfg.alaska.gov/static/research/wildlife/species/woodbisonrestoration/pdfs/woodbison_news_10_spring_2018.pdf.

Meyer, H., Schirrmeister, L., Andreev, A., Wagner, D., Hubberten, H.W., Yoshikawa, K., Bobrov, A., Wetterich, S., Opel, T., Kandiano, E., and Brown, J. 2010. Lateglacial and Holocene isotopic and environmental history of northern coastal Alaska - Results from a buried ice-wedge system at Barrow. Quat. Sci. Rev. 29(27–28): 3720–3735. Elsevier Ltd. doi:10.1016/j.quascirev.2010.08.005.

Misarti, N., Finney, B., Maschner, H., and Wooller, M.J. 2009. Changes in northeast Pacific marine ecosystems over the last 4500 years: evidence from stable isotope analysis of bone collagen from archeological middens. The Holocene 19(8): 1139–1151. doi:10.1177/0959683609345075.

Mooney, W.D., Laske, G., and Masters, T.G. 1998. CRUST 5.1: A global crustal model at 5° × 5°. J. Geophys. Res. Solid Earth 103(B1): 727–747. doi:10.1029/97jb02122.

Nicholson, K.L., Arthur, S.M., Horne, J.S., Garton, E.O., and Del Vecchio, P.A. 2016. Modeling caribou movements: Seasonal ranges and migration routes of the central arctic herd. PLoS One 11(4): 1–20. doi:10.1371/journal.pone.0150333.

O'Brien, D.M., and Wooller, M.J. 2007. Tracking human travel using stable oxygen and hydrogen isotope analysis of hair and urine. Rapid Commun. Mass Spectrom. 21: 2951–2954. doi:10.1002/rcm.

Pelletier, J.D., Broxton, P.D., Havenberg, P., Zeng, X., Trocj, P.A., Niu, G.-Y., Williams, Z., Brunke, M.A., and Gochis, D. 2015. A gridded global data set of soil, intact regolith, and sedimentary deposit thicknessess for regional and global land surface modeling. J. Adv. Model. Earth Syst. 7: 1339–1350. doi:10.1002/2017MS001065.

Plumb, G.E., White, P.J., Coughenour, M.B., and Wallen, R.L. 2009. Carrying capacity, migration, and dispersal in Yellowstone bison. Biol. Conserv. 142(11): 2377–2387. Elsevier Ltd. doi:10.1016/j.biocon.2009.05.019.

Porter, T.J., Froese, D.G., Feakins, S.J., Bindeman, I.N., Mahony, M.E., Pautler, B.G., Reichart, G., Sanborn, P.T., Simpson, M.J., and Weijers, J.W.H. 2016. Multiple water isotope proxy reconstruction of extremely low last glacial temperatures in Eastern Beringia (Western Arctic). Quat. Sci. Rev. 137: 113–125. Elsevier Ltd. doi:10.1016/j.quascirev.2016.02.006.

Potter, B.A., Holmes, C.E., and Yesner, D.R. 2013. Technology and economy among the earliest prehistoric foragers in Interior Eastern Beringia. Paleoamerican Odyssey: 81–103.

Potter, B.A., Reuther, J.D., Holliday, V.T., Holmes, C.E., Miller, D.S., and Schmuck, N. 2017. Early colonization of Beringia and Northern North America: Chronology, routes, and adaptive strategies. Quat. Int. 444: 36–55. Elsevier Ltd. doi:10.1016/j.quaint.2017.02.034.

Price, T.D., Burton, J.H., and Bentley, R.A. 2002. The characterization of biologically available strontium isotope ratios for the studyof prehistoric migration. Archaeometry 44(1): 117–135.

Rasic, J.T., and Matheus, P.E. 2007. A reconsideration of purported Holocene bison bones from northern Alaska. Arctic 60(4): 381–388.

Rasmussen, S.O., Bigler, M., Blockley, S.P., Blunier, T., Buchardt, S.L., Clausen, H.B., Cvijanovic, I., Dahl-Jensen, D., Johnsen, S.J., Fischer, H., Gkinis, V., Guillevic, M., Hoek, W.Z., Lowe, J.J., Pedro, J.B., Popp, T., Seierstad, I.K., Steffensen, J.P., Svensson, A.M., Vallelonga, P., Vinther, B.M., Walker, M.J.C., Wheatley, J.J., and Winstrup, M. 2014. A stratigraphic framework for abrupt climatic changes during the Last Glacial period based on three synchronized Greenland ice-core records: Refining and extending the INTIMATE event stratigraphy. Quat. Sci. Rev. 106: 14–28. Elsevier Ltd. doi:10.1016/j.quascirev.2014.09.007.

Reynolds, A.C., Quade, J., and Betancourt, J.L. 2012. Strontium isotopes and nutrient sourcing in a semi-arid woodland. Geoderma 189–190: 574–584. Elsevier B.V. doi:10.1016/j.geoderma.2012.06.029.

Rich, S., Manning, S.W., Degryse, P., Vanhaecke, F., and Van Lerberghe, K. 2012. Strontium isotopic and tree-ring signatures of Cedrus brevifolia in Cyprus. J. Anal. At. Spectrom. 27(5): 796. doi:10.1039/c2ja10345a.

Risnes, S. 1998. Growth tracks in dental enamel. J Hum Evol. (4–5): 331–50.

Shand, P., Darbyshire, D.P.F., Love, A.J., and Edmunds, W.M. 2009. Sr isotopes in natural waters: Applications to source characterisation and water-rock interaction in contrasting landscapes. Appl. Geochemistry 24(4): 574–586. Elsevier Ltd. doi:10.1016/j.apgeochem.2008.12.011.

Shapiro, B., and Cooper, A. 2003. Beringia as an Ice Age genetic museum. Quat. Res. 60(1): 94–100. doi:10.1016/S0033-5894(03)00009-7.

Shapiro, B., Pybus, O.G., Gilbert, M.T.P., Barnes, I., Baryshnikov, G.F., Burns, J.A., and Davydov, S. 2004. Rise and Fall of the Beringian Steppe Bison. Science (80-.). 306: 1561–1565. doi:10.1126/science.1101074.

Stenseth, N.C., Lidicker, W.Z., and Lidicker, W.Z.J. 1992. Animal Dispersal: Small Mammals As a Model. Chapman & Hall, London.

Stephenson, R.O., Gerlach, S.C., Guthrie, R.D., Harington, C.R., Mills, R.O., and Hare, G. 2001. Wood Bison in Late Holocene Alaska and Adjacent Canada: Paleontological, Archaeological and Historical Records. In People and Wildlife in Northern North America. BAR International Series. pp. 125–148.

Stuiver, M., Reimer, P.J., and Reimer, R.W. 2019. CALIB 7.1. Available from http://calib.org.

Van Klinken, G.J. 1999. Bone collagen quality indicators for palaeodietary and radiocarbon measurements. J. Archaeol. Sci. 26(6): 687–695. doi:10.1006/jasc.1998.0385.

Verkouteren, R.M., and Klinedinst, D.B. 2004. Value Assignment and Uncertainty Estimation of Selected Light Stable Isotope Reference Materials: RMs 8543-8545, RMs 8562-8564, and RM 8566. In National Institute of Standards and Technology Special Publication. Available from http://www.nist.gov/srm/upload/SP260-149.pdf.

VertNet. 2016. Georeferencing. Available from http://www.vertnet.org/resources/georef.html.

Viner, S., Evans, J., Albarella, U., and Parker Pearson, M. 2010. Cattle mobility in prehistoric Britain: Strontium isotope analysis of cattle teeth from Durrington Walls (Wiltshire, Britain). J. Archaeol. Sci. 37(11): 2812–2820. doi:10.1016/j.jas.2010.06.017.

West, J.B., Bowen, G.J., Dawson, T., and Tu, K. 2009. Isoscapes: Understanding movment, pattern, and process on Earth through isotope mapping. Springer, Dordrecht.

Widga, C., Walker, J.D., and Stockli, L.D. 2010. Middle Holocene Bison diet and mobility in the eastern Great Plains (USA) based on 13C, 18O, and 87Sr/86Sr analyses of tooth enamel carbonate. Quat. Res. 73(3): 449–463. doi:10.1016/j.yqres.2009.12.001.

Wooller, M.J., Zazula, G.D., Edwards, M., Froese, D.G., Boone, R.D., Parker, C., and Bennett, B. 2007. Stable carbon isotope compositions of Eastern Beringian grasses and sedges: Investigating their potential as paleoenvironmental indicators. Arct. Antarct. Alp. Res. 39(2): 318–331. doi:10.1657/1523-0430(2007)39[318:SCICOE]2.0.CO;2.

Wunder, M.B. 2012. Determining geographic patterns of migration and dispersal using stable isotopes in keratins. J. Mammal. 93(2): 360–367. doi:10.1644/11-mamm-s-182.1.

Zazula, G.D., Hall, E., Hare, P.G., Thomas, C., Mathewes, R., La Farge, C., Martel, A.L., Heintzman, P.D., and Shapiro, B. 2017. A middle holocene steppe bison and paleoenvironments from the Versleuce Meadows, Whitehorse, Yukon, Canada. Can. J. Earth Sci. 54(11): 1138–1152. doi:10.1139/cjes-2017-0100.

Zomer, R.J., Trabucco, A., Bossio, D.A., and Verchot, L. V. 2008. Climate change mitigation: A spatial analysis of global land suitability for clean development mechanism afforestation and reforestation. Agric. Ecosyst. Environ. 126(1–2): 67–80. doi:10.1016/j.agee.2008.01.014.

2.9 Supplementary Figures

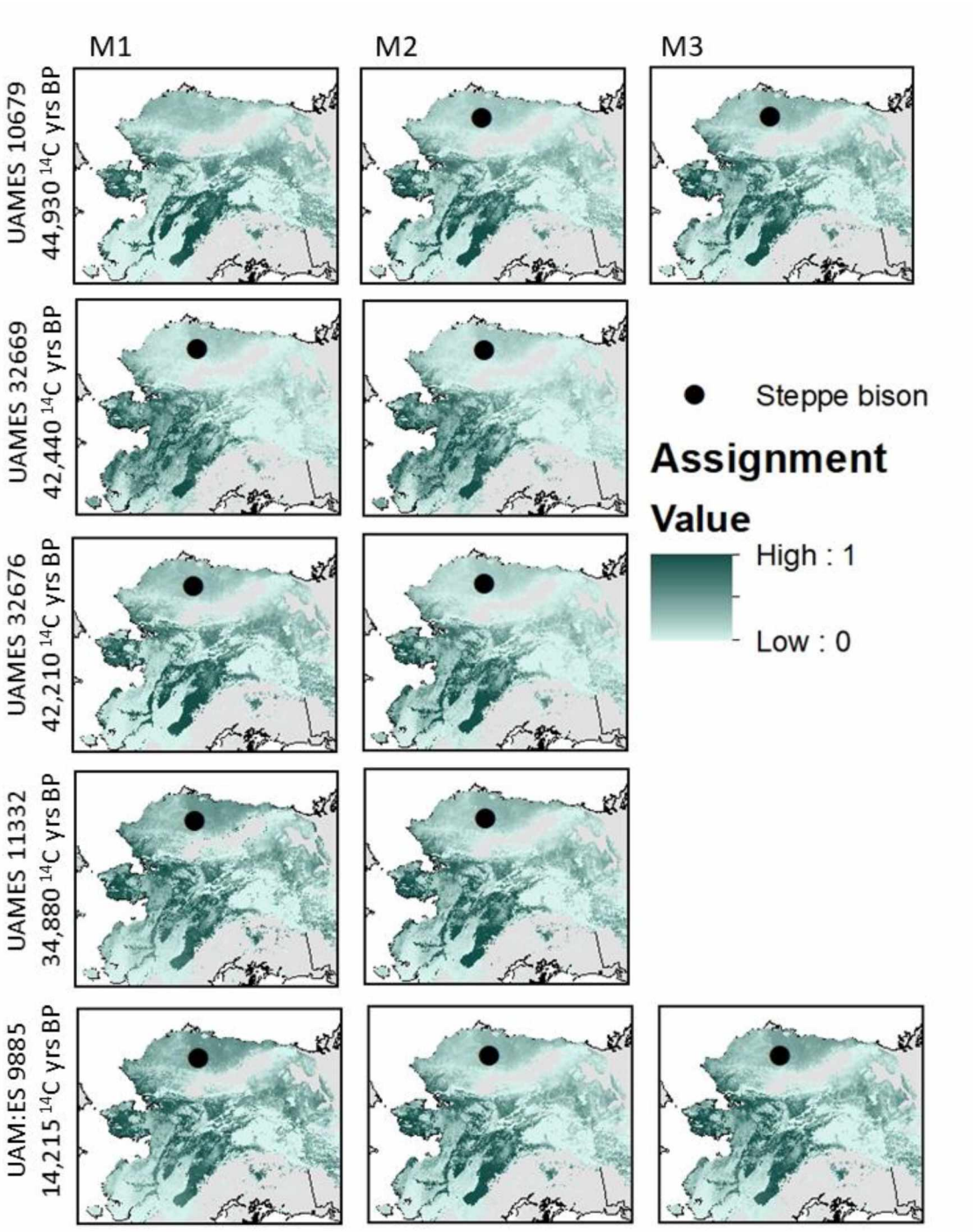

Figure 2.S1 Assignment of bison molar 1 (M1), molar 2 (M2) and molar 3 (M3), with probability assignment based on dual models of bioavailable strontium map and oxygen isoscape (Lachniet et al., 2016) adjusted by Δ $\delta^{18}O$ offset of nearest peak value from age (Figure 11, Table 3).

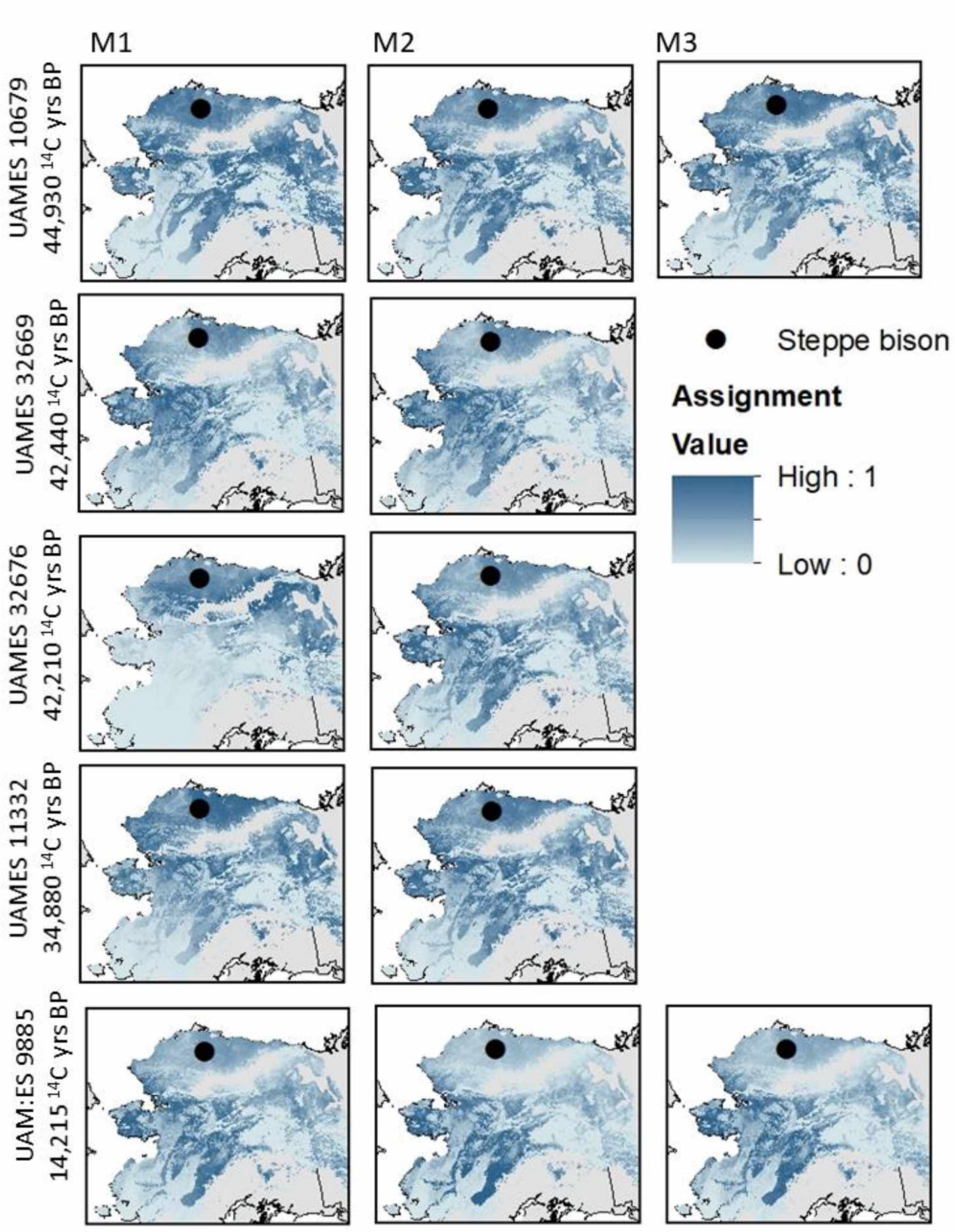

Figure S2 Assignment of bison molar 1 (M1), molar 2 (M2) and molar 3 (M3), with probability assignment based on dual models of bioavailable strontium map and oxygen isoscape (Lachniet et al., 2016) with no adjustment for age.

Table 2.S1 Full list of UAM:Mamm Rodents samples analyzed for $^{87}Sr/^{86}Sr$

UAM: Mamm	Species	Locality	Collection date	Latitude	Longitude	Coordinate uncertainty (m)	$^{87}Sr/^{86}Sr$
130	*Microtus oeconomus operarius*	Wales	6/4/1952	65.617	-168.083	2000	0.70967
150	*Microtus oeconomus*	Steese Hwy at Eagle Summit	10/29/1951	65.333	-147.500	1041	0.73414
204	*Microtus oeconomus*	Fort Yukon	5/23/1952	66.560	-145.250	3615	0.71119
1850	*Microtus miurus*	<Null>	6/4/1956	68.083	-143.750	1041	0.71012
1979	*Microtus oeconomus macfarlani*	<Null>	7/31/1956	68.600	-143.750	1041	0.70929
2971	*Myodes rutilus*	Black River	7/5/1957	66.733	-143.583	1041	0.71327
3100	*Myodes rutilus*	Small Lake, A-6	7/25/1957	67.367	-143.800	1041	0.71213
3237	*Lemmus trimucronatus*	Old John Lake	8/7/1957	67.067	-145.050	1041	0.71079
3269	*Microtus oeconomus macfarlani*	Old John Lake	8/8/1957	68.050	-145.000	3615	0.71004
3981	*Microtus pennsylvanicus*	Huslia R, North Fork, Yatlin's cabin	8/23/1957	66.540	-156.833	3615	0.70669
4057	*Myodes rutilus*	Porcupine River @ Old Rampart	7/22/1957	67.250	-141.667	1041	0.71416
4069	*Lemmus trimucronatus*	<Null>	7/25/1957	67.183	-141.917	1041	0.7127
4477	*Microtus oeconomus*	Golden Gate Cr at Pilgrim River	23 Jul 195?	65.083	-164.667	1041	0.7111
4650	*Microtus oeconomus*	Meade River village	10/11/1960	70.481	-157.417	1041	0.71007
4658	*Lemmus trimucronatus*	Mead River village	9/20/1960	70.483	-157.417	1041	0.71204
6238	*Myodes rutilus*	BSMS camp 2, Noatak River	6/28/1963	67.883	-160.800	1041	0.71323
6241	*Myodes rutilus*	BSMS camp 4, Walker Lake	8/29/1963	67.200	-154.550	1041	0.71675
6243	*Myodes rutilus*	BSMS camp 4, Walker Lake	8/27/1963	67.200	-154.550	1041	0.71921

Table 2.S1, continued.

UAM: Mamm	Species	Locality	Collection date	Latitude	Longitude	Coordinate uncertainty (m)	$^{87}Sr/^{86}Sr$
6362	*Myodes rutilus*	Redstone River Valley, BSMS Camp 3, Mt edge of camp	7/9/1963	67.233	-157.617	1041	0.72174
7988	*Microtus oeconomus*	Allakaket, near river	8/9/1955	66.567	-152.633	1041	0.71242
8005	*Lemmus trimucronatus*	Ogotoruk Cr region, 1 1/2 mi NNW of Cr mouth	7/25/1959	68.100	-165.750	1041	0.71185
8163	*Microtus oeconomus*	Umiat region, 1 mi N Umiat	8/18/1954	69.367	-152.133	1041	0.71309
8432	*Microtus miurus*	Colville River region	8/18/1961	69.967	-155.767	1041	0.71111
8452	*Microtus oeconomus*	Point Hope	5/20/1956	68.348	-166.808	2000	0.70945
8963	*Microtus miurus*	BSMS camp 5, Omelaktavik Lake	8/8/1963	67.657	-155.539	0	0.71392
10376	*Microtus oeconomus*	Cape Thompson	8/16/1960	68.144	-165.978	2000	0.7105
10377	*Microtus oeconomus*	Elliot Hwy, Riverbank at Tolvana R	5/15/1954	65.517	-148.533	1041	0.71078
10390	*Microtus oeconomus*	Cape Dyer region	7/17/1960	68.650	-166.233	1041	0.71454
10401	*Microtus oeconomus*	Baldwin Peninsula, mouth of Sadie Cr	7/7/1960	66.750	-162.333	1041	0.70951
11018	*Myodes rutilus*	Seward Peninsula, Imuruk Lake	7/14/1973	65.617	-163.129	0	0.70829
11018	*Myodes rutilus*	Seward Peninsula, Imuruk Lake	7/14/1973	65.617	-163.129	0	0.70822
11024	*Myodes rutilus*	Seward Peninsula, Serpentine Hot Springs	8/6/1973	65.859	-163.727	0	0.70968
11044	*Microtus oeconomus*	Seward Peninsula, Lava Lake	7/8/1973	65.583	-163.895	1041	0.70789
11051	*Microtus oeconomus*	Seward Peninsula, Inmachuk River	8/1/1973	66.070	-162.738	0	0.71012
11149	*Microtus oeconomus*	Kikitaliorak Lake, Noatak drainage, ca 18 mi ESE Howard Pass	7/13/1973	68.125	-156.233	1041	0.71721

Table 2.S1, continued.

UAM: Mamm	*Species*	Locality	Collection date	Latitude	Longitude	Coordinate uncertainty (m)	$^{87}Sr/^{86}Sr$
11157	*Microtus oeconomus*	Kaluich Cr, Noatak Vally, Anuk Lake, easternmost lake, *	8/3/1973	67.533	-158.467	1041	0.71306
11166	*Microtus oeconomus*	Feniak Lake (Noatak Valley, Feniak Lake, Makpik Cr)	7/3/1973	68.250	-158.333	1041	0.71372
11183	*Myodes rutilus*	Tulugak Lake, (Noatak Valley)	8/17/1973	67.967	-161.717	1041	0.70973
11669	*Microtus oeconomus*	Happy Valley Pipeline camp	10/25/1975	69.250	-148.083	1041	0.71068
13444	*Microtus miurus*	Sagavanirktok River	6/13/1974	69.383	-148.683	1041	0.70923
13584	*Microtus oeconomus*	Mancha Cr	8/25/1979	68.667	-141.250	1041	0.70897
13611	*Dicrostonyx groenlandicus rubricatus*	Anaktuvuk Pass	8/17/1963	68.133	-151.750	1041	0.71003
13614	*Microtus oeconomus*	Barrow, NARL research facilities	3/1/1976	71.283	-156.783	1041	0.7094
13708	*Microtus oeconomus*	N Slope, Dalton Hwy, Franklin Bluffs	7/12/1979	69.800	-148.683	1041	0.7093
14401	*Lemmus trimucronatus*	Barrow area, 2 mi E of ARL	11/14/1960	71.333	-156.567	1041	0.71097
14555	*Myodes rutilus*	Nulato River, 1/2 mi N, 3 1/4 mi W of Nulato cemetery	7/3/1982	64.717	-158.183	1041	0.70775
15052	*Myodes rutilus*	Ray Mts, headwaters of Moose Creek	8/16/1979	65.600	-150.633	1041	0.71053
15056	*Microtus oeconomus*	<Null>	7/9/1979	65.817	-151.433	1041	0.71927
15300	*Microtus xanthognathus*	(Horseshoe L) Koyukuk R, 1.25 mi N, 8.75 mi E Kateel R mouth	5/30/1983	65.467	-157.317	1041	0.7116
15307	*Microtus oeconomus*	<Null>	3/24/1983	64.750	-157.950	1041	0.71292
15311	*Myodes rutilus*	Old Town Galena	10/12/1982	64.733	-156.933	1041	0.71257

Table 2.S1, continued.

UAM: Mamm	Species	Locality	Collection date	Latitude	Longitude	Coordinate uncertainty (m)	$^{87}Sr/^{86}Sr$
15756	*Dicrostonyx groenlandicus rubricatus*	Prudhoe Bay	6/26/1984	70.200	-148.417	1041	0.70885
15814	*Myodes rutilus*	upper Hulahula River	8/17/1984	69.083	-144.617	1041	0.72738
15849	*Microtus oeconomus*	Ninemile Point, E of Deering	4/25/1984	66.067	-162.467	1041	0.7102
15872	*Microtus pennsylvanicus*	small pond 0.25mi E of Hozatka Lake,T35,R11E,Sec14. 219ft.	7/17/1984	65.233	-156.550	1041	0.71042
18599	*Myodes rutilus*	Tuluksak R, vicinity of Slate Cr	8/19/1981	60.983	-160.067	1041	0.70657
19770	*Microtus oeconomus*	Cape Krusenstern, shore	5/28/1989	67.067	-162.750	1041	0.70933
20990	*Microtus miurus*	<Null>	8/14/1972	65.400	-167.100	1041	0.70918
21532	*Myodes rutilus dawsoni*	Izembek Lagoon	6/17/1970	55.333	-162.800	1041	0.70742
22994	*Myodes rutilus*	Dietrich River, mile 207 Dalton Hwy	8/31/1993	67.617	-149.783	1041	0.7122
23024	*Microtus oeconomus*	Slope Mountain, mile 301 Dalton Hwy	8/26/1993	68.733	-149.033	1041	0.71032
23031	*Microtus oeconomus*	Chandalar Shelf, mile 239.4 Dalton Hwy	8/29/1993	68.067	-149.583	1041	0.71655
23331	*Microtus xanthognathus*	2 mi E of Akpelik Creek and Kobuk River confluence	8/24/1993	66.750	-155.283	1041	0.71303
24695	*Myodes rutilus*	73 km ESE of Ruby	8/9/1992	64.683	-153.917	1041	0.71042
31929	*Microtus pennsylvanicus*	Mouse Lake, Grid 3	8/26/1993	66.312	-151.775	200	0.70935
34138	*Myodes rutilus*	13.5 mi N Coldfoot	6/12/1994	67.434	-150.071	0	0.71521
34256	*Myodes rutilus*	Grayling Creek Cabin	8/13/1994	66.129	-165.129	0	0.70887
37729	*Microtus oeconomus*	Candle	8/23/1968	65.917	-161.933	2000	0.7125

Table 2.S1, continued.

UAM: Mamm	Species	Locality	Collection date	Latitude	Longitude	Coordinate uncertainty (m)	$^{87}Sr/^{86}Sr$
37738	*Microtus oeconomus*	Nome	5/4/1968	64.500	-165.417	2000	0.70906
37777	*Microtus oeconomus*	Council	7/21/1966	64.900	-163.667	2000	0.70967
37924	*Microtus xanthognathus*	8.1 km E, 5.7 km S Horner Hot Springs, Twin Slough	8/10/1981	64.883	-154.244	0	0.71272
43125	*Myodes rutilus*	0.5 mi S, 4 mi E Bishop Rock	8/25/1995	64.801	-157.227	0	0.71286
43142	*mus trimucronatus*	Colville River delta, Colville village airport	9/25/1996	70.383	-150.800	1041	0.71065
43144	*Lemmus trimucronatus*	Colville River delta, Colville village airport	9/29/1996	70.383	-150.800	1041	0.7102
47577	*Myodes rutilus*	Buttes Gap	8/29/1991	66.100	-148.117	1041	0.71266
51183	*Lemmus trimucronatus*	Colville River delta, Colville Village	9/24/1996	70.383	-150.800	2000	0.71107
51183	*Lemmus trimucronatus*	Colville River delta, Colville Village	9/24/1996	70.383	-150.800	2000	0.71012
51184	*Lemmus trimucronatus*	Colville River delta, Colville Village	9/28/1996	70.383	-150.800	2000	0.71043
51848	*Myodes rutilus*	Kuzitrin River between Igloo and Bridge	7/12/1969	65.167	-165.417	2000	0.71138
51850	*Myodes rutilus*	Pilgrim Hot Springs	7/10/1969	65.100	-164.917	2000	0.71143
54687	*Microtus oeconomus*	Grand Central River	7/28/2000	64.902	-165.113	0	0.71104
54819	*Microtus oeconomus*	8 km south of Kotzebue	7/23/2000	66.927	-162.596	0	0.70969
54959	*Microtus oeconomus*	Wesley Creek	8/11/2000	64.914	-166.216	200	0.71029
55120	*Myodes rutilus*	Tukrok River	7/26/2000	66.927	-162.596	200	0.71106
55457	*Myodes rutilus*	mile 56 Dalton Hwy.	8/25/2001	65.888	-149.729	30	0.71276
55526	*Myodes rutilus*	rock formations N. Finger Mountain, Dalton Hwy.	8/31/2001	66.363	-150.460	30	0.70898

Table 2.S1, continued.

UAM: Mamm	Species	Locality	Collection date	Latitude	Longitude	Coordinate uncertainty (m)	$^{87}Sr/^{86}Sr$
55566	*Microtus oeconomus*	Kuzitrin Lake	7/30/2001	65.389	-163.264	152	0.70835
55624	*Microtus oeconomus*	Serpentine Hot Springs	8/7/2001	65.853	-164.696	152	0.7119
55855	*Myodes rutilus*	W bank Rabbit Creek	7/16/2001	67.515	-163.590	152	0.71287
55961	*Myodes rutilus*	7 mile Red Dog Mine Road	7/21/2001	67.627	-163.855	0	0.71068
55969	*Dicrostonyx groenlandicus*	Red Dog Mine Road	7/21/2001	67.749	-163.609	152	0.70902
55970	*Myodes rutilus*	base of Kaksusok Mountain, W of Situkuyok River	7/13/2001	67.205	-163.175	152	0.71064
56154	*Microtus miurus*	Devil Mountain Lakes	7/27/2001	66.387	-164.454	152	0.70596
56271	*Myodes rutilus*	Sidik Lake	7/17/2001	68.148	-158.981	100	0.71191
56272	*Myodes rutilus*	Sidik Lake	7/17/2001	68.148	-158.981	100	0.71194
56280	*Myodes rutilus*	Sidik Lake	7/15/2001	68.149	-158.988	100	0.71114
56318	*Myodes rutilus*	Sidik Lake	7/18/2001	68.149	-158.988	100	0.71224
56327	*Microtus oeconomus*	Desperation Lake	7/13/2001	68.338	-158.728	200	0.70619
56386	*Myodes rutilus*	Kaluich Creek Upland	7/21/2001	67.664	-158.191	200	0.71239
56429	*Microtus oeconomus*	Aniralik Lake	8/1/2001	68.210	-159.831	100	0.71212
56525	*Myodes rutilus*	Onion Portage	8/10/2001	67.106	-158.270	100	0.71465
56534	*Myodes rutilus*	Onion Portage	8/10/2001	67.106	-158.270	100	0.71363
56536	*Myodes rutilus*	Onion Portage	8/10/2001	67.106	-158.270	100	0.71345
56597	*Lemmus trimucronatus*	8 km W of Copter Peak	7/25/2001	68.474	-161.482	100	0.70956
56639	*Microtus oeconomus*	5 km E of Asik Mountain	7/28/2001	67.474	-162.216	100	0.71006
56640	*Microtus oeconomus*	5 km E of Asik Mountain	7/28/2001	67.474	-162.216	100	0.71234
56641	*Microtus oeconomus*	5 km E of Asik Mountain	7/28/2001	67.474	-162.216	100	0.7104

Table 2.S1, continued.

UAM: Mamm	Species	Locality	Collection date	Latitude	Longitude	Coordinate uncertainty (m)	$^{87}Sr/^{86}Sr$
56650	*Microtus oeconomus*	5 km E of Asik Mountain	7/28/2001	67.474	-162.216	100	0.71041
56667	*Myodes rutilus*	5 km E of Asik Mountain	7/30/2001	67.474	-162.216	100	0.71091
57008	*Myodes rutilus*	confluence of Kallarichuk River and Kobuk River	8/6/2001	67.086	-159.779	100	0.714
57441	*Myodes rutilus*	12.5 km ENE of Kathul Mountain	7/27/2001	65.372	-142.018	500	0.70764
57879	*Myodes rutilus*	SW of Summit Lake	8/8/2001	61.318	-144.240	100	0.7062
61393	*Microtus miurus*	Polychrome	8/21/2000	63.498	-149.888	10	0.70731
62430	*Microtus oeconomus*	Noorvik Airport	10/1/2000	66.831	-161.032	1609	0.71344
62431	*Microtus oeconomus*	Noorvik Airport	10/1/2000	66.831	-161.032	1609	0.71385
64352	*Microtus miurus*	2 miles N of Bold Peak	7/20/2002	61.365	-148.908	600	0.70539
64468	*Myodes rutilus*	Reindeer Creek	7/6/2002	56.993	-158.644	500	0.70492
66866	*Microtus miurus*	<Null>	7/22/1999	68.617	-153.000	2000	0.71274
72483	*Myodes rutilus*	Tundra Lake near Sparrevohn Air Base	7/25/1999	61.181	-155.685	0	0.70669
72503	*Myodes rutilus*	1.5 mi S McGrath	7/28/1999	62.946	-155.561	0	0.71003
75346	*Microtus oeconomus*	Skookum River	7/17/2000	64.715	-164.012	3615	0.71145
75852	*Microtus oeconomus*	Toolik Lake Research Station	8/11/2000	68.628	-149.593	2500	0.71938
75854	*Microtus oeconomus*	Toolik Lake Research Station	8/11/2000	68.628	-149.593	2500	0.71578
75868	*Microtus oeconomus*	Toolik Lake Research Station	8/11/2000	68.628	-149.593	2500	0.71371
75871	*Microtus oeconomus*	Toolik Lake Research Station	8/11/2000	68.628	-149.593	2500	0.71113

Table 2.S1, continued.

UAM: Mamm	Species	Locality	Collection date	Latitude	Longitude	Coordinate uncertainty (m)	$^{87}Sr/^{86}Sr$
76134	*Microtus oeconomus*	Toolik Lake Research Station	8/10/2000	68.628	-149.593	2500	0.71381
77006	*Myodes rutilus*	2 mi S of confluence of Fox River and Lil Creek	7/23/2000	64.763	-163.815	0	0.71249
77040	*Myodes rutilus*	Rock Creek	7/2/1996	63.729	-148.990	150	0.72298
78696	*Microtus oeconomus*	unnamed lake near North Fork Koyukuk River	7/23/2002	67.453	-150.850	200	0.71577
78833	*Microtus miurus*	Agiak Lake	7/17/2002	68.078	-152.924	200	0.71502
79046	*Microtus miurus*	Nanushuk River	8/4/2002	68.275	-150.655	150	0.71695
79102	*Microtus oeconomus*	Agiak Lake	7/13/2002	68.081	-152.944	200	0.71661
79609	*Microtus oeconomus*	S side of Takahula Lake	7/29/2002	67.347	-153.665	150	0.71082
81573	*Myodes rutilus*	Noorvik Airport	9/25/1999	66.833	-161.017	2000	0.71284
81972	*Microtus miurus*	E side of Lake Isiak	7/22/2002	67.719	-156.138	200	0.71344
82113	*Microtus oeconomus*	N side of Lake Tulilik	7/12/2002	68.117	-154.120	250	0.72047
83081	*Microtus oeconomus*	5 km NE confluence of Noatak River and Kelly River	8/1/2000	67.945	-162.232	2000	0.71181
85806	*Myodes rutilus*	0.41 mi SE of Research Station, SE side of Lake Peters	7/26/2006	69.300	-145.022	300	0.73519
89229	*Myodes rutilus*	Galbrath Lake	1/13/2005	68.529	-144.471	274	0.7112
92451	*Myodes rutilus*	3 miles north of Kvichak River, 4 miles east of Yellow Creek	7/21/2003	59.230	-156.693	150	0.7056
93431	*Myodes rutilus*	Waring Mountains	7/29/2003	67.013	-158.499	75	0.71719

Table 2.S1, continued.

UAM: Mamm	***Species***	***Locality***	***Collection date***	***Latitude***	***Longitude***	***Coordinate uncertainty (m)***	***$^{87}Sr/^{86}Sr$***
94310	*Myodes rutilus*	Igisukruk Mountain	7/14/2003	67.136	-162.884	100	0.70984
94336	*Microtus miurus*	Kakagrak Hills	7/9/2003	67.270	-163.647	250	0.70994
94524	*Microtus oeconomus*	North Fork Unalakleet River	7/7/2005	64.373	-159.546	137	0.71034
98326	*Microtus oeconomus*	North Fork Unalakleet River	7/7/2005	64.373	-159.546	137	0.70766
99108	*Microtus oeconomus*	0.160 mi east of south tip of Cooper Lake, Kenai Peninsula	8/18/2005	60.383	-149.716	150	0.70645
99510	*Microtus oeconomus*	Coyote Lake, Kenai Peninsula	8/21/2005	60.725	-150.445	190	0.70567
106231	*Myodes rutilus*	Fish Creek	9/24/2007	66.577	-150.970	6	0.71744
125703	*Microtus oeconomus*	Colville River - confluence of Kiligwa	6/13/2015	69.007	-158.268	<Null>	0.71107
125706	*Dicrostonyx groenlandicus*	Colville R and confluence of Ipnavik	6/15/2015	68.899	-156.470	10	0.71494
125713	*Microtus oeconomus*	Colville River - SE of Kakvuiyat Bend	6/18/2015	69.060	-154.244	<Null>	0.71312
131749	*Lemmus trimucronatus*	Cape Nome	5/20/1905	64.438	-165.006	1000	0.70746
7991a	*Dicrostonyx groenlandicus*	Mead River site, 46 mi S of Barrow	8/21/1954	70.867	-155.917	1041	0.71179
7991b	*Dicrostonyx groenlandicus*	Mead River site, 46 mi S of Barrow	8/21/1954	70.867	-155.917	1041	0.71172
7991c	*Dicrostonyx groenlandicus*	Mead River site, 46 mi S of Barrow	8/21/1954	70.867	-155.917	1041	0.71293
7991d	*Dicrostonyx groenlandicus*	Mead River site, 46 mi S of Barrow	8/21/1954	70.867	-155.917	1041	0.71139

Table 2.S2 Previously published data used for modelling in this study

Analysis ID	*Sample ID*	*Type*	*Location*	*Latitude*	*Longitude*	*87Sr/86Sr*	*Citation*
2131	DH-01.07	Minerals	Hot Springs Pluton	66.3417	-150.4513	0.70787	Keller et al., 2007
2132	DH-02.07	Minerals	Bonanza Pluton	66.6889	-150.6594	0.70947	Keller et al., 2007
2133	DH-03.09	Minerals	Jim River Pluton Quarry Site	66.9910	-150.2886	0.70924	Keller et al., 2007
2134	DH-03.10	Minerals	Jim River Pluton Quarry Site	66.9910	-150.2886	0.70877	Keller et al., 2007
2135	DH-03.11	Minerals	Jim River Pluton Quarry Site	66.9910	-150.2886	0.70851	Keller et al., 2007
2136	1996-0112	Water	Milky Way Upper Stream	68.6191	-149.5806	0.71256	Keller et al., 2007
2137	1996-0194	Water	Milky Way Upper Stream	68.6191	-149.5806	0.71232	Keller et al., 2007
2138	1996-0233	Water	Milky Way Upper Stream	68.6191	-149.5806	0.71246	Keller et al., 2007
2139	1996-0726	Water	Milky Way Upper Stream	68.6191	-149.5806	0.71234	Keller et al., 2007
2140	1996-0784	Water	Milky Way Upper Stream	68.6191	-149.5806	0.71226	Keller et al., 2007
2141	2002-0093	Water	Milky Way Upper Stream	68.6191	-149.5806	0.71254	Keller et al., 2007
2142	2002-0152	Water	Milky Way Upper Stream	68.6191	-149.5806	0.71263	Keller et al., 2007
2143	2002-0213	Water	Milky Way Upper Stream	68.6191	-149.5806	0.71258	Keller et al., 2007
2144	2002-0297	Water	Milky Way Upper Stream	68.6191	-149.5806	0.71255	Keller et al., 2007
2145	2002-0376	Water	Milky Way Upper Stream	68.6191	-149.5806	0.71241	Keller et al., 2007
2146	2002-0417	Water	Milky Way Upper Stream	68.6191	-149.5806	0.71236	Keller et al., 2007
2147	2002-0517	Water	Milky Way Upper Stream	68.6191	-149.5806	0.71224	Keller et al., 2007
2148	2002-0572	Water	Milky Way Upper Stream	68.6191	-149.5806	0.71200	Keller et al., 2007
2149	2002-0658	Water	Milky Way Upper Stream	68.6191	-149.5806	0.71198	Keller et al., 2007

Table 2.S2, continued.

Analysis ID	*Sample ID*	*Type*	*Location*	*Latitude*	*Longitude*	*87Sr/86Sr*	*Citation*
2151	2002-0702.0-gff	Water	Milky Way Upper Stream	68.6191	-149.5806	0.71203	Keller et al., 2007
2152	2003-0241	Water	Milky Way Upper Stream	68.6191	-149.5806	0.71241	Keller et al., 2007
2153	2003-0247	Water	Milky Way Upper Stream	68.6191	-149.5806	0.71218	Keller et al., 2007
2154	2003-0253	Water	Milky Way Upper Stream	68.6191	-149.5806	0.71252	Keller et al., 2007
2155	2003-0259	Water	Milky Way Upper Stream	68.6191	-149.5806	0.71255	Keller et al., 2007
2156	2003-0271	Water	Milky Way Upper Stream	68.6191	-149.5806	0.71257	Keller et al., 2007
2157	2003-0277	Water	Milky Way Upper Stream	68.6191	-149.5806	0.71256	Keller et al., 2007
2158	2003-0283	Water	Milky Way Upper Stream	68.6191	-149.5806	0.71260	Keller et al., 2007
2159	2003-0307	Water	Milky Way Upper Stream	68.6191	-149.5806	0.71230	Keller et al., 2007
2160	2003-0331	Water	Milky Way Upper Stream	68.6191	-149.5806	0.71257	Keller et al., 2007
2161	2003-0355	Water	Milky Way Upper Stream	68.6191	-149.5806	0.71259	Keller et al., 2007
2162	NS-08.07	Minerals	lt 1 pit	68.6255	-149.5774	0.71281	Keller et al., 2007
2163	NS-08.08	Minerals	lt 1 pit	68.6255	-149.5774	0.71274	Keller et al., 2007
2164	NS-08.10	Minerals	lt 1 pit	68.6255	-149.5774	0.71240	Keller et al., 2007
2165	NS-101.01	Minerals	lt1 Pit 2	68.6251	-149.5718	0.71992	Keller et al., 2007
2166	NS-101.02	Minerals	lt1 Pit 2	68.6251	-149.5718	0.71414	Keller et al., 2007
2167	NS-101.03	Minerals	lt1 Pit 2	68.6251	-149.5718	0.71264	Keller et al., 2007
2168	NS-101.04	Minerals	lt1 Pit 2	68.6251	-149.5718	0.71261	Keller et al., 2007

Table 2.S2 continued.

Analysis ID	*Sample ID*	*Type*	*Location*	*Latitude*	*Longitude*	*87Sr/86Sr*	*Citation*
2170	NS-101.06	Minerals	lt1 Pit 2	68.6251	-149.5718	0.70908	Keller et al., 2007
2171	NS-102.01	Minerals	lt1 Pit 3	68.6247	-149.5708	0.72138	Keller et al., 2007
2172	NS-102.02	Minerals	lt1 Pit 3	68.6247	-149.5708	0.71304	Keller et al., 2007
2173	NS-102.03	Minerals	lt1 Pit 3	68.6247	-149.5708	0.71350	Keller et al., 2007
2174	NS-102.04	Minerals	lt1 Pit 3	68.6247	-149.5708	0.71311	Keller et al., 2007
2175	NS-102.05	Minerals	lt1 Pit 3	68.6247	-149.5708	0.71272	Keller et al., 2007
2176	NS-102.06	Minerals	lt1 Pit 3	68.6247	-149.5708	0.71120	Keller et al., 2007
2177	NS-103.01	Minerals	Sag 2, Pit 2	68.6451	-149.4352	0.71478	Keller et al., 2007
2178	NS-103.02	Minerals	Sag 2, Pit 2	68.6451	-149.4352	0.71219	Keller et al., 2007
2179	NS-103.03	Minerals	Sag 2, Pit 2	68.6451	-149.4352	0.71191	Keller et al., 2007
2180	NS-103.04	Minerals	Sag 2, Pit 2	68.6451	-149.4352	0.71171	Keller et al., 2007
2181	NS-103.05	Minerals	Sag 2, Pit 2	68.6451	-149.4352	0.71193	Keller et al., 2007
2182	NS-103.06	Minerals	Sag 2, Pit 2	68.6451	-149.4352	0.71174	Keller et al., 2007
2183	NS-104.01	Minerals	Sag 2 Pit 3	68.6445	-149.4306	0.71673	Keller et al., 2007
2184	NS-104.02	Minerals	Sag 2 Pit 3	68.6445	-149.4306	0.71304	Keller et al., 2007
2185	NS-104.03	Minerals	Sag 2 Pit 3	68.6445	-149.4306	0.71276	Keller et al., 2007
2186	NS-104.04	Minerals	Sag 2 Pit 3	68.6445	-149.4306	0.71240	Keller et al., 2007
Analysis ID	*Sample ID*	*Type*	*Location*	*Latitude*	*Longitude*	*87Sr/86Sr*	*Citation*
2187	NS-104.05	Minerals	Sag 2 Pit 3	68.6445	-149.4306	0.71287	Keller et al., 2007

Table 2.S2 continued.

2188	NS-104.06	Minerals	Sag 2 Pit 3	68.6445	-149.4306	0.71204	Keller et al., 2007
2189	NS-105.01	Minerals	Sag 1 Pit 2	68.6178	-149.3231	0.71653	Keller et al., 2007
2190	NS-105.02	Minerals	Sag 1 Pit 2	68.6178	-149.3231	0.71423	Keller et al., 2007
2191	NS-105.03	Minerals	Sag 1 Pit 2	68.6178	-149.3231	0.71444	Keller et al., 2007
2192	NS-105.04	Minerals	Sag 1 Pit 2	68.6178	-149.3231	0.71345	Keller et al., 2007
2193	NS-105.05	Minerals	Sag 1 Pit 2	68.6178	-149.3231	0.71321	Keller et al., 2007
2194	NS-106.01	Minerals	Sag 1 Pit 3	68.6517	-149.3071	0.71718	Keller et al., 2007
2195	NS-106.02	Minerals	Sag 1 Pit 3	68.6517	-149.3071	0.71546	Keller et al., 2007
2196	NS-106.03	Minerals	Sag 1 Pit 3	68.6517	-149.3071	0.71487	Keller et al., 2007
2197	NS-106.04	Minerals	Sag 1 Pit 3	68.6517	-149.3071	0.71376	Keller et al., 2007
2198	NS-106.05	Minerals	Sag 1 Pit 3	68.6517	-149.3071	0.71308	Keller et al., 2007
2199	NS-107.01	Minerals	lt3 Pit 2	68.5135	-149.4467	0.71066	Keller et al., 2007
2200	NS-107.02	Minerals	lt3 Pit 2	68.5135	-149.4467	0.71318	Keller et al., 2007
2201	NS-107.03	Minerals	lt3 Pit 2	68.5135	-149.4467	0.71290	Keller et al., 2007
2202	NS-107.04	Minerals	lt3 Pit 2	68.5135	-149.4467	0.71295	Keller et al., 2007
2203	NS-107.05	Minerals	lt3 Pit 2	68.5135	-149.4467	0.71368	Keller et al., 2007
2204	NS-108.01	Minerals	lt3 Pit 3	68.5117	-149.4661	0.71167	Keller et al., 2007
2205	NS-108.02	Minerals	lt3 Pit 3	68.5117	-149.4661	0.71291	Keller et al., 2007
2206	NS-108.03	Minerals	lt3 Pit 3	68.5117	-149.4661	0.71256	Keller et al., 2007

Table 2.S2 continued.

Analysis ID	*Sample ID*	*Type*	*Location*	*Latitude*	*Longitude*	*87Sr/86Sr*	*Citation*
2208	NS-108.05	Minerals	lt3 Pit 3	68.5117	-149.4661	0.71445	Keller et al., 2007
2209	NS-108.06	Minerals	lt3 Pit 3	68.5117	-149.4661	0.71359	Keller et al., 2007
2210	NS-109.01	Minerals	lt2 Pit 2	68.6343	-149.6415	0.70978	Keller et al., 2007
2211	NS-109.02	Minerals	lt2 Pit 2	68.6343	-149.6415	0.70990	Keller et al., 2007
2212	NS-109.03	Minerals	lt2 Pit 2	68.6343	-149.6415	0.71050	Keller et al., 2007
2213	NS-109.04	Minerals	lt2 Pit 2	68.6343	-149.6415	0.71010	Keller et al., 2007
2214	NS-109.05	Minerals	lt2 Pit 2	68.6343	-149.6415	0.71046	Keller et al., 2007
2215	NS-110.01	Minerals	lt2 Pit 3	68.6414	-149.5995	0.70957	Keller et al., 2007
2216	NS-110.02	Minerals	lt2 Pit 3	68.6414	-149.5995	0.70978	Keller et al., 2007
2217	NS-110.03	Minerals	lt2 Pit 3	68.6414	-149.5995	0.70947	Keller et al., 2007
2218	NS-110.04	Minerals	lt2 Pit 3	68.6414	-149.5995	0.70946	Keller et al., 2007
2219	NS-110.05	Minerals	lt2 Pit 3	68.6414	-149.5995	0.71000	Keller et al., 2007
2220	NS-112.01	Minerals	neo 1 pit 1	68.3641	-149.5262	0.71166	Keller et al., 2007
2221	NS-112.02	Minerals	neo 1 pit 1	68.3641	-149.5262	0.71277	Keller et al., 2007
2222	NS-113.01	Minerals	neo 2 pit 1	68.3506	-149.5376	0.71174	Keller et al., 2007
2223	NS-113.02	Minerals	neo 2 pit 1	68.3506	-149.5376	0.70985	Keller et al., 2007
2224	NS-113.03	Minerals	neo 2 pit 1	68.3506	-149.5376	0.71066	Keller et al., 2007
2225	NS-113.04	Minerals	neo 2 pit 1	68.3506	-149.5376	0.71156	Keller et al., 2007

Table 2.S2 continued.

Analysis ID	*Sample ID*	*Type*	*Location*	*Latitude*	*Longitude*	*87Sr/86Sr*	*Citation*
2227	NS-114.02	Minerals	neo 3 pit 1	68.3776	-149.5216	0.70845	Keller et al., 2007
2228	NS-114.03	Minerals	neo 3 pit 1	68.3776	-149.5216	0.70936	Keller et al., 2007
2229	NS-114.04	Minerals	neo 3 pit 1	68.3776	-149.5216	0.70939	Keller et al., 2007
2230	NS-119.01	Minerals	Anak Pit 3	68.9070	-149.3841	0.70876	Keller et al., 2007
2231	NS-119.02	Minerals	Anak Pit 3	68.9070	-149.3841	0.70906	Keller et al., 2007
2232	NS-119.03	Minerals	Anak Pit 3	68.9070	-149.3841	0.70858	Keller et al., 2007
2233	NS-119.04	Minerals	Anak Pit 3	68.9070	-149.3841	0.70824	Keller et al., 2007
2234	NS-119.05	Minerals	Anak Pit 3	68.9070	-149.3841	0.70835	Keller et al., 2007
2235	NS-119.06	Minerals	Anak Pit 3	68.9070	-149.3841	0.70843	Keller et al., 2007
2236	NS-121.02	Minerals	Ice Lens Melt-Out	68.6924	-149.2033	0.71163	Keller et al., 2007
2237	NS-121.03	Minerals	Ice Lens Melt-Out	68.6924	-149.2033	0.71107	Keller et al., 2007
2238	NS-122.01	Minerals	Gunsight Pit 1	69.2663	-148.9047	0.71063	Keller et al., 2007
2239	NS-122.02	Minerals	Gunsight Pit 1	69.2663	-148.9047	0.71187	Keller et al., 2007
2240	NS-122.03	Minerals	Gunsight Pit 1	69.2663	-148.9047	0.71104	Keller et al., 2007
2241	NS-122.04	Minerals	Gunsight Pit 1	69.2663	-148.9047	0.71084	Keller et al., 2007
2242	NS-122.05	Minerals	Gunsight Pit 1	69.2663	-148.9047	0.70952	Keller et al., 2007
2243	NS-122.06	Minerals	Gunsight Pit 1	69.2663	-148.9047	0.70968	Keller et al., 2007
2244	NS-122.07	Minerals	Gunsight Pit 1	69.2663	-148.9047	0.70908	Keller et al., 2007

Table 2.S2 continued.

Analysis ID	*Sample ID*	*Type*	*Location*	*Latitude*	*Longitude*	*87Sr/86Sr*	*Citation*
2246	NS-13.14	Minerals	lt2pit	68.6412	-149.6030	0.71047	Keller et al., 2007
2247	NS-13.15	Minerals	lt2pit	68.6412	-149.6030	0.71006	Keller et al., 2007
2248	NS-13.16	Minerals	lt2pit	68.6412	-149.6030	0.70963	Keller et al., 2007
2249	NS-13.23	Minerals	lt2pit	68.6412	-149.6030	0.70923	Keller et al., 2007
2250	NS-22.07	Plant	200 m from Dalton Highway on the Sag 2 glacial surface	68.6445	-149.4504	0.71535	Keller et al., 2007
2251	NS-22.07b	Plant	200 m from Dalton Highway on the Sag 2 glacial surface	68.6445	-149.4504	0.71660	Keller et al., 2007
2252	NS-22.08	Minerals	Sag 2 pit	68.6425	-149.4591	0.71370	Keller et al., 2007
2253	NS-22.08 HNO3 leach	Minerals	200 m from Dalton Highway on the Sag 2 glacial surface	68.6445	-149.4504	0.71370	Keller et al., 2007
2254	NS-22.09	Minerals	Sag 2 pit	68.6425	-149.4592	0.71278	Keller et al., 2007
2255	NS-22.09 HNO3 leach	Minerals	200 m from Dalton Highway on the Sag 2 glacial surface	68.6445	-149.4504	0.71278	Keller et al., 2007
2256	NS-22.10	Minerals	Sag 2 pit	68.6425	-149.4592	0.71330	Keller et al., 2007
2257	NS-22.10 HNO3 leach	Minerals	200 m from Dalton Highway on the Sag 2 glacial surface	68.6445	-149.4504	0.71330	Keller et al., 2007
2258	NS-22.11	Minerals	Sag 2 pit	68.6425	-149.4592	0.71198	Keller et al., 2007
2259	NS-22.11 HNO3 leach	Minerals	200 m from Dalton Highway on the Sag 2 glacial surface	68.6445	-149.4504	0.71198	Keller et al., 2007
2260	NS-22.22	Plant	200 m from Dalton Highway on the Sag 2 glacial surface	68.6445	-149.4504	0.71366	Keller et al., 2007

Table 2.S2 continued.

Analysis ID	*Sample ID*	*Type*	*Location*	*Latitude*	*Longitude*	*87Sr/86Sr*	*Citation*
2263	NS-22.25	Plant	200 m from Dalton Highway on the Sag 2 glacial surface	68.6445	-149.4504	0.71578	Keller et al., 2007
2264	NS-22.26	Minerals	Sag 2 pit b/w pit and road-50 m south of the road	68.6554	-149.4584	0.70994	Keller et al., 2007
2265	NS-22.26 HNO3 leach	Minerals	50 m from Dalton Highway on the Sag 2 glacial surface	68.6458	-149.4512	0.70994	Keller et al., 2007
2266	NS-22.27	Minerals	Sag 2 pit b/w pit and road-50 m south of the road	68.6554	-149.4584	0.71250	Keller et al., 2007
2267	NS-22.27 HNO3 leach	Minerals	50 m from Dalton Highway on the Sag 2 glacial surface	68.6458	-149.4512	0.71250	Keller et al., 2007
2268	NS-22.30	Plant	50 m from Dalton Highway on the Sag 2 glacial surface	68.6458	-149.4512	0.71131	Keller et al., 2007
2269	NS-22.31	Plant	50 m from Dalton Highway on the Sag 2 glacial surface	68.6458	-149.4512	0.71179	Keller et al., 2007
2270	NS-22.32	Plant	50 m from Dalton Highway on the Sag 2 glacial surface	68.6458	-149.4512	0.71157	Keller et al., 2007
2271	NS-22.33	Plant	50 m from Dalton Highway on the Sag 2 glacial surface	68.6458	-149.4512	0.71157	Keller et al., 2007
2272	NS-22.33b	Plant	50 m from Dalton Highway on the Sag 2 glacial surface	68.6458	-149.4512	0.71276	Keller et al., 2007
2273	NS-22.34	Plant	250 m from Dalton Highway on the Sag 2 glacial surface	68.6441	-149.4501	0.71338	Keller et al., 2007
2274	NS-22.35	Plant	250 m from Dalton Highway on the Sag 2 glacial surface	68.6441	-149.4501	0.71414	Keller et al., 2007

Table 2.S2 continued.

Analysis ID	*Sample ID*	*Type*	*Location*	*Latitude*	*Longitude*	*87Sr/86Sr*	*Citation*
2276	NS-22.37	Plant	250 m from Dalton Highway on the Sag 2 glacial surface	68.6441	-149.4501	0.71400	Keller et al., 2007
2277	NS-22.38 (average of 2 reruns)	Plant	250 m from Dalton Highway on the Sag 2 glacial surface	68.6441	-149.4501	0.71310	Keller et al., 2007
2278	NS-22.39	Plant	250 m from Dalton Highway on the Sag 2 glacial surface	68.6441	-149.4501	0.71413	Keller et al., 2007
2279	NS-23A.06	Minerals	Imnavait lower slope pit	68.6485	-149.3479	0.71124	Keller et al., 2007
2280	NS-23A.07	Minerals	Imnavait lower slope pit	68.6485	-149.3479	0.71110	Keller et al., 2007
2281	NS-23A.08	Minerals	Imnavait lower slope pit	68.6485	-149.3479	0.71072	Keller et al., 2007
2282	NS-23A.09	Minerals	Imnavait lower slope pit	68.6485	-149.3479	0.71056	Keller et al., 2007
2283	NS-23B.06	Minerals	Imnavait middle slope pit	68.6342	-149.3341	0.71129	Keller et al., 2007
2284	NS-23B.07	Minerals	Imnavait middle slope pit	68.6342	-149.3341	0.71005	Keller et al., 2007
2285	NS-23B.08	Minerals	Imnavait middle slope pit	68.6342	-149.3341	0.70981	Keller et al., 2007
2286	NS-23C.06	Minerals	Imnavait upper slope pit	68.6234	-149.3214	0.71143	Keller et al., 2007
2287	NS-23C.07	Minerals	Imnavait upper slope pit	68.6234	-149.3214	0.71086	Keller et al., 2007
2288	NS-23C.08	Minerals	Imnavait upper slope pit	68.6234	-149.3214	0.71045	Keller et al., 2007
2289	NS-23D.07	Minerals	Imnavait crest pit	68.6205	-149.3080	0.70994	Keller et al., 2007
2290	NS-23D.08	Minerals	Imnavait crest pit	68.6205	-149.3080	0.70948	Keller et al., 2007
2291	NS-23D.09	Minerals	Imnavait crest pit	68.6205	-149.3080	0.70887	Keller et al., 2007

Table 2.S2 continued.

Analysis ID	*Sample ID*	*Type*	*Location*	*Latitude*	*Longitude*	*87Sr/86Sr*	*Citation*
2293	NS-28.07	Minerals	lt3 Pit	68.4978	-149.4833	0.71771	Keller et al., 2007
2294	NS-28.08	Minerals	lt3 Pit	68.4978	-149.4833	0.71396	Keller et al., 2007
2295	NS-28.09	Minerals	lt3 Pit	68.4978	-149.4833	0.71667	Keller et al., 2007
2296	NS-28.10	Minerals	lt3 Pit	68.4978	-149.4833	0.71367	Keller et al., 2007
2297	NS-29.01	Minerals	Imnavait bedrock pit	68.6187	-149.3162	0.70782	Keller et al., 2007
2298	NS-37.06	Minerals	Acidic vegetation pit on lt2 surface	68.6413	-149.6285	0.71605	Keller et al., 2007
2299	NS-37.07	Minerals	Acidic vegetation pit on lt2 surface	68.6413	-149.6285	0.71088	Keller et al., 2007
2300	NS-37.08	Minerals	Acidic vegetation pit on lt2 surface	68.6413	-149.6285	0.71149	Keller et al., 2007
2301	NS-38.08	Minerals	Non-acidic vegetation pit on lt2 surface	68.6414	-149.6279	0.71166	Keller et al., 2007
2302	NS-38.09	Minerals	Non-acidic vegetation pit on lt2 surface	68.6414	-149.6279	0.71010	Keller et al., 2007
2303	NS-38.10	Minerals	Non-acidic vegetation pit on lt2 surface	68.6414	-149.6279	0.70993	Keller et al., 2007
2304	NS-47.03	Minerals	Sag 2 E5 10 m from road	68.6425	-149.4591	0.71219	Keller et al., 2007
2305	NS-47.03 HNO3 leach	Minerals	10 m from Dalton Highway on the Sag 2 glacial surface	68.6461	-149.4515	0.71219	Keller et al., 2007
2306	NS-47.04	Minerals	Sag2 E5 10 m from road	68.6425	-149.4591	0.71220	Keller et al., 2007
2307	NS-47.04 HNO3 leach	Minerals	10 m from Dalton Highway on the Sag 2 glacial surface	68.6461	-149.4515	0.71220	Keller et al., 2007

Table 2.S2 continued.

Analysis ID	*Sample ID*	*Type*	*Location*	*Latitude*	*Longitude*	*87Sr/86Sr*	*Citation*
2308	NS-47.05	Plant	10 m from Dalton Highway on the Sag 2 glacial surface	68.6461	-149.4515	0.71415	Keller et al., 2007
2309	NS-47.06	Plant	10 m from Dalton Highway on the Sag 2 glacial surface	68.6461	-149.4515	0.71261	Keller et al., 2007
2310	NS-47.07	Plant	10 m from Dalton Highway on the Sag 2 glacial surface	68.6461	-149.4515	0.71128	Keller et al., 2007
2311	NS-47.08	Plant	10 m from Dalton Highway on the Sag 2 glacial surface	68.6461	-149.4515	0.71097	Keller et al., 2007
2312	NS-48.01	Minerals	middle of Dalton Highway, mile 287	68.6425	-149.4591	0.70841	Keller et al., 2007
2313	1993-0338	Water	Toolik Inlet Stream	68.6256	-149.5961	0.71214	Keller et al., 2007
2314	1993-1386	Water	Toolik Inlet Stream	68.6256	-149.5961	0.71223	Keller et al., 2007
2315	1994-0371	Water	Toolik Inlet Stream	68.6256	-149.5961	0.71226	Keller et al., 2007
2316	1994-0434	Water	Toolik Inlet Stream	68.6256	-149.5961	0.71225	Keller et al., 2007
2317	1994-0489	Water	Toolik Inlet Stream	68.6256	-149.5961	0.71227	Keller et al., 2007
2318	1994-0603	Water	Toolik Inlet Stream	68.6256	-149.5961	0.71220	Keller et al., 2007
2319	1994-0655	Water	Toolik Inlet Stream	68.6256	-149.5961	0.71235	Keller et al., 2007
2320	1994-0718	Water	Toolik Inlet Stream	68.6256	-149.5961	0.71218	Keller et al., 2007
2321	1994-0776	Water	Toolik Inlet Stream	68.6256	-149.5961	0.71205	Keller et al., 2007
2322	1994-0882	Water	Toolik Inlet Stream	68.6256	-149.5961	0.71221	Keller et al., 2007
2323	1994-0927	Water	Toolik Inlet Stream	68.6256	-149.5961	0.71212	Keller et al., 2007
2324	1994-1040	Water	Toolik Inlet Stream	68.6256	-149.5961	0.71223	Keller et al., 2007

Table 2.S2 continued.

Analysis ID	*Sample ID*	*Type*	*Location*	*Latitude*	*Longitude*	*87Sr/86Sr*	*Citation*
2326	1994-1152	Water	Toolik Inlet Stream	68.6256	-149.5961	0.71213	Keller et al., 2007
2327	1994-1214	Water	Toolik Inlet Stream	68.6256	-149.5961	0.71227	Keller et al., 2007
2328	1996-0002	Water	Toolik Inlet Stream	68.6256	-149.5961	0.71215	Keller et al., 2007
2329	1996-0019	Water	Toolik Inlet Stream	68.6256	-149.5961	0.71216	Keller et al., 2007
2330	1996-0023	Water	Toolik Inlet Stream	68.6256	-149.5961	0.71221	Keller et al., 2007
2331	1996-0024	Water	Toolik Inlet Stream	68.6256	-149.5961	0.71239	Keller et al., 2007
2332	1996-0033	Water	Toolik Inlet Stream	68.6256	-149.5961	0.71248	Keller et al., 2007
2333	1996-0071	Water	Toolik Inlet Stream	68.6256	-149.5961	0.71251	Keller et al., 2007
2334	1996-0074	Water	Toolik Inlet Stream	68.6256	-149.5961	0.71250	Keller et al., 2007
2335	1996-0077	Water	Toolik Inlet Stream	68.6256	-149.5961	0.71245	Keller et al., 2007
2336	1996-0081	Water	Toolik Inlet Stream	68.6256	-149.5961	0.71245	Keller et al., 2007
2337	1996-0088	Water	Toolik Inlet Stream	68.6256	-149.5961	0.71251	Keller et al., 2007
2338	1996-0095	Water	Toolik Inlet Stream	68.6256	-149.5961	0.71244	Keller et al., 2007
2339	1996-0192	Water	Toolik Inlet Stream	68.6256	-149.5961	0.71216	Keller et al., 2007
2340	1996-0231	Water	Toolik Inlet Stream	68.6256	-149.5961	0.71214	Keller et al., 2007
2341	1996-0234	Water	Toolik Inlet Stream	68.6256	-149.5961	0.71209	Keller et al., 2007
2342	1996-0312	Water	Toolik Inlet Stream	68.6256	-149.5961	0.71206	Keller et al., 2007
2343	1996-0332	Water	Toolik Inlet Stream	68.6256	-149.5961	0.71194	Keller et al., 2007
2344	1996-0389	Water	Toolik Inlet Stream	68.6256	-149.5961	0.71218	Keller et al., 2007

Table 2.S2 continued.

Analysis ID	*Sample ID*	*Type*	*Location*	*Latitude*	*Longitude*	*87Sr/86Sr*	*Citation*
2345	1996-0389.1	Water	Toolik Inlet Stream	68.6256	-149.5961	0.71225	Keller et al., 2007
2346	1996-0469	Water	Toolik Inlet Stream	68.6256	-149.5961	0.71210	Keller et al., 2007
2347	1996-0502	Water	Toolik Inlet Stream	68.6256	-149.5961	0.71206	Keller et al., 2007
2348	1996-0524	Water	Toolik Inlet Stream	68.6256	-149.5961	0.71218	Keller et al., 2007
2349	1996-0638	Water	Toolik Inlet Stream	68.6256	-149.5961	0.71199	Keller et al., 2007
2350	1996-0724	Water	Toolik Inlet Stream	68.6256	-149.5961	0.71197	Keller et al., 2007
2351	1996-0737	Water	Toolik Inlet Stream	68.6256	-149.5961	0.71195	Keller et al., 2007
2352	1996-0798	Water	Toolik Inlet Stream	68.6256	-149.5961	0.71192	Keller et al., 2007
2353	1996-0824	Water	Toolik Inlet Stream	68.6256	-149.5961	0.71256	Keller et al., 2007
2354	1996-0832	Water	Toolik Inlet Stream	68.6256	-149.5961	0.71224	Keller et al., 2007
2355	1997-0001	Water	Toolik Inlet Stream	68.6256	-149.5961	0.71237	Keller et al., 2007
2356	1997-0012	Water	Toolik Inlet Stream	68.6256	-149.5961	0.71237	Keller et al., 2007
2357	1997-0065	Water	Toolik Inlet Stream	68.6256	-149.5961	0.71239	Keller et al., 2007
2358	1997-0094	Water	Toolik Inlet Stream	68.6256	-149.5961	0.71229	Keller et al., 2007
2359	1997-0163	Water	Toolik Inlet Stream	68.6256	-149.5961	0.71201	Keller et al., 2007
2360	1997-0265	Water	Toolik Inlet Stream	68.6256	-149.5961	0.71210	Keller et al., 2007
2361	1997-0455	Water	Toolik Inlet Stream	68.6256	-149.5961	0.71207	Keller et al., 2007
2362	1997-0547	Water	Toolik Inlet Stream	68.6256	-149.5961	0.71215	Keller et al., 2007
2363	1997-0641	Water	Toolik Inlet Stream	68.6256	-149.5961	0.71200	Keller et al., 2007

Table 2.S2 continued.

Analysis ID	*Sample ID*	*Type*	*Location*	*Latitude*	*Longitude*	*87Sr/86Sr*	*Citation*
2364	1997-0807	Water	Toolik Inlet Stream	68.6256	-149.5961	0.71232	Keller et al., 2007
2365	1997-0810	Water	Toolik Inlet Stream	68.6256	-149.5961	0.71222	Keller et al., 2007
2366	1997-0831	Water	Toolik Inlet Stream	68.6256	-149.5961	0.71216	Keller et al., 2007
2367	1998-0001	Water	Toolik Inlet Stream	68.6256	-149.5961	0.71211	Keller et al., 2007
2368	1998-0025	Water	Toolik Inlet Stream	68.6256	-149.5961	0.71224	Keller et al., 2007
2369	1998-0123	Water	Toolik Inlet Stream	68.6256	-149.5961	0.71202	Keller et al., 2007
2370	1998-0222	Water	Toolik Inlet Stream	68.6256	-149.5961	0.71202	Keller et al., 2007
2371	1998-0335	Water	Toolik Inlet Stream	68.6256	-149.5961	0.71190	Keller et al., 2007
2372	1998-0400	Water	Toolik Inlet Stream	68.6256	-149.5961	0.71187	Keller et al., 2007
2373	1998-0464	Water	Toolik Inlet Stream	68.6256	-149.5961	0.71184	Keller et al., 2007
2374	1998-0608	Water	Toolik Inlet Stream	68.6256	-149.5961	0.71205	Keller et al., 2007
2375	1998-0639	Water	Toolik Inlet Stream	68.6256	-149.5961	0.71210	Keller et al., 2007
2376	1998-0686	Water	Toolik Inlet Stream	68.6256	-149.5961	0.71201	Keller et al., 2007
2377	1999-0075	Water	Toolik Inlet Stream	68.6256	-149.5961	0.71212	Keller et al., 2007
2378	1999-0080	Water	Toolik Inlet Stream	68.6256	-149.5961	0.71206	Keller et al., 2007
2379	1999-0125	Water	Toolik Inlet Stream	68.6256	-149.5961	0.71199	Keller et al., 2007
2380	1999-0251	Water	Toolik Inlet Stream	68.6256	-149.5961	0.71193	Keller et al., 2007
2381	1999-0282	Water	Toolik Inlet Stream	68.6256	-149.5961	0.71202	Keller et al., 2007
2382	1999-0385	Water	Toolik Inlet Stream	68.6256	-149.5961	0.71200	Keller et al., 2007

Table 2.S2 continued.

Analysis ID	*Sample ID*	*Type*	*Location*	*Latitude*	*Longitude*	*87Sr/86Sr*	*Citation*
2383	1999-0613	Water	Toolik Inlet Stream	68.6256	-149.5961	0.71200	Keller et al., 2007
2384	1999-0682	Water	Toolik Inlet Stream	68.6256	-149.5961	0.71193	Keller et al., 2007
2385	1999-0734	Water	Toolik Inlet Stream	68.6256	-149.5961	0.71187	Keller et al., 2007
2386	1999-0806	Water	Toolik Inlet Stream	68.6256	-149.5961	0.71202	Keller et al., 2007
2387	1999-0827	Water	Toolik Inlet Stream	68.6256	-149.5961	0.71205	Keller et al., 2007
2388	2000-0017	Water	Toolik Inlet Stream	68.6256	-149.5961	0.71218	Keller et al., 2007
2389	2000-0099	Water	Toolik Inlet Stream	68.6256	-149.5961	0.71208	Keller et al., 2007
2390	2000-0181	Water	Toolik Inlet Stream	68.6256	-149.5961	0.71208	Keller et al., 2007
2391	2000-0227	Water	Toolik Inlet Stream	68.6256	-149.5961	0.71219	Keller et al., 2007
2392	2000-0308	Water	Toolik Inlet Stream	68.6256	-149.5961	0.71202	Keller et al., 2007
2393	2000-0434	Water	Toolik Inlet Stream	68.6256	-149.5961	0.71201	Keller et al., 2007
2394	2000-0501	Water	Toolik Inlet Stream	68.6256	-149.5961	0.71168	Keller et al., 2007
2395	2000-0539	Water	Toolik Inlet Stream	68.6256	-149.5961	0.71192	Keller et al., 2007
2396	2000-0580	Water	Toolik Inlet Stream	68.6256	-149.5961	0.71185	Keller et al., 2007
2397	2000-0655	Water	Toolik Inlet Stream	68.6256	-149.5961	0.71201	Keller et al., 2007
2398	2001-0136	Water	Toolik Inlet Stream	68.6256	-149.5961	0.71201	Keller et al., 2007
2399	2001-0220	Water	Toolik Inlet Stream	68.6256	-149.5961	0.71210	Keller et al., 2007
2400	2001-0232	Water	Toolik Inlet Stream	68.6256	-149.5961	0.71206	Keller et al., 2007
2401	2001-0249	Water	Toolik Inlet Stream	68.6256	-149.5961	0.71214	Keller et al., 2007

Table 2.S2 continued.

Analysis ID	*Sample ID*	*Type*	*Location*	*Latitude*	*Longitude*	*87Sr/86Sr*	*Citation*
2402	2001-0377	Water	Toolik Inlet Stream	68.6256	-149.5961	0.71198	Keller et al., 2007
2403	2001-0444	Water	Toolik Inlet Stream	68.6256	-149.5961	0.71199	Keller et al., 2007
2404	2001-0529	Water	Toolik Inlet Stream	68.6256	-149.5961	0.71209	Keller et al., 2007
2405	2001-0554	Water	Toolik Inlet Stream	68.6256	-149.5961	0.71215	Keller et al., 2007
2406	2001-0630	Water	Toolik Inlet Stream	68.6256	-149.5961	0.71211	Keller et al., 2007
2407	2001-0696	Water	Toolik Inlet Stream	68.6256	-149.5961	0.71207	Keller et al., 2007
2408	2002-0040	Water	Toolik Inlet Stream	68.6256	-149.5961	0.71209	Keller et al., 2007
2409	2002-0094	Water	Toolik Inlet Stream	68.6256	-149.5961	0.71212	Keller et al., 2007
2410	2002-0150	Water	Toolik Inlet Stream	68.6256	-149.5961	0.71216	Keller et al., 2007
2411	2002-0218	Water	Toolik Inlet Stream	68.6256	-149.5961	0.71217	Keller et al., 2007
2412	2002-0301	Water	Toolik Inlet Stream	68.6256	-149.5961	0.71211	Keller et al., 2007
2413	2002-0377	Water	Toolik Inlet Stream	68.6256	-149.5961	0.71209	Keller et al., 2007
2414	2002-0421	Water	Toolik Inlet Stream	68.6256	-149.5961	0.71206	Keller et al., 2007
2415	2002-0521	Water	Toolik Inlet Stream	68.6256	-149.5961	0.71197	Keller et al., 2007
2416	2002-0576	Water	Toolik Inlet Stream	68.6256	-149.5961	0.71187	Keller et al., 2007
2417	2002-0659	Water	Toolik Inlet Stream	68.6256	-149.5961	0.71194	Keller et al., 2007
2418	2002-0703	Water	Toolik Inlet Stream	68.6256	-149.5961	0.71189	Keller et al., 2007
2419	2003-0047	Water	Toolik Inlet Stream	68.6256	-149.5961	0.71192	Keller et al., 2007
2420	2003-0239	Water	Toolik Inlet Stream	68.6256	-149.5961	0.71211	Keller et al., 2007

Table 2.S2 continued.

Analysis ID	*Sample ID*	*Type*	*Location*	*Latitude*	*Longitude*	*87Sr/86Sr*	*Citation*
2421	2003-0245	Water	Toolik Inlet Stream	68.6256	-149.5961	0.71205	Keller et al., 2007
2422	2003-0251	Water	Toolik Inlet Stream	68.6256	-149.5961	0.71213	Keller et al., 2007
2423	2003-0257	Water	Toolik Inlet Stream	68.6256	-149.5961	0.71217	Keller et al., 2007
2424	2003-0275	Water	Toolik Inlet Stream	68.6256	-149.5961	0.71220	Keller et al., 2007
2425	2003-0281	Water	Toolik Inlet Stream	68.6256	-149.5961	0.71224	Keller et al., 2007
2426	2003-0310	Water	Toolik Inlet Stream	68.6256	-149.5961	0.71205	Keller et al., 2007
2427	2003-0334	Water	Toolik Inlet Stream	68.6256	-149.5961	0.71221	Keller et al., 2007
2428	2003-0358	Water	Toolik Inlet Stream	68.6256	-149.5961	0.71210	Keller et al., 2007
2429	2003-0473	Water	Toolik Inlet Stream	68.6256	-149.5961	0.71195	Keller et al., 2007
2430	2003-0474	Water	Toolik Inlet Stream	68.6256	-149.5961	0.71192	Keller et al., 2007
2431	2003-0475	Water	Toolik Inlet Stream	68.6256	-149.5961	0.71184	Keller et al., 2007
2432	2003-0478	Water	Toolik Inlet Stream	68.6256	-149.5961	0.71185	Keller et al., 2007
2433	2003-0478	Water	Toolik Inlet Stream	68.6256	-149.5961	0.71198	Keller et al., 2007
2434	2003-0480	Water	Toolik Inlet Stream	68.6256	-149.5961	0.71216	Keller et al., 2007
2435	2003-0481	Water	Toolik Inlet Stream	68.6256	-149.5961	0.71219	Keller et al., 2007
2436	2003-0482	Water	Toolik Inlet Stream	68.6256	-149.5961	0.71225	Keller et al., 2007
2437	2003-0488	Water	Toolik Inlet Stream	68.6256	-149.5961	0.71225	Keller et al., 2007
2438	2003-0492	Water	Toolik Inlet Stream	68.6256	-149.5961	0.71243	Keller et al., 2007
2439	2003-0499	Water	Toolik Inlet Stream	68.6256	-149.5961	0.71242	Keller et al., 2007

Table 2.S2 continued.

Analysis ID	*Sample ID*	*Type*	*Location*	*Latitude*	*Longitude*	*87Sr/86Sr*	*Citation*
2440	2003-0500	Water	Toolik Inlet Stream	68.6256	-149.5961	0.71247	Keller et al., 2007
2441	2003-0507	Water	Toolik Inlet Stream	68.6256	-149.5961	0.71245	Keller et al., 2007
2442	2003-0529	Water	Toolik Inlet Stream	68.6256	-149.5961	0.71228	Keller et al., 2007
2443	2003-0539	Water	Toolik Inlet Stream	68.6256	-149.5961	0.71220	Keller et al., 2007
2444	2003-0760	Water	Toolik Inlet Stream	68.6256	-149.5961	0.71228	Keller et al., 2007
2445	2003-0841	Water	Toolik Inlet Stream	68.6256	-149.5961	0.71228	Keller et al., 2007
2446	2004-0130	Water	Toolik Inlet Stream	68.6256	-149.5961	0.71183	Keller et al., 2007
2447	2004-0178	Water	Toolik Inlet Stream	68.6256	-149.5961	0.71181	Keller et al., 2007
2448	2004-0179	Water	Toolik Inlet Stream	68.6256	-149.5961	0.71181	Keller et al., 2007
2449	2004-0238	Water	Toolik Inlet Stream	68.6256	-149.5961	0.71180	Keller et al., 2007
2450	2004-0296	Water	Toolik Inlet Stream	68.6256	-149.5961	0.71187	Keller et al., 2007
2451	2004-0344	Water	Toolik Inlet Stream	68.6256	-149.5961	0.71200	Keller et al., 2007
2452	2004-0345	Water	Toolik Inlet Stream	68.6256	-149.5961	0.71202	Keller et al., 2007
2453	2004-0404	Water	Toolik Inlet Stream	68.6256	-149.5961	0.71211	Keller et al., 2007
2454	2004-0462	Water	Toolik Inlet Stream	68.6256	-149.5961	0.71200	Keller et al., 2007
2455	2004-0510	Water	Toolik Inlet Stream	68.6256	-149.5961	0.71222	Keller et al., 2007
2456	2004-0511	Water	Toolik Inlet Stream	68.6256	-149.5961	0.71205	Keller et al., 2007
2457	2004-0570	Water	Toolik Inlet Stream	68.6256	-149.5961	0.71193	Keller et al., 2007
2458	2004-0628	Water	Toolik Inlet Stream	68.6256	-149.5961	0.71196	Keller et al., 2007

Table 2.S2 continued.

Analysis ID	*Sample ID*	*Type*	*Location*	*Latitude*	*Longitude*	*87Sr/86Sr*	*Citation*
2459	2005-tk1	Water	Toolik River Ice Lens Melt-out upstream	68.6924	-149.2033	0.71731	Keller et al., 2007
2460	2005-tk2	Water	Toolik River Ice Lens Melt-out downstream	68.6924	-149.2033	0.71529	Keller et al., 2007
2461	2005-tk3	Water	Toolik River Ice Lens Melt-out downstream	68.6924	-149.2033	0.71398	Keller et al., 2007
2462	2005-tk4	Water	Toolik River Ice Lens Melt-out downstream	68.6924	-149.2033	0.71419	Keller et al., 2007
2463	DH-101.01	Water	Bonanza Creek	66.6590	-150.5457	0.71344	Keller et al., 2007
2464	DH-130.01	Water	Yukon River	62.5986	-164.8000	0.71323	Keller et al., 2007
2465	KP-02.01	Water	Kanuti Stream	66.4748	-150.6651	0.70926	Keller et al., 2007
2466	NS-04.01	Water	E5 inlet S	68.6444	-149.4306	0.71641	Keller et al., 2007
2467	NS-04.02	Water	E5 inlet W	68.6450	-149.4600	0.71881	Keller et al., 2007
2468	NS-04.03	Water	E5 outlet	68.6461	-149.4556	0.71515	Keller et al., 2007
2469	NS-04.05	Water	E5 inlet S	68.6444	-149.4306	0.71633	Keller et al., 2007
2470	NS-07.01	Water	Imnavait weir	68.6170	-149.3179	0.71719	Keller et al., 2007
2471	NS-07.04	Water	Imnavait site 4	68.6234	-149.3214	0.71653	Keller et al., 2007
2472	NS-07.05	Water	Imnavait weir	68.6170	-149.3179	0.71691	Keller et al., 2007
2473	NS-07.21	Water	Imnavait weir	68.6170	-149.3179	0.71695	Keller et al., 2007
2474	NS-08.20	Water	lt 1 pit	68.6255	-149.5774	0.71959	Keller et al., 2007
2475	NS-101.15	Water	lt1 pit2 lysimeter	68.6251	-149.5718	0.71754	Keller et al., 2007

Table 2.S2 continued.

Analysis ID	*Sample ID*	*Type*	*Location*	*Latitude*	*Longitude*	*87Sr/86Sr*	*Citation*
2477	NS-103.13	Water	Sag 2 Pit 2	68.6451	-149.4352	0.71538	Keller et al., 2007
2478	NS-103.14	Water	Sag 2 Pit 2	68.6451	-149.4352	0.71367	Keller et al., 2007
2479	NS-105.11	Water	Sag 1 Pit 2	68.6178	-149.3231	0.71613	Keller et al., 2007
2480	NS-105.12	Water	Sag 1 Pit 2	68.6178	-149.3231	0.71556	Keller et al., 2007
2481	NS-110.16	Water	lt2 Pit 3	68.6414	-149.5995	0.70954	Keller et al., 2007
2482	NS-110.17	Water	lt 2 Pit 3	68.6414	-149.5995	0.70951	Keller et al., 2007
2483	NS-112.05	Water	upper glacier stream near neo pit 1	68.3641	-149.5262	0.71730	Keller et al., 2007
2484	NS-115.01	Water	middle glacier stream	68.3506	-149.5376	0.71823	Keller et al., 2007
2485	NS-116.01	Water	lower glacier stream	68.3776	-149.5216	0.71383	Keller et al., 2007
2486	NS-120.01	Water	Anak stream	68.9050	-149.3842	0.71242	Keller et al., 2007
2487	NS-125.01	Water	Gunsight stream	69.2764	-148.9274	0.71136	Keller et al., 2007
2488	NS-126.01	Water	Toolik River Ice Lens Melt-out upstream	68.6924	-149.2033	0.71734	Keller et al., 2007
2489	NS-127.01	Water	Toolik River Ice Lens Melt-out downstream	68.6924	-149.2033	0.71312	Keller et al., 2007
2490	NS-129.01	Water	Underwillow stream	68.3342	-149.3200	0.71989	Keller et al., 2007
2491	NS-13.25	Water	lt2 pit/lysimeter	68.6412	-149.6030	0.71146	Keller et al., 2007
2495	NS-17.01	Water	N1 feeder stream	68.6412	-149.6107	0.71060	Keller et al., 2007
2496	NS-1OUT.08	Water	l1 outlet	68.5724	-149.5812	0.71502	Keller et al., 2007
2497	NS-20.01	Water	Roche Moutonee Creek	68.3739	-149.3101	0.71338	Keller et al., 2007

Table 2.S2 continued.

Analysis ID	*Sample ID*	*Type*	*Location*	*Latitude*	*Longitude*	*87Sr/86Sr*	*Citation*
2498	NS-20.21	Water	Roche Moutonee Creek	68.3739	-149.3101	0.71384	Keller et al., 2007
2499	NS-21.01	Water	lt 1 stream	68.6255	-149.5774	0.71100	Keller et al., 2007
2500	NS-25.01	Water	TW Lower Stream	68.6198	-149.6095	0.71331	Keller et al., 2007
2501	NS-30.01	Water	PMI Atigun feeder stream	68.4503	-149.3464	0.71055	Keller et al., 2007
2502	NS-31.01	Water	Atigun river	68.4614	-149.3279	0.71446	Keller et al., 2007
2503	NS-33.01	Water	It3 stream	68.4818	-149.4757	0.71039	Keller et al., 2007
2504	NS-35.01	Water	Sagavanirktok River	68.9585	-148.8591	0.71045	Keller et al., 2007
2505	NS-36.04	Water	Aufeis near Galbraith	68.4639	-149.5402	0.70880	Keller et al., 2007
2506	NS-39.01	Water	Island Lake	68.5200	-149.4917	0.71023	Keller et al., 2007
2507	NS-40.01	Water	Kuparuk	68.6471	-149.4086	0.70787	Keller et al., 2007
2508	NS-41.01	Water	Holden Creek	68.4074	-149.3194	0.70982	Keller et al., 2007
2509	NS-41.21	Water	Holden Creek	68.4074	-149.3194	0.70977	Keller et al., 2007
2510	NS-42.01	Water	Bad idea stream drains MDk only	68.3905	-149.3122	0.71123	Keller et al., 2007
2511	NS-42.21	Water	Bad idea stream	68.3905	-149.3122	0.71138	Keller et al., 2007
2512	NS-43.01	Water	Kuparuk upstream from dripper	68.6363	-149.4050	0.70788	Keller et al., 2007
2513	NS-44.01	Water	Atigun upstream	68.2144	-149.4070	0.71966	Keller et al., 2007
2514	NS-45.01	Water	Trevor Creek	68.2839	-149.3688	0.71486	Keller et al., 2007
2515	NS-45.21	Water	Trevor Creek	68.2839	-149.3688	0.71505	Keller et al., 2007
2516	NS-46.01	Water	Kayak Creek	68.4116	-149.3282	0.70847	Keller et al., 2007

Table 2.S2 continued.

Analysis ID	*Sample ID*	*Type*	*Location*	*Latitude*	*Longitude*	*87Sr/86Sr*	*Citation*
2517	NS-46.21	Water	Kayak stream	68.4116	-149.3282	0.70849	Keller et al., 2007
2518	NS-l1OUT.01	Water	l1 outlet	68.5724	-149.5812	0.71493	Keller et al., 2007
2519	NS-l2OUT.01	Water	l2 outlet	68.5727	-149.5705	0.71640	Keller et al., 2007
2520	NS-l2OUT.03	Water	l2 outlet	68.5727	-149.5705	0.71647	Keller et al., 2007
2521	NS-l2OUT.08	Water	l2 outlet	68.5727	-149.5705	0.71668	Keller et al., 2007
2522	NS-l4OUT.01	Water	l4 outlet	68.5815	-149.5864	0.71566	Keller et al., 2007
2523	NS-l4OUT.04	Water	l4 outlet	68.5815	-149.5864	0.71559	Keller et al., 2007
2524	NS-l6HWIN.01	Water	l6 headwater inlet	68.5790	-149.6225	0.71142	Keller et al., 2007
2525	NS-l6HWIN.08	Water	l6 headwater inlet	68.5790	-149.6225	0.71095	Keller et al., 2007
2526	NS-l6INE.08	Water	l6 inlet east	68.5802	-149.6195	0.71541	Keller et al., 2007
2527	NS-l6INEAST.01	Water	l5 into l6	68.5949	-149.5863	0.71536	Keller et al., 2007
2528	NS-l6INEAST.04	Water	l5 into l6	68.5949	-149.5863	0.71526	Keller et al., 2007
2529	NS-l6INWEST.01	Water	l6 HW into l6	68.5969	-149.6013	0.71132	Keller et al., 2007
2530	NS-l6INWEST.03	Water	l6 HW into l6	68.5969	-149.6013	0.71086	Keller et al., 2007
2531	NS-l6INWEST.08	Water	l6 HW into l6	68.5969	-149.6013	0.71126	Keller et al., 2007
2532	NS-l6WIN.04	Water	l6 headwater inlet	68.5790	-149.6225	0.71128	Keller et al., 2007
2533	NS-l7OUT.01	Water	l7 outlet	68.6020	-149.5969	0.71262	Keller et al., 2007
2534	NS-l7OUT.03	Water	l7 outlet	68.6020	-149.5969	0.71252	Keller et al., 2007
2535	NS-l8HW.01	Water	l8 headwater	68.5723	-149.5409	0.71346	Keller et al., 2007

Table 2.S2 continued.

Analysis ID	*Sample ID*	*Type*	*Location*	*Latitude*	*Longitude*	*87Sr/86Sr*	*Citation*
2536	NS-l8HW.08	Water	l8 headwater	68.5723	-149.5409	0.71255	Keller et al., 2007
2537	NS-l8IN.01	Water	l8 inlet	68.6085	-149.5876	0.71252	Keller et al., 2007
2538	NS-l8IN.03	Water	l8 inlet	68.6085	-149.5876	0.71221	Keller et al., 2007
2539	NS-l9INEAST.01	Water	l8 into l9	68.6184	-149.5965	0.71217	Keller et al., 2007
2540	NS-l9INEAST.03	Water	l8 into l9	68.6184	-149.5965	0.71202	Keller et al., 2007
2541	NS-l9INW.08	Water	l9 inlet west	68.6182	-149.5968	0.71254	Keller et al., 2007
2542	NS-l9INWEST.01	Water	l7 into l9	68.6182	-149.5968	0.71250	Keller et al., 2007
2543	NS-l9INWEST.03	Water	l7 into l9	68.6182	-149.5968	0.71214	Keller et al., 2007
2544	NS-l9OUT.01	Water	l9 outlet	68.6194	-149.5953	0.71225	Keller et al., 2007
2545	NS-l9OUT.05	Water	l9 outlet	68.6194	-149.5953	0.71203	Keller et al., 2007
2546	NS-lMINUSIN.01	Water	l minus inlet	68.5568	-149.5551	0.71297	Keller et al., 2007
2547	NS-lMINUSOUT.01	Water	l minus outlet	68.5567	-149.5747	0.71313	Keller et al., 2007
2548	NS-lOUT.03	Water	l1 outlet	68.5724	-149.5812	0.71519	Keller et al., 2007
2549	NS-MWL.01	Water	Milky Way lower	68.6197	-149.5961	0.71094	Keller et al., 2007
2550	NS-MWL.03	Water	Milky Way lower	68.6197	-149.5961	0.71060	Keller et al., 2007
2551	NS-MWL.08	Water	Milky Way lower	68.6197	-149.5961	0.71095	Keller et al., 2007
2552	NS-MWL.09	Water	Milky Way lower	68.6197	-149.5961	0.71158	Keller et al., 2007
2553	NS-MWU.03	Water	Milky Way upper	68.6191	-149.5806	0.71281	Keller et al., 2007
2554	NS-MWU.08	Water	Milky Way upper	68.6191	-149.5806	0.71255	Keller et al., 2007

Table 2.S2 continued.

Analysis ID	*Sample ID*	*Type*	*Location*	*Latitude*	*Longitude*	*87Sr/86Sr*	*Citation*
2555	NS-MWU.09	Water	Milky Way upper	68.6191	-149.5806	0.71263	Keller et al., 2007
2556	NS-TOOLIKIN.01	Water	Toolik Inlet	68.6256	-149.5961	0.71232	Keller et al., 2007
2557	NS-TOOLIKIN.03	Water	Toolik Inlet	68.6256	-149.5961	0.71185	Keller et al., 2007
2558	NS-TOOLIKIN.08	Water	Toolik Inlet	68.6256	-149.5961	0.71211	Keller et al., 2007
2559	NS-TOOLIKIN.09	Water	Toolik Inlet	68.6256	-149.5961	0.71225	Keller et al., 2007
2560	NS-TOOLIKIN.10	Water	Toolik Inlet	68.6256	-149.5961	0.71207	Keller et al., 2007
2561	NS-TOOLIKIN.11	Water	Toolik Inlet	68.6256	-149.5961	0.71207	Keller et al., 2007
2857	Copper River	Water	Copper River	60.3851	-144.9802	0.70710	Keller et al., 2007
2859	Kuskokwim River	Water	Kuskokwim River	60.2068	-162.4065	0.70900	Keller et al., 2007
2861	Yukon River	Water	Yukon River	62.5968	-164.7853	0.71370	Keller et al., 2007
8735	27	Water	Aleknagik Lake	59.2740	-158.5990	0.70463	Brennan et al., 2014
8736	30	Water	Snake Lake	59.1510	-158.8870	0.70435	Brennan et al., 2014
8737	34	Water	Upper Talarik	59.9170	-155.2700	0.70432	Brennan et al., 2014
8738	36	Water	Lake Amanka	59.0480	-159.2720	0.70422	Brennan et al., 2014
8739	40	Water	Nushagak upstream Mulchatna	59.6420	-157.1230	0.70778	Brennan et al., 2014
8740	41	Water	Nushagak downstream Mulchatna	59.4470	-157.3030	0.70653	Brennan et al., 2014
8741	42	Water	Mulchatna	59.6700	-157.0530	0.70572	Brennan et al., 2014
8742	55	Water	Nushagak mouth	59.2680	-157.6490	0.70693	Brennan et al., 2014

Table 2.S2 continued.

Analysis ID	*Sample ID*	*Type*	*Location*	*Latitude*	*Longitude*	*87Sr/86Sr*	*Citation*
8744	57	Water	Tanalian	60.1890	-154.3190	0.70519	Brennan et al., 2014
8745	59	Water	Lake Clark mouth	60.0120	-154.7610	0.70466	Brennan et al., 2014
8746	61	Water	Gibraltar	59.4300	-154.8320	0.70432	Brennan et al., 2014
8747	7	Water	Nizina	61.3800	-143.1540	0.70618	Brennan et al., 2014
8748	8	Water	Kennicott	61.4330	-142.9440	0.70630	Brennan et al., 2014
8749	9	Water	Chitina	61.5180	-144.3330	0.70723	Brennan et al., 2014
8750	10	Water	Copper upstream Chitina	61.5310	-144.4080	0.70637	Brennan et al., 2014
8751	11	Water	Copper downstream Chitina	61.4750	-144.4550	0.70694	Brennan et al., 2014
8752	12	Water	Tonsina downstream Little Tonsina	61.6630	-145.1820	0.70568	Brennan et al., 2014
8753	13	Water	Klutina	61.9470	-145.3540	0.70540	Brennan et al., 2014
8754	14	Water	Little Tonsina	61.5950	-145.2230	0.70558	Brennan et al., 2014
8755	15	Water	Tonsina upstream Little Tonsina	61.5980	-145.2250	0.70566	Brennan et al., 2014
8756	16	Water	Tazlina	62.0580	-145.4310	0.70561	Brennan et al., 2014
8757	17	Water	Gulkana	62.2700	-145.3850	0.70573	Brennan et al., 2014
8758	3	Water	Kenai	60.4870	-149.9350	0.70652	Brennan et al., 2014
8759	4	Water	Resurrection	60.1630	-149.4540	0.70601	Brennan et al., 2014
8760	5	Water	Knik	61.4760	-148.8760	0.70607	Brennan et al., 2014
8761	6	Water	Matanuska	61.7340	-148.7650	0.70571	Brennan et al., 2014
8762	35	Water	South Fork Kuskokwim	63.0390	-154.5730	0.70932	Brennan et al., 2014

Table 2.S2 continued.

Analysis ID	*Sample ID*	*Type*	*Location*	*Latitude*	*Longitude*	*87Sr/86Sr*	*Citation*
8763	43	Water	Takotna	62.9680	-156.0920	0.70825	Brennan et al., 2014
8764	44	Water	Kwethuk old wier	60.4940	-161.1000	0.70498	Brennan et al., 2014
8765	45	Water	Tulusak	60.9650	-160.1700	0.70649	Brennan et al., 2014
8766	46	Water	Kwethluk elbow	60.2980	-160.9600	0.70498	Brennan et al., 2014
8767	47	Water	Kipchuk	61.0120	-159.1770	0.70558	Brennan et al., 2014
8768	48	Water	Salmon	61.0630	-159.1950	0.70684	Brennan et al., 2014
8769	49	Water	Aniak upstream Kipchuk and Salmon	61.0080	-159.1170	0.70553	Brennan et al., 2014
8770	50	Water	Aniak downstream Timber	61.1260	-159.1210	0.70584	Brennan et al., 2014
8771	51	Water	Kisaralik	60.7370	-160.4470	0.70752	Brennan et al., 2014
8772	52	Water	Holitina upstream Kokcugluk wier	60.8290	-157.8290	0.70868	Brennan et al., 2014
8773	53	Water	George	61.9840	-157.6280	0.70812	Brennan et al., 2014
8774	21	Water	Sagavanirktok	68.8340	-148.8210	0.71219	Brennan et al., 2014
8775	22	Water	Kuparuk	68.6470	-149.4110	0.70780	Brennan et al., 2014
8776	23	Water	Atigan	68.4370	-149.3680	0.71634	Brennan et al., 2014
8777	54	Water	Canning	69.9720	-146.2760	0.71108	Brennan et al., 2014
8778	58	Water	Inigok	70.1620	-152.9030	0.70966	Brennan et al., 2014
8779	60	Water	Etivluk	68.6010	-156.2710	0.71533	Brennan et al., 2014
8780	1	Water	Chulitna	62.5680	-150.2360	0.70895	Brennan et al., 2014
8781	2	Water	Susitna	62.1780	-150.1720	0.70813	Brennan et al., 2014

Table 2.S2 continued.

Analysis ID	*Sample ID*	*Type*	*Location*	*Latitude*	*Longitude*	*87Sr/86Sr*	*Citation*
8782	18	Water	Yukon	65.8770	-149.7100	0.71329	Brennan et al., 2014
8783	19	Water	South Fork Koyukuk	67.0170	-150.2860	0.71263	Brennan et al., 2014
8784	20	Water	Middle Fork Koyukuk	67.2580	-150.1950	0.71457	Brennan et al., 2014
8785	24	Water	Dietrich	67.9160	-149.8230	0.71824	Brennan et al., 2014
8786	25	Water	Jim's	66.8380	-150.6070	0.71002	Brennan et al., 2014
8787	26	Water	Innoko	63.6380	-158.0380	0.70869	Brennan et al., 2014
8788	28	Water	Tanana	64.5590	-149.0660	0.71854	Brennan et al., 2014
8789	29	Water	Hogatza	66.0010	-155.3970	0.70816	Brennan et al., 2014
8790	31	Water	Nenana	64.5290	-149.1310	0.71317	Brennan et al., 2014
8791	32	Water	Dulbi	65.3990	-156.5230	0.70763	Brennan et al., 2014
8792	33	Water	Chatanika	65.0850	-147.7240	0.74041	Brennan et al., 2014
8793	37	Water	Chena	64.8300	-147.5660	0.72520	Brennan et al., 2014
8794	38	Water	Salcha	64.4730	-146.9170	0.72282	Brennan et al., 2014
8795	39	Water	Koyukuk mainstem	65.6650	-156.3840	0.71365	Brennan et al., 2014

Chapter 3: A detailed life history from a Pleistocene steppe bison (Bison priscus) skeleton unearthed in Arctic Alaska

Juliette Funck1,2*, Peter D. Heintzman3,4, Gemma G. R. Murray5, Beth Shapiro3,6, Holly McKinney7, Jean-Bernard Huchet8, Nancy Bigelow9, Pat Druckenmiller2,10, Matthew J. Wooller1,11*

1. Alaska Stable Isotope Facility, Water and Environmental Research Center, Institute of Northern Engineering, University of Alaska Fairbanks, Fairbanks, AK 99775, USA.

2. Department of Geosciences, University of Alaska Fairbanks, Fairbanks, AK 99775, USA.

3. Department of Ecology and Evolutionary Biology, University of California Santa Cruz, Santa Cruz, CA 95064, USA.

4. The Arctic University Museum of Norway, UiT - The Arctic University of Norway, NO-9037 Tromsø, Norway.

5. Department of Veterinary Medicine, University of Cambridge, Cambridge, CB3 0ES, UK.

6. Howard Hughes Medical Institute, University of California Santa Cruz, Santa Cruz, CA 95064, USA.

7. Department of Anthropology, University of Alaska Fairbanks, Fairbanks, AK 99775, USA.

8. Muséum National d'Histoire Naturelle, Institut de Systématique, Evolution, Biodiversité (ISYEB), Unit Mixte de Recherche 7205, CP50, Entomologie, 45, rue Buffon, F-75005 Paris, France.

9. Alaska Quaternary Center, University of Alaska Fairbanks, Fairbanks, AK 99775, USA

10. University of Alaska Museum of the North, Fairbanks, University of Alaska Fairbanks, AK 99775, USA.

11. College of Fisheries and Ocean Sciences, University of Alaska Fairbanks, Fairbanks, AK 99775, USA.

* Corresponding author e-mails: jmfunck@alaska.edu and mjwooller@alaska.edu

Abstract

Detailed paleoecological evidence from Arctic Alaska's past megafauna can help reconstruct paleoenvironmental conditions and can illustrate ecological adaptation to varying environments. We examined a rare, largely articulated and almost complete skeleton of a steppe bison (Bison priscus) recently unearthed in Northern Alaska using a multi-proxy paleoecological approach to reconstruct the past ecology of an individual representing a key ancient taxon. Radiocarbon dating of horn keratin revealed that the specimen has a finite radiocarbon age ~46,000 +/- 1000 Cal yr BP, very close to the limit of radiocarbon dating. We also employed Bayesian age modeling of the mitochondrial genome, which estimated an age of ~33,000-87,000 Cal yr BP. Our taphonomic investigations show that the bison was scavenged post-mortem and infested by blowflies before burial. Stable carbon and oxygen isotope (δ13C and δ15N) analyses of sequentially sampled horn keratin reveal a seasonal cycle; furthermore, high δ15N values during its first few years of life are consistent with patterns observed in modern bison that undertook dispersal. We compared sequential analyses of tooth enamel for strontium isotope ratios ($^{87}Sr/^{86}Sr$) to a spatial model of $^{87}Sr/^{86}Sr$ values providing evidence for dispersal across the landscape. Synthesis of the paleoecological findings indicates the specimen lived during interstadial conditions. Our multi-proxy, paleoecological approach, combining light and heavy isotope ratios along with genetic information, adds to the broader understanding of ancient bison ecology during the Late Pleistocene, indicating that ancient bison adopted different degrees of paleo-mobility according to the prevailing paleoecological conditions and climate.

Keywords

Quaternary; Beringia, Paleoecology; Stable Isotopes; Strontium; Oxygen; Carbon; Nitrogen; Steppe Bison

3.2 Introduction

3.2.1 Paleoecological context:

Northern Alaska is currently experiencing environmental changes as the result of global warming, which is occurring most rapidly at northern latitudes (Moon *et al.*, 2019). These changes impact the mobility and ecologies of extant megafauna including caribou, moose, and muskoxen (Post and Forchhammer, 2008; Sharma, Couturier and Côté, 2009). For example, migratory species are experiencing mismatch in timing of migration and peak resource availability (Post and Forchhammer, 2008), while caribou are losing habitat in the north due to warmer Arctic summers and winters (Sharma, Couturier and Côté, 2009). Detailed paleoecological evidence from the remains of past megafauna from this region provides an opportunity to examine how past megafauna lived in this environment (Guthrie, 1989), and therefore help predict responses of living megafauna to present and projected environmental changes.

During the height of the last glaciation (~28-18 thousand years ago (kya)) (Clark *et al.*, 2009), the North Slope of Alaska was part of an expansive land-mass known as Beringia. Sea levels were ~130 meters lower than today (Lambeck *et al.*, 2014), exposing a shallow continental shelf between northeast Asia and North America known as the Bering Land Bridge (BLB). The BLB extended approximately from the Lena River, Russia, in the west and the Mackenzie River, Yukon, Canada, in the east (Elias and Crocker 2008) (Figure 1). The Beringian ecosystem was primarily that of a mammoth steppe, a graminoid-dominated grassland ecosystem that supported a community of large herbivorous mammals, dominated by mammoths (*Mamamuthus primigenius*), horses (*Equus* sp.), and steppe bison (*Bison priscus*) (Guthrie, 2001; Mann et al., 2013; Shapiro and Cooper, 2003; Zimov et al., 2012). The mammoth steppe supported large populations of these herbivores, many of which had larger body sizes than their descendants today at similar latitudes (Zimov *et al.*, 2012). Bison, in particular, had larger body sizes and horns than present-day American bison (*Bison bison*) (Martin, Mead and Barboza, 2018), and were present throughout most of Eurasia and North America in what has been termed "The Bison Belt" (Guthrie, 1989). Steppe bison

first arrived in North America ~195-135 kya (Froese *et al.*, 2017) and their population began to decline around 37 kya (Shapiro *et al.*, 2004; Heintzman *et al.*, 2016).

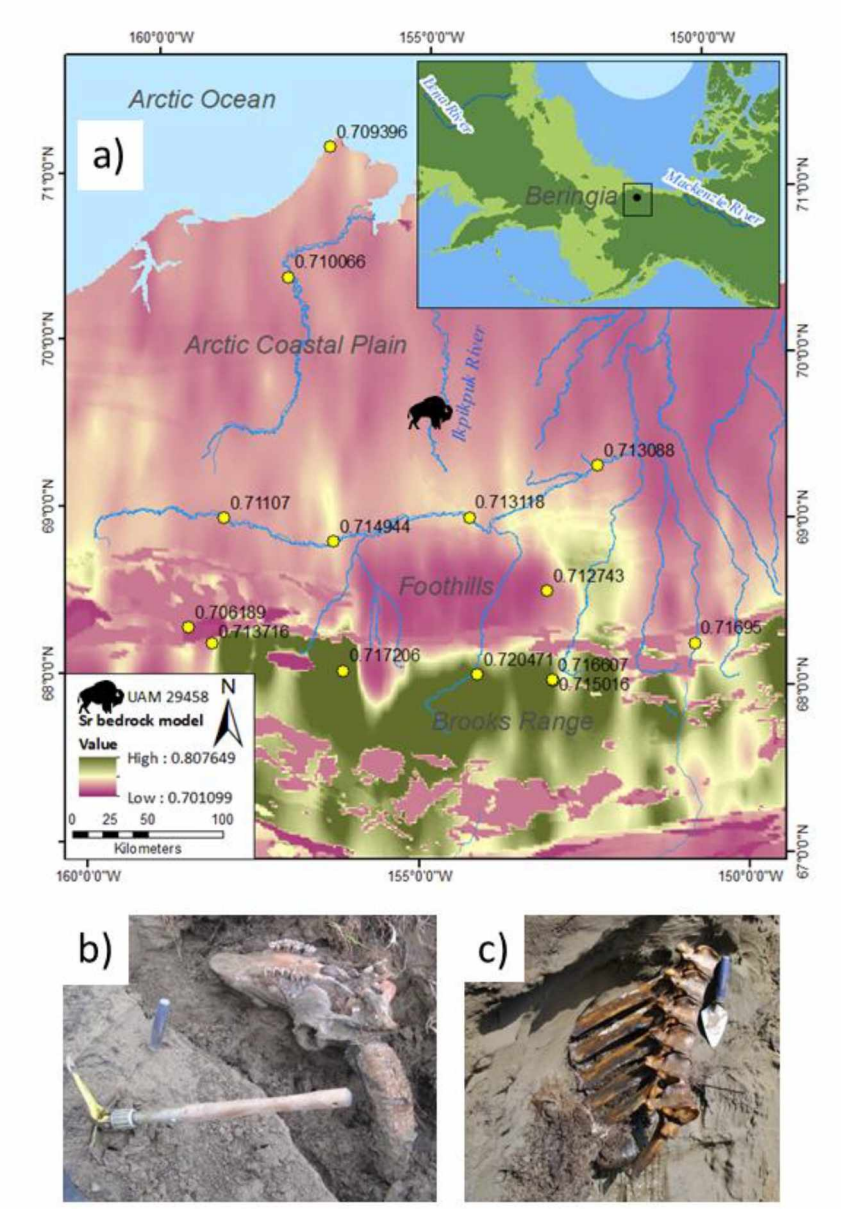

Figure 3.1 A map on northern Alaska, with the provenance of steppe bison (Bison priscus) specimen UAMES 29458 indicated by the red star. Yellow dots show rodent specimen localities and strontium values measured from their teeth. The underlying map is modified from

Modern bison ecology can provide an analog for inferring ancient bison behavior as well as the basis for comparative (paleo) biology and anatomy. Although modern bison are grassland grazing specialists

(Bamforth, 1987), some evidence from macro and micro tooth-wear analysis indicates that steppe bison may have had a broader herbivorous diet and ecological niche that included browsing (Rivals, Solounias and Mihlbachler, 2007). The long-distance (>100km) (Berger, 2004; Plumb *et al.*, 2009; Hanson, 2015) migrations of American bison (*Bison bison*) across the American Great Plains were legendary and a key component of bison life history (Bamforth, 1987; Flores, 1991). However, isotopic (strontium) analyses of ancient (~18,500 ^{14}C yr BP) bison (*Bison priscus*) from a site in Ukraine found no evidence of paleomobility (Julien *et al.*, 2012). Analyses of ancient bison specimens can provide opportunities to flesh out the paleoecological life-history of a taxon that shaped Beringian ecosystems (Zimov *et al.*, 2011). Fortunately for paleoecologists, bones, teeth, and horns of bison are some of the most numerous fossil remains found in Alaska (Guthrie, 1970; Mann *et al.*, 2013). On rare occasions, high sediment deposition rates along with freezing temperatures can result in preservation of virtually complete carcasses or skeletons of past Beringian fauna, revealing vivid paleoecological snap-shots of life in Beringia (Boeskorov et al., 2016; Kirillova et al., 2015; Van Geel et al., 2014; Zazula et al., 2017; Zazula et al., 2009). These rare and well-preserved glimpses of past megafaunal paleoecology can emerge from eroding river-banks (Zazula *et al.*, 2009b; Mann *et al.*, 2013), during mining operations (Guthrie, 1968), and during construction activities (Zazula et al., 2017). In some instances, soft tissue such as hair, skin, organs, and stomach contents are preserved (Van Geel *et al.*, 2014; Kirillova *et al.*, 2015), as well as associated insects. These remains, along with bones and teeth, can retain chemical clues about an individual's paleoecology. Isotopic analyses (Kirillova *et al.*, 2015) and analyses of ancient DNA (aDNA) (Zazula et al., 2017) can reveal past mobility patterns and population interconnectivity, contributing to an understanding of past ecosystems, landscapes, and evolution (Froese et al., 2017; Haile et al., 2009; Marsolier-Kergoat et al., 2015; Shapiro and Cooper, 2003, Heintzman et al., 2016; Shapiro et al., 2004).

3.2.2 Stable Isotopes

Isotopic analyses have become a popular tool in paleoecology for determining the ecological and life-history traits of ancient fauna (Bocherens, 2003; Britton *et al.*, 2009). Tissues that form in discrete layers

over a period of an individual's life, such as tooth enamel, hair, or horn, can be subsampled to allow inference of inter- and intra-annual paleo-mobility and paleoecology using isotopic analyses of these sample types (Balasse *et al.*, 2001; Britton *et al.*, 2009; Stevens, Balasse and O'Connell, 2011; Zazzo *et al.*, 2012). Intra-tooth strontium analysis has been developed as a useful tool to track the mobility of past animals and humans (Koch, Heisinger, Moss, Carlson, Marilyn, *et al.*, 1995; Hoppe *et al.*, 1999; Balasse, 2002; Hoppe, 2004; Pellegrini *et al.*, 2008; Britton, 2009; Widga, Walker and Stockli, 2010; Radloff *et al.*, 2010; Viner *et al.*, 2010; Britton *et al.*, 2011; Julien *et al.*, 2012). Strontium isotope ratios ($^{87}Sr/^{86}Sr$) can vary across landscapes depending in part on the age and rock type of the underlying geology (Bataille *et al.*, 2014; Brennan *et al.*, 2014). These landscape $^{87}Sr/^{86}Sr$ signatures can enter animals through their diet and drinking water, replacing calcium in tissues such as teeth and bones (Capo, Stewart and Chadwick, 1998). The combination of $^{87}Sr/^{86}Sr$ and oxygen isotopic ($\delta^{18}O$) values from analyses of animal tissues have proved to be a powerful predictor of geographic location (Britton *et al.*, 2009; Knudson *et al.*, 2009; Gigleux *et al.*, 2017). The $\delta^{18}O$ values from a specimen can indicate location based on latitude and distance from the coast (Hoppe, 2006; Lachniet *et al.*, 2016). The $\delta^{18}O$ values from analyses of bison teeth have also been used to determine approximate local climate and seasonal temperature variation, because $\delta^{18}O$ values in water can be closely related to temperature (Hoppe, Paytan and Chamberlain, 2006; Bernard *et al.*, 2009; Scherler, Tütken and Becker, 2014). Examining bison mobility has been one of the more common applications of this isotopic methodology, partly due to the abundance of bison remains in the archaeological and paleontological records (Widga, Walker and Stockli, 2010; Britton *et al.*, 2012; Julien *et al.*, 2012).

Stable carbon and nitrogen isotope ratios (expressed as $\delta^{13}C$ and $\delta^{15}N$ values, respectively) from analyses of sub-fossils of animals can add a dietary dimension to a paleoecological reconstruction (Stevens and Hedges, 2004; Drucker *et al.*, 2008). $\delta^{13}C$, along with $\delta^{18}O$, values can be generated from the analysis of inorganic carbon in the bones and teeth (Koch, Tuross and Fogel, 1997). Bison horns, which grow throughout the life of a bison, are a carbon and nitrogen-rich keratin tissue that allows intra- and inter-annual paleoecological inferences. $\delta^{13}C$ values can also be generated from analyses of organic carbon

preserved as bone collagen and horn keratin, these methods also produce $\delta^{15}N$ values (Schoeninger and DeNiro, 1984; Iacumin, Bocherens and Chaix, 2001). In order to interpret the $\delta^{13}C$ and $\delta^{15}N$ values of these analyses, potential sources of variability need to be evaluated. One common source of $\delta^{13}C$ variation in the diet of herbivores is variation in the proportional contribution C4 vs. C3 plants. However, C4 plants are exceedingly rare or non-existent in the Arctic (Wooller *et al.*, 2007). Furthermore, a lack of trees in the Arctic also excludes "the canopy effect" caused by the concentration of CO_2 in dense forest (Drucker *et al.*, 2008). Thus, the main source of variability in $\delta^{13}C$ values we can expect in Arctic vegetation is between wetter and drier environments (Wooller *et al.*, 2007). The $\delta^{15}N$ values in ecosystems and organisms can vary for a range of reasons, often being used to infer the past trophic positions of organisms (Bocherens and Drucker, 2003). In the case of herbivores, changes in $\delta^{15}N$ values have been used to infer past environmental conditions, including past levels of precipitation (Heaton *et al.*, 1986; Graham *et al.*, 2016; Rabanus-Wallace *et al.*, 2017) and dietary stress (Lee et al., 2012; Mekota et al., 2006; Funck et al., in review). Overall, a combination of isotopic approaches can provide a multi-proxy perspective of an individual's life-history.

3.2.3 Ancient DNA

Ancient DNA (aDNA) from ancient bison specimens from Beringia has been used to monitor gene-flow across the BLB and through the ice-free corridor that connected eastern Beringia to the rest of the Americas (Heintzman *et al.*, 2016; Froese *et al.*, 2017). It has also been used to estimate past changes in effective population size (Lorenzen *et al.*, 2011), which has been used to identify the decline of steppe bison since ~37 kya in Beringia (Shapiro *et al.*, 2004). Analyses using aDNA can also add a further perspective on individual steppe bison specimens. They can provide information on an individual's genomic sex and population affinity, and help constrain age estimates for specimens potentially outside the range or towards the limits of radiocarbon dating. For the latter analysis, one such approach uses Bayesian analysis of aDNA sequences from dated specimens that lived at different time periods to calibrate a molecular clock, and then use this calibration to estimate the age of the undatable individual

(Shapiro *et al.*, 2011). The mitochondrial genealogy of Pleistocene bison in North America has been relatively well sampled, both geographically and temporally (Shapiro *et al.*, 2004; Heintzman *et al.*, 2016; Froese *et al.*, 2017), and is therefore likely to be well suited for estimating the age of ancient bison specimens.

In this study, we conducted a multi-proxy study, combining isotopic and aDNA analyses, with supporting paleo-forensic analyses, to investigate the sex, age, paleoecology and life history of an exceptionally well-preserved and largely articulated steppe bison (*Bison priscus*) found on the North Slope of Alaska (Figure 1 a-c). We combined isotopic and aDNA analyses with more traditional methods of taphonomic analyses. We further assess peri- and post-mortem events together with the taphonomic history of skeletal remains using a taphonomic analysis of the skeleton and of the plant and insect remains present. Our examination of the physical condition of the remains (bones and teeth) from the specimen provides clues about an individual's age, sex, and appearance (Fuller, 1959). The taphonomy and geology associated with the specimen provides information about the context surrounding an organism's death and a possible cause of death. We used insect (Elias, Berman and Alfimov, 2000) and plant (Bigelow, Zazula and Atkinson, 2013) macrofossils associated with megafaunal remains to provide valuable paleoecological information. Our multi-proxy, paleoecological approach adds to the broader understanding of ancient bison ecology during the Late Pleistocene.

3.1 Material and methods

3.3.1 Specimen and study site

Dr. Dan Mann and Dr. Pamela Grooves found a nearly complete, and partially articulated specimen of steppe bison (*Bison priscus*) eroding out of a bank of the Ikpikpuk River on the North Slope of Alaska (Figure 1 a-c) located at 69.71563 N, -154.863 W (WGS 84) (Figure 1). They excavated and transported to the University of Alaska Museum of the North (UAMN), where the University of Alaska Museum

Earth Sciences collections (UAMES) assigned an identification number UAMES 29458. The North Slope of Alaska is delimited by the Brooks Range of mountains to the south and the Arctic Ocean to the north (Figure 1). The southern portion is predominantly low foothills that become a coastal plain at ~69° north. The Ikpikpuk River cuts through Quaternary-aged aeolian sand deposits, known as the Ikpikpuk Sand Sea (Carter, 1981). These deposits preserve an abundance of Quaternary vertebrate fossils that erode from banks of the Ikpikpuk River, though rarely in such excellent and complete condition (Mann *et al.*, 2015).

3.3.2 Fossil Material

We removed skeletal elements of specimen UAMES 29458 from the encasing sediment, cleaned, and anatomically re-articulated (Figure 2a). Hair, preserved soft tissue, and associated sediment was stored by individual body element and kept frozen. We rearticulated the specimen at the UAMES (Figure 2 a, b) and examined it for signs of scavenging and other taphonomic processes. We found a large number of invertebrate and plant macrofossils within the interstices of the skull, particularly the brain cavity of UAMES 29458. These were collected and identified to provide taphonomic and paleoenvironmental context. We removed larger macrofossils and examined them using a dissecting microscope. We wet sieved sediments at 150 μm and 250 μm. All diagnostic plant macrofossils were collected from sediments large than 250 μm and all invertebrate materials were collected and archived.

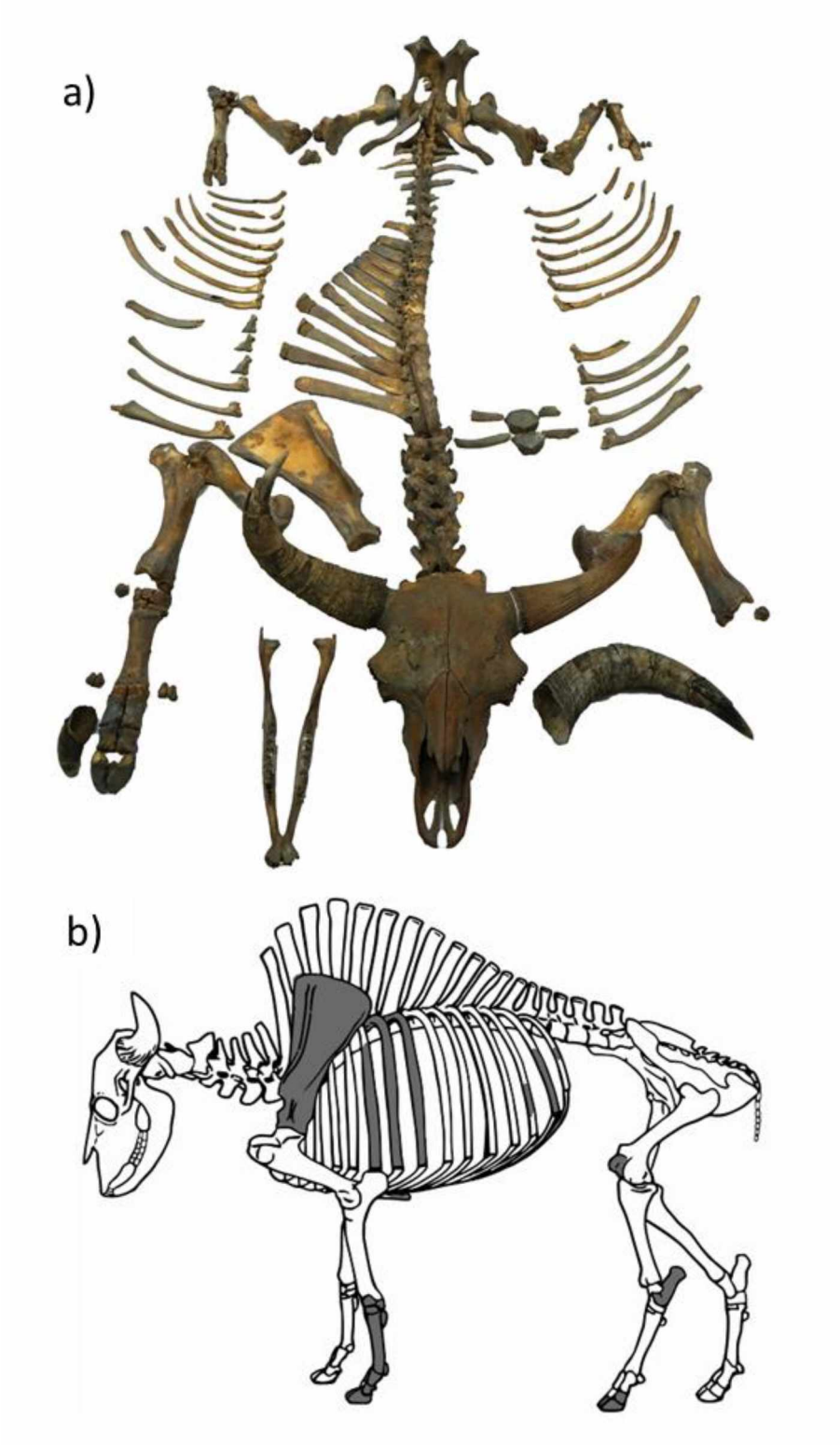

Figure 3.2 Specimen UAMES 29458 rearticulated for taphonomic analysis. b) Skeletal elements missing from specimen are indicated in gray. All elements from the right side were present.

3.3.3 Radiocarbon analysis

Radiocarbon dating was conducted on different materials associated with specimen UAMES 29458. Previously the bone collagen from the cap of a spinous process, extracted without ultrafiltration, was analyzed at Beta Analytic (Miami, Florida), and found to be none finite in age >43,500 radiocarbon years (Mann *et al.*, 2013). However, collagen is porous and can be subject to contamination, so we selected additional materials for further analysis: keratin from the horn sheath, a fly pupal case, and a plant macrofossil (herbaceous stem), both recovered from inside the bison skull. W. M. Keck Carbon Cycle Accelerator Mass Spectrometry Laboratory analyzed the samples on a National Electrostatics Corporation (NEC 0.5MV 1.5SDH-2 AMS system). The horn sheath keratin was run alongside three infinite-^{14}C aged bison horn sheath samples and the mean blank from these three was subtracted from sample results, with an assumed 30% uncertainty. All of the sample preparation backgrounds were also subtracted, based on measurements of a ^{14}C-free wood standard, with an assumed 30% uncertainty.

3.3.4 Isotopic analyses

We removed thirty-three intra-tooth subsamples of enamel from the right mandibular molars 1, 2, and 3 (M1, M2, M3) of UAMES 29458 (Supplemental Figure 1). We collected samples in a laminar flow hood at the Alaska Stable Isotope Facility (ASIF) at the University of Alaska Fairbanks (UAF). We used a Dremel buffing bit to abraded the exterior surface of a target section of the tooth on each molar. Subsequently, we used a Dremel diamond-coated circular saw to divide samples along each tooth parallel to the growth plane (Figure S1). We then used a dental pick to break off chips from the enamel surface, which were placed in labeled sealable vials. Rather than removing enamel as a ground powder, this method has been found to reduce the potential for the introduction of contaminates during the preparation process (Diego Fernendez, University of Utah, ICPMS Facility 2018 personal communication).

We divided enamel samples into two with each subsample. The University of Utah, Department of Geology and Geophysics, ICPMS facility analyzed the other half of sample for ^{87}Sr/^{86}Sr isotope ratios using a multi-collector inductively coupled plasma mass spectrometer (MC-ICPMS - ThermoFisher

Scientific, High Resolution NEPTUNE, Bremen, Germany). Strontium isotope analyses followed previously published protocols (Glassburn *et al.*, 2018; Nelson *et al.*, 2018). Additionally, we sampled molars from 14 modern rodents (*Microtus oeconomus*, *Microtus mirus, Dicrostonyx groenlandicus*) from within a 250-km radius surrounding the UAMES 29458 locality (Figure 1a) to determine the bioavailable $^{87}Sr/^{86}Sr$ values in the region. This method has previously been used to determine local bioavailable $^{87}Sr/^{86}Sr$ values for comparison to mobile individuals (Hoppe *et al.*, 1999; Radloff *et al.*, 2010; Kootker *et al.*, 2016)). The results of this investigation augment existing spatial models of variability in $^{87}Sr/^{86}Sr$ values in Alaska (Bataille *et al.*, 2014).

We chemically pre-treated remaining half of each bison enamel sample to remove contaminants from gas exchange using the modified method from Pellegrini and Snoeck (2016, 2015) in order to produce $\delta^{18}O$ and $\delta^{13}C$ values. To compensate for the use of small (~1 × 2 mm) enamel chips rather than powder we increased soaking time. We added one milliliter of 2% sodium hypochlorite (NaOCl) to each sample, shaken to mix, and soaked for 48 hours to remove organic particulates. We then rinsed samples with deionized water and soaked them in 1 M acetate buffered acetic acid (0.1 M) (CH_3CO_2H) for 48 hours to removed carbonate portion. Finally, we rinsed the samples three times with deionized water before freezing and then freeze-drying them for approximately 10 hours on a VirTiS benchtop Lyo-Centre lyophilizer to remove any moisture prior to isotopic analysis. We analyzed the carbonate fraction using a Thermo Scientific GasBench II carbonate analyzer attached to a Thermo Scientific DeltaV^{Plus} Isotope Ratio Mass Spectrometer at ASIF following previously published protocols (Glassburn et al., 2018). Stable carbon and oxygen isotope ratios are reported in δ notation as parts per thousand (‰) relative to the international standard Vienna Pee Dee Belemnite (VPDB). We ran the samples with laboratory standards of calcium carbonate (Merck, Suprapur 99.95% Lot # B510959 313) every 10 samples to determine analytical precision for $\delta^{13}C$ values (0.3 ‰) and $\delta^{18}O$ values (0.2 ‰) (all errors are expressed as one standard deviations). The $\delta^{18}O$ and $\delta^{13}C$ values were initially determined relative to VPDB for oxygen and carbon, but the $\delta^{18}O$ values were subsequently converted to the Vienna Standard Mean Ocean Water (VSMOW) scale to allow the comparison of the values to meteoric water values. The $\delta^{18}O$ values

were converted to VSMOW using Formula 1 (below) (Verkouteren and Klinedinst, 2004) and then Formula 2 (below), a conversion developed by Hoppe et al. (2006) and Velivetskaya et al (2016) to compare bison enamel to meteoric water $\delta^{18}O$ values:

Formula 1: VSMOW = 30.92+1.03092*VPDB

Formula 2: Enamel carbonate = 0.7(±0.12)*VSMOW- 30.06(±1.40)

We removed horn sheath keratin as a wedge perpendicular to the direction of the keratin growth layers (Figure S2). We selected the location to maximize the years of horn growth covered by the core. We then subsampled the core by peeling off thin layers between 0.1-0.3 mm in thickness with a razor blade, for a total of n = 113 sub-samples. Sub-samples were analyzed to produce $\delta^{15}N$ and $\delta^{13}C$ values (vs. AIR for nitrogen and VPDB for carbon) using a Flash 2000 Organic Elemental Analyzer (EA) connected via a Conflo IV to an IRMS (DeltaV Plus) at ASIF. Internal reference checks using peptone (No. P-7750 meat-based protein. Sigma Chemical Company, Lot #76f-0300) were run every 10th sample, and blanks were run every 20th sample. Repeated measurements of standards provided the analytical precisions, which were ±0.1 ‰ and ±0.6 ‰ for $\delta^{15}N$ and $\delta^{13}C$ values, respectively.

3.3.5 aDNA analyses

The first premolar (PM1) of specimen UAMES 29458 was sent to the specialized Paleogenomics Laboratory at the University of California Santa Cruz (UCSC) for aDNA analysis. We followed standard protocols as outlined in Froese et al. (2017) to extract and analyze ancient DNA unless stated otherwise. Briefly, we extracted aDNA using a silica column method (Dabney *et al.*, 2013), and then converted extracts into an Illumina-compatible double-stranded DNA library (Meyer and Kircher, 2010). We enriched an aliquot of this DNA library for bison mitochondrial genomic fragments using a commercial

MyBaits target capture kit (Arbor Biosciences, Ann Arbor, MI). We sequenced both the enriched and remaining unenriched library on separate runs of an Illumina MiSeq using v3 150 cycle chemistry75 cyc, with paired-end 75 bp reads. We then merged the paired-end read data, trimmed adapters, and removed short (<25 base pairs (bp) for the enriched library; <30 bp for the unenriched library) and low-complexity sequences (DUST cutoff: 7) using SeqPrep and PRINSEQ-lite v0.20.4 (Schmieder and Edwards, 2011). We aligned the filtered reads from the unenriched library to a reference database that included the cow (*Bos taurus*) genome (Genbank: Btau_4.6.1) and an American bison (*Bison bison*) mitochondrial genome (Genbank: NC_012346), using the Burrows Wheeler Aligner (BWA; Li and Durbin, 2009) aln algorithm with the seed disabled (-l 1024). We filtered aligned reads by map quality score (minimum of 20) and removed duplicates using SAMtools v0.1.19 (Li and Durbin, 2009). We assessed ancient DNA damage patterns using mapDamage v2.0.9 (Jónsson *et al.*, 2013). To infer the genomic sex of UAMES 29458, we followed the method of Heintzman et al. (2017), which compares the relative mapping frequency of the X chromosome to the autosomes. A male is inferred if this ratio is 0.45-0.55, whereas the expectation for a female is 0.95-1.05.

We mapped the filtered reads from the enriched library to a steppe bison reference mitochondrial genome (Genbank: KX269138) using the multiple iterative assembler (MIA; Briggs et al. 2009) and BWA, as above. For aDNA damage assessment of the enriched data, we used the BWA mapping consensus results as the reference sequence for mapDamage. We calculated a mitochondrial genome consensus sequence from the MIA mapping results using the criteria outlined in Froese et al. (2017), and added this sequence to the full mitochondrial genome alignment of Froese et al. (2017), as modified by Zazula et al. (2017). This alignment consisted of four yak and 47 Siberian or North American bison mitochondrial sequences. Before estimating the age of UAMES 29458 with Bayesian time-tree methods, we tested for temporal signal in the data set. Tip-dating methods are only valid if this signal is present, as these methods will usually converge on an estimate whether or not there is a temporal signal present (Firth *et al.*, 2010). We used a linear regression of phylogenetic root-to-tip distance against the sampling date to test for temporal signal (following Murray et al., 2016). We estimated a neighbor-joining tree of the data set (excluding the

yak and two radiocarbon non-finite bison sequences) using a K80 nucleotide substitution model with pairwise deletion, using the ape package in R (Paradis, Claude and Strimmer, 2004), in which the root was fit simultaneously with the regression, so as to minimize the residual mean squares, with the resulting root matching the root obtained by using the yak sequences as an outgroup. Analyses of the full alignment and a reduced alignment, with MS022 omitted (see below), returned positive correlations that are significantly different from random permutations over clusters of samples with similar dates (full: $r = 0.50$, $p = 0.010$; reduced: $r = 0.44$, $p = 0.025$; Figure S3). We defined similar-date clusters (n=34-35) as monophyletic clades that had the same date after rounding to the nearest thousand years (kya BP). A Mantel test suggested that this clustering was sufficient to eliminate a correlation between genetic and temporal distances in the data (without clustering: $p = 0.001$, with clustering: $p = 0.18$) (Murray *et al.*, 2016), which can result in a false positive result. Overall, these analyses suggest the presence of temporal signal in the bison mitochondrial genome data set.

We then estimated a time-tree in BEAST (v1.10.4, Drummond et al., 2012) so as to estimate both the age of UAMES 29458 and its placement in the bison mitochondrial genome phylogeny. We used a strict molecular clock with either finite radiocarbon dates or stratigraphic data associated with the other sequences in the analysis as priors, following Froese et al. (2017) and Zazula et al. (2017). To estimate the age of UAMES 29458, we used a uniform prior distribution of between 30 kya BP (as this specimen is borderline radiocarbon finite; see results) and 195 kya BP (the earliest mitochondrial estimate for the arrival of bison in North America; Froese et al., 2017), following the method of Shapiro et al. (2011). To test the robustness of the oldest age estimates, we also ran analyses with the minimum age prior set at 0, 20, 40, or 50 kya BP. We ran analyses with each set of priors twice, each time with the Markov chain Monte Carlo (MCMC) chains run for 60 million iterations, sampling every 3,000 iterations, and discarding the first 10% as burn-in. Using Tracer v1.6, we observed that all parameters reached convergence with the exception of the tree likelihood, which swapped between two optima in all analyses. This was due to the shifting placement of sequence MS022 (KX269130; Froese et al., 2017). This sequence was therefore removed from the alignment and all analyses were re-run. Convergence was then

observed for all parameters. For each prior and alignment result set, we summarized trees and calculated a maximum clade credibility tree. All ages are reported as 95% highest posterior density (HPD) credibility intervals.

3.2 Results

3.4.1 Physical description:

Overall, we observed specimen UAMES 29458 to be relatively complete and well preserved (Figure 2). Based on the observed number of annual growth cycles visible in the horn sheath, we estimated the bison specimen to be minimally 12 years old, which is considered a mature individual (Fuller, 1959). The specimen's horn span was 90 cm at the widest point and the comparative angle and length of the horns indicate that it was a male (Guthrie, 1966). Much of the hair had sloughed off the specimen and was found in the surrounding sediment. In some areas, hair and skin had dried to the bone and were still attached. Hair from the front and hind limbs was yellow ochre in color, as were the shorter undercoat hairs from the body. The longer hairs were a reddish-brown or dark brown and tail hairs were black to dark brown. Long hairs found in the surrounding sediment, which likely came from the cape, beard or cap, were light to dark brown.

The skull was in excellent condition and the left and right mandibles were fused at the symphysis. The incisors were missing from a pre-burial break, apparently from gnawing. Evidence of root etching was observed on the ventral surfaces of the mandible with vivianite deposits observed on the articular surface. We observed that the cervical vertebra 2 (C2) through thoracic vertebra 7 (T7) had the dorsal portion of the spinous process gnawed and bitten off. We also observed T4 and T5 had evidence of damage from a carnivore, including puncture marks (Figure 3 a). Lumbar vertebra 1 (L1) to the sacrum also had evidence of carnivore damage on the ventral surface of the vertebrae (Figure 3 b). The distal ends of four thoracic ribs (towards the anterior portion of the body) also had canine puncture marks and gnawing. There were several pre- and post-burial breaks, and several medial portions of the ribs were

missing. One rib on the right side had a pathology consistent with a healed break. The left side was missing two thoracic ribs. The costal cartilage had carnivore gnawing damage on two fragments and the manubrium was missing one section.

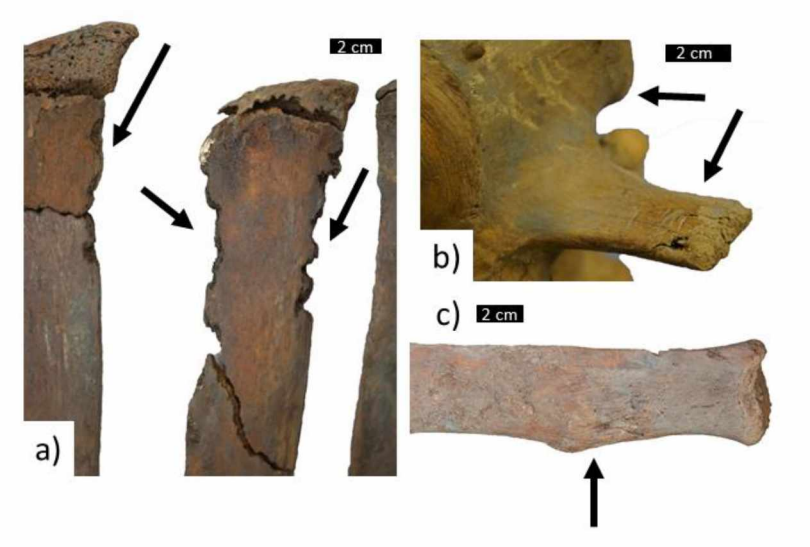

Figure 3.3 Scavenger dentition marks on the a) thoracic vertebral processes of Bison priscus specimen UAMES 29458 indicated by the arrows, and b) ventral side of lumbar vertebrae. c) Vertebrae with healed pathology.

The right appendicular skeleton was complete and we observed no evidence of carnivore damage. In addition, there was soft tissue (keratinous hoof sheathes, leather-like flesh and connective tissue) and vivianite present. There were gnaw marks and canine marks observed on the proximal end of the left humerus (lateral tuberosity) near its articulation with the scapula; the scapula was missing. There was root etching on the medial surface of the humerus where it would have rested on the ground after the specimen's death and we observed soft tissue adhering to the bone. The left metacarpal, carpals, and proximal, medial, and distal phalanges were missing, which could be consistent with loss during taphonomic processes upon emerging from the riverbank because the bones would have been exposed first and eroded out of the bank. In addition to the lack of carnivore marks near the articulations, they do not possess much food value for a carnivore and would not have been a primary target. On the left femur there was a pre-burial break at the greater trochanter, but no obvious carnivore damage. The left patella,

calcaneus, several left tarsals, one sesamoid, one proximal, medial and distal phalanx was missing, which is also consistent with secondary loss upon the specimen eroding out of the riverbank.

3.4.2 Radiocarbon analysis

We generated three new radiocarbon dates associated with specimen UAMES 29458 (Table 1). The background-subtracted fraction modern values for both the keratin and insect chitin are different from zero by ~6 standard deviations, which indicates the ages are finite. The age of the keratin from the bison horn sheath was 46,000 ± 1,100 ^{14}C yr BP (46,962 cal yr BP using CALIB 7.1; (Stuiver, Reimer and Reimer, 2019), which was very similar to the radiocarbon date produced from the keratinous fly puparium (Table 1 , Figure 4) taken from inside the bison skull cavity (46,800 ± 1,200 ^{4}C yr BP, just outside the range for calibration using CALIB 7.1 (Stuiver, Reimer and Reimer, 2019). The dated plant macrofossil found in the skull, along with the puparia, had a radiocarbon date of >49,900 radiocarbon years, which was outside the range for calibration (Table 1).

Table 3.1 Summary of radiocarbon dates.

Material	*^{14}C yrs*	*Error*	*Cal yr BP CALIB*	*Laboratory*	*Accession Number*
Collagen	>43,500	NA		BETA	324600
Keratin	46,000	1100	46,962	Keck	209861
Chitin	46,800	1200		Keck	209862
Plant	>49,990	NA		Keck	209863

3.4.3 Macrofossils

3.4.3.1 Fossil plant remains

The contents of the neural canal of the spine and skull from specimen UAMES 29458 included a sand-rich matrix with abundant moss, wood, and we could identify other plant fragments to species in some instances (Figures 4 and 5). The plant macrofossil assemblage from inside the skull is consistent with a mesic tundra or a wet flood plain surrounded by a shrub tundra (Figure 5). The presence of *Daphnia* spp. ephippia indicate that the sediment was also, at least partially, aquatic in origin. Bryophytic material,

likely from wet tundra and rivers, was abundant and well preserved in the skull cavity. Wood was very common and possibly came from the shrubs identified from seeds, leaves, and other materials in the skull cavity, including *Salix* spp. (willow), *Betula* spp. (birch), and *Andromeda polifolia* (bog rosemary) (Figure 4 n). These shrubs are typical of wet tundra and tend to be more abundant in more protected areas (Hulten, 1968; Cody, 2000), suggesting an interstadial environment. In addition, *Potentilla palustris* and *Juncus* spp. were also present and are typically associated with riparian habitats and bogs (Cody, 2000). In contrast, the remains of *Papaver* spp. (poppies) and *Polygonum bistorta* (Figure 4 l), which favor drier open slopes (Hulten, 1968), were also present in the bison skull cavity. The largest number of plant macrofossils from the skull cavity was the mustard and *Draba*-type seeds (Figures 4 m and 5), which are from a large and very diverse family making it difficult to use these specimens to characterize paleoecological conditions (Hulten, 1968; Cody, 2000). However, many of the species from this group are typical of open slopes, gravel and/or sandy river banks (Cody, 2000). In addition, there is a portion of grasses (Poaceae) (Figure 4 k) (and *Carex* Figure 4 i and j) that are typical of tundra or steppe ecosystems in the Arctic, and are consistent with an open landscape with no large shrubs (Hulten, 1968). The depositional sequence seems to have been relatively gentle due to the exceptional preservation of some of the delicate plant macrofossils, which included pollen anthers, intact herbaceous materials, and leaves with glands preserved. The spine contained 10 times more specimens per gram of sediment than the skull, possibly due to how accessible the cavity was.

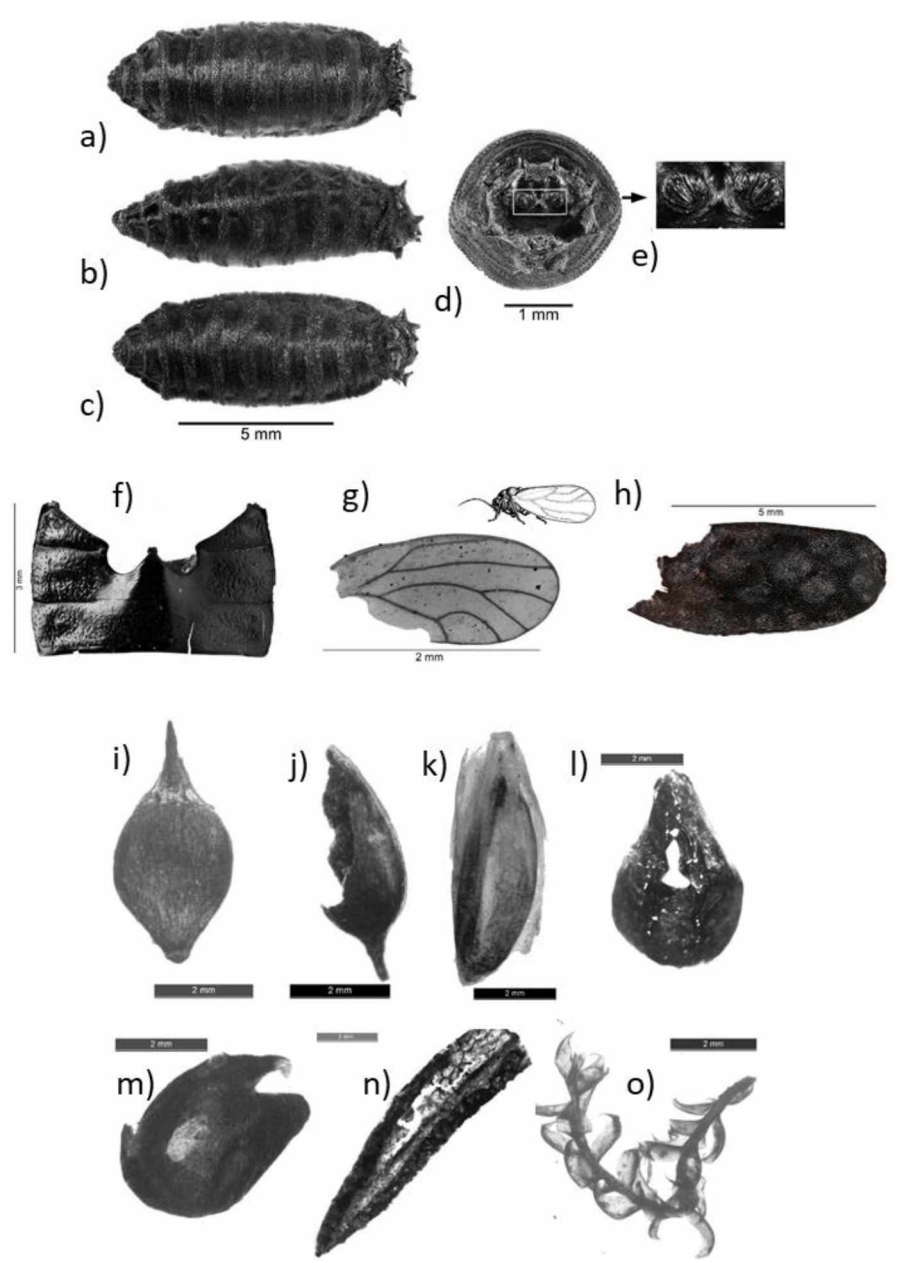

Figure 3.4 The macrofossil assemblage taken from skull of specimen UAMES 29458: Protophormia terraenovae puparium UAMES 52319. a), dorsal view b), lateral view c), ventral view d), posterior view, the posterior spiracles surrounded by a rectangle e), the posterior spiracles in close-up view. (photos: J.-B. Huchet, 2018), f) Partial abdomen sternites of a ground beetle UAMES 52334 (Carabidae: Pterostichinae) (photo: J.-B. Huchet, 2018), g) Psyllid forewing recovered from inside the bison skull UAMES 52331 (photo: J.-B. Huchet, 2018), h) Right elytron of a ripicolous ground beetle of the genus Elaphrus Fabricius UAMES 52333 (Carabidae: Elaphrinae) (photo: J.-B. Huchet, 2018), i) Carex seed lenticular, j) Carex seed Trigonal, k) Poaceae caryopsis, l) Polygonum bistorta, m) Draba-type seed, n) Andromeda polifolia, o) Bryophyta sp.

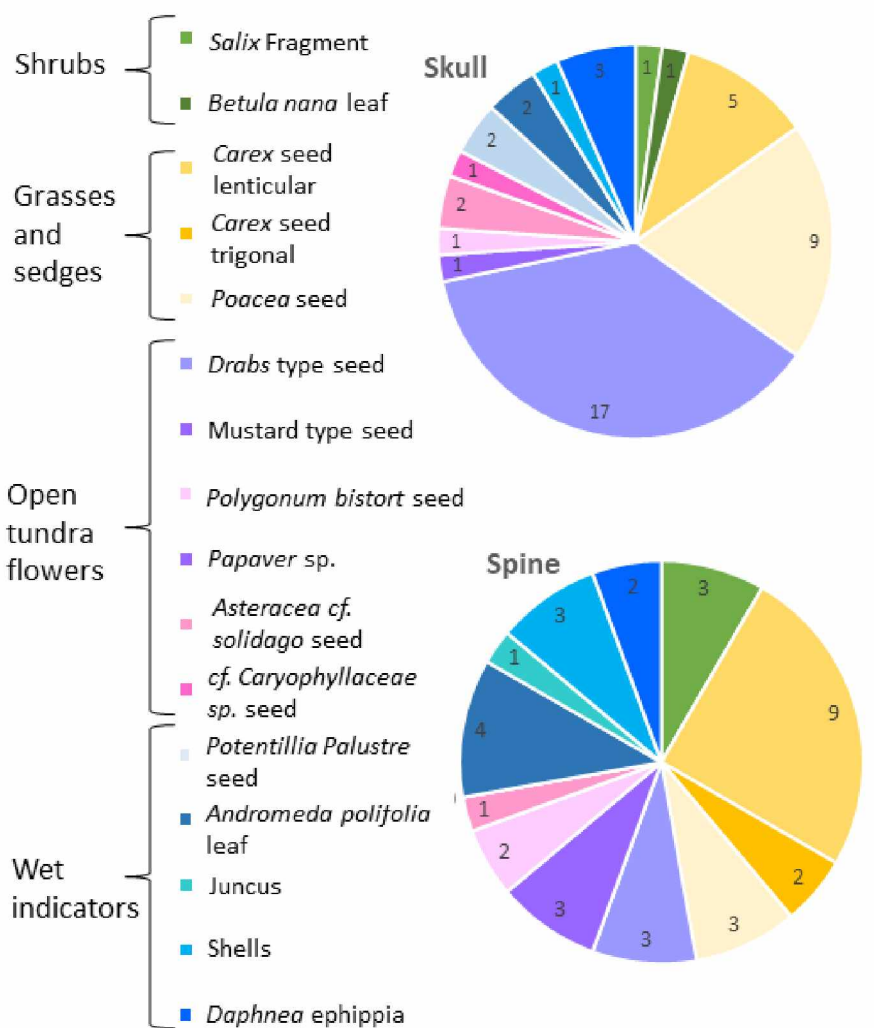

Figure 3.5 The relative abundance of plant macrofossil specimens in the skull and spine of specimen UAMES 29458, categorized by characteristic eco-type.

3.4.3.2 Fossil insect remains

Analysis of the skull cavity of UAMES 29458 revealed the presence of insect remains, including complete or incomplete blowfly puparia (Calliphoridae) (n = 15, UAMES 52319-52330). From their excellent state of preservation, a determination at the species level was possible and the taxon that colonized the bison at the time of its death was identified as the northern blowfly *Protophormia*

terraenovae (Robineau-Desvoidy) (Figure 4 a-e). With the exception of 4 fragmentary specimens, all the puparia were complete and unhatched indicating that the life cycle was interrupted before adult emergence. An attempt to open two fossil puparia (#29458c, (#29458g), in order to find a possible nymph and to observe its maturity stage, proved unsuccessful since the pupa had disintegrated inside.

Partial abdomen remains of a carabid beetle (Pterostichinae: cf. *Pterostichus* sp.) was also found inside the skull (UAMES 52334; Figure 4 f). Thirty-five *Pterostichus* species occur in Alaska (Bousquet *et al.*, 2013). Some representatives of this genus (i.e. *Pterostichus costatus* Ménétriés), live in the damp peaty areas of lowland tundra regions (Lindroth, 1966). Other insect remains belonging to several distinct orders were also recovered from inside the skull: a complete wing of Psylloidea (Homoptera) (UAMES 52331; Figure 4 g); a cephalic capsule of a larval Chironomidae (Diptera), an incomplete elytron of Elaphrinae (Coleoptera, Carabidae) (UAMES 52332; Figure 4 h) and finally, some disarticulated coleopteran remains, too fragmented to be identified. The presence of a psylloidean species in this context is not surprising since fossil remains of the three main plants (*Salix, Betula, Polygonum*) exploited by these insects were preserved evidenced within the skull cavity of the bison. The larval stages of chironomids develop in almost any aquatic or semiaquatic habitat, both standing and flowing waters, but also occur in tree-holes, rotting vegetation, and damp soils. Finally, the presence of *Elaphrus* sp. (*cf. trossulus* Semenov) (UAMES 52333; Figure 4 h), another ground beetle, is recorded. The species belonging to this genus are representative of riparian communities. Adults of all species of *Elaphrus* live along rivers, small streams, swamps, sloughs, or bogs, which is fully consistent with the bison discovery site. Overall, these taxa are typical of mesic to wet tundra habitats at the time of burial.

3.4.4 Isotopic analyses

The $\delta^{13}C$ and $\delta^{15}N$ values from the collagen sample were -20.0 ‰ (±0.6) and 4.2 ‰ (±0.1), respectively. The $\delta^{13}C$ value is consistent with a diet of vegetation consists of plants using C3 photosynthesis in a relatively open environment (Drucker *et al.*, 2008). The $\delta^{15}N$ value is consistent with values from other bison specimens dated to interstadial conditions, and contrast with stadial conditions,

which can have higher values (Hedges, Stevens and Richards, 2004; Rabanus-Wallace *et al.*, 2017). Based on an 8-10 year collagen turn-over rate (Hedges *et al.*, 2007), the collagen would exclude the higher $\delta^{15}N$ values from this individual's early life based on analyses of the horn sheath (described below), and thus the bone collagen and horn can be considered in the same range. The mean horn keratin $\delta^{13}C$ value was slightly lower than the collagen values (mean $\delta^{13}C$ value -21.3 ‰ ±1.1; -20.0 ‰ respectively), which is consistent with the difference in fractionation factors associated with the two different tissue types (keratin Δ=3.1 ‰ ±0.3; collagen Δ=5.1 ‰ ±0.3 (Drucker *et al.*, 2008)).

The mean $\delta^{15}N$ value from analyses of the horn keratin (4.6 ‰ ±1.1) was similar to the $\delta^{15}N$ value from the collagen value (4.2 ‰ ±0.1). The periodicity of the isotopic fluctuations in the horn sheath (Figure 6) appears to reflect annual cycles because the number of oscillations (n = 11) is consistent with the number of observed annual growth layers observed from the horn (11-12). The first two oscillations (~2 years) likely correspond with the period covered by the tooth record (~2.5 years) from the same specimen (described below). These apparently annual fluctuations would be consistent with the peaks in $\delta^{15}N$ values reflecting a seasonal shift to greater nutritional stress and a more water-limited plant diet during the winter (Funck et al., in review).. Shortly before the death of the bison, the $\delta^{15}N$ values from the horn sheath increases (Figure 6), which would correspond with a transition from summer to winter that is observed in modern bison from Alaska (Funck et al., in review), indicating the bison may have died in the late summer/early fall. Two peaks in the $\delta^{15}N$ values from the horn sheath occurred towards the start of the life of the bison and the second of these corresponds with a decrease in $\delta^{13}C$ values from the horn sheath. These features are consistent with periods of nutritional stress (Funck et al., in review). Most notably, this pattern seems consistent with catabolism and the use of lipid reserves respectively (Funck et al., in review). A marked decrease in $\delta^{13}C$ values is evident in the year prior to the bison's death, which also seems consistent with the use of the animal's lipid reserves (Funck et al., in review).

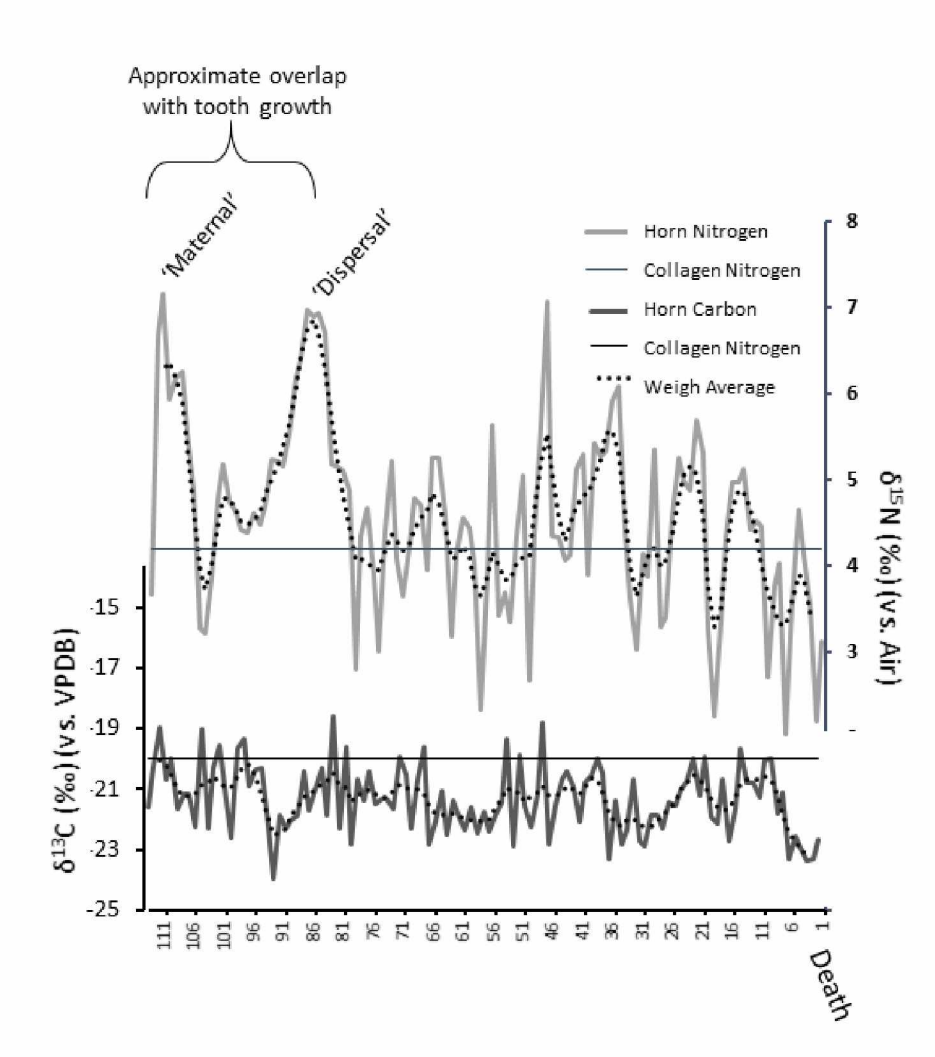

Figure 3.6 Carbon and nitrogen stable isotope values of serial horn sheath samples (n=113) with dotted trend-line of weighted moving averaging and collagen carbon and nitrogen stable isotope values.

The results of the strontium isotope analyses (n = 33) from specimen UAMES 29458 (Table 2), with an analytical precision of 0.00001, show a mean $^{87}Sr/^{86}Sr$ value from the first molar (M1) of 0.71139 (±0.00028). These values are consistent with the rodent teeth values from the Arctic Coastal Plain, which range from 0.70940 to 0.71107 (Table 3, Figure 7). The mean $^{87}Sr/^{86}Sr$ value from the M2 was higher compared to the values from the M1 ($p < 0.000$, t.test), averaging at 0.71206 (±0.00025). The mean $^{87}Sr/^{86}Sr$ value from the M3 was 0.71398 (± 0.00008) and was higher than the values from both the M1 and M2 ($p < 0.000$, t.test). The range of the M3 values was similar to the values found from the modern

rodents found in the foothills of the Brooks Range mountains (Table 3) (from 0.7137 to 0.7205) (Figure 8). Based on the bedrock $^{87}Sr/^{86}Sr$ model (Bataille and Bowen, 2012), the expected $^{87}Sr/^{86}Sr$ value at the place of death of specimen UAMES 29458 was ~0.70982 (Figure 8). Overall, the M1, M2 and M3 sequential data show a marked increase in $^{87}Sr/^{86}Sr$ values throughout the tooth sequence ($p < 0.000$, ANOVA) (Figure 7).

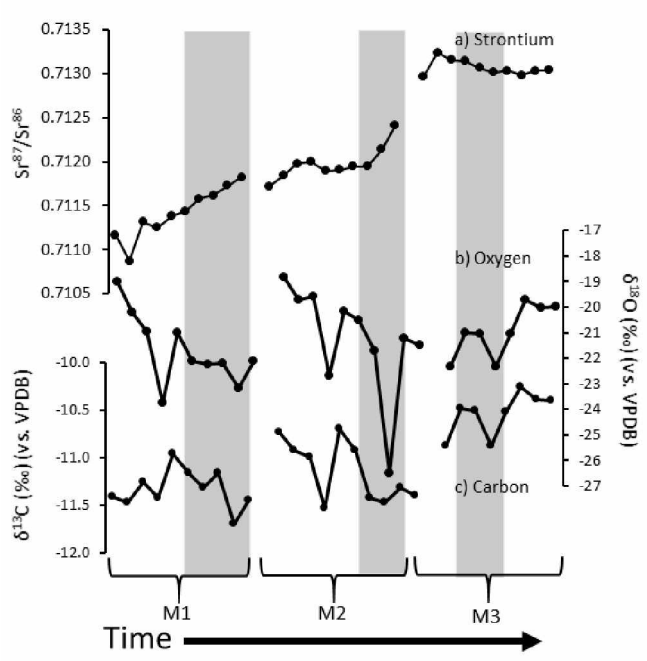

Figure 3.7 Isotope data from analyses of molar 1 (M1), molar 2 (M2), and molar 3 (M3) from specimen UAMES 29458. a) Strontium 87Sr/86Sr values, b) Oxygen stable isotope ratios expressed as δ18O values and c) Stable carbon isotope ratios (expressed as δ13C values).

Table 3.2 Results of isotopic analysis of strontium, carbon and oxygen of UAMES specimen 29458.

Tooth	Sample #	Distance from base of enamel (cm)	87Sr/86Sr	δ13C ‰ (VPDB)	δ13C ‰ Std dev	δ18O ‰ (VPDB)	δ18O ‰ Std dev
M1	1	1.8	0.71117	-11.4	0.1	-19.0	0.1
	2	1.7	0.71087	-11.5	0.3	-20.2	0.3
	3	2.55	0.71116	No data	No data	No data	No data
	4	1.3	0.71132	-11.3	0.4	-21.0	0.5
	5	1.15	0.71125	-11.4	0.5	-23.8	0.9
	6	1	0.71138	-11.0	0.2	-21.0	0.2
	7	0.8	0.71144	-11.2	0.3	-22.1	0.4
	8	0.65	0.71158	-11.3	0.1	-22.2	0.2
	9	0.5	0.71162	-11.2	0.1	-22.2	0.2
	10	0.3	0.71172	-11.7	0.4	-23.2	0.4
	11	0.2	0.71182	-11.4	0.2	-22.1	0.3
M2	1	2.1	0.71172	-10.7	0.1	-18.8	0.3
	2	1.95	0.71184	-10.9	0.2	-19.7	0.6
	3	1.8	0.71198	-11.0	0.1	-19.6	0.1
	4	1.65	0.712	-11.5	0.3	-22.7	0.4
	5	1.45	0.71189	-10.7	0.2	-20.2	0.4
	6	1.35	0.71191	-10.9	0.2	-20.5	0.5
	7	1.1	0.71195	-11.4	0.2	-21.7	0.3
	8	0.95	0.71195	-11.5	0.5	-26.5	0.9
	9	0.75	0.71214	-11.3	0.1	-21.2	0.3
	10	0.6	0.71242	-11.4	0.1	-21.5	0.3
	11	0.45	0.71236	No data	No data	No data	No data
	12	0.3	0.71255	No data	No data	No data	No data
M3	1	2.25	0.71297	-10.9	0.1	-22.3	0.3
	2	2.05	0.71324	-10.5	0.1	-21.0	0.1
	3	1.8	0.71315	-10.5	0.4	-21.0	0.1
	4	1.60	0.71314	-10.9	0.2	-22.3	0.2
	5	1.4	0.71307	-10.5	0.2	-21.1	0.3
	6	1.2	0.71302	-10.3	0.1	-19.7	0.1

Table3.2, Continued.

Tooth	*Sample #*	*Distance from base of enamel (cm)*	*87Sr/86Sr*	*δ13C ‰ (VPDB)*	*δ13C ‰ Std dev*	*δ18O ‰ (VPDB)*	*δ18O ‰ Std dev*
	7	1	0.71303	-10.4	0.2	-20.0	0.2
	8	0.85	0.71298	-10.4	0.2	-20.0	0.2
	9	0.6	0.71303	-10.4	0.1	-18.4	0.2
	10	0.45	0.71304	-10.6	0.2	-20.0	0.2

Table 3.3 Rodents use for characterizing 87Sr/86Sr isoscape.

UAM Mamm #	*Species*	*Locality*	$^{87}Sr/^{86}Sr$
4650	Microtus oeconomus	Meade River village	0.71007
8163	Microtus oeconomus	Umiat region, 1 mi N Umiat	0.71309
11149	Microtus oeconomus	Kikitaliorak Lake, Noatak drainage, ca 18 mi ESE Howard Pass	0.71721
11166	Microtus oeconomus	Feniak Lake (Noatak Valley, Feniak Lake, Makpik Cr)	0.71372
13614	Microtus oeconomus	Barrow, NARL research facilities	0.70940
56327	Microtus oeconomus	Desperation Lake	0.70619
66866	Microtus miurus	Unknown	0.71274
78833	Microtus miurus	Agiak Lake	0.71502
79046	Microtus miurus	Nanushuk River	0.71695
79102	Microtus oeconomus	Agiak Lake	0.71661
82113	Microtus oeconomus	N side of Lake Tulilik	0.72047
125703	Microtus oeconomus	Colville River - confluence of Kiligwa	0.71107
125706	Dicrostonyx groenlandicus	Colville R and confluence of Ipnavik	0.71494
125713	Microtus oeconomus	Colville River - SE of Kakvuiyat Bend	0.71312

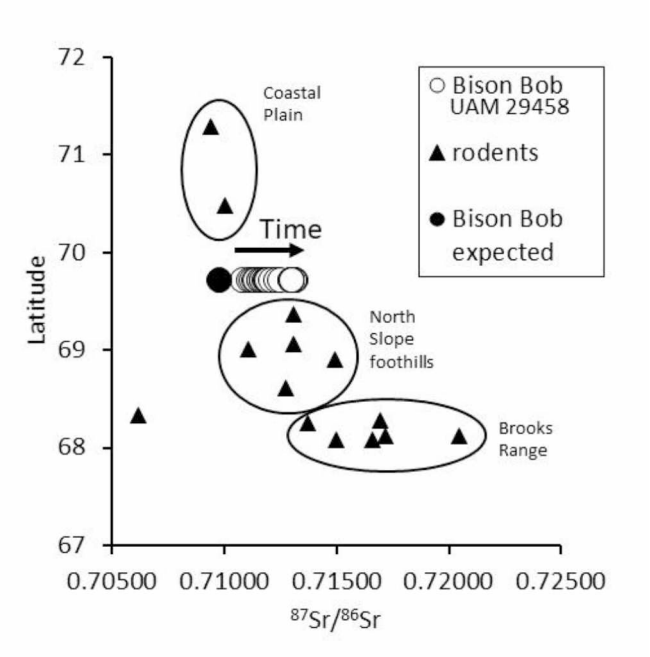

Figure 3.8 Rodent 87Sr/86Sr values grouped by region, compared to 87Sr/86Sr values from specimen UAMES 29458 over time and a model-predicted 87Sr/86Sr value for the death location of specimen UAMES 29458.

The mean $\delta^{18}O$ value across all teeth samples from specimen UAMES 29458 (n = 30) was -21.1 ‰ (±0.4) vs. VPDB (with an analytical precision of 0.2 ‰) (Table 4). Values were highly variable across the M1-M3 sequence (Figure 7) ranging from -18.4 ‰ to -26.5 ‰, but were not significantly different between teeth ($p = 0.34$, ANOVA). The values appear to cycle through approximately two full years, with three peaks representing summers, which seasonally have higher $\delta^{18}O$ values (Velivetskaya *et al.*, 2016) and separated by two cooler periods with lower values (Figure 7).

Table 3.4 Summary of isotopic results (δ13C‰ and δ18O‰ reported here vs. VPDB).

	Mean	***Max***	***Min***	***Range***
$^{87}Sr/^{86}Sr$	0.71214	0.71324	0.71087	0.00237
$\delta^{13}C$‰	-11.0	-10.3	-11.7	1.5
$\delta^{18}O$‰	-21.2	-18.4	-26.5	8.1

The mean $\delta^{13}C$ value of the enamel calcium carbonate from the teeth of specimen UAMES 29458 was -11.0 ‰ (±2.0) (with an analytical precision of 0.03) and had a relatively small range of values (-10.3 ‰ to -11.7 ‰) (Table 4), which are consistent with a C3 diet. Typical values for C3 plants are ~-27 ‰ (Wooller *et al.*, 2007) and the difference between animal diets and tooth calcium carbonate is Δ+14.6 - (Cerling and Harris 1999; Passey et al. 2005). Overall the $\delta^{13}C$ values started at their lowest during early life (M1) and gradually became higher in the M2 (-11.1 ‰ ±0.2) and M3 (-10.5 ‰ ±0.1) ($p < 0.000$, ANOVA), a trend that appears to correlate with the temporal shift from lower to higher $^{87}Sr/^{86}Sr$ values from the same teeth (Figure 7).

3.4.5 aDNA analyses

We generated 1.15 million reads from the unenriched library of UAMES 29458 (raw reads available at the NCBI Short Read Archive under BioProject PRJNA613249), which had an endogenous DNA content of 15.4% based on reads aligning to the cow genome. The relative mapping frequency ratio between the X chromosome and autosomes was 0.528, with a range of 0.493-0.561 across all 29 autosomes (Table 5). This is consistent with UAMES 29458 representing a genomic male individual.

Table 3.5 Results of the genomic sex determination analysis. X:A ratio is the ratio of the relative mapping frequency of the X chromosome to that of an autosome (1-29, all). Chr.: chromosome. The minimum and maximum X:A ratios are highlighted in bold.

Chr.	*Length*	*Reads mapped*	*X:A ratio*	*Chr.*	*Length*	*Reads mapped*	*X:A ratio*
1	161428367	10474	0.543	17	76280064	4915	0.547
2	141965563	9334	0.536	18	65811054	4640	0.500
3	126844711	8357	0.535	19	64845320	4500	0.508
4	123809850	8237	0.530	20	75686341	4995	0.534
5	125249322	8237	0.536	21	69078422	4622	0.527
6	122519025	8008	0.539	22	61598339	4384	0.495
7	113029157	7598	0.525	23	52334015	3652	0.505
8	116846264	7802	0.528	24	64508398	4447	0.511

Table 3.5, continued.

Chr.	*Length*	*Reads mapped*	*X:A ratio*	*Chr.*	*Length*	*Reads mapped*	*X:A ratio*
9	108503706	6828	0.560	25	44081797	3137	0.495
10	105982576	7023	0.532	26	51826547	3480	0.525
11	109987751	7605	0.510	27	48460478	3046	0.561
12	85119472	5420	0.554	28	45964680	3144	0.516
13	84213851	6029	0.493	29	51812796	3432	0.532
14	81216349	5748	0.498	all	2541187220	169841	0.528
15	84472747	5548	0.537				
16	77710258	5199	0.527	X	88654062	3126	NA

A full mitochondrial genome (JK319) was generated from the enriched library, with an average coverage of 139× (Genbank: MN549280). The phylogenetic placement of the UAMES 29458 mitochondrial genome was marginally impacted by the minimum age prior used, and was found either to fall at the base of Clade 2 (prior of 50 kya BP) or to be sister to MS002 within bison mitochondrial Clade 2 (all other tested priors) (Figure 9, Table 6). The inclusion or exclusion of MS022 did not affect the phylogenetic placement of UAMES 29458. Across all analyses, the age of UAMES 29458 was estimated to be ~33-87 kya BP (Table 6). Analyses with MS022 excluded generally yielded slightly older age estimates, but varying the minimum age prior did not greatly impact this individual's maximum estimated age (range of ~81-87 kya BP across all analyses). This suggests that the priors did not drive the estimated age results. Mapped reads from both the unenriched (primarily nuclear) and enriched (mitochondrial) DNA libraries exhibit damage patterns characteristic of authentic aDNA, including short DNA fragments and elevated relative deamination frequencies at the ends of reads (Figure S4).

Table 3.6 Summary of the Bayesian molecular analyses of JK319/UAMES 29458, with overall maximum age ranges highlighted in bold

Analysis variables		***Phylogenetic placement***		***Estimated age***		
Min. age prior	***MS022***	***Placement***	***Posterior probability***	***Minimum***	***Maximum***	***ESS***
0	Included	1	0.276	32,653	85,157	11376
0	Excluded	1	0.410	36,022	86,643	20465
20,000	Included	1	0.261	34,300	85,618	15546
20,000	Excluded	1	0.409	34,929	85,827	18525
30,000	Included	1	0.268	34,708	83,346	19814
30,000	Excluded	1	0.407	36,696	85,376	18945
40,000	Included	1	0.241	40,021	81,074	19367
40,000	Excluded	1	0.391	40,227	82,423	19013
50,000	Included	2	0.678	50,000	82,285	20687
50,000	Excluded	2	1.000	50,007	82,935	18967

Phylogenetic placements are: 1) sister to MS002, and 2) at the base of Clade 2 (see Figure 9). Minimum and maximum ages are based on 95% highest posterior density credibility intervals. Note that, for analyses with a minimum age prior of 40 and 50 kya BP, the estimated minimum ages are likely to have been truncated by the prior. ESS: estimated sample size.

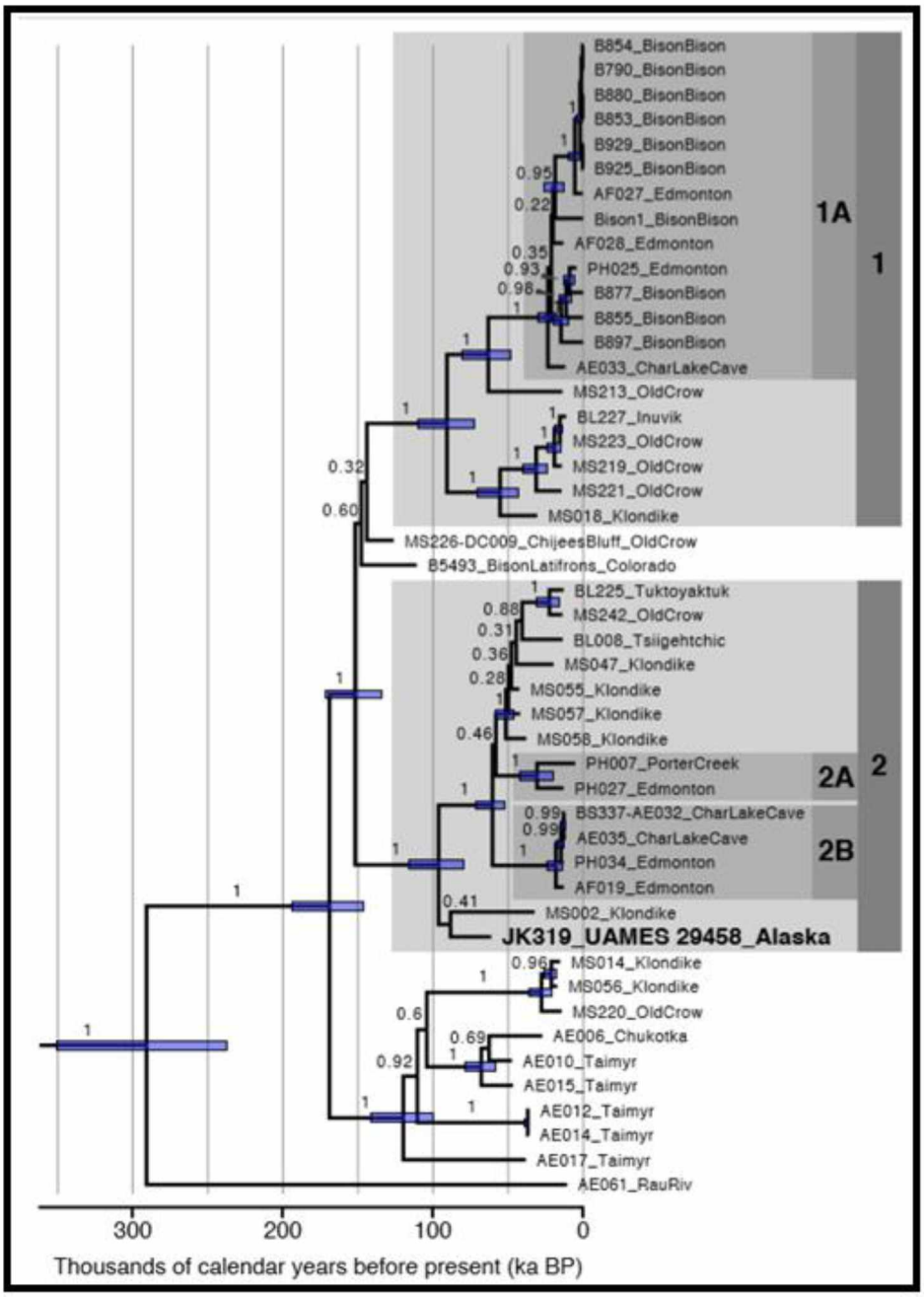

Figure 3.9 A Bayesian time-calibrated genealogy of bison mitochondrial genomes, with major well-supported Clades (1, 1A, 2, 2A, 2B) highlighted (following Heintzman et al., 2016 and Zazula et al., 2017). All living bison fall within Clade 1A, whereas the specimen UAMES 29458 falls near the base of Clade 2. Purple bars are 95% highest posterior density intervals for node heights and are shown for nodes with posterior probability >0.95. This maximum clade credibility tree resulted from the analysis that excluded MS022 and had a minimum age prior of 30 kya BP for UAMES 29458. Results from the other analyses can be found in Table 6. The diverged yak tips have been removed.

3.3 Discussion

4.3.1 Constraining a chronological age for UAMES 29458

Specimen UAMES 29458 provides several lines of evidence that can be used to constrain the individual's chronological age (Figure 11). The radiocarbon dates from the keratin and the blow fly puparium (chitin) are nearly identical (46,000 ±1100 ^{14}C yrs and 46,800 ±1200 ^{14}C yrs – inside and outside the range for calibration, respectively). Keratin is a structurally dense tissue and less susceptible to contamination than collagen (Taylor *et al.*, 1995). The blow flies *P. terraenovae*, which colonizes a corpse within hours or days following death, seemed a good candidate for precise ^{14}C dating of specimen UAMES 29458. The congruence of the keratin and chitin ^{14}C dates lends support for a finite age of approximately 46,900 ^{14}C yrs. In contrast, the radiocarbon dates from collagen and from plant material are non-finite. Collagen, from porous bone material, can be contaminated or degraded. The sample from the bone of UAMES 29458 was also run on a lower energy ^{14}C instrument, which cannot discriminate low levels of ^{14}C from old samples compared with the chitin and keratin, which were run on a more powerful instrument. The radiocarbon date of the plant material and its apparent older age compared to the puparium and keratin is difficult to interpret. The plant material recovered from the skull was specifically selected because it was a delicate herbaceous structure that would not have endured high energy reworking or be influenced by variations in carbon sources that can occur in aquatic plants (Marcenko *et al.*, 1989). However, the radiocarbon date of the plant was determined to be non-finite (>49,000) and could have been reworked from older sediments in a low-energy environment. Given that the dates from keratin and chitin are on the margins of radiocarbon limits we must consider two possibilities; first, that the finite dates are accurate, or second, that these dates are not distinguishable from non-finite dates.

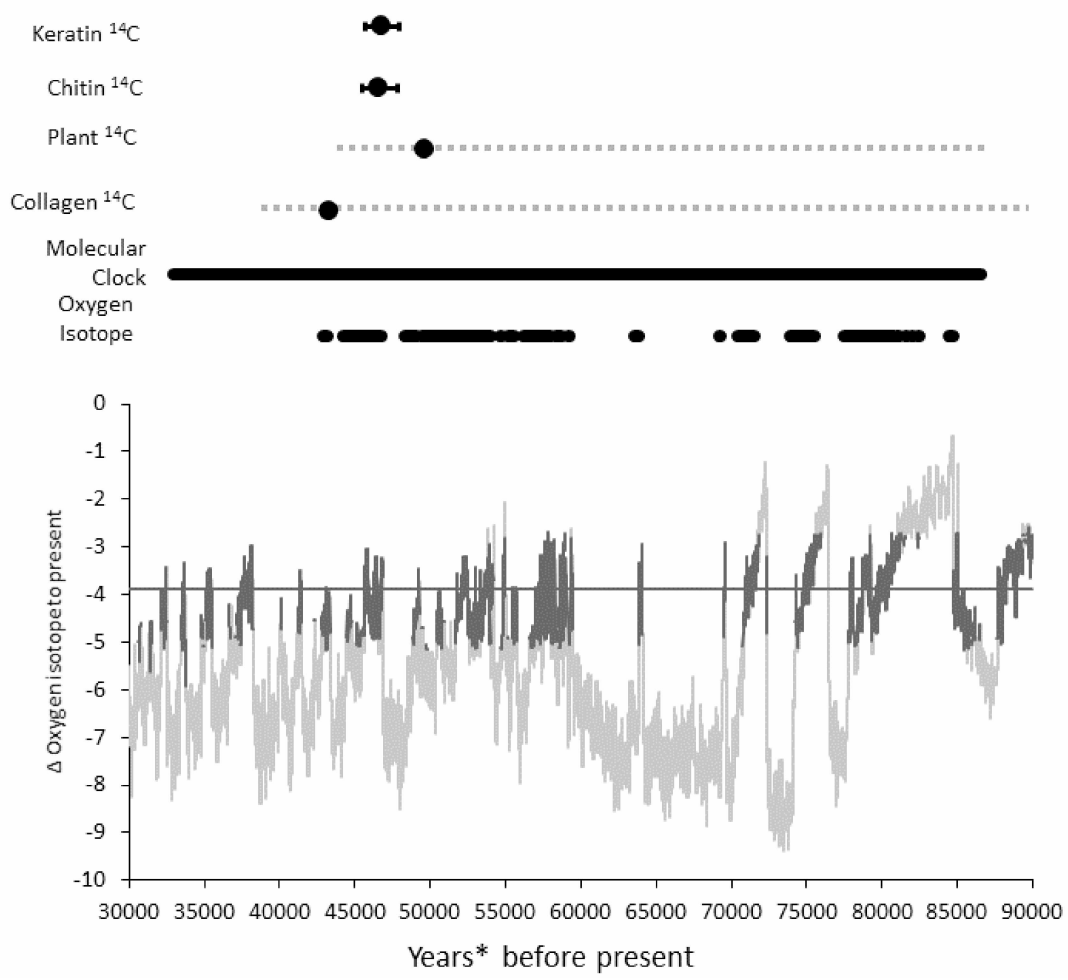

*Figure 3.10 Summary of all radiocarbon dates (14C), molecular clock estimates, and compatible δ18O value periods based on Greenland Ice core values (Rasmussen et al., 2014) and a □4‰ lower values than present. *dates are calibrated radiocarbon dates where possible,*

Other evidence supports the hypothesis that UAMES 29458 dates are finite in age. Environmental information from the $\delta^{18}O$ values from the bison specimen and plant macrofossils add further dimensions that help constrain the chronological age estimation for UAMES 29458. The mean $\delta^{18}O$ value (as VSMOW) from analyses of the bison's molars is -3.9 ‰ (±1.2) lower than the mean modern precipitation values. In contrast, full stadial $\delta^{18}O$ values for precipitation tend to be around -8 ‰ lower than modern precipitation values (Bowen, 2018; Gaglioti et al., 2017; Meyer et al., 2010; Rasmussen et al., 2014). The $\delta^{18}O$ values from UAMES 29458 therefore indicate that although the climate was slightly colder than modern it was not full stadial (Figure 11). The finite radiocarbon date from the keratin coincides with a

period of time that had an offset in $\delta^{18}O$ values of Δ -3.9 ‰ (±1.2), between 44,380 cal yrs BP and 46,880 cal yrs BP (Rasmussen *et al.*, 2014). This inference that the bison specimen may have lived during a more moderate (interstadial) climate is also supported by the plant macrofossils and insect remains found in the skull, which represent a typical flood plain in tundra ecosystems of the Arctic. However, as stated above, the plant remains may not be exactly contemporaneous with the specimen.

The Bayesian molecular age estimate for the specimen was between ~33-87 kya BP, which is consistent with the radiocarbon ages and corresponds to Marine Isotope Stage (MIS) 3 through to MIS 5b (Lisiecki and Raymo, 2005). Although the results of this analysis are not informative as to whether UAMES 29458 is of older radiocarbon finite or non-finite age, they do suggest that, if the individual were radiocarbon non-finite, it lived after MIS 5e. The finite radiocarbon age from the bison's keratin is within the range of this molecular-clock derived age estimate, which could narrow the age estimate to within MIS 3 (29-57 kya BP). Our phylogenetic analyses show that UAMES 29458 belonged to bison mitochondrial clade 2 (Heintzman *et al.*, 2016). This lineage did not contribute to extant bison diversity, and instead became extinct during the late Holocene, by as long as ~400 years ago (Shapiro *et al.*, 2004; Heintzman *et al.*, 2016). Given the varied methods used for dating this specimen, it is expected that there might be some disagreement between results. However, the two nearly identical dates from the chemically stable portions associated with the specimen (i.e. keratin and insect chitin, 46,000 ±1100 ^{14}C yr BP and 46,800 ±1200 ^{14}C yr BP, respectively) provide support for this as a finite-aged specimen very close to the limit of radiocarbon dating. This age is congruent with an appropriate climatic period suggested by the $\delta^{18}O$ values (Figure 11) and the macrofossil assemblage of flora.

4.3.2 Life history of an individual steppe bison

Multiple lines of evidence suggest that specimen UAMES 29458 was a large bull that was 11 to 12 years old at the time of death. Present-day male bison of this age are typically lone bulls, either in or just past their prime (Soper, 1941; Maher and Byers, 1987). During his life, this individual incurred injury to a rib and the bone callous clearly indicates it healed (Figure 3c). This type of injury typically occurs in present-

day bison during the rut when bison compete for access to females (Lott, 1971). In addition to this evidence of injury, the early stages of this bison's life, recorded as the $\delta^{15}N$ values from the horn sheath (Figure 6), indicate some periods of nutritional stress. Increases in $\delta^{15}N$ values in the tissues of animals can represent stressors, such as starvation, illness, or long-distance movement (Funck et al., in review). Shifts in $\delta^{15}N$ values are generally used to determine changes in the trophic level, an interpretation that is not appropriate for a herbivore (Post, 2002). However, during nutritional stress an animal can break down its muscles to build new proteins, during which tissues fractionate and lead to elevated $\delta^{15}N$ values (Lee *et al.*, 2012). The bison specimen analyzed here exhibited two periods of elevated $\delta^{15}N$ values towards the start of its life (Figure 6). Horn stubs begin developing in utero but do not solidify into horn spikes until the calves are older (Wiener *et al.*, 2015). The two periods of higher $\delta^{15}N$ values likely occurred in the first 2-3 years of life, overlapping with some of the time periods represented by the molar development, which was used to produce the $\delta^{18}O$ and $^{87}Sr/^{86}Sr$ values.

The interpretation of intra-tooth serial samples as a measure of change over time requires an understanding of how teeth develop and mineralize. For example, the molars of bison have been shown to grow over 2 to 2.5 years (Gadbury *et al.*, 2000; Higgins and MacFadden, 2004; Velivetskaya *et al.*, 2016) and the pattern of molar eruption occurs in a particular sequence and time in an animal's life. As each molar develops, discrete layers of enamel are laid down and retain the isotopic composition of conditions at each point in time. However, as a tooth develops it continues to mineralize over 6 to 7 months leading to a degree of isotopic averaging (Balasse, 2002; Montgomery, Evans and Horstwood, 2010). As a result, changes that may appear progressive could in fact occur over much shorter periods of time and the exact timing of tooth development and mineralization can be subject to some degree of variation between individuals and species. However, Velivetskaya et al. (2016) used high-resolution sampling for analysis of stable oxygen isotope composition (expressed as $\delta^{18}O$ values) to pinpoint the timing of tooth development in two late-Pleistocene steppe bison from the Middle Urals, Russia and found it to be close to those of present-day bison. Seasonal oscillation in $\delta^{18}O$ values can also be compared to those of present-day animals to track the speed of tooth development.

The M1 is formed in utero and shortly after birth (Bernard *et al.*, 2009; Widga, Walker and Stockli, 2010), and thus represents the mother's home range and the calving grounds. The M1 formation likely corresponds with the timing of the first $\delta^{15}N$ value peak (Figure 6). The $^{87}Sr/^{86}Sr$ values from the M1 had little variation suggesting the mother remained in a relatively consistent geological area. When the M1 $^{87}Sr/^{86}Sr$ values are compared to bioavailable $^{87}Sr/^{86}Sr$ values from the region, it appears that this bison began life on the Alaska coastal plain (Figure 8). Contemporary caribou from similar regions of Alaska currently use the coastal plain as calving grounds, taking advantage of the emerging grasses and open terrain (Fancy *et al.*, 1990; Post and Forchhammer, 2008). Subsequently, they move to higher ground to avoid insects and to take advantage of abundant lichens that sustain them during non-calving seasons (Fancy *et al.*, 1990). The first peak in $\delta^{15}N$ values from the horn (Figure 6) likely corresponds to this M1 period and could be interpreted as a maternal/weening signal (Gadbury *et al.*, 2000; Reitsema and Muir, 2015), either attributed to the bison being at a higher trophic level than its mother from which it was nursing, or the effect of weening and the nutritional stress that it may have imparted (Fuller, Richards and Mays, 2003).

After the period of initial geographic stability inferred from the $^{87}Sr/^{86}Sr$ values in the M1, which likely represented the first year of life, the bison seems to have dispersed into a new geographic area during its second summer according to the $^{87}Sr/^{86}Sr$ values from the M2 and M3. The M2 development starts at ~2 to 3 months of age and continues for 12-15 months (Gadbury *et al.*, 2000; Velivetskaya *et al.*, 2016). The M3 subsequently develops from the beginning of the second summer after weaning, ~10-11 months until the age of about 2 to 2.5 years (Gadbury *et al.*, 2000; Velivetskaya *et al.*, 2016). Comparisons of the bison's $^{87}Sr/^{86}Sr$ values from the M2 and M3 to bioavailable $^{87}Sr/^{86}Sr$ values from the region indicate that the bison may have moved into the foothills of the Brooks Range (Figure 1 and Figure 8). The second peak in $\delta^{15}N$ values from the analyses of the horn sheath (Figure 6) could correspond to mobility on the landscape, which seems to have occurred during this period. A study on present-day wood bison in Alaska (Funck et al., in review) found that bison that traveled long distances, or experienced nutritional stress, produced elevated $\delta^{15}N$ values due to the energetic costs of travel. In the present study, the

carbonate $\delta^{13}C$ values show an overall increase (+1 ‰) during this same period (~2.5 years), consistent with a change from a wetter environment to a drier one (Wooller *et al.*, 2007), which also seems to correspond with a shift towards the higher and drier elevations of the foothills compared to the wetter, lower reaches of the coastal plain. Later in the bison's life, after the record preserved in the molars is fully mineralized (~2.5 years), we lose track of the specimen's geolocation based on the strontium isotope record. However, this bison must have eventually returned to the coastal plain to the location where he eventually died and was found (Figure 1).

In contrast to the tooth record, the horn sheath continues to develop over approximately the lifetime of the individual. The $\delta^{15}N$ fluctuates through what appear to be seasonal oscillations of slightly more elevated $\delta^{15}N$ values in the winter, likely due to nutritional stress during this season, then lower $\delta^{15}N$ values during more favorable summers, interpreted based on isotopic patterns exhibited in present-day bison from Alaska (Funck et al., in review). Present-day wood bison south of the Brooks Range in Alaska only had changes in $\delta^{15}N$ values during particularly hard winters (Funck et al., in review). Thus, these winters were likely harder than the conditions experienced by present-day analogous populations. Applying this seasonal pattern implies that the sample closest to the horn core (i.e. the period leading to the animal's death) represented the start of the transition from the summer to winter. This indicates that the bison was not experiencing unusual nutritional stress and did not appear to have been in a weakened state prior to death. However, the low $\delta^{13}C$ values from the horn sheath in the last year of life, relative to the rest of the record from the horn, could indicate that the animal may have begun to draw on its lipid reserves (Funck et al., in review).

The degree of mobility of the bison specimen analyzed, based on the $^{87}Sr/^{86}Sr$ data from the North Slope specimen, is relatively high compared to data from other ancient and present-day bison (Figure 11, Table 7; Britton et al., 2011; Glassburn, et al., 2015; Julien et al. 2012; Widga et al., 2010). Although the range of $^{87}Sr/^{86}Sr$ values cannot be directly compared, because variability is highly dependent on the geological heterogeneity of a landscape that individuals inhabit, the bison specimen from the North Slope does demonstrate a very high comparative range. Britton et al. (2011) examined a single bison from

western France dating to 49,000 ±5,000 BP and demonstrated high fidelity to an area, with almost no variability in $^{87}Sr/^{86}Sr$ values. Julien et al. (2012) found that steppe bison from the Last Glacial Maximum (LGM) (~20.5 kya BP) in Amrosievika in Eastern Ukraine had a $^{87}Sr/^{86}Sr$ range of 0.00074 and attributed this low degree of variability to minimal mobility on the landscape (Julien *et al.*, 2012). A study of bison herds on the Great Plains of North America from the Middle Holocene indicated that bison also had limited seasonal mobility (<50 km), while inter-annual movement of herds over ~4-5 yrs moved further afield (<500 km) (Widga et al., 2010a). In contrast, present-day *Bison bison* from the interior of Alaska, with an observed seasonal and regional migration route, had a range $^{87}Sr/^{86}Sr$ of 0.71714 to 0.71540 (0.00174) (Glassburn *et al.*, 2018). Overall, the range of $^{87}Sr/^{86}Sr$ variation from the North Slope bison specimen analyzed here (0.00237) is relatively large compared to all these previous measures, indicating that he was likely a gregarious individual who traveled some distance during his early years of life. The variability in $^{87}Sr/^{86}Sr$ ranges among bison from different localities and periods suggests that bison utilize different mobility strategies that are dependent on (paleo)ecological conditions. Future research could integrate genetic testing of sex from specimens to determine if males and females used different mobility strategies.

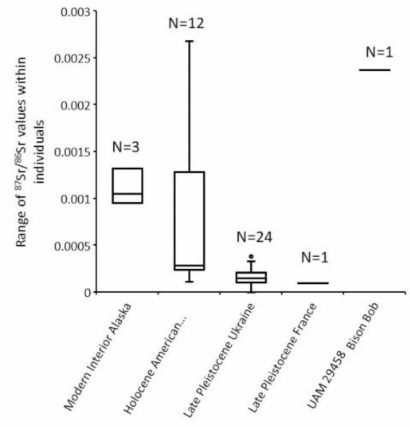

Figure 3.11 Comparison of the ranges (□) of 87Sr/86Sr values recorded within the teeth of different bison including, present-day plains bison (Bison bison) from interior Alaska (Glassburn et al., 2018); Holocene plains bison (Bison bison) from the American Plains (Widga et al., 2010); Late Pleistocene steppe bison (Bison priscus) from Ukraine (Julien et al., 2012) and Late Pleistocene steppe bison (Bison priscus) from France (Britton et al., 2011).

*Table 3.7 Comparison to other Bison strontium data. See Figure 10 *Stratigraphically determined to be from MIS4 **Molecular clock*

Context	*Species*	*N*	*Date*	*Average Range*	*Citation*
Present-day Interior Alaska	Bison bison	3	2014	0.00111	Glassburn et al. 2018
Holocene American Plaines	Bison bison	12	8930-6980 cal yr BP	0.00077	Widga et al. 2010
Late Pleistocene Ukraine	Bison priscus	24	20557-20,491 cal yr BP	0.00016	Julien et al. 2012
Late Pleistocene France	Bison priscus	1	49,000±5 yr BP*	0.00010	Britton et al. 2011
UAMES 29458	Bison priscus	1	33-87,000 yr BP**	0.00237	This paper

4.3.3 Necrology and Biostratinomy

Evidence from the specimen UAMES 29458 helps shape a paleoecological picture leading up to the individual's death, decomposition, and the mechanism of burial. The bones from the bison specimen were overall in a state of excellent preservation as evidenced by the presence of intact horn, hooves, fur, spinal cord, cartilage, and possible brain tissues. Specimens of this level of completeness are extremely rare in Quaternary deposits. There were no obvious signs of the cause of death, such as bite marks around the nose or neck, and all carnivore marks were related to scavenging (Andersson, Norman and Werdelin, 2011) but predation cannot be ruled out. After death, the specimen came to finally rest on his right side, which protected that side from scavenging, this is further supported by the presence of vivianite. Vivianite deposits tended to be on the bone surfaces that were exposed to the ground surface and root etching also tended to be present on the surfaces of the bones that rested on the ground (Supplemental data). Carnivore tooth marks are present at various locations on the specimen, indicating scavenging of the bison carcass occurred post mortem (Figure 3 a and b and Supplemental data). There are four major carnivore taxa present contemporaneously that could cause the type of damage seen on UAMES 29458: *Arctodus simus* (short-faced bear), *Canis Lupus* (wolf), *Homotherium serum* (scimitar cat), and *Panthera*

atrox (American lion) (Fox-dobbs, Leonard and Koch, 2008; Schubert, 2010). The dentition marks (Figure 3) were consistently narrow punctures, which are not consistent with the wide teeth of *A. simus* (Sorkin, 2006) or *H. serum* (Ewald *et al.*, 2018). The incisor punctures indicated that the space between the canines is at least 6 cm apart, which is consistent with *P. atrox* (Baryshnikov and Boeskorov, 2001; Christiansen and Harris, 2010). This may be out of the range of the smaller *C. lupus* (Sorkin, 2006), leaving large *felidae* as the most likely scavenger. Indication of lion scavenging have also been found on other preserved bison specimens from in Alaska (Guthrie, 1989). It is likely that only one individual scavenger caused all of the damage based on the consistency in size of the tooth marks. The limited scavenging also supports a single scavenger, as more individuals would require less time to remove meat, disarticulate the corpse, and scavenge from a greater area of the carcass (Blumenschine, 1986). The carnivore appears to have consumed the bison carcass and ate portions of the back strap based on observed damage along the spinous processes of several vertebrae (Figure 3 a and b). The carnivore also seems to have consumed the carcass from the inside of the body and likely ate the internal organs and tenderloin based on damage to the costal cartilage, the distal ribs, the transverse processes of the lumbar vertebrae, and the sacrum. In addition, the carnivore gnawed the left humerus and likely removed the left scapula, in an attempt to get at the flesh of the left fore-limb. Scavenging only seems to have occurred in high-value areas, supporting an inference that the carcass was likely buried rapidly. In most contexts a carcass on an open landscape with carnivores can be consumed and disarticulated within hours to a few days (Blumenschine, 1986). It is for this reason that complete specimens are extremely rare. Thus, for this specimen to preserve, something exceptional must have occurred to protect it. During the erosion that re-exposed the bison it seems the left extremities of the front and hind limbs (phalanxes, carpals, tarsals, etc.) may have been lost due to erosional processes (Figure 2). These skeletal elements would be the first to be exposed and vulnerable to gravity, weathering, and would have been preferentially removed via taphonomic agents (e.g., eroded into the river and lost). These skeletal elements of the lower extremities are also not associated with high food value flesh and likely would not have been a target for scavenging.

The presence of the blow fly puparia recovered from inside the skull made it possible to propose some "paleoforensics" hypotheses associated with postmortem events. Blow flies figure among the most relevant witnesses in forensic entomology in order to determine the time elapsed since death, namely the postmortem interval (PMI) because blow flies (Calliphoridae) are the first and predominant organisms to colonize a body after death. Within hours of death, these insects are attracted to the smell of the decomposing remains, which are both a site for laying eggs and a source of protein for larval development. Under normal circumstances, egg laying occurs soon after death (1–3 days) (Gomes, Augusto and Godoy, 2006). The favored egg-laying sites are the natural openings of the body (mouth, eyes, anus) as well as any wounds present on the corpse (Gomes, Augusto and Godoy, 2006). The species preserved on the carcass *Protophormia terraenovae* (Robineau Desvoidy) is a Holarctic, cold-adapted species, present throughout northern Europe and Asia. Very common in the cooler high latitude regions and notably in the Arctic, representatives of this species are found within 890 km of the North Pole (Smith, 1986). Experiments conducted by Marchenko (2001) found that the development period of *P. terraenovae* (from egg to adult) is relatively long. According to Warren and Anderson (2013), egg-carrying females of *P. terraenovae* do not lay eggs at temperatures lower than 10.3°C. In the North Slope region, temperatures only reach above 10°C during the summer period (https://www.weatherbase.com). Insects, like all arthropods, are coldblooded and the duration of their life-cycle is primarily temperature driven. Rate of development is species-specific and influenced by biotic (e.g. maggot mass that can significantly accelerate rate of development) and environmental factors (exposure of the carcass to sunlight or shade, rain, and wind). Following the biological data provided by Marchenko (2001), and focusing on temperatures ranging from 11 to 18°C (respectively the average minimal temperature required for laying eggs and the current maximum temperatures recorded on the paleontological site), *P. terraenovae* development extends from 15 to 50 days (egg to pupal stage) and adult emergence from 24 to 78 days. In the case of UAMES 29458, all of the puparia were intact with no evidence of adult emergence.

The fact that the bison's skeleton was almost complete and articulated, and not fully scavenged by carnivores suggests that the fly pupal stage intervened fairly quickly, indicating relatively high temperatures at the time of death (e.g., at 18°C, the pupal stage would have started on the 15th day). The bison carcass was then quickly covered with sediment or snow precluding further access to predators; however, a few centimeters of soil cover would not prevent the development and emergence of flies (Balme *et al.*, 2012). Trapped in the skull, the pupae would have preserved in situ. The presence of unhatched fly puparia of *P. terraenovae* recovered from the bison individual indicates that its carcass had been subaerially exposed for at least 2 weeks before the life cycle was interrupted either due to a more complete burial or freezing. Moreover, we can argue that the ambient temperature was very likely over 10°C when the fly infestation occurred, requiring the events to occur during a warm period of the year. This warm period seems to have been at the transition from summer to winter, based on the isotopic evidence from the horn sheath.

Fluvial sediments including plant macrofossils likely entered the skull after this initial burial during which the *P. terraenovae* puparia developed. The plant macrofossils recovered from inside the skull and neural canal are unlikely penecontemporaneous with the death of this bison individual, but could indicate an overall glimpse of the surroundings. The macrofossil assemblage of plants is consistent with an Arctic flood plain. The immediate surrounding of the river was probably covered in moss, low shrubs, and bogs (Figure 5). Further away from the banks of the river were likely drier tundra with grasses, sedges, and a variety of tundra flowers including *Papaver* sp., *Polygonum bistorta,* and *Draba* type (Figure 5). Overall, the plant assemblage is more typical of a mesic tundra than a steppe and possibly originated from an inter-glacial or interstadial environment (Gaglioti *et al.*, 2018).

Overall, we conclude that this bison died on a flood plain during the warm period prior to the onset of winter and fell on to its right side. A carnivore, possibly a large *felidae*, quickly consumed high-value areas of meat and blow flies swiftly laid eggs within the skull. Alluvial sediments or possibly snow then quickly buried the carcass before the carcass could be further disarticulated. At least two weeks

passed before temperatures inside the carcass or the oxygen availability fell too low for the puparia to continue developing.

3.4 Conclusion

Our multi-proxy paleoecological evidence from UAMES 29458 fills out the details of an individual bison's life and death in the Arctic, where bison were once a dominant herbivore. Combining serial isotope analyses with aDNA allowed us to combine mobility information with genealogical information, and to place the individual within bison meta-population dynamics over millennia. This augments a paleoecological picture based on the physical evidence of the skeletal remains alone, providing a more vivid image of a highly mobile individual moving across the North Slope of Alaska. The mitochondrial lineage of this bison is one that thrived in Beringia but ultimately died out. Our multiproxy evaluation indicates that this bison likely lived during an interstadial period, which in some ways may have been somewhat similar to today. Strontium isotope data from the specimen indicates that he dispersed across the Northern Alaska landscape from possible calving grounds located on the Arctic coastal plain to the foothills of the Brooks Range in early life and ultimately back to his place of death on the Arctic coastal plain. Nitrogen isotopes from the horn sheath indicate that the mobility of his early life may have resulted in significant nutritional stress, and that this individual suffered somewhat harsher winters than those on the North Slope today. The taphonomic analysis revealed that this bison was scavenged in parts of high nutritional value, which was followed by a rapid burial in a riverine environment, likely in the early summer. In this case, a multiproxy approach has uncovered a life history and detailed examination of a member of a dominant Pleistocene species in the Arctic.

3.5 Acknowledgments

First and foremost, we recognize and are very grateful for the efforts of Dr. Dan Mann and Dr. Pam Groves in discovering, excavating, and transporting this exceptional specimen, affectionately known as 'Bison Bob' to the UAMN. Without them none of this work would have been possible and we thank them for discussions. The bison specimen was collected during fieldwork directed by Mike Kunz and funded by the Bureau of Land Management. Kathrine Anderson at the Museum of the North Earth Sciences managed curating the bison specimen. In addition, she assisted Stormy Fields and Juliette Funck in preparing the specimen for taphonomic analysis. Aren Gunderson helped locate and select rodent specimens at the Museum of the North Mammalogy. Diego Fernandez at the University of Utah conducted strontium isotope analysis. We thank Tim Howe at the Alaska Stable Isotope Facility for assistance conducting the stable isotope analyses of the specimen. Amanda Barker provided support and advice on chemistry preparation. Radiocarbon analysis was conducted by W. M. Keck Carbon Cycle Accelerator Mass Spectrometry Laboratory by Dr. John Southon, who provided expertise in evaluating radiocarbon results from the bison specimen. The Bureau of Land Management oversaw specimen management and permitted destructive analysis of necessary materials for this study. The 2016 and 2017 David and Rachel Hopkins Fellowship provided funds for strontium anaylsis. Dr. Beth Shapiro was supported by IMLS MG-30-17-0045-17. Gemma Murray and Peter Heintzman were partially supported by NSF DEB 1754451. Joshua D. Kapp assisted in the aDNA analysis. Dr. Derek Sikes, Dr. Denise Gemmellaro, and Dr. Martin Hall were all contacted for their expertise with forensic entomology.

3.6 References

Andersson, K., Norman, D., Werdelin, L., 2011. Sabretoothed carnivores and the killing of large prey. PLoS One 6, 8–13. https://doi.org/10.1371/journal.pone.0024971

Balasse, M., 2002. Reconstructing dietary and environmental history from enamel isotopic analysis: Time resolution of intra-tooth sequential sampling. Int. J. Osteoarchaeol. 12, 155–165. https://doi.org/10.1002/oa.601

Balasse, M., Bocherens, H., Mariotti, A., Ambrose, S.H., 2001. Detection of Dietary Changes by Intra-tooth Carbon and Nitrogen Isotopic Analysis: An Experimental Study of Dentine Collagen of Cattle (Bos taurus). J. Archaeol. Sci. 28, 235–245. https://doi.org/10.1006/jasc.1999.0535

Balme, G.R., Denning, S.S., Cammack, J.A., Watson, D.W., 2012. Blow flies (Diptera : Calliphoridae) survive burial : Evidence of ascending vertical dispersal. Forensic Sci. Int. 216, e1–e4. https://doi.org/10.1016/j.forsciint.2011.07.017

Bamforth, D.B., 1987. Historical Documents and Bison Ecology on the Great Plains. Plains Antrhoplogist 32, 1–16. https://doi.org/10.1080/2052546.1987.11909364

Baryshnikov, G., Boeskorov, G., 2001. The pleistocene cave lion, Panthera spelaea (Carnivora, Felidae) from Yakutia, Russia. Cranium 18.

Bataille, C.P., Bowen, G.J., 2012. Sr / 86 Sr variations in bedrock and water for large scale provenance studies. Chem. Geol. 304–305, 39–52. https://doi.org/10.1016/j.chemgeo.2012.01.028

Bataille, C.P., Brennan, S.R., Hartmann, J., Moosdorf, N., Wooller, M.J., Bowen, G.J., 2014. A geostatistical framework for predicting variability in strontium concentrations and isotope ratios in Alaskan rivers. Chem. Geol. 389, 1–15. https://doi.org/10.1016/j.chemgeo.2014.08.030

Berger, J., 2004. The last mile: How to sustain long-distance migration in mammals. Conserv. Biol. 18, 320–331. https://doi.org/10.1111/j.1523-1739.2004.00548.x

Bernard, A., Daux, V., Lécuyer, C., Brugal, J.P., Genty, D., Wainer, K., Gardien, V., Fourel, F., Jaubert, J., 2009. Pleistocene seasonal temperature variations recorded in the δ18O of Bison priscus teeth. Earth Planet. Sci. Lett. 283, 133–143. https://doi.org/10.1016/j.epsl.2009.04.005

Bigelow, N.H., Zazula, G.D., Atkinson, D.E., 2013. Plant Macrofossil Records: Arctic North America, in: Elias, S.A., Mock, C.J. (Eds.), Encyclopedia of Quaternary Science. Elsevier, Amsterdam, pp. 746–759.

Blumenschine, R.J., 1986. Carcass consumption sequences and the archaeological distinction of scavenging and hunting. J. Hum. Evol. 15, 639–659. https://doi.org/10.1016/S0047-2484(86)80002-1

Bocherens, H., 2003. Isotopic biogeochemistry and the paleoecology, in: Advances in Mammoth Research. pp. 57–76.

Bocherens, H., Drucker, D., 2003. Trophic level isotopic enrichment of carbon and nitrogen in bone collagen: case studies from recent and ancient terrestrial ecosystems. Int. J. Osteoarchaeol. 13, 46–53. https://doi.org/10.1002/oa.662

Boeskorov, G.G., Potapova, O.R., Protopopov, A. V., Plotnikov, V. V., Agenbroad, L.D., Kirikov, K.S., Pavlov, I.S., Shchelchkova, M. V., Belolyubskii, I.N., Tomshin, M.D., Kowalczyk, R., Davydov, S.P., Kolesov, S.D., Tikhonov, A.N., van der Plicht, J., 2016. The Yukagir Bison: The exterior morphology of a complete frozen mummy of the extinct steppe bison, Bison priscus from the early Holocene of northern Yakutia, Russia. Quat. Int. 406, 94–110. https://doi.org/10.1016/j.quaint.2015.11.084

Bousquet, Y., Bouchard, P., Davies, A.E., Sikes, D.S., 2013. Checklist of beetles (Coleoptera) of Canada and Alaska . Second edition. Zookeys 44, 1–44. https://doi.org/10.3897/zookeys.360.4742

Bowen, G.J., 2018. WaterIsotopes.org [WWW Document]. Univ. Utah.

Brennan, S.R., Fernandez, D.P., Mackey, G., Cerling, T.E., Bataille, C.P., Bowen, G.J., Wooller, M.J., 2014. Strontium isotope variation and carbonate versus silicate weathering in rivers from across Alaska: Implications for provenance studies. Chem. Geol. 389, 167–181. https://doi.org/10.1016/j.chemgeo.2014.08.018

Briggs, A.W., Good, J.M., Green, R.E., Krause, J., Maricic, T., Stenzel, U., Lalueza-fox, C., Rudan, P., Brajković, D., Kućan, Ž., Rasilla, M. De, Fortea, J., Rosas, A., Pääbo, S., 2009. Five Neandertal mtDNA Genomes. Science (80-.). 325, 318–321.

Britton, K., 2009. Reconstructing faunal migrations using intra- tooth sampling and strontium and oxygen isotope analyses : A case study of modern caribou (Rangifer tarandus granti). https://doi.org/10.1016/j.jas.2009.01.003

Britton, K., Gaudzinski-Windheuser, S., Roebroeks, W., Kindler, L., Richards, M.P., 2012. Stable isotope analysis of well-preserved 120,000-year-old herbivore bone collagen from the Middle Palaeolithic site of Neumark-Nord 2, Germany reveals niche separation between bovids and equids. Palaeogeogr. Palaeoclimatol. Palaeoecol. 333–334, 168–177. https://doi.org/10.1016/j.palaeo.2012.03.028

Britton, K., Grimes, V., Dau, J., Richards, M.P., 2009. Reconstructing faunal migrations using intra-tooth sampling and strontium and oxygen isotope analyses: a case study of modern caribou (Rangifer tarandus granti). J. Archaeol. Sci. 36, 1163–1172. https://doi.org/10.1016/j.jas.2009.01.003

Britton, K., Grimes, V., Niven, L., Steele, T.E., McPherron, S., Soressi, M., Kelly, T.E., Jaubert, J., Hublin, J.J., Richards, M.P., 2011. Strontium isotope evidence for migration in late Pleistocene Rangifer: Implications for Neanderthal hunting strategies at the Middle Palaeolithic site of Jonzac, France. J. Hum. Evol. 61, 176–185. https://doi.org/10.1016/j.jhevol.2011.03.004

Capo, R.C., Stewart, B.W., Chadwick, O.A., 1998. Strontium isotopes as tracers of ecosystem processes: theory and methods. Geoderma 82, 197-225 (pp.21). https://doi.org/10.1016/S0016-7061(97)00102-X

Carter, L.D., 1981. A pleistocene sand sea on the alaskan arctic coastal plain. Science 211, 381–3. https://doi.org/10.1126/science.211.4480.381

Cerling, T.E., Harris, J.M., 1999. Carbon isotope fractionation between diet and bioapatite in ungulate mammals and implications for ecological and paleoecological studies. Oecologia 120, 347–363. https://doi.org/10.1007/s004420050868

Christiansen, P., Harris, J.M., 2010. Craniomandibular morphology and phylogenetic affinities of Panthera atrox : implications for the evolution and paleobiology of the lion lineage. J. Vertebr. Paelontology 4634. https://doi.org/10.1671/039.029.0314

Clark, P.U., Dyke, A.S., Shakun, J.D., Carlson, A.E., Clark, J., Wohlfarth, B., Mitrovica, J.X., Hostetler, S.W., McCabe, A.M., 2009. The Last Glacial Maximum. Science (80-.). 325, 710–714. https://doi.org/10.1126/science.1172873

Cody, W.J., 2000. Flora of the Yukon Territory, Second Edi. ed. NRC Research Press, Ottawa, Ontario, Canada.

Dabney, J., Knapp, M., Glocke, I., Gansauge, M.-T., Weihmann, A., Nickel, B., Valdiosera, C., Garcia, N., Paabo, S., Arsuaga, J.-L., Meyer, M., 2013. Complete mitochondrial genome sequence of a Middle Pleistocene cave bear reconstructed from ultrashort DNA fragments. Proc. Natl. Acad. Sci. 110, 15758–15763. https://doi.org/10.1073/pnas.1314445110

Drucker, D.G., Bridault, A., Hobson, K. a., Szuma, E., Bocherens, H., 2008. Can carbon-13 in large herbivores reflect the canopy effect in temperate and boreal ecosystems? Evidence from modern and ancient ungulates. Palaeogeogr. Palaeoclimatol. Palaeoecol. 266, 69–82. https://doi.org/10.1016/j.palaeo.2008.03.020

Drummond, A.J., Suchard, M.A., Xie, D., Rambaut, A., 2012. Bayesian phylogenetics with BEAUti and the BEAST 1.7. Mol. Biol. Evol. 29, 1969–1973. https://doi.org/10.1093/molbev/mss075

Elias, S.A., Berman, D., Alfimov, A., 2000. Late pleistocene beetle faunas of beringia: Where east met west. J. Biogeogr. 27, 1349–1363. https://doi.org/10.1046/j.1365-2699.2000.00503.x

Elias, S.A., Crocker, B., 2008. The Bering Land Bridge: a moisture barrier to the dispersal of steppe-tundra biota? Quat. Sci. Rev. 27, 2473–2483. https://doi.org/10.1016/j.quascirev.2008.09.011

Ewald, T., Hills, L. V., Tolman, S., Kooyman, B., 2018. Scimitar cat (Homotherium serum Cope) from southwestern Alberta, Canada. Can. J. Earth Sci. 55, 8–17. https://doi.org/10.1139/cjes-2017-0130

Fancy, S.G., Pank, L.F., Whitten, K.R., Regelin, W.L., 1990. Seasonal movements of caribou in arctic Alaska as determined by satellite. Rangifer 10, 167. https://doi.org/10.7557/2.10.3.850

Firth, C., Kitchen, A., Shapiro, B., Suchard, M.A., Holmes, E.C., Rambaut, A., 2010. Using time-structured data to estimate evolutionary rates of double-stranded DNA viruses. Mol. Biol. Evol. 27, 2038–2051. https://doi.org/10.1093/molbev/msq088

Flores, D., 1991. Bison Ecology and Bison Diplomacy: The Southern Plains from 1800 to 1850. J. Am. Hist. 78, 465. https://doi.org/10.2307/2079530

Fox-dobbs, K., Leonard, J.A., Koch, P.L., 2008. Pleistocene megafauna from eastern Beringia : Paleoecological and paleoenvironmental interpretations of stable carbon and nitrogen isotope and radiocarbon records. Palaeogeogr. Palaeoclimatol. Palaeoecol. 261, 30–46. https://doi.org/10.1016/j.palaeo.2007.12.011

Froese, D., Stiller, M., Heintzman, P.D., Reyes, A. V., Zazula, G.D., Soares, A.E.R., Meyer, M., Hall, E., Jensen, B.J.L., Arnold, L.J., MacPhee, R.D.E., Shapiro, B., 2017. Fossil and genomic evidence constrains the timing of bison arrival in North America. Proc. Natl. Acad. Sci. 114, 3457–3462. https://doi.org/10.1073/pnas.1620754114

Fuller, B.T., Richards, M.P., Mays, S.A., 2003. Stable carbon and nitrogen isotope variations in tooth dentine serial sections from Wharram Percy. J. Archaeol. Sci. 30, 1673–1684. https://doi.org/10.1016/S0305-4403(03)00073-6

Fuller, W.A., 1959. The horns and teeth as indicators of age in bison. J. Wildl. Manage. 23, 342–344. https://doi.org/10.2307/3796894

Funck, J., Kellam, C., Seaton, T., Wooller, M.J., in review. Stable isotopic signatures in modern wood bison (Bison bison athabascae) hairs as telltale biomarkers of nutritional stress. Can. J. Zool.

Gadbury, C., Todd, L., Jahren, A.H., Amundson, R., 2000. Spatial and temporal variations in the isotopic composition of bison tooth enamel from the Early Holocene Hudson-Meng Bone Bed, Nebraska. Palaeogeogr. Palaeoclimatol. Palaeoecol. 157, 79–93. https://doi.org/10.1016/S0031-0182(99)00151-0

Gaglioti, B. V., Mann, D.H., Groves, P., Kunz, M.L., Farquharson, L.M., Reanier, R.E., Jones, B.M., Wooller, M.J., 2018. Aeolian stratigraphy describes ice-age paleoenvironments in unglaciated Arctic Alaska. Quat. Sci. Rev. 182, 175–190. https://doi.org/10.1016/j.quascirev.2018.01.002

Gaglioti, B. V., Mann, D.H., Wooller, M.J., Jones, B.M., Wiles, G.C., Groves, P., Kunz, M.L., Baughman, C.A., Reanier, R.E., 2017. Younger-Dryas cooling and sea-ice feedbacks were prominent features of the Pleistocene-Holocene transition in Arctic Alaska. Quat. Sci. Rev. 169, 330–343. https://doi.org/10.1016/j.quascirev.2017.05.012

Gigleux, C., Grimes, V., Tütken, T., Knecht, R., Britton, K., 2017. Reconstructing caribou seasonal biogeography in Little Ice Age (late Holocene) Western Alaska using intra-tooth strontium and oxygen isotope analysis. J. Archaeol. Sci. Reports 0–1. https://doi.org/10.1016/j.jasrep.2017.10.043

Glassburn, C.L., Potter, B.A., Clark, J.L., Reuther, J.D., Bruning, D.L., Wooller, M.J., 2018. Strontium and Oxygen Isotope Profiles of Sequentially Sampled Modern Bison (Bison bison bison) Teeth from Interior Alaska as Proxies of Seasonal Mobility 71, 185–202.

Glassburn, C.L., Potter, B.A., Clark, J.L., Reuther, J.D., Bruning, D.L., Wooller, M.J., Clark, J.L., Reuther, J.D., Bruning, D.L., Wooller, M.J., 2015. Application of strontium and oxygen isotope analyses

to sequentially-sampled modern bison (Bison bison bison) teeth from Interior Alaska as a proxy of seasonal mobility. (Masters Thesis). Univ. Alaska Fairbanks.

Gomes, L., Augusto, W., Godoy, C., 2006. A review of postfeeding larval dispersal in blowflies : implications for forensic entomology. Naturwissenschaften 93, 207–215. https://doi.org/10.1007/s00114-006-0082-5

Graham, R.W., Belmecheri, S., Choy, K., Culleton, B.J., Davies, L.J., Froese, D., Heintzman, P.D., Hritz, C., Kapp, J.D., Newsom, L.A., Rawcliffe, R., Saulnier-Talbot, É., Shapiro, B., Wang, Y., Williams, J.W., Wooller, M.J., 2016. Timing and causes of mid-Holocene mammoth extinction on St. Paul Island, Alaska. Proc. Natl. Acad. Sci. 201604903. https://doi.org/10.1073/pnas.1604903113

Guthrie, A.R.D., 1966. Bison Horn Cores : Character Choice and Systematics. J. Paleontol. 40, 738–740.

Guthrie, R.D., 2001. Origin and causes of the mammoth steppe: A story of cloud cover, woolly mammal tooth pits, buckles, and inside-out Beringia. Quat. Sci. Rev. 20, 549–574. https://doi.org/10.1016/S0277-3791(00)00099-8

Guthrie, R.D., 1989. Frozen Fauna of Mammoth Steppe: The Story of Blue Babe. University of Chicago Press, Chicago.

Guthrie, R.D., 1970. Bison Evolution and Zoogeography in North America During the Pleistocene. Q. Rev. Biol. 45, 1–15.

Guthrie, R.D., 1968. Paleoecology of the Large-Mammal Community in Interior Alaska during the Late Pleistocene in of the Large-mammal Community. Am. Midl. Nat. 79, 346–363.

Haile, J., Froese, D.G., Macphee, R.D.E., Roberts, R.G., Arnold, L.J., Reyes, A. V, Rasmussen, M., Nielsen, R., Brook, B.W., Robinson, S., Demuro, M., Gilbert, M.T.P., Willerslev, E., Munch, K., Austin, J.J., Cooper, A., Barnes, I., Mo, P., 2009. Ancient DNA reveals late survival of mammoth and horse in interior Alaska. PNAS 106, 22352–22357.

Hanson, J.R., 2015. Bison ecology in the Northern Plains and a reconstruction of bison patterns for the North Dakota Region. Plains Anthr. 29, 93–113.

Heaton, T.H.E., Vogel, J.C., von la Chevallerie, G., Collett, G., 1986. Climatic influence on the isotopic composition of bone nitrogen. Nature 322, 822. https://doi.org/https://doi.org/10.1038/322822a0

Hedges, R.E.M., Clement, J.G., Thomas, D.L., O'Connell, T.C., 2007. Collagen Turnover in the Adult Femoral Mid-Shaft Modeled from Anthropogenic Radiocarbon Traver Measurements. Am. J. Phys. Anthr. 133, 808–816. https://doi.org/10.1002/ajpa

Hedges, R.E.M., Stevens, R.E., Richards, M.P., 2004. Bone as a stable isotope archive for local climatic information. Quat. Sci. Rev. 23, 959–965. https://doi.org/10.1016/j.quascirev.2003.06.022

Heintzman, P.D., Froese, D., Ives, J.W., Soares, A.E.R., Zazula, G.D., Letts, B., Andrews, T.D., Driver, J.C., Hall, E., Gregory Hare, P., Jass, C.N., Mackay, G., Southon, J.R., Stiller, M., Woywitka, R., Suchard, M.A., Shapiro, B., 2016. Bison phylogeography constrains dispersal and viability of the Ice Free Corridor in western Canada. PNAS 1–7. https://doi.org/10.1073/pnas.1601077113

Higgins, P., MacFadden, B.J., 2004. "Amount Effect" recorded in oxygen isotopes of Late Glacial horse (Equus) and bison (Bison) teeth from the Sonoran and Chihuahuan deserts, southwestern United States. Palaeogeogr. Palaeoclimatol. Palaeoecol. 206, 337–353. https://doi.org/10.1016/j.palaeo.2004.01.011

Hoppe, K. a, Koch, P.L., Carlson, R.W., Webb, S.D., 1999. Tracking mammoths and mastodons : Reconstruction of migratory behavior using strontium isotope ratios. Geology 27, 439–442. https://doi.org/10.1130/0091-7613(1999)027<0439

Hoppe, K.A., 2006. Correlation between the oxygen isotope ratio of North American bison teeth and local waters: Implication for paleoclimatic reconstructions. Earth Planet. Sci. Lett. 244, 408–417. https://doi.org/10.1016/j.epsl.2006.01.062

Hoppe, K.A., 2004. Late Pleistocene mammoth herd structure, migration patterns, and Clovis hunting strategies inferred from isotopic analyses of multiple death assemblages. Paleobiology 30, 129–145.

Hoppe, K.A., Paytan, A., Chamberlain, P., 2006. Reconstructing grassland vegetation and paleotemperatures using carbon isotope ratios of bison tooth enamel. Geology 34, 649–652. https://doi.org/10.1130/G22745.1

Hulten, E., 1968. Flora of Alaska and Neighboring Territories. Standford University Press, Standford, California.

Iacumin, P., Bocherens, H., Chaix, L., 2001. C and N stable isotope ratios of fossil cattle keratin horn from Kerma (Sudan): A record of dietary changes. Ital. J. Int. Sci. 14, 41–46.

Jónsson, H., Ginolhac, A., Schubert, M., Johnson, P.L.F., Orlando, L., 2013. MapDamage2.0: Fast approximate Bayesian estimates of ancient DNA damage parameters. Bioinformatics 29, 1682–1684. https://doi.org/10.1093/bioinformatics/btt193

Julien, M., Bocherens, H., Burke, A., Drucker, D.G., Patou-mathis, M., Krotova, O., Péan, S., 2012. Were European steppe bison migratory? d18O, d13C and Sr intra-tooth isotopic variations applied to a palaeoethological reconstruction. Quat. Int. 271, 106–119. https://doi.org/10.1016/j.quaint.2012.06.011

Kirillova, I. V., Zanina, O.G., Chernova, O.F., Lapteva, E.G., Trofimova, S.S., Lebedev, V.S., Tiunov, A. V., Soares, A.E.R., Shidlovskiy, F.K., Shapiro, B., 2015. An ancient bison from the mouth of the Rauchua River (Chukotka, Russia). Quat. Res. 84, 232–245. https://doi.org/10.1016/j.yqres.2015.06.003

Knudson, K.J., Williams, S.R., Osborn, R., Forgey, K., Ryan, P., 2009. The geographic origins of Nasca trophy heads using strontium, oxygen, and carbon isotope data. J. Anthropol. Archaeol. 28, 244–257. https://doi.org/10.1016/j.jaa.2008.10.006

Koch, P.L., Heisinger, J., Moss, C., Carlson, R.W., Marilyn, L., Koch, P.L., Heisinger, J., Moss, C., Carlson, R.W., Fogel, M.L., Behrensmeyer, A.K., 1995. Isotopic Tracking of Change in Diet and Habitat Use in African Elephants. Science (80-.). 267, 1340–1343.

Koch, P.P.L., Tuross, N., Fogel, M.L., 1997. The effects of sample treatment and diagenesis on the isotopic integrity of carbonate in biogenic hydroxylapatite. J. Archaeol. Sci. 24, 417–429. https://doi.org/10.1006/jasc.1996.0126

Kootker, L.M., van Lanen, R.J., Kars, H., Davies, G.R., 2016. Strontium isoscapes in The Netherlands. Spatial variations in87Sr/86Sr as a proxy for palaeomobility. J. Archaeol. Sci. Reports 6, 1–13. https://doi.org/10.1016/j.jasrep.2016.01.015

Lachniet, M.S., Lawson, D.E., Stephen, H., Sloat, A.R., Patterson, W.P., 2016. Isoscapes of d18O and d2H reveal climatic forcings on Alaska and Yukon precipitation. Water Resour. Res. 52, 6575–6586. https://doi.org/10.1002/2016WR019436.Received

Lambeck, K., Rouby, H., Purcell, A., Sun, Y., Sambridge, M., 2014. Sea level and global ice volumes from the Last Glacial Maximum to the Holocene. Proc. Natl. Acad. Sci. U. S. A. 111, 15296–15303. https://doi.org/10.1073/pnas.1411762111

Lee, T.N., Buck, C.L., Barnes, B.M., O'Brien, D.M., 2012. A test of alternative models for increased tissue nitrogen isotope ratios during fasting in hibernating arctic ground squirrels. J. Exp. Biol. 215, 3354–61. https://doi.org/10.1242/jeb.068528

Li, H., Durbin, R., 2009. Fast and accurate short read alignment with Burrows-Wheeler transform. Bioinformatics 25, 1754–1760. https://doi.org/10.1093/bioinformatics/btp324

Lindroth, C.H., 1966. The ground beetles (Carabidae, excl. Cicindellidae) of Canada and Alaska, Part 4. Opusc. Entomol. Suppl. 29, 409–648.

Lisiecki, L.E., Raymo, M.E., 2005. A Pliocene-Pleistocene stack of 57 globally distributed benthic δ 18O records. Paleoceanography 20, 1–17. https://doi.org/10.1029/2004PA001071

Lloyd, A.H., Duffy, P. a., Mann, D.H., 2013. Nonlinear responses of white spruce growth to climate variability in interior Alaska. Can. J. For. Res. 43, 331–343. https://doi.org/10.1139/cjfr-2012-0372

Lorenzen, E.D., Nogués-Bravo, D., Orlando, L., Weinstock, J., Binladen, J., Marske, K.A., Ugan, A., Borregaard, M.K., Gilbert, M.T.P., Nielsen, R., Ho, S.Y.W., Goebel, T., Graf, K.E., Byers, D., Stenderup, J.T., Rasmussen, M., Campos, P.F., Leonard, J.A., Koepfli, K.P., Froese, D., Zazula, G., Stafford, T.W., Aaris-Sørensen, K., Batra, P., Haywood, A.M., Singarayer, J.S., Valdes, P.J., Boeskorov, G., Burns, J.A., Davydov, S.P., Haile, J., Jenkins, D.L., Kosintsev, P., Kuznetsova, T., Lai, X., Martin, L.D., McDonald, H.G., Mol, D., Meldgaard, M., Munch, K., Stephan, E., Sablin, M., Sommer, R.S., Sipko, T., Scott, E., Suchard, M.A., Tikhonov, A., Willerslev, R., Wayne, R.K., Cooper, A., Hofreiter, M., Sher, A., Shapiro, B., Rahbek, C., Willerslev, E., 2011. Species-specific responses of Late Quaternary megafauna to climate and humans. Nature 479, 359–364. https://doi.org/10.1038/nature10574

Lott, D.F., 1971. Sexual and aggressive behavior of American bison (Bison bison), in: The Behaviour of Ungulates and Its Relation to Management. pp. 382–394.

Maher, C.R., Byers, J.A., 1987. Age-related changes in reproductive effort of male bison. Behav. Ecol. Sociobiol. 21, 91–96. https://doi.org/10.1007/PL00020232

Mann, D.H., Groves, P., Kunz, M.L., Reanier, R.E., Gaglioti, B. V., 2013. Ice-age megafauna in Arctic Alaska: Extinction, invasion, survival. Quat. Sci. Rev. 70, 91–108. https://doi.org/10.1016/j.quascirev.2013.03.015

Mann, D.H., Groves, P., Reanier, R.E., Gaglioti, B. V, Kunz, M.L., Shapiro, B., 2015. Life and extinction of megafauna in the ice-age Arctic. Proc. Natl. Acad. Sci. 112, 14301–14306. https://doi.org/10.1073/pnas.1516573112

Marcenko, E., Srdoc, D., Golubic, S., Pezdic, J., Head, M.J., 1989. Carbon uptake in aquatic plants deduced from their natural 13C and 14C content. Radiocarbon 31, 785–794. https://doi.org/10.1017/S0033822200012406

Marchenko, M.I., 2001. Medicolegal relevance of cadaver entomofauna for the determination of the time of death. Forensic Sci. Int. 120, 89–109.

Marsolier-Kergoat, M.C., Palacio, P., Berthonaud, V., Maksud, F., Stafford, T., Begouen, R., Elalouf, J.M., 2015. Hunting the Extinct Steppe Bison (Bison priscus) Mitochondrial Genome in the Trois-Freres Paleolithic Painted Cave. PLoS One 10, e0128267. https://doi.org/10.1371/journal.pone.0128267

Martin, J.M., Mead, J.I., Barboza, P.S., 2018. Bison body size and climate change. J. Mammal. 8, 1–11. https://doi.org/10.1002/ece3.4019

Mekota, A.-M., Grupe, G., Ufer, S., Cuntz, U., 2006. Serial analysis of stable nitrogen and carbon isotopes in hair: monitoring starvation and recovery phase of patients suffering from anorexia nervosa. Rapid Commun. Mass Spectrom. 20, 1604–1610. https://doi.org/10.1002/rcm

Meyer, H., Schirrmeister, L., Andreev, A., Wagner, D., Hubberten, H.W., Yoshikawa, K., Bobrov, A., Wetterich, S., Opel, T., Kandiano, E., Brown, J., 2010. Lateglacial and Holocene isotopic and environmental history of northern coastal Alaska - Results from a buried ice-wedge system at Barrow. Quat. Sci. Rev. 29, 3720–3735. https://doi.org/10.1016/j.quascirev.2010.08.005

Meyer, M., Kircher, M., 2010. Illumina Sequencing Library Preparation for Highly Multiplexed Target Capture and Sequencing. Cold Spring Harb. Protoc. https://doi.org/10.1101/pdb.prot5448

Montgomery, J., Evans, J., Horstwood, M.S.A., 2010. Evidence for long-term averaging of strontium in bovine enamel using TIMS and LA-MC-ICP-MS strontium isotope intra-molar profiles, Environmental archeology. https://doi.org/10.1063/1.2756072

Moon, T.A., Overeem, I., Druckenmiller, M., Holland, M., Huntington, H., Kling, G., Lovecraft, A.L., Miller, G., Scambos, T., Schädel, C., Schuur, E.A.G., Trochim, E., Wiese, F., Williams, D., Wong, G., 2019. The Expanding Footprint of Rapid Arctic Change. Earth's Futur. 7, 212–218. https://doi.org/10.1029/2018EF001088

Murray, G.G.R., Wang, F., Harrison, E.M., Paterson, G.K., Mather, A.E., Harris, S.R., Holmes, M.A., Rambaut, A., Welch, J.J., 2016. The effect of genetic structure on molecular dating and tests for temporal signal. Methods Ecol. Evol. 7, 80–89. https://doi.org/10.1111/2041-210X.12466

Nelson, M.A., Quakenbush, L.T., Mahoney, B.A., Taras, B.D., Wooller, M.J., 2018. Fifty years of Cook Inlet beluga whale feeding ecology from isotopes in bone and teeth. Endanger. Species Res. 36, 77–87. https://doi.org/10.3354/ESR00890

Paradis, E., Claude, J., Strimmer, K., 2004. APE: Analyses of phylogenetics and evolution in R language. Bioinformatics 20, 289–290. https://doi.org/10.1093/bioinformatics/btg412

Passey, B.H., Robinson, T.F., Ayliffe, L.K., Cerling, T.E., Sponheimer, M., Dearing, M.D., Roeder, B.L., Ehleringer, J.R., 2005. Carbon isotope fractionation between diet, breath CO2, and bioapatite in different mammals. J. Archaeol. Sci. 32, 1459–1470. https://doi.org/10.1016/j.jas.2005.03.015

Pellegrini, M., Donahue, R.E., Chenery, C., Evans, J., Lee-Thorp, J., Montgomery, J., Mussi, M., 2008. Faunal migration in late-glacial central Italy: Implications for human resource exploitation. Rapid Commun. Mass Spectrom. 22, 1714–1726. https://doi.org/10.1002/rcm.3521

Pellegrini, M., Snoeck, C., 2016. Comparing bioapatite carbonate pre-treatments for isotopic measurements: Part 2 - Impact on carbon and oxygen isotope compositions. Chem. Geol. 420, 88–96. https://doi.org/10.1016/j.chemgeo.2015.10.038

Plumb, G.E., White, P.J., Coughenour, M.B., Wallen, R.L., 2009. Carrying capacity, migration, and dispersal in Yellowstone bison. Biol. Conserv. 142, 2377–2387. https://doi.org/10.1016/j.biocon.2009.05.019

Post, D.M., 2002. Using Stable Isotopes to Estimate Trophic Position: Models, Methods and Assumptions. Ecology 83, 703–718.

Post, E., Forchhammer, M.C., 2008. Climate change reduces reproductive success of an Arctic herbivore through trophic mismatch. Philos. Trans. R. Soc. B Biol. Sci. 363, 2369–2375. https://doi.org/10.1098/rstb.2007.2207

Rabanus-Wallace, M.T., Wooller, M.J., Zazula, G.D., Shute, E., Jahren, A.H., Kosintsev, P., Burns, J.A., Breen, J., Llamas, B., Cooper, A., 2017. Megafaunal isotopes reveal role of increased moisture on rangeland during late Pleistocene extinctions. Nat. Ecol. Evol. 1, 1–5. https://doi.org/10.1038/s41559-017-0125

Radloff, F.G.T., Mucina, L., Bond, W.J., le Roux, P.J., 2010. Strontium isotope analyses of large herbivore habitat use in the Cape Fynbos region of South Africa. Oecologia 164, 567–578. https://doi.org/10.1007/s00442-010-1731-0

Rasmussen, S.O., Bigler, M., Blockley, S.P., Blunier, T., Buchardt, S.L., Clausen, H.B., Cvijanovic, I., Dahl-Jensen, D., Johnsen, S.J., Fischer, H., Gkinis, V., Guillevic, M., Hoek, W.Z., Lowe, J.J., Pedro, J.B., Popp, T., Seierstad, I.K., Steffensen, J.P., Svensson, A.M., Vallelonga, P., Vinther, B.M., Walker, M.J.C., Wheatley, J.J., Winstrup, M., 2014. A stratigraphic framework for abrupt climatic changes during the Last Glacial period based on three synchronized Greenland ice-core records: Refining and extending the

INTIMATE event stratigraphy. Quat. Sci. Rev. 106, 14–28. https://doi.org/10.1016/j.quascirev.2014.09.007

Reitsema, L.J., Muir, A.B., 2015. Brief communication: Growth velocity and weaning $\delta^{15}N$ "dips" during ontogeny in Macaca mulatta. Am. J. Phys. Anthropol. 157, 347–357. https://doi.org/10.1002/ajpa.22713

Rivals, F., Solounias, N., Mihlbachler, M.C., 2007. Evidence for geographic variation in the diets of late Pleistocene and early Holocene Bison in North America, and differences from the diets of recent Bison. Quat. Res. 68, 338–346. https://doi.org/10.1016/j.yqres.2007.07.012

Scherler, L., Tütken, T., Becker, D., 2014. Carbon and oxygen stable isotope compositions of late Pleistocene mammal teeth from dolines of Ajoie (Northwestern Switzerland). Quat. Res. 82, 378–387. https://doi.org/10.1016/j.yqres.2014.05.004

Schmieder, R., Edwards, R., 2011. Quality control and preprocessing of metagenomic datasets. Bioinformatics 27, 863–864. https://doi.org/10.1093/bioinformatics/btr026

Schoeninger, M.J., DeNiro, M.J., 1984. Nitrogen and carbon isotopic composition of bone collagen from marine and terrestrial animals. Geochim. Cosmochim. Acta 48, 625–639. https://doi.org/10.1016/0016-7037(84)90091-7

Schubert, B.W., 2010. Late Quaternary chronology and extinction of North American giant short-faced bears (Arctodus simus). Quat. Int. 217, 188–194. https://doi.org/10.1016/j.quaint.2009.11.010

Shapiro, B., Cooper, A., 2003. Beringia as an Ice Age genetic museum. Quat. Res. 60, 94–100. https://doi.org/10.1016/S0033-5894(03)00009-7

Shapiro, B., Ho, S.Y.W., Drummond, A.J., Suchard, M.A., Pybus, O.G., Rambaut, A., 2011. A bayesian phylogenetic method to estimate unknown sequence ages. Mol. Biol. Evol. 28, 879–887. https://doi.org/10.1093/molbev/msq262

Shapiro, B., Pybus, O.G., Gilbert, M.T.P., Barnes, I., Baryshnikov, G.F., Burns, J.A., Davydov, S., 2004. Rise and Fall of the Beringian Steppe Bison. Science (80-.). 306, 1561–1565. https://doi.org/10.1126/science.1101074

Sharma, S., Couturier, S., Côté, S.D., 2009. Impacts of climate change on the seasonal distribution of migratory caribou. Glob. Chang. Biol. 15, 2549–2562. https://doi.org/10.1111/j.1365-2486.2009.01945.x

Smith, K.G.V., 1986. A Manual of Forensic Entomology. Trustees of the British Museum, Oxford.

Snoeck, C., Pellegrini, M., 2015. Comparing bioapatite carbonate pre-treatments for isotopic measurements: Part 1-Impact on structure and chemical composition. Chem. Geol. 417, 349–403. https://doi.org/10.1016/j.chemgeo.2015.10.004

Soper, J.D., 1941. History, Range and Home Life of the Northern Bison. Ecol. Monogr. 11, 347–412. https://doi.org/10.2307/1943298

Sorkin, B., 2006. Ecomorphology of the giant short-faced bears Agriotherium and Arctodus. Hist. Biol. 18, 1–20. https://doi.org/10.1080/08912960500476366

Stevens, R.E., Balasse, M., O'Connell, T.C., 2011. Intra-tooth oxygen isotope variation in a known population of red deer: Implications for past climate and seasonality reconstructions. Palaeogeogr. Palaeoclimatol. Palaeoecol. 301, 64–74. https://doi.org/10.1016/j.palaeo.2010.12.021

Stevens, R.E., Hedges, R.E.., 2004. Carbon and nitrogen stable isotope analysis of northwest European horse bone and tooth collagen, 40,000BP–present: Palaeoclimatic interpretations. Quat. Sci. Rev. 23, 977–991. https://doi.org/10.1016/j.quascirev.2003.06.024

Stuiver, M., Reimer, P.J., Reimer, R.W., 2019. CALIB 7.1.

Taylor, R.E., Hare, P.E., Prior, C.A., Kirner, D.L., Want, L., Burkyi, R.R., 1995. Radiocarbon dating of biochemically characterized hair. Radiocarbon 37, 319–330. https://doi.org/10.1017/S0033822200030794

Van Geel, B., Protopopov, A., Bull, I., Duijm, E., Gill, F., Lammers, Y., Nieman, A., Rudaya, N., Trofimova, S., Tikhonov, A.N., Vos, R., Zhilich, S., Gravendeel, B., 2014. Multiproxy diet analysis of the last meal of an early Holocene Yakutian bison. J. Quat. Sci. 29, 261–268. https://doi.org/10.1002/jqs.2698

Velivetskaya, T.A., Smirnov, N.G., Kiyashko, S.I., Ignatiev, A. V., Ulitko, A.I., 2016. Resolution-enhanced stable isotope profiles within the complete tooth rows of Late Pleistocene bisons (Middle Urals, Russia) as a record of their individual development and environmental changes. Quat. Int. 400, 212–226. https://doi.org/10.1016/j.quaint.2014.12.011

Verkouteren, R.M., Klinedinst, D.B., 2004. Value Assignment and Uncertainty Estimation of Selected Light Stable Isotope Reference Materials: RMs 8543-8545, RMs 8562-8564, and RM 8566, National Institute of Standards and Technology Special Publication.

Viner, S., Evans, J., Albarella, U., Parker Pearson, M., 2010. Cattle mobility in prehistoric Britain: Strontium isotope analysis of cattle teeth from Durrington Walls (Wiltshire, Britain). J. Archaeol. Sci. 37, 2812–2820. https://doi.org/10.1016/j.jas.2010.06.017

Warren, J., Anderson, G.S., 2013. The development of Protophormia terraenovae (Robineau-Desvoidy) at constant temperatures and its minimum temperature threshold. Forensic Sci. Int. 233, 374–379. https://doi.org/10.1016/j.forsciint.2013.10.012

Widga, C., Walker, J.D., Stockli, L.D., 2010. Middle Holocene Bison diet and mobility in the eastern Great Plains (USA) based on 13C, 18O, and 87Sr/86Sr analyses of tooth enamel carbonate. Quat. Res. 73, 449–463. https://doi.org/10.1016/j.yqres.2009.12.001

Wiener, D.J., Wiedemar, N., Welle, M.M., Drögemüller, C., 2015. Novel features of the prenatal horn bud development in cattle (Bos taurus). PLoS One 10, 1–13. https://doi.org/10.1371/journal.pone.0127691

Wooller, M.J., Zazula, G.D., Edwards, M., Froese, D.G., Boone, R.D., Parker, C., Bennett, B., 2007. Stable carbon isotope compositions of Eastern Beringian grasses and sedges: Investigating their potential as paleoenvironmental indicators. Arct. Antarct. Alp. Res. 39, 318–331. https://doi.org/10.1657/1523-0430(2007)39[318:SCICOE]2.0.CO;2

Zazula, G., Hare, P., Thomas, C., Mathewes, R.W., La Farge, C., Martel, A., Heintzman, P.D., Shapiro, B., 2017. A middle Holocene steppe bison and paleoenvironments from the Versleuce Meadows, Whitehorse, Yukon, Canada. Can. J. Earth Sci.

Zazula, G.D., Hall, E., Hare, P.G., Thomas, C., Mathewes, R., La Farge, C., Martel, A.L., Heintzman, P.D., Shapiro, B., 2017. A middle holocene steppe bison and paleoenvironments from the Versleuce Meadows, Whitehorse, Yukon, Canada. Can. J. Earth Sci. 54, 1138–1152. https://doi.org/10.1139/cjes-2017-0100

Zazula, G.D., MacKay, G., Andrews, T.D., Shapiro, B., Letts, B., Brock, F., 2009a. A late Pleistocene steppe bison (Bison priscus) partial carcass from Tsiigehtchic, Northwest Territories, Canada. Quat. Sci. Rev. 28, 2734–2742. https://doi.org/10.1016/j.quascirev.2009.06.012

Zazula, G.D., MacKay, G., Andrews, T.D., Shapiro, B., Letts, B., Brock, F., 2009b. A late Pleistocene steppe bison (Bison priscus) partial carcass from Tsiigehtchic, Northwest Territories, Canada. Quat. Sci. Rev. 28, 2734–2742. https://doi.org/10.1016/j.quascirev.2009.06.012

Zazzo, A., Bendrey, R., Vella, D., Moloney, A.P., Monahan, F.J., Schmidt, O., 2012. A refined sampling strategy for intra-tooth stable isotope analysis of mammalian enamel. Geochim. Cosmochim. Acta 84, 1–13. https://doi.org/10.1016/j.gca.2012.01.012

Zimov, A.S.A., Chuprynin, V.I., Oreshko, A.P., Iii, F.S.C., Reynolds, J.F., 2011. Steppe-Tundra Transition : A Herbivore-Driven Biome Shift at the End of the Pleistocene. Am. Soc. Nat. 146, 765–794. https://doi.org/10.1086/285824

Zimov, S.A., Zimov, N.S., Tikhonov, A.N., Chapin, I.S., 2012. Mammoth steppe: A high-productivity phenomenon. Quat. Sci. Rev. 57, 26–45. https://doi.org/10.1016/j.quascirev.2012.10.005

3.7 Supplementary figures

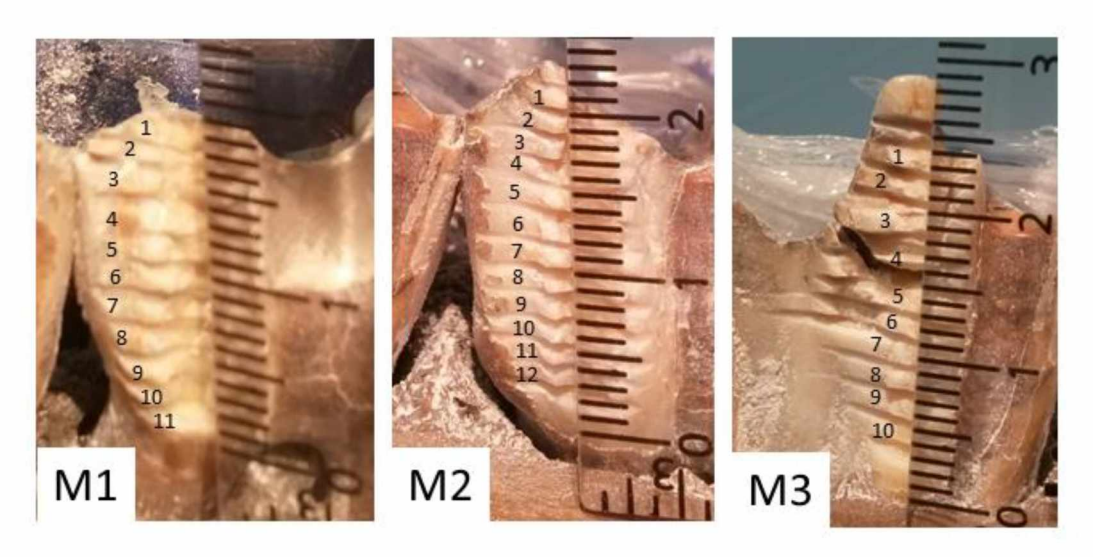

Figure 3.S1 Intra tooth sampling of molar 1 (M1), molar 2 (M2) and molar 3 (M3) from Bison priscus specimen UAMES 29458, number indicates sample number.

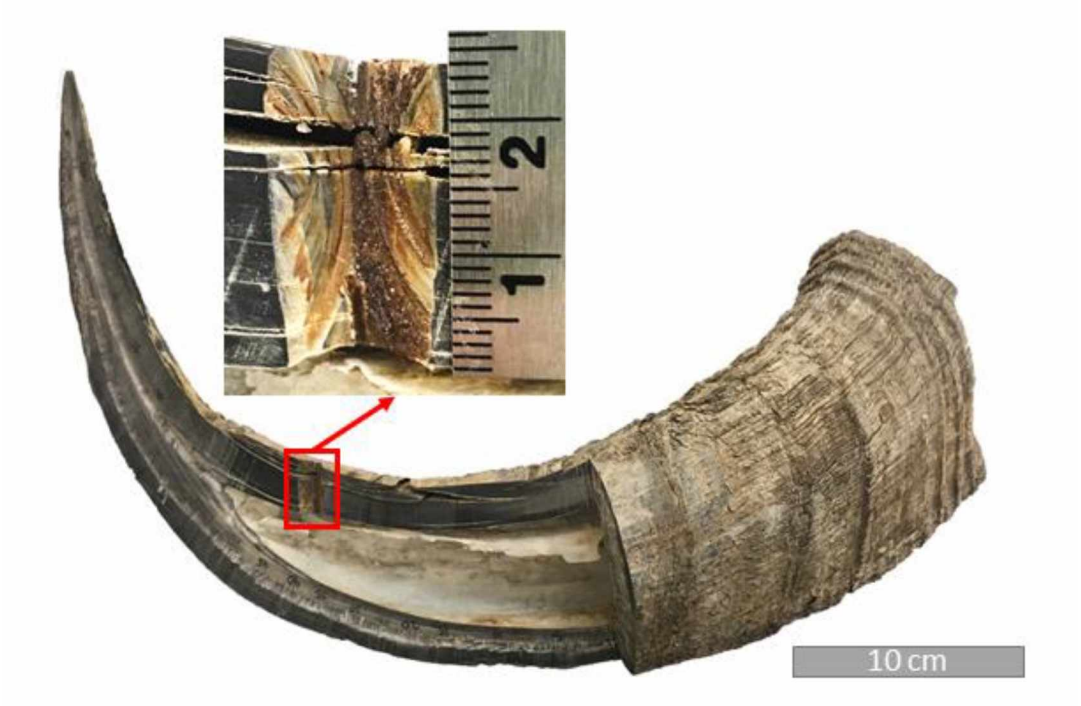

Figure 3.S2 Serial sampling scheme for bison horn sheath from Bison priscus specimen UAMES 29458.

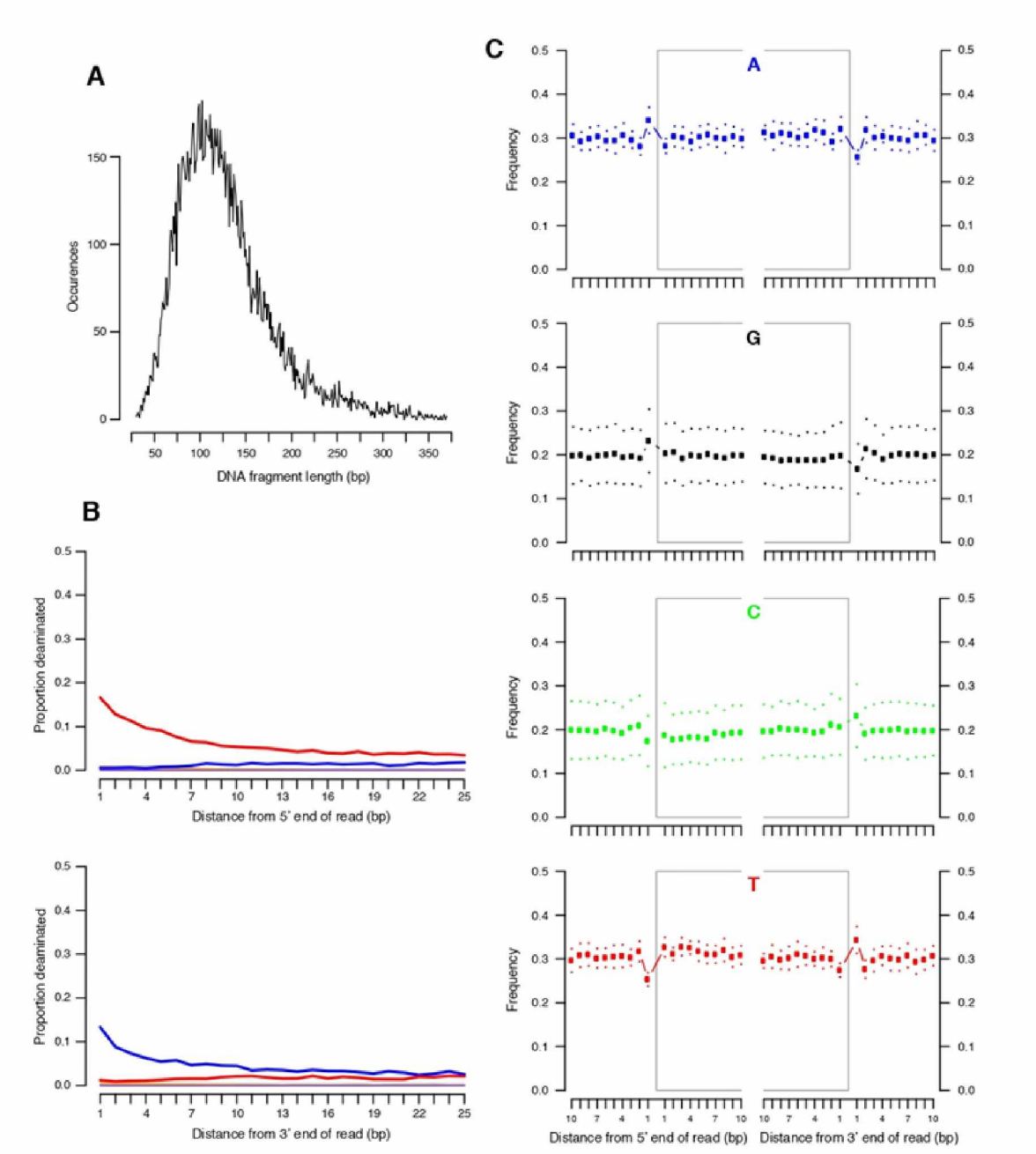

Figure 3.S3 Results of the tests for temporal signal in the bison mitochondrial genome data set. a) Full alignment data set, and b) reduced alignment data set (excluding MS022). Left panels: linear regression of phylogenetic root-to-tip distance against sampling date. Center panels: similar-date clusters (rounded to the nearest thousand years). Right panels: testing the results against random permutations over the clusters presented in b).

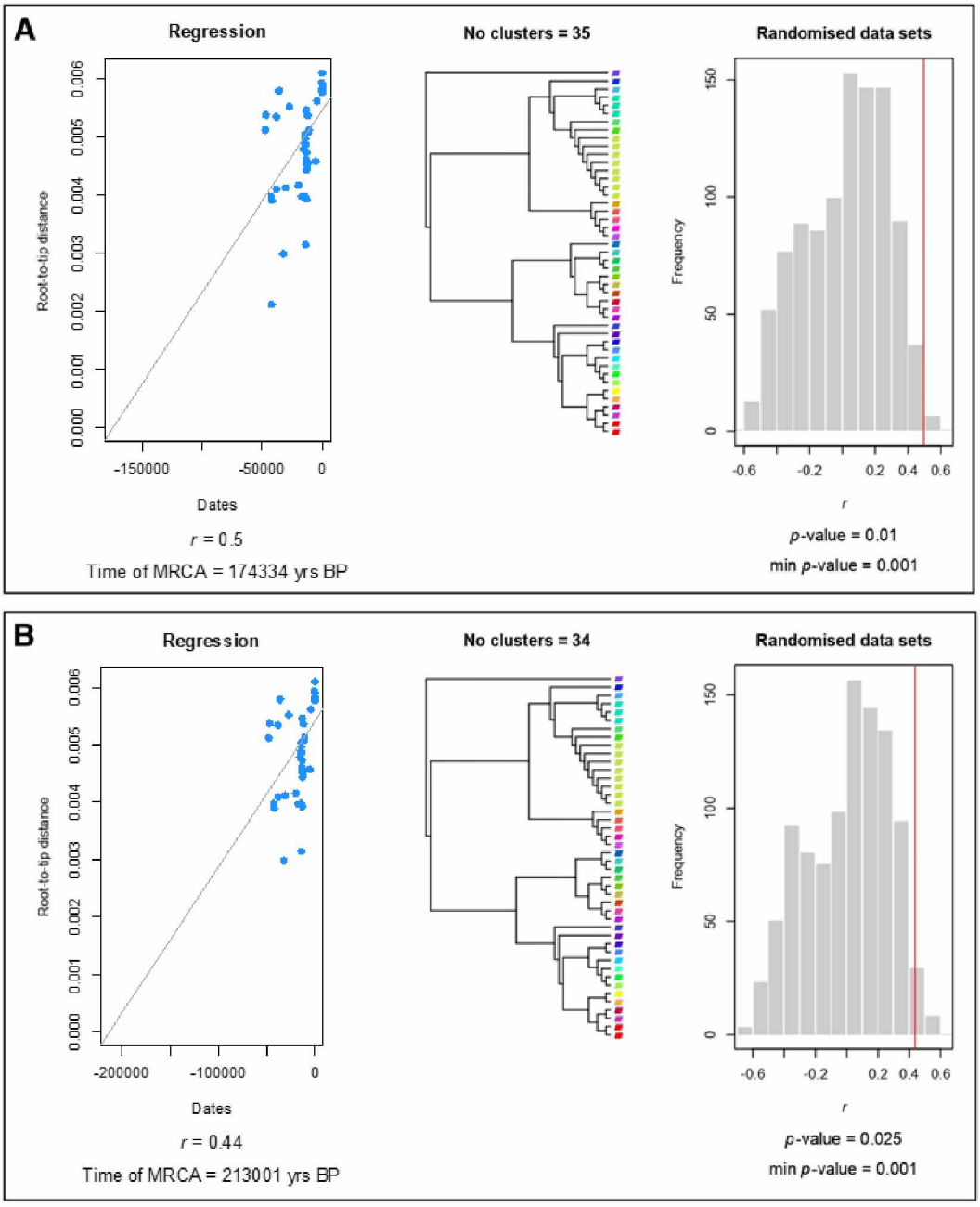

Figure 3.S4 Assessment of damage patterns in nuclear (A-C) and mitochondrial (D-F) DNA fragments from Bison priscus specimen UAMES 29458. (A, D) DNA fragment length distributions, with means of 90 bp (nuclear) and 127 bp (mitochondrial). (B, E) The relative frequency of cytosine to thymine deamination (red line) and observed guanine to adenine misincorporation (blue line) from cytosine deamination on the opposite DNA strand. Deamination is more prevalent at the ends of ancient DNA fragments. (C, F) DNA fragmentation plots showing an elevated occurrence of purines (guanine, adenine) immediately upstream of the ancient DNA fragment (to the left of the grey box) and the opposite signal immediately downstream of the fragment (to the right of the grey box).

General Conclusions

This thesis has laid out several examples of approaches that bring "new life to old bones," including by cross-fertilizing ancient and contemporary data analysis. With these promising advances, we can ask new questions of our fossils.

The first data chapter explored the isotope ecology of the newly reestablished wood bison herd in Alaska - with a view towards developing tools applicable to ancient ones. By tracking the carbon and nitrogen isotopes along their tail length, I was able to understand some of the ecological physiology and seasonal patterns of their wild lives. This could prove useful to herd managers trying to obtain information effectively about an extremely remote population. In addition, I gained insight into how events in an individual's life might be recorded in the keratin tissues of a bison. Of particular interest is the fact that animals that travelled long distances appeared to have a elevate nitrogen isotope signals during this period. This helps characterize the energetic cost of long-distance travel. Although long and intact hairs may be relatively rare in Pleistocene fossil beds, horn sheaths made of a similar material are among the most common fossils found in northern regions. Indeed, this wood bison study informs my analysis of the horn sheath of ancient bison in data chapter 3.

In chapter 2, we again used isotope analyses of present-day animals to help in the studies of ancient megafauna, including bison. In this case, present-day rodents were successfully used to characterize the local bioavailable strontium of an area. A reliance on contemporary archived specimens helped to overcome the obstacle of sampling from remote locations and allowed for sample collection across Alaska. These specimens were used to develop a new strontium isoscape of Alaska to better characterize terrestrial bioavailable strontium across the landscape. I then demonstrated the usefulness of these tools to identify the potential home range of ancient bison. This approach will drive exciting new research into regional studies of larger collection of ancient bison, other megafauna, and humans.

Finally, in chapter 3, I used the knowledge gained from the previous chapters to describe an in-depth life history of a single exceptionally well-preserved ancient steppe bison. Nitrogen stable isotopes of the horn

demonstrated nutritional stress associated with early life mobility identified from strontium isotopes in the teeth. When compared to the strontium isoscape and local rodents, it appears that this bison was likely moving from the coastal plain to the foothills during this period. The aDNA from this specimen helped place this bison into temporal context and identified its lineage. This information added to more traditional tools of zooarchaeology and taphonomy that helped explain the circumstances surrounding its death. Together, these methodologies demonstrate the potential depth of understanding fossil analysis can reach, not just in taphonomic terms, but also in terms of the life history and biogeography of its subject.

In this thesis, I have presented several novel ways of investigating landscape use and ecological physiology in ancient animal fossils and present-day animal tissues. Moving forward, it will be possible to apply these techniques to a much larger number of samples. The emergence of new techniques such as laser ablation means that expensive and labor-intensive strontium isotope analysis by solution can now be done quickly and at higher resolution. The large collections being collected from mines and eroding riverbeds produce many samples for future research to look at population trends over time.

Bison are regaining an important role in Alaska's landscape. They are crucial for wilderness restoration and add important economic stimulus in environmental services, hunting and tourism. In Alaska, we are privileged to work with stakeholders who value the bison and provide strong support for reintroduction programs and share their finds of ancient specimens with researchers. Without the support of native communities, hunters and miners, a lot of this research would not be possible.

Works cited

Balasse, M., 2002. Reconstructing dietary and environmental history from enamel isotopic analysis: Time resolution of intra-tooth sequential sampling. Int. J. Osteoarchaeol. 12, 155–165. https://doi.org/10.1002/oa.601

Bataille, C.P., Brennan, S.R., Hartmann, J., Moosdorf, N., Wooller, M.J., Bowen, G.J., 2014. A geostatistical framework for predicting variability in strontium concentrations and isotope ratios in Alaskan rivers. Chem. Geol. 389, 1–15. https://doi.org/10.1016/j.chemgeo.2014.08.030

Ceballos, G., Ehrlich, P.R., Dirzo, R., 2017. Biological annihilation via the ongoing sixth mass extinction signaled by vertebrate population losses and declines. Proc. Natl. Acad. Sci. U. S. A. 114, E6089–E6096. https://doi.org/10.1073/pnas.1704949114

Clementz, M.T., 2012. New insight from old bones: stable isotope analysis of fossil mammals. J. Mammal. 93, 368–380. https://doi.org/10.1644/11-MAMM-S-179.1

de Silva, S., Leimgruber, P., 2019. Demographic Tipping Points as Early Indicators of Vulnerability for Slow-Breeding Megafaunal Populations. Front. Ecol. Evol. 7, 1–13. https://doi.org/10.3389/fevo.2019.00171

Fritz, H., 2017. Long-term field studies of elephants: understanding the ecology and conservation of a long-lived ecosystem engineer. J. Mammal. 98, 603–611. https://doi.org/10.1093/jmammal/gyx023

Geremia, C., Merkle, J.A., Eacker, D.R., Wallen, R.L., White, P.J., Hebblewhite, M., 2019. Migrating bison engineer the green wave 1–7. https://doi.org/10.1073/pnas.1913783116

Glassburn, C.L., Potter, B.A., Clark, J.L., Reuther, J.D., Bruning, D.L., Wooller, M.J., 2018. Strontium and Oxygen Isotope Profiles of Sequentially Sampled Modern Bison (Bison bison bison) Teeth from Interior Alaska as Proxies of Seasonal Mobility 71, 185–202.

Juarez, C.A., 2008. Strontium and geolocation, the pathway to identification for deceased undocumented Mexican border-crossers: A preliminary report. J. Forensic Sci. 53, 46–49. https://doi.org/10.1111/j.1556-4029.2007.00610.x

Lee, T.N., Buck, C.L., Barnes, B.M., O'Brien, D.M., 2012. A test of alternative models for increased tissue nitrogen isotope ratios during fasting in hibernating arctic ground squirrels. J. Exp. Biol. 215, 3354–61. https://doi.org/10.1242/jeb.068528

Mann, D.H., Groves, P., Kunz, M.L., Reanier, R.E., Gaglioti, B. V., 2013. Ice-age megafauna in Arctic Alaska: Extinction, invasion, survival. Quat. Sci. Rev. 70, 91–108. https://doi.org/10.1016/j.quascirev.2013.03.015

O'Brien, D.M., 2015. Stable Isotope Ratios as Biomarkers of Diet for Health Research. Annu Rev Nutr. 35, 565–594. https://doi.org/10.1161/CIRCRESAHA.116.303790.The

Shepherd, T.G., 2016. grounds, climate change is ex- tically significant. This is rather. Science (80-.). 353, 989–990.

Widga, C., Walker, J.D., Stockli, L.D., 2010. Middle Holocene Bison diet and mobility in the eastern Great Plains (USA) based on 13C, 18O, and 87Sr/86Sr analyses of tooth enamel carbonate. Quat. Res. 73, 449–463. https://doi.org/10.1016/j.yqres.2009.12.001

Zimov, A.S.A., Chuprynin, V.I., Oreshko, A.P., Iii, F.S.C., Reynolds, J.F., 2011. Steppe-Tundra Transition : A Herbivore-Driven Biome Shift at the End of the Pleistocene. Am. Soc. Nat. 146, 765–794. https://doi.org/10.1086/285824